SYNTHESIS, COORDINATION CHEMISTRY, AND REACTIVITY OF FUNCTIONALIZED PHOSPHINES: TOWARD WATER-SOLUBLE MACROCYCLIC PHOSPHINE COMPLEXES

by

CHARLES D. SWOR

A DISSERTATION

Presented to the Department of Chemistry
and the Graduate School of the University of Oregon
in partial fulfillment of the requirements
for the degree of
Doctor of Philosophy

March 2011

DISSERTATION APPROVAL PAGE

Student: Charles D. Swor

Title: Synthesis, Coordination Chemistry, and Reactivity of Functionalized Phosphines: Toward Water-soluble Macrocyclic Phosphine Complexes

This dissertation has been accepted and approved in partial fulfillment of the requirements for the Doctor of Philosophy degree in the Department of Chemistry by:

Dr. Michael M. Haley	Chairperson
Dr. David R. Tyler	Advisor
Dr. Darren W. Johnson	Member
Dr. Shih-Yuan Liu	Member
Dr. Mark H. Reed	Outside Member

and

Richard Linton	Vice President for Research and Graduate Studies/Dean of the Graduate School

Original approval signatures are on file with the University of Oregon Graduate School.

Degree awarded March 2011

© 2011 Charles David Swor

DISSERTATION ABSTRACT

Charles David Swor

Doctor of Philosophy

Department of Chemistry

March 2011

Title: Synthesis, Coordination Chemistry, and Reactivity of Functionalized Phosphines: Toward Water-soluble Macrocyclic Phosphine Complexes

Approved: _____
Dr. David R. Tyler

Macrocyclic phosphine compounds have long been sought as ligands for transition metal complexes because of their strong binding properties. Despite considerable effort in this field, no general methods for synthesizing phosphine macrocycles or their complexes have been developed. This dissertation describes attempts to synthesize an iron complex with a water-soluble macrocyclic tetraphosphine ligand for use in separating nitrogen from natural gas. Chapter I reviews previous syntheses of macrocyclic phosphine ligands and their complexes, focusing on ligand synthesis, coordination chemistry, and demetallation of the complexes.

Chapter II reports on the synthesis of water-soluble secondary bidentate phosphine ligands, their coordination chemistry with iron(II), and attempts to use these complexes as templates for forming a macrocyclic iron-phosphine complex by reactions with carbon electrophiles.

Over the course of treating these iron complexes with various carbon electrophiles, an interesting reaction between bromomaleic anhydride and proton sponge was discovered. Chapter III explores the product, 4-maleicanhydrido-1,8-bis-

(dimethylamino)naphthalene (MAPS). Due to its conjugated donor-acceptor network, which is disrupted upon protonation, MAPS acts as a colorimetric version of a proton sponge. The attachment of MAPS to amine-functionalized solid supports, forming solid-supported proton sponge reagents, is also described.

Chapter IV discusses the synthesis of an iron(II) complex of the water-soluble phosphine 1,2-bis(di(hydroxymethyl)phosphino)ethane (DHMPE). Although unbound hydroxymethylphosphines commonly react with NH-functional amines via the phosphorus Mannich reaction, this and other complexes of DHMPE do not undergo this reaction. Further investigation with hydroxymethylphosphine-boranes suggests that the currently-accepted mechanism of the phosphorus Mannich reaction is incorrect, and an alternate mechanism is proposed.

Chapter V discusses the synthesis and functionalization of copper(I) complexes of water-soluble phosphines. Unlike the complexes described in Chapter I, these complexes readily react with α,ω-dihalides or di(acyl chloride)s, forming complexes whose mass spectra correspond to those with macrocyclic phosphine ligands. Unlike most macrocyclic tetraphosphine complexes, these complexes can be demetallated by treatment with sulfide. Finally, a new synthesis of water-soluble macrocycles, based on lessons learned during the course of these investigations, is proposed.

This dissertation includes previously published and unpublished co-authored material.

CURRICULUM VITAE

NAME OF AUTHOR: Charles David Swor

GRADUATE AND UNDERGRADUATE SCHOOLS ATTENDED:

University of Oregon, Eugene, OR
Tennessee Technological University, Cookeville, TN

DEGREES AWARDED:

Doctor of Philosophy in Chemistry, 2011, University of Oregon
Master of Science in Chemistry, 2007, University of Oregon
Bachelor of Science in Chemistry, 2004, Tennessee Technological University

AREAS OF SPECIAL INTEREST:

Phosphine Synthesis
Coordination Chemistry
Macrocyclic Ligands
Reactions of Coordinated Ligands

PROFESSIONAL EXPERIENCE:

Co-op Engineer, Fleetguard, Inc., 2004-2005
Graduate Teaching Fellow, University of Oregon, 2005-2007
Graduate Research Assistant, University of Oregon, 2010-2011

GRANTS, AWARDS, AND HONORS:

NSF GK-12 Fellowship, University of Oregon, 2007-2010
Ferris U. Foster Scholarship, Department of Chemistry, Tennessee Technological University, 2004
Outstanding Senior Award, Department of Chemistry, Tennessee Technological University, 2004

PUBLICATIONS:

Swor, C. D.; Hanson, K. R.; Zakharov, L. N.; Tyler, D. R. Reactions of Coordinated Hydroxymethylphosphines with NH-Functional Amines: Investigation of the Phosphorus Mannich Reaction. *Submitted to Inorganic Chemistry.*

Swor, C. D. and Tyler, D. R. Solid-supported proton sponges. U.S. Patent Application No. 61/383,688. September 16, 2010.

Swor, C. D.; Zakharov, L. N.; Tyler, D. R. A colorimetric proton sponge. *J. Org. Chem.* **2010**, *75*, 6977-6999.

ACKNOWLEDGMENTS

I would first like to thank my advisor, Professor David R. Tyler, for his guidance over the course of my graduate studies. He has been a great mentor, and has provided an excellent environment for me to enhance my knowledge and skills in science. By setting a lofty example, he has given me the commitment, motivation, and the desire to conduct scientific research which will provide an important contribution to society. Thanks also to all members of my committee, who have demonstrated a genuine interest in my project and in my development as a chemist.

I would also like to thank previous graduate students in the Tyler Group, especially Justin Crossland, Bevin Daglen, and Takiya Ahmed, who mentored me throughout my graduate career. Thanks also to rotation students Brandy Fox, Kyle Hanson, Jesse Gavette, and Andy Hughett, as well as undergraduates McKenzie Floyd, Erika Hanson, and Ian Doxsee, for the work they contributed to the project. Thanks also to Bryan Nell, who is continuing this research project after I leave, and I wish him the best of luck in his graduate career.

I thank Lev Zakharov for the crystal structures presented in this dissertation. Thanks also to Mike Strain for all his help with NMR spectrometers, and Tim Carter and Erich Chapman for their help with the mass spectrometers.

Thank you to all the wonderful friends I have met during my graduate career. There are too many of you to mention by name, but because of you I will always remember my graduate school experience as a great one.

I was fortunate to receive funding through the UO GK-12 program (NSF Grant # DGE-0742540). I am also deeply grateful to directors Anae Rosenberg and Dean

Livelybrooks for allowing me to participate in this program. The GK-12 does an excellent job promoting science in schools across Oregon. In addition, my experience as a GK-12 fellow in these schools has helped immensely with my development as a science educator. I am privileged to have been a part of this program.

Finally, I would like to thank my family. Thanks to my parents Tom and Sallie, and my brother Steve, for their continued love and encouragement during my graduate career. I would especially like to thank my beautiful wife Rachel for being my steadfast partner throughout this endeavour. She has provided me with support, confidence, and stability during these challenging years. I am grateful and blessed that she has chosen me to accompany her on this adventure of life, and I can't wait to see what's next.

Dedicated to every good teacher I've ever had. I could never have achieved any of my success without the skills they have given me.

TABLE OF CONTENTS

Chapter Page

Chapter Page

LIST OF FIGURES

Figure Page

CHAPTER V

LIST OF TABLES

LIST OF SCHEMES

Scheme Page

CHAPTER I

Scheme Page

Scheme Page

CHAPTER IV

CHAPTER V

CHAPTER VI

CHAPTER I

SYNTHESIS AND COORDINATION CHEMISTRY OF MACROCYCLIC PHOSPHINE LIGANDS

1.1. Introduction

Phosphines (PR_3) are an important class of compounds because of their widespread use as ligands for transition-metal complexes. Phosphine ligands are soft, strong σ-donors, and their electronic, steric, and stereochemical properties vary based on the substituents attached to the phosphorus atoms.[1-3] Thus, choosing the correct phosphine ligands for a metal complex allows control over the electronic and steric environment of the complex.[4] Such tunability is most useful for optimizing the activity of homogeneous catalysts, and as such a plethora of phosphine-containing homogeneous catalysts have been developed for a wide variety of organic reactions including hydrogenation, hydroformylation, hydration, hydrolysis, cross-couplings, and carbon-heteroatom bond formations.[5] In addition, transition-metal phosphine complexes are able to activate small molecules such as H_2, O_2, N_2, H_2O, and CO_2,[6] which makes them promising candidates for use in hydrogen fuel cells, water-splitting, ambient-pressure ammonia synthesis, and artificial photosynthesis.

Macrocyclic ligands – ligands which form a large, continuous ring around a metal ion – form extremely robust complexes because of the *macrocyclic effect*.[7] This is both a thermodynamic effect as well as a kinetic effect. The *thermodynamic macrocyclic effect* is a stronger binding constant (log*β*) for a macrocyclic ligand compared to an analogous open-chain ligand (eq. 1):

$$\text{macrocyclic effect} = \Delta\log\beta = \log\beta_{\text{macrocycle}} - \log\beta_{\text{open-chain}} \qquad (1)$$

Also, because the macrocyclic ring lacks a "free end", stepwise removal of the donor atoms is exceedingly difficult. This results in very slow dissociation rates of macrocyclic ligands from their complexes (the *kinetic macrocyclic effect*).

The exact entropic and enthalpic sources of the macrocyclic effect depend on a number of variables including the donor atoms, the metal, chelate ring size, and solvent interactions;[8-10] however, the macrocyclic effect can be most easily understood by comparing the relative stabilities of *unbound* macrocyclic ligands to open-chain ligands, while arbitrarily setting the *coordinated* macrocyclic and open-chain complexes at equal energy (Figures 1 and 2). A free macrocyclic ligand in solution is less stable than its open-chain analog because of reduced flexibility and the resulting loss of configurational entropy. Macrocycles also have less solvent-accessible surface area, and cannot be as efficiently stabilized by interactions with solvent molecules. This is especially important for nitrogen macrocycles in aqueous solution, where the free open-chain ligand can extend, and the nitrogen atoms can accept hydrogen bonds from the solvent. By contrast, macrocyclic nitrogen ligands are conformationally restricted, and the nitrogen

atoms are not as accessible for hydrogen bonding, resulting in poor stabilization of the free macrocycle. Because of this, the macrocyclic effect in nitrogen ligands is especially large (up to log $\beta \sim 10$).[11] Macrocyclic oxygen ligands (crown ethers), which bind electrostatically to alkali metals and other cations, show smaller macrocyclic effects (log $\beta \sim 3\text{-}4$),[12] which are primarily attributed to enthalpic contributions.[13] Macrocyclic sulfur ligands show an even smaller macrocyclic effect (log $\beta \sim 2$),[14] although it has been shown that additional functionalization (installation of *gem*-dimethyl groups) can help to further stabilize macrocyclic sulfur complexes.[15]

Figure 1. Origin of the thermodynamic macrocyclic effect.

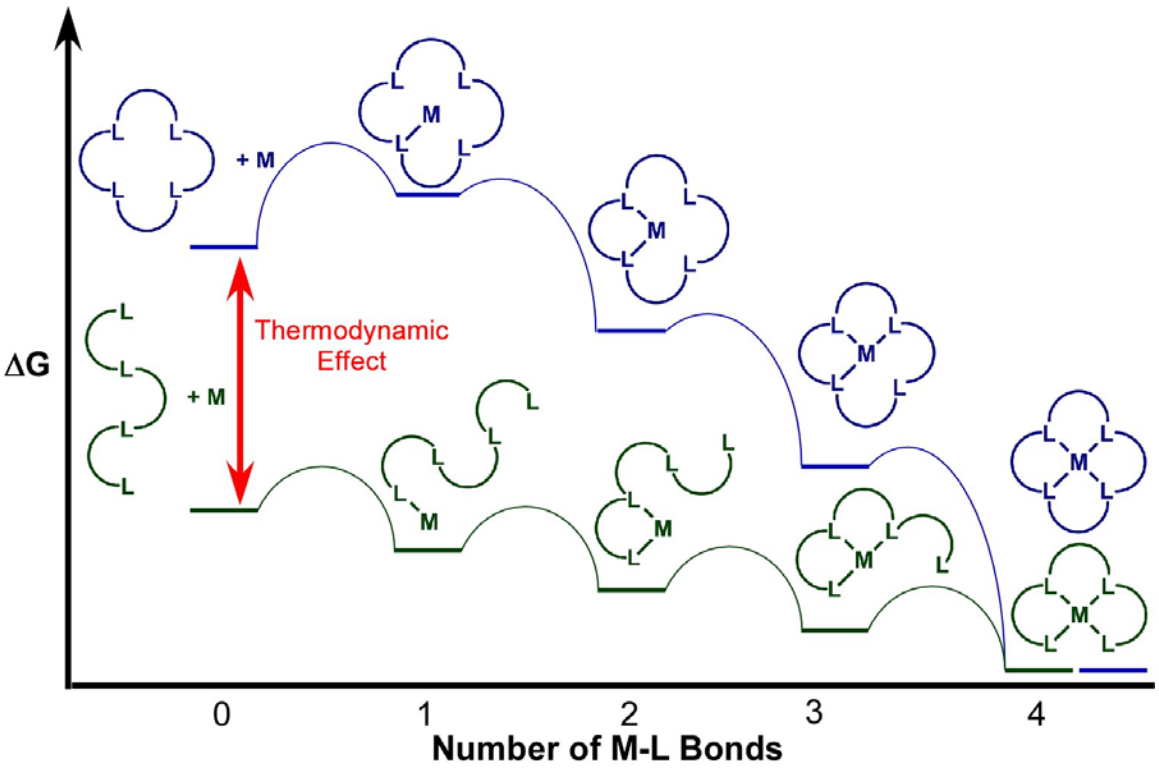

Figure 2. Origin of the kinetic macrocyclic effect.

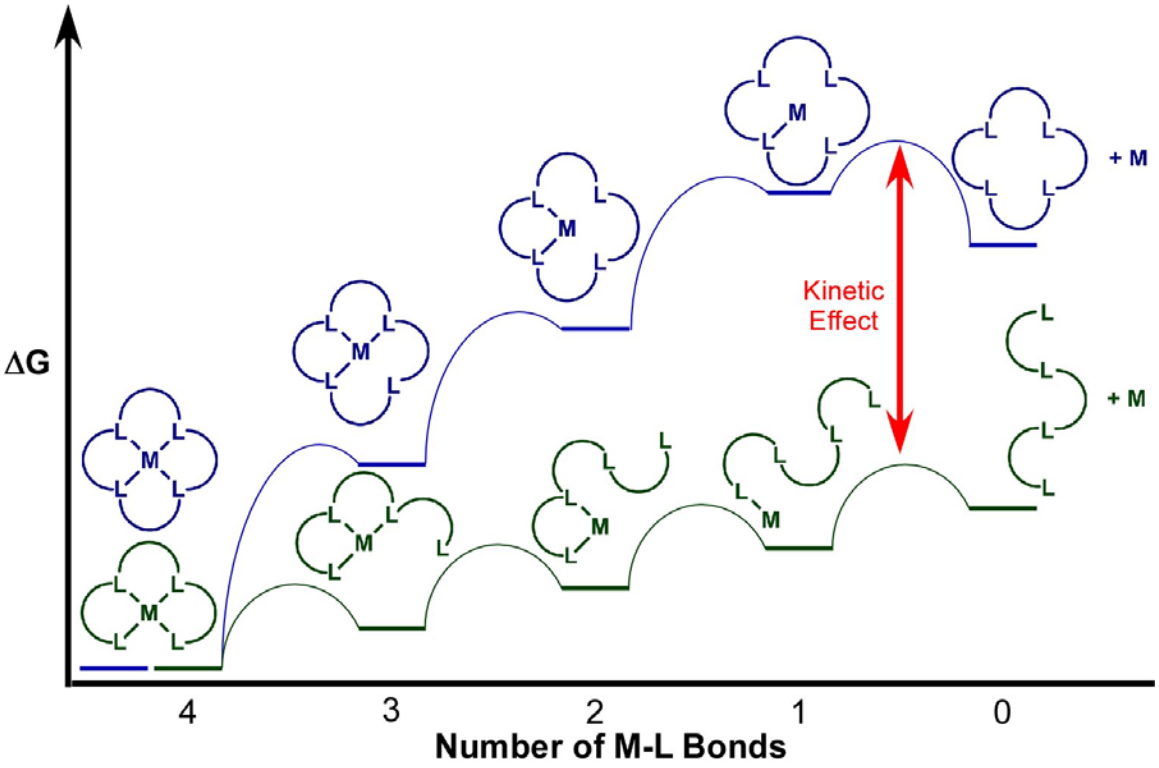

Macrocyclic phosphines hold promise as incredibly stable ligands for applications requiring robust complexes, such as radioactive transition metal complexes for use as radiopharmaceuticals.[16,17] Because of this, these ligands and their complexes have been synthetic targets since soon after the macrocyclic effect was discovered. Unfortunately, macrocyclic phosphine ligands have historically been difficult to synthesize in good yield. A general, versatile synthesis of phosphine macrocycles has not yet been developed, for reasons that will be discussed below. Also, the macrocyclic effect has not yet been measured for a phosphine ligand. This is due to the difficulty in synthesizing macrocyclic ligands, as well as open-chain reference ligands, as will be discussed further below.

The focus of this chapter will be to review advances in both the synthesis and coordination chemistry of macrocyclic phosphine (PR_3) ligands. A few reviews of phosphorus-containing macrocycles have been published,[18-21] but none focused specifically on macrocyclic phosphine ligands. Generally, the term *macrocycle* is used when describing a ring of at least nine covalently-bonded atoms, which is not part of a system of fused or bridged smaller rings. This review, then, will only consider macrocycles with at least nine-membered rings. Also, because macrocyclic ligands are generally considered to be polydentate, this review will only cover macrocycles with at least three phosphorus donor atoms as part of the ring. Mixed-donor macrocycles will not be thoroughly reviewed, but will be mentioned in instances when they accompany similar all-phosphorus-donor macrocycles. Other functional groups are routinely converted to phosphines, such as phosphine oxides and phosphine sulfides (by reduction with $LiAlH_4$ or silanes) or quaternary phenylphosphonium or benzylphosphonium ions (by either reductive cleavage with LAH or base hydrolysis to the phosphine oxide, followed by reduction). Because of this, the synthesis of these macrocycles can be thought of as *formal* syntheses of phosphine macrocycles; as such, these cases are included in this review.

1.2. Synthesis of Macrocyclic Phosphine Ligands

1.2.1. Cyclocondensation Reactions

1.2.1.1. Early Syntheses

The first macrocyclic phosphine ligands were synthesized in 1975 by Horner, et. al.[22,23] These phosphines were generated by the tetramolecular "2:2" reaction of two

equivalents of α,ω-bis(dibenzyl)phosphines with 2 equivalents of α,ω-dialkyl halides to form 16-, 18-, and 20-membered macrocyclic quaternary benzylphosphonium salts **1** (Scheme 1, Method A). The yields of the phosphonium macrocycles generated by this method were very low (3-11%). In most cases the bimolecular "1:1" small-ring compounds were formed in addition to the macrocycles and the mixtures were separated by differential solubility. It should be noted that the 2:2 macrocycles are essentially dimers of the 1:1 small-ring products; thus, their molecular formula is exactly twice that of the small rings, and their elemental ratios are the same. In this case, the macrocycles were characterized by having higher melting points than the small-ring products.

Scheme 1. Summary of Horner's benzylphosphonium macrocycle syntheses.

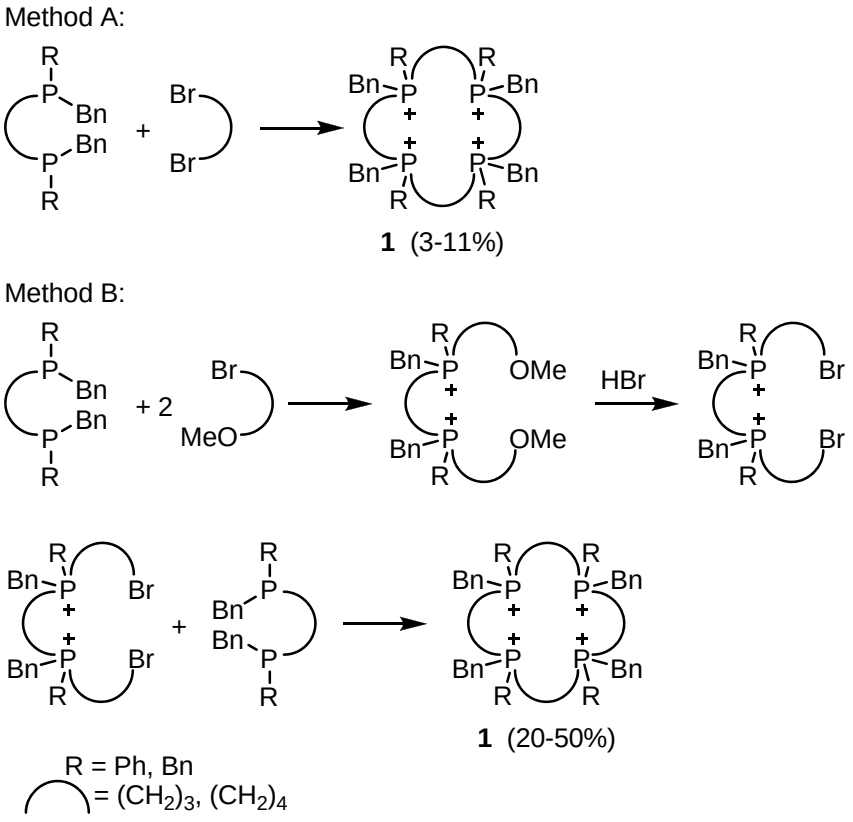

Later syntheses involved stepwise building-up of the macrocyclic ring by first alkylating the phosphine with $MeO(CH_2)_3Br$, followed by conversion of the methoxy groups to bromides, forming an α,ω-brominated bis(phosphonium) compound (Scheme 1, Method B). This compound was then reacted with a second equivalent of bisphosphine to form the tetraphosphonium macrocycle. This stepwise synthesis resulted in higher yields for the macrocyclization step (20-50%). Strangely, the use of high-dilution conditions did not improve the yields of these macrocycles. Reductive cleavage of **1** with $LiAlH_4$ (typically 6 to 24 hours in refluxing THF) gave the corresponding phosphine macrocycles **2** in yields of 77-89% (Scheme 2). The phosphonium macrocycles could also be converted to phosphine oxides (**3**) by hydrolysis with base. The coordination chemistry of these compounds was not studied.

Scheme 2. Reductive and oxidative cleavage of benzylphosphonium macrocycles.

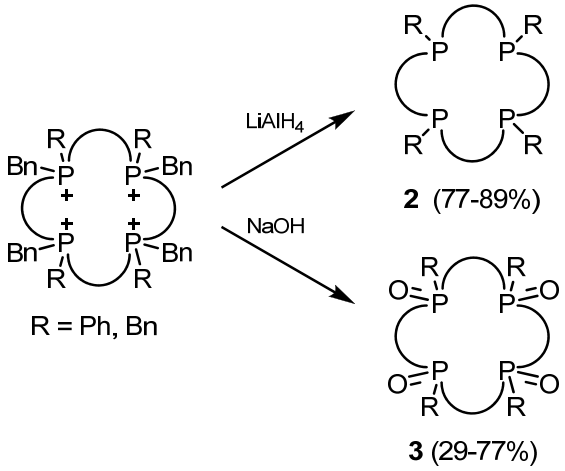

In 1977, Kyba et al. synthesized 11-membered triphosphine (P3) macrocycles **4** and 14-membered tetraphosphine (P4) macrocycles **5**[24] (Scheme 3) using a special high-dilution apparatus (Figure 3).[25,26] The apparatus contained reservoirs that pre-diluted

each reagent with condensing solvent. These reservoirs then overflowed, combining the pre-diluted reagents into a large volume of refluxing solvent. As the reaction proceeded, small amounts of pre-diluted reactants were slowly added so that the concentration of each reactant at any given time was kept to a minimum to prevent polymerization. Even using such an apparatus, the best yield of a macrocycle achieved was only 22%. The structure of each macrocycle was confirmed by X-ray crystallography and their coordination chemistry investigated (see Section 1.3.1).[27-29] Mixed phosphorus/oxygen, phosphorus/nitrogen, and phosphorus/sulfur donor macrocycles were also synthesized by this method, including a 14-membered P3S macrocycle in 26% yield.[30,31]

Scheme 3. Kyba's P3 and P4 macrocyles.

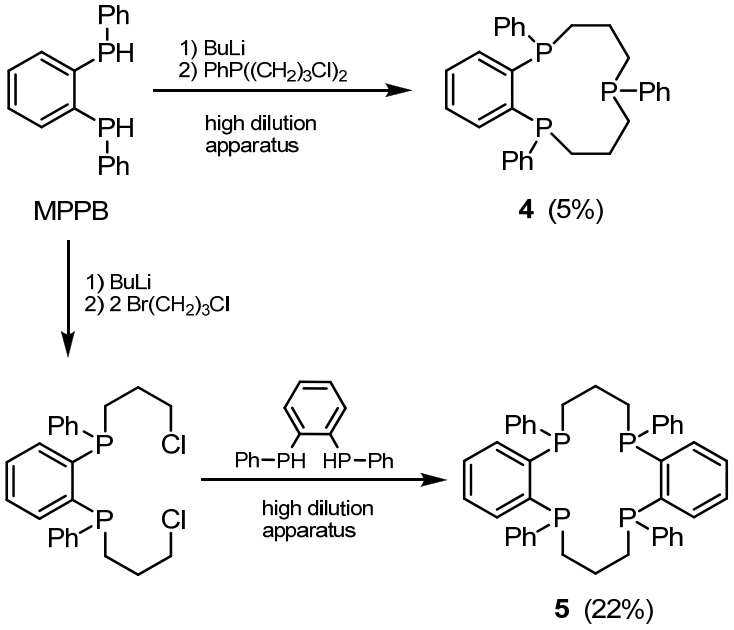

Figure 3. High-dilution apparatus.

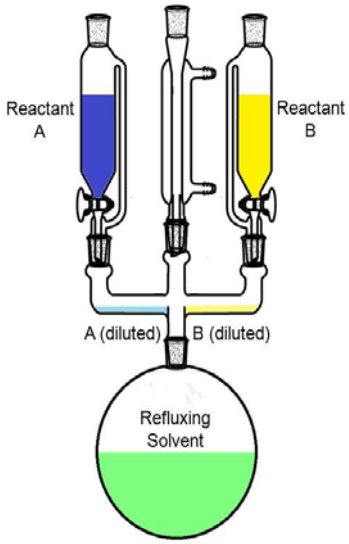

Most macrocyclic phosphine ligands consist entirely of tertiary phosphine groups. This often limits the ability to functionalize the phosphine after the macrocyclic ring is

formed. The first macrocycle containing a secondary phosphine was synthesized by the 1:1 reaction between 1,2-bis(phenylphosphino)benzene (MPPB) and a chloride-functionalized phosphine sulfide containing a 1-naphthylmethyl group.[32] Following macrocyclization (36% yield), the naphthylmethyl protecting group was cleaved using potassium naphthalenide, followed by reduction of the phosphine sulfide group with $LiAlH_4$ to form **8** (Scheme 4). The coordination chemistry of this macrocycle will be discussed in Section 1.3.1.

Scheme 4. Synthesis of a secondary triphosphine macrocycle.

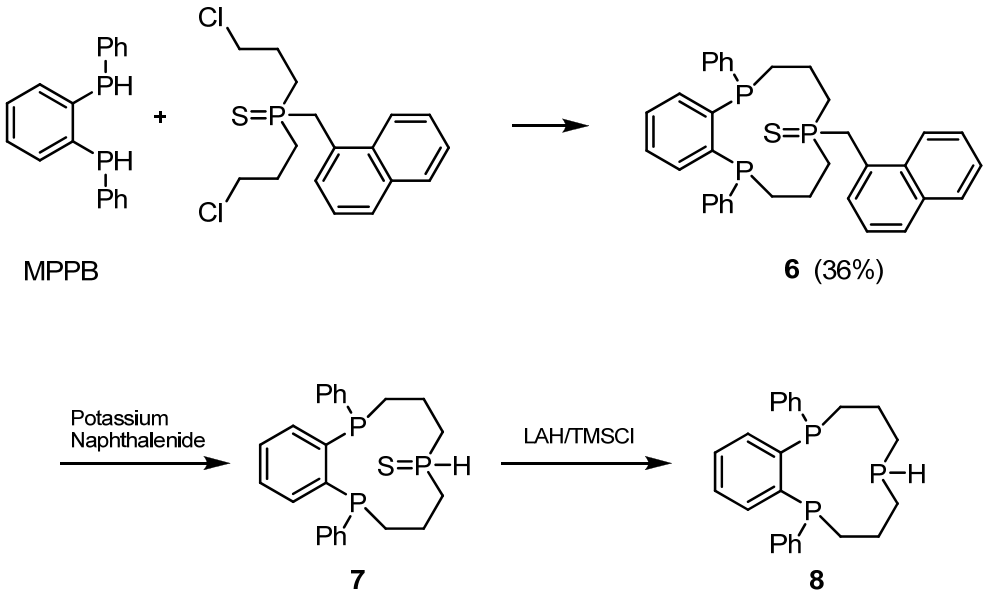

Ciampolini's 18-membered crown ether-type mixed P4O2[33,34], P4S2[35], and P4N2[36] macrocycles were synthesized by 2:2 cyclocondensations between 1,2-bis(phenylphosphino)ethane (MPPE) and $(ClCH_2CH_2)_2L$ (L = O, S, N*n*-Pr), in yields up to 12% (Scheme 5). These ligands showed interesting coordination chemistry with cobalt and nickel, where the ligands could act as tetradentate, pentadentate, or

hexadentate ligands depending on the metal, the identity of the non-phosphorus donor, and the presence of other ligands such as chloride or solvent (see Section 1.3.2).

Scheme 5. Ciampolini's phosphine macrocycles.

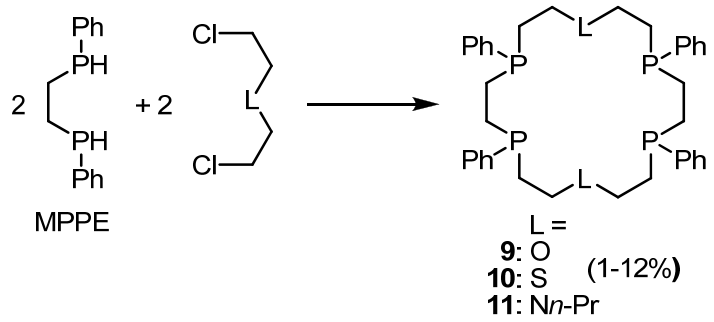

The low yields of these early syntheses illustrate the inherent difficulties involved in the synthesis of macrocyclic phosphines by cyclocondensation reactions. Control of stoichiometry is often difficult when flexible linkers are used to join phosphine units. In the case of 2:2 cyclocondensations, where two bisphosphine molecules are connected by two difunctional linker molecules, two types of by-products are more favorably generated, depending on the reaction conditions (Scheme 6). After the first coupling between reactants A and B, complementary reactive ends are present on the same molecule. Under concentrated conditions, the reactive ends are more likely to encounter other reactant molecules and form polymers. On the other hand, dilute conditions encourage the formation of small rings because the complementary reactive ends of a single molecule are more likely to find each other than to find another reactant molecule. However, in practice even under "ideal" high-dilution conditions, the macrocyclic products are only formed in small amounts.

Scheme 6. Macrocyclization via a 2:2 cyclocondensation method.

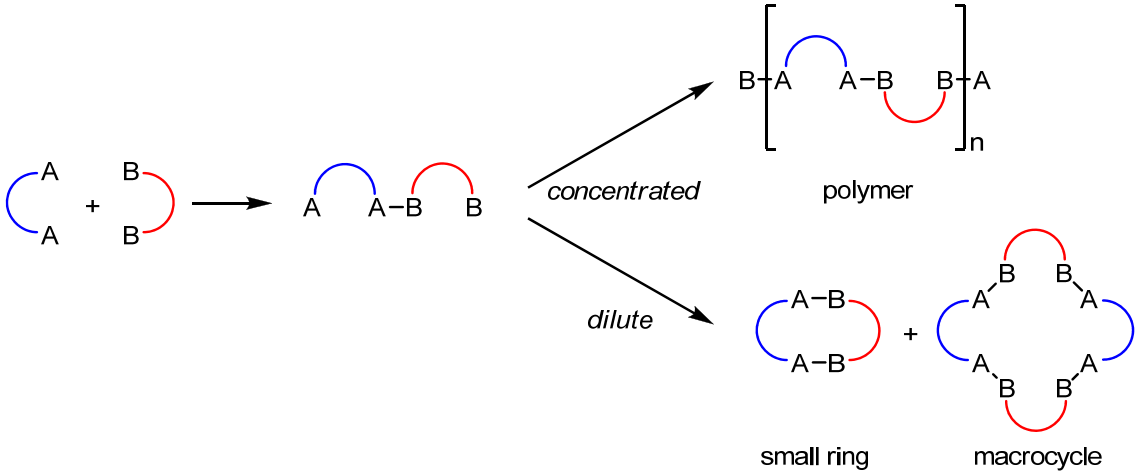

Small-ring products can be avoided if a stepwise synthesis is employed in which the linkers are attached first to one phosphine, followed by a 1:1 macrocyclization step with a second phosphine (Scheme 7). For 1:1 macrocyclizations, the macrocycle is the smallest ring possible and is favored over polymeric products if sufficiently dilute reaction conditions are employed. However, the yields are often low even under optimal conditions because of slow kinetics and the entropic penalty of closing a large ring.[37] Also, as more synthetic steps are required, including functional group transformations, the overall yield of the macrocycle from its starting components is still often low.

Scheme 7. Macrocycle synthesis by stepwise buildup, followed by 1:1 cyclization.

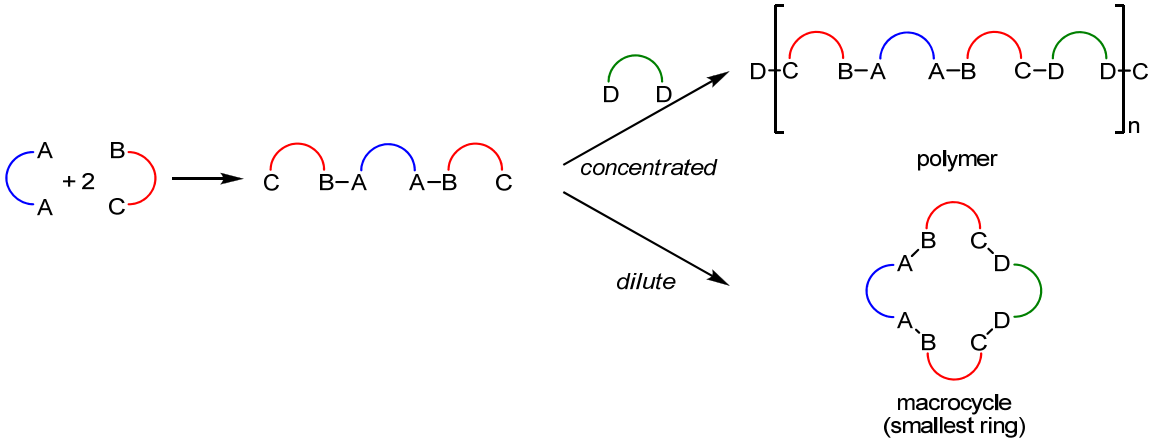

A pair of 15- and 16-membered, mixed phosphine oxide/phosphonium macrocycles **12a** and **12b** were synthesized in a stepwise fashion in 50% and 57% yield, respectively.[38] In the first step, a secondary bisphosphine was alkylated with allyl alcohol, followed by conversion of the hydroxyl groups to bromides using Br_2 (which also oxidized the phosphine groups to phosphine oxides), then cyclocondensation with 1,3-bis(diphenylphosphino)propane (DPPP) (Scheme 8). The phosphonium groups were hydrolyzed to form the corresponding tetra(phosphine oxide) macrocycles. Reduction to the macrocyclic phosphines was suggested, but not reported.

Scheme 8. Stepwise synthesis of a mixed phosphonium/phosphine oxide macrocycle.

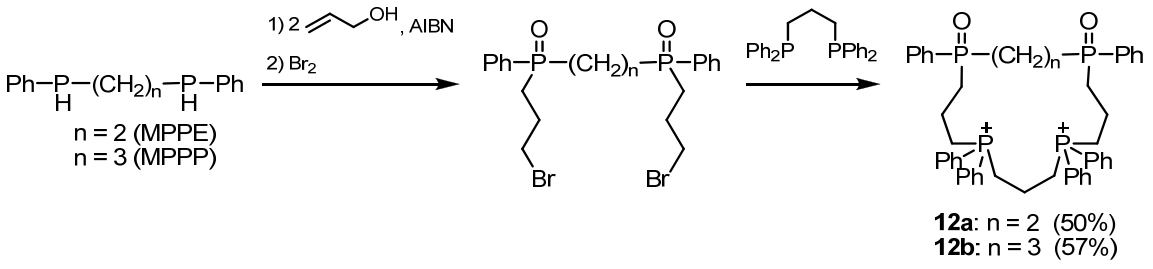

1.2.1.2. Cyclocondensations Using Rigid Linkers

Syntheses of macrocycles by cyclocondensation are more successful when rigid linker units are used, which favor the conformations necessary for macrocyclization. This was first realized with tetraphosphonium macrocycles containing *p*-xylene linkers (Scheme 9), which formed in yields up to 98%.[39] Although direct evidence of a macrocycle (molecular weight measurement) was not obtained for this compound, the open-chain macrocycle precursor $Ph_2P(CH_2)_2P^+PhCH_2(p\text{-}C_6Cl_4)CH_2P^+Ph(CH_2)_2PPh_2$ was isolated when the reaction was stopped before reaching completion. Also, simple molecular modeling revealed that the small-ring product is strained because of the length and rigidity of the *p*-xylene linker and is likely to be disfavored over the macrocyclic product. Unfortunately, base hydrolysis of the tetraphosphonium macrocycle preferentially cleaved the benzylphosphine linkages in the macrocyclic ring as opposed to the phenyl groups, resulting in decomposition of the macrocycle.

Scheme 9. Macrocyclizations using *p*-xylene linkers.

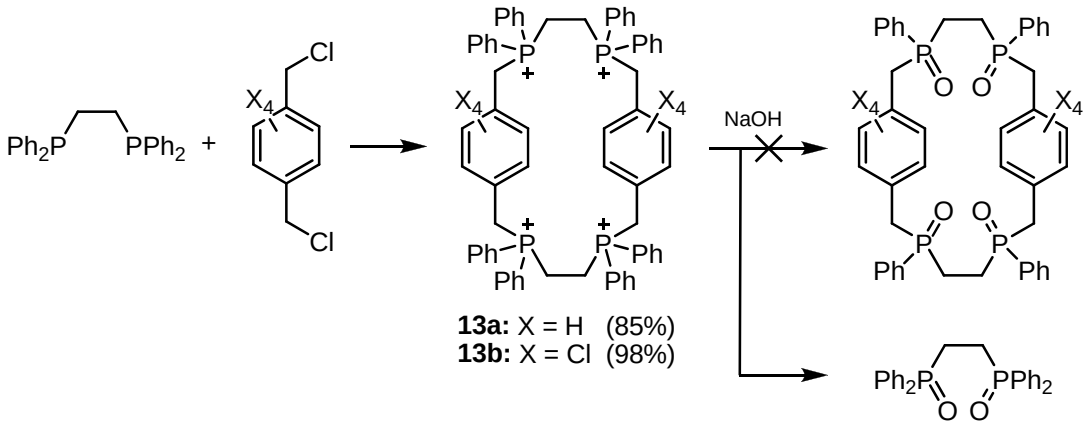

Rigid *trans*-2-butene linkers have been used to synthesize phosphonium and phosphine oxide macrocycles (Scheme 10). Reaction of 1,2-bis(diphenylphosphino)-ethane (DPPE) with *trans*-1,4-dichloro-2-butene gave a 16-membered phosphonium macrocycle in 80% yield.[40] The macrocyclic structure was identified by molecular weight determinations using vapor pressure osmometry. This linker was also used to form 16- and 18-membered phosphine oxide macrocycles.[41,42] The *trans*-butene linkers probably enforce the wrong geometry for chelation to a transition metal, but these molecules could be hydrogenated to generate the saturated, flexible macrocycles.

Scheme 10. Macrocyclizations using *trans*-2-butene linkers.

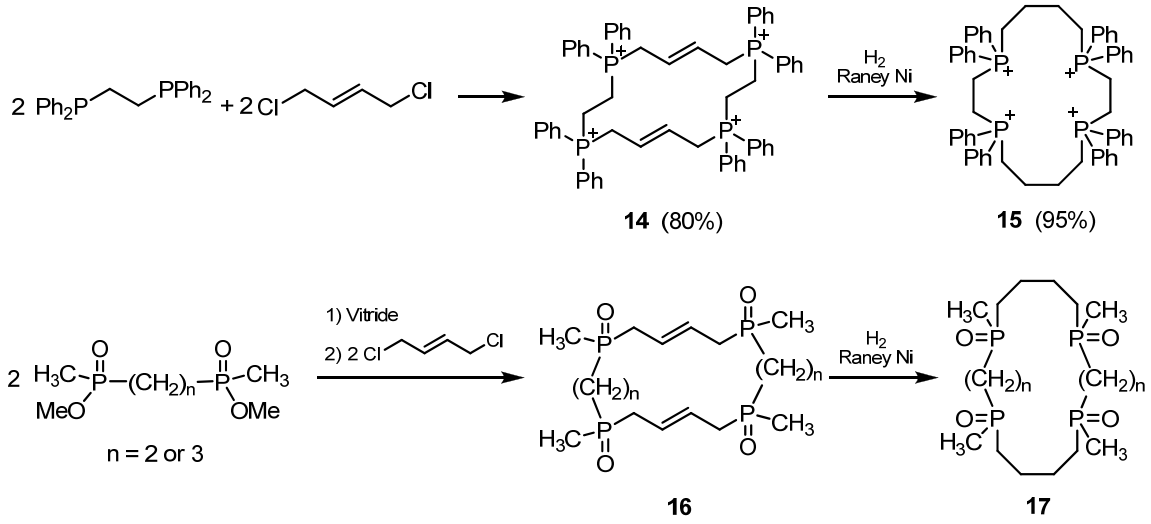

Interestingly, rigid 2-butene linkers with the *opposite* (*cis*) stereochemistry were also shown to give tetraphosphonium macrocycles in some instances (Scheme 11).[43] This result suggests that the absolute stereochemistry of the linker is not always important for successful macrocyclization, as long as the linker is generally inflexible.

Ortho-xylene linkers have also been used, although the yields of macrocycles were very low.[44]

Scheme 11. Phosphine macrocycle synthesis using a *cis*-2-butene linker.

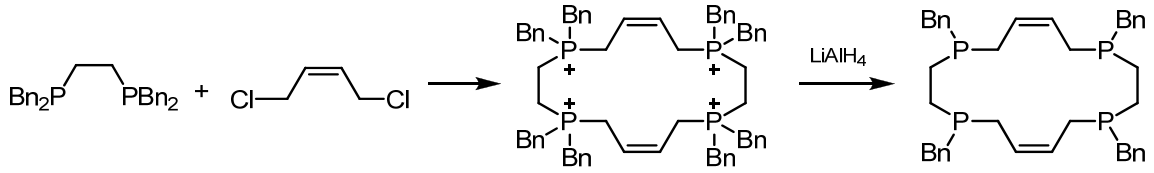

18: (85%) **19**

1.2.1.3. Stereochemical Control

Another difficulty associated with macrocyclic phosphine synthesis is control of the stereochemistry at the phosphorus atoms. Most macrocyclic phosphine ligands contain asymmetric phosphine groups ($PR^1R^2R^3$), where each substituent attached to the phosphorus is different. Unlike tertiary amines, the inversion barrier of phosphines is sufficiently high (30-35 kcal/mol) that they do not undergo inversion at room temperature.[45] This means that the $PR^1R^2R^3$ groups of macrocyclic phosphines are chiral, resulting in multiple possible stereoisomers for each macrocycle. None of the syntheses described so far have attempted to control the stereochemistry of the phosphine groups. This limits these macrocycles' utility as ligands because the relative orientations of the phosphorus lone pairs will vary in each stereoisomer, and this can affect the coordination behavior of the various stereoisomers.

In an attempt to bypass this problem of stereochemistry, Mathey et al. synthesized a series of phosphole macrocycles (Scheme 12).[46] Reductive cleavage of the bis(diphosphole) **20** to bis(phospholide) **21** with Na^0, followed by linking with

dibromomethane under high-dilution conditions, generated the 10-membered tetraphosphole macrocycle **22a** in moderate yield. In addition, 13- and 16-membered macrocycles **22b** and **22c** could be obtained by stepwise reductive cleavage and reaction with either dibromomethane or 1,4-dibromobutane. These macrocycles were then derivatized to the corresponding phosphine sulfides for complete characterization.

Scheme 12. Synthesis of phosphole macrocycles.

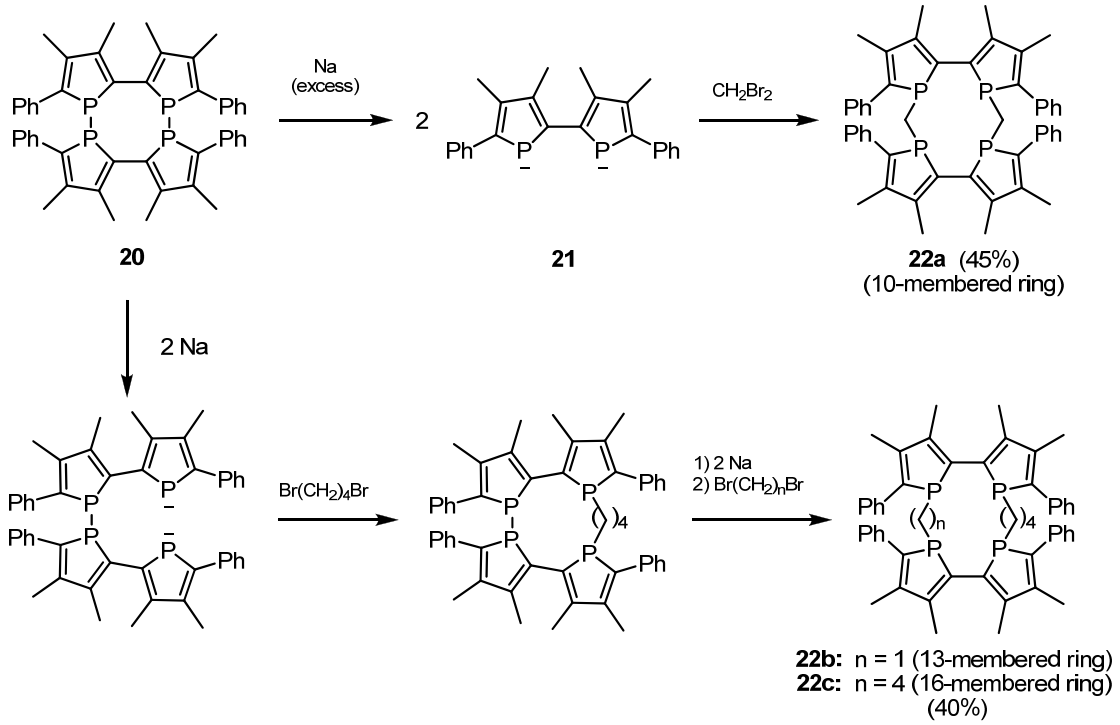

Phosphole groups are not planar but have an inversion barrier of ~16 kcal/mol,[47] which allows them to undergo inversion at room temperature. In macrocycles **22a-c**, multiple stereoisomers are still observed, but they readily interconvert so that potentially problematic isomers (i.e. those that may not be the correct geometry for a desired

coordination mode) can convert to those better suited for coordination once a metal is introduced.

Another solution to the problem of chiral phosphines is phosphinine (a.k.a. "phosphorine" or "phosphabenzene") macrocycles. P3 and P4 phosphinine macrocycles **23** and **24** were successfully synthesized by high-dilution reactions involving bis(1,2-azaphosphinines) and bis(acetylenes) (Scheme 13).[48] Yields are low (20%), owing to formation of oligomeric by-products. Fortunately, the macrocycles are less soluble than the by-products, which can simply be rinsed away. Both of these structures were confirmed by x-ray crystallography. Another advantage of phosphinine groups over normal phosphines is that they are air-stable. This synthetic route has also generated mixed phosphinine/furan (**25**), phosphinine/thiophene (**26**), and phosphinine/ether macrocycles **27a-c** (Figure 4).[49,50]

Scheme 13. Synthesis of phosphinine macrocycles.

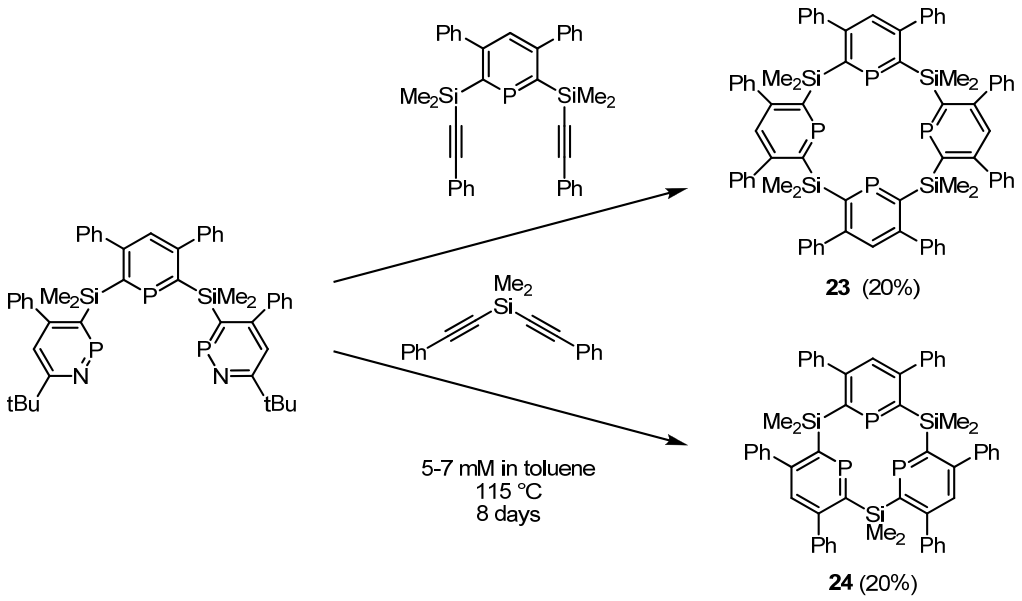

Figure 4. Mixed phosphinine macrocycles.

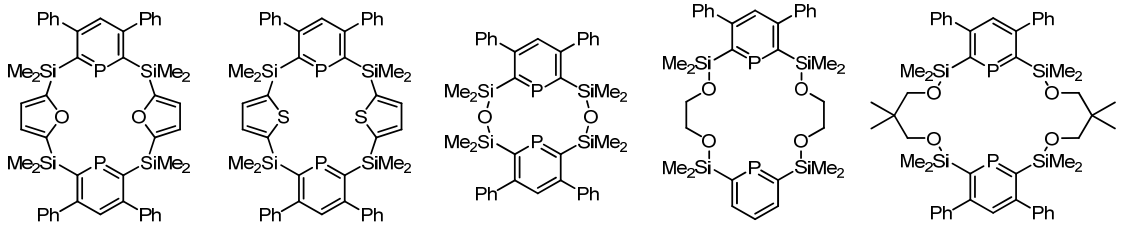

Morisaki recently synthesized a chiral, crown-ether type phosphine-borane macrocycle by stepwise oxidative coupling of chiral methylphosphine-borane oligomers (Scheme 14).[51] The major product was an 8-phosphorus oligomer; however, macrocycle **28** was also generated and isolated in 15% yield. Its structure was confirmed by X-ray crystallography. This is the only example of a 12-phosphacrown-4 macrocycle. Phosphine-boranes are routinely converted to phosphines by refluxing with excess amine, although this method was not reported for this macrocycle. Although the coordination chemistry of this macrocycle has not been studied, the coordination chemistry of 12-membered N4[52-54] and S4[55] macrocycles suggests that it would likely not be large enough to fully encircle a transition metal atom.

Scheme 14. Synthesis of a borane-protected 12-phosphacrown-4 macrocycle.

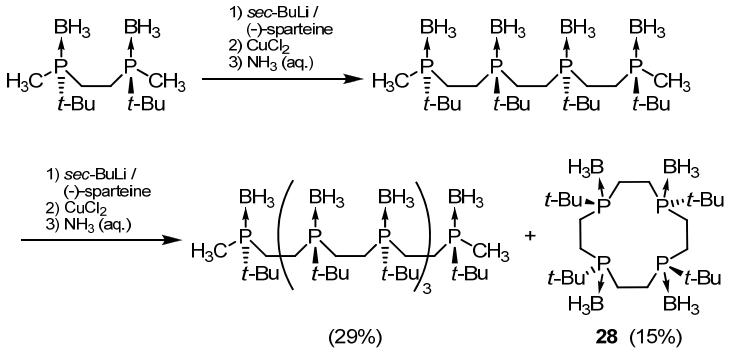

Recently a nine-membered P3 macrocycle **32** was synthesized in high yield[56] by reductive cleavage of bis(2-diphenylphosphinoethyl)phenylphosphine (TRIPHOS) to generate the bis(phosphide) **29**,[57] followed by the 1:1 cyclocondensation with 1,2-dichloroethane (Scheme 15). Both the *syn-syn* isomer **30a** and the *syn-anti* isomer **30b** were observed by ^{31}P NMR spectroscopy (*syn-syn*:*syn-anti* = 3:7), although these isomers were not separated. See Section 1.3.1 for a discussion of this ligand's coordination chemistry.

Scheme 15. Synthesis of a 9-membered P3 macrocycle by a cyclocondensation method.

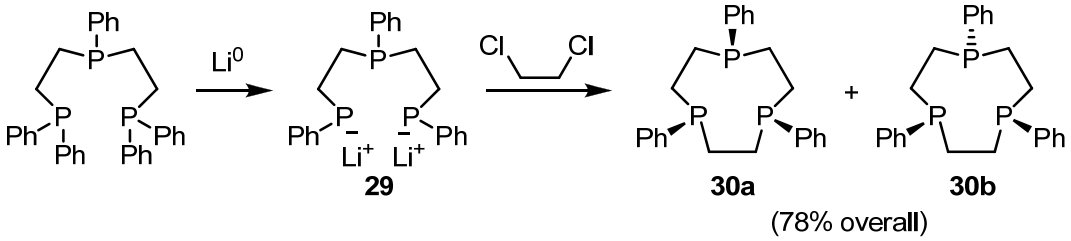

A unique ferrocene-bridged P3 macrocycle has been isolated, and its crystal structure obtained.[58,59] While synthesizing phosphine-containing poly(ferrocenes) **34** by photoinitiated ring-opening polymerization of the strained phosphine-bridged ferrocene **31**, the dimer **32** and macrocyclic trimer **33** were obtained as side-products. The two isomers all-*syn* **33a** and *syn-anti* **33b** were isolated by conversion to the phosphine sulfide, separated from other oligomers by preparative-scale recycling gel permeation chromatography (GPC), and converted back to the phosphines with MeOTf and $P(NMe_2)_3$. Crystal structures of both **33a** and its phosphine sulfide were obtained.

Scheme 16. Synthesis of a ferrocene-bridged P3 macrocycle.

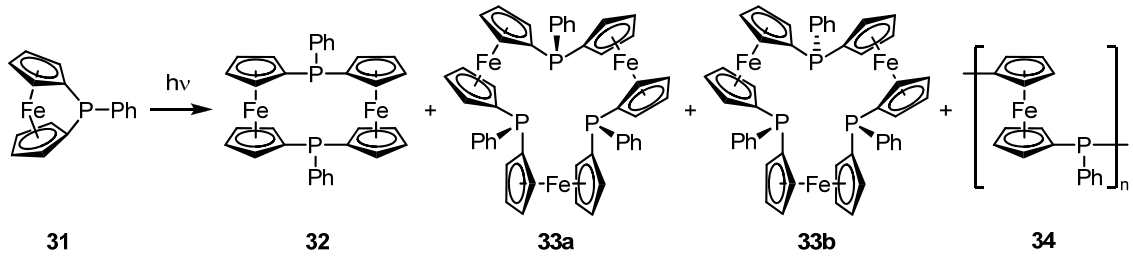

1.2.1.4. Self-Assembling Phosphine Macrocyles

Balueva and colleagues prepared large phosphorus macrocycles that self-assembled by the phosphorus Mannich reaction between hydroxymethylphosphines and NH-functional amines. The first series is the 28-membered P4 macrocycles **35a-f** (Scheme 17),[60,61] with semi-rigid *p*-diphenyl linkers spanning two 1,5-diaza-3,7-diphosphacyclooctane rings. These macrocycles form under high-dilution conditions in DMF. The phosphorus Mannich reaction is reversible in solution, allowing the six individual components to self-assemble into the thermodynamically favored macrocycles. The self-assembly was observed by monitoring the reactions by ^{31}P NMR spectroscopy, which showed the appearance and disappearance of a variety of intermediates over the course of the reactions and which reached completion between 4 h and 60 h at 110 °C. Four of these macrocycles (**35a, d, e,** and **f**) were structurally confirmed by XRD, with the others characterized by FAB-MS. The 120° angle between the amine groups on the linking agent is crucial for formation of the macrocycle; for example, using a 3,3'-diaminodiphenylmethane linking agent did not give a discrete product. A 36-membered macrocycle (**36**) was synthesized in the same manner using the more flexible spacer, 4,4'-(1,3-phenylenedioxy)dianiline.[62]

Scheme 17. 28- and 36-membered self-assembled macrocycles.

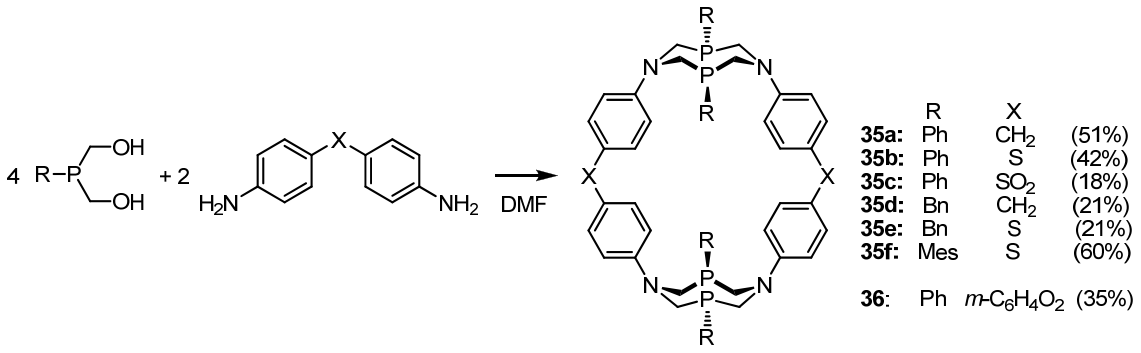

A 16-membered macrocycle was also synthesized by self-assembly using the phosphorus Mannich reaction (Scheme 18).[63] The bidentate secondary phosphine 1,3-bis(mesitylphosphino)propane reacted with formaldehyde and benzylamine, precipitating macrocycle **37a** in 51% yield after 7 days. In a similar manner, chiral macrocycle **37b** was synthesized using *R*- or *S*-α-methylbenzylamine,[64] and cryptand **38** was generated when *m*-xylylenediamine was used as a tetrafunctional linker.[65] The authors later reported the synthesis of more 16-membered phosphine macrocycles including water-soluble and chiral versions, by using other amine linkers.[66] However, no experimental data or crystal structures were reported for any of these compounds so this route cannot yet be considered a generalized method for the synthesis of macrocyclic phosphines. Indeed, when aromatic amines were used as linkers, the eight-membered small-ring products were generated instead of the macrocycles, showing that there are limits to this synthetic strategy.[67]

Scheme 18. Self-assembly of 16-membered tetraphosphine macrocycles and cryptand.

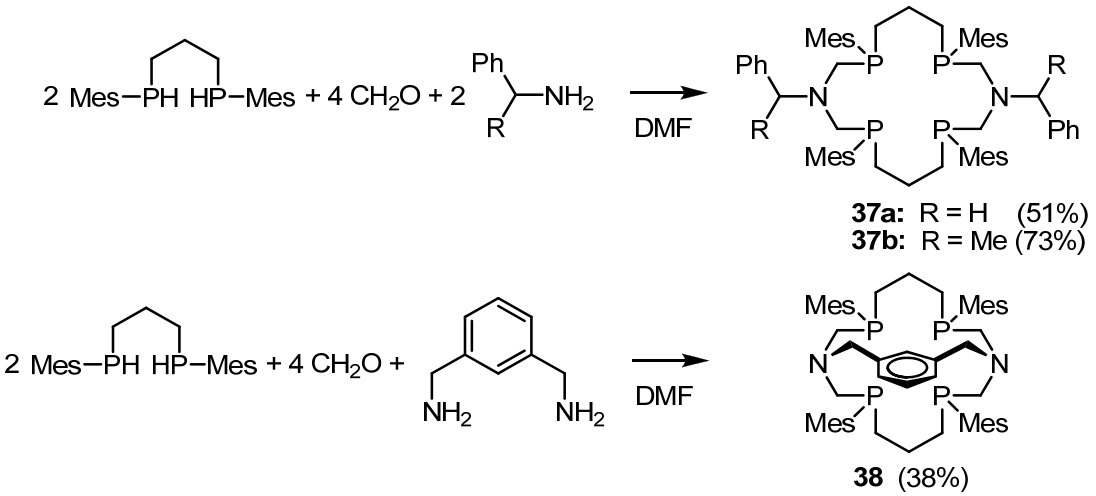

1.2.1.5. Summary

Cyclocondensation reactions have been employed to synthesize phosphorus macrocycles with varying degrees of success. High-dilution conditions are usually necessary, and as such the reactions often require long reaction times. The 2:2 cyclocondensation method using flexible linkers is the least successful strategy, while rigid linkers and/or self-assembling components can be used to favor macrocycle formation over either 1:1 small-ring products or polymers. Formation of small-ring products can be avoided if a multi-step approach is employed, in which a linear compound is built then cyclized in a 1:1 cyclocondensation reaction. However, formation of the macrocyclic ring still requires high dilution conditions and can suffer from low yields.

1.2.2. Template Syntheses

As discussed in the previous section, cyclocondensation reactions often suffer from side-reactions and slow kinetics, resulting in low yields of macrocycles. An

alternative strategy is the *template synthesis*,[68] where components are coordinated to a transition-metal template before being linked together to form the macrocycle. The metal acts as a collection point, controlling the stoichiometry and increasing the likelihood of the macrocyclization by placing reactive groups in close proximity to each other. In the case of primary and secondary phosphines, the metal may also activate the ligand toward alkylation by increasing the acidity of the P-H bond and the nucleophilicity of the deprotonated phosphido ligand.[69]

1.2.2.1. Triphosphine Macrocycles

In 1982, Norman et al. synthesized the 12-membered P3 macrocycle **39a** from *fac*-Mo(allylphosphine)$(CO)_3$ (Scheme 19).[70] AIBN-initiated hydrophosphination of the terminal olefins around the Mo template gave the macrocycle in 85% yield. This reaction also worked with 4-phosphino-1-butene, generating the 15-membered P3 macrocycle **39b** in 70% yield.[71] The progress of the reaction, showing each partially-formed intermediate, could be followed by ^{31}P NMR spectroscopy. The Edwards group later synthesized tungsten and chromium analogs **39c**[72] and **39d.**[73] Synthesis of the $W(CO)_3$(allylphosphine)$_3$ template from $W(CO)_3$(mesitylene) was similar to the synthesis of the Mo analog, although heating was required, which resulted in some oligomerization of the allylphosphine as a side-reaction. The $Cr(CO)_3$(allylphosphine)$_3$ template could not be formed from the mesitylene complex but was synthesized instead from $Cr(CO)_3(MeCN)_3$. Radical-initiated intramolecular hydrophosphination of each of these templates then led to macrocyclization.

Scheme 19. Group 4 metal-templated triphosphorous macrocyclizations.

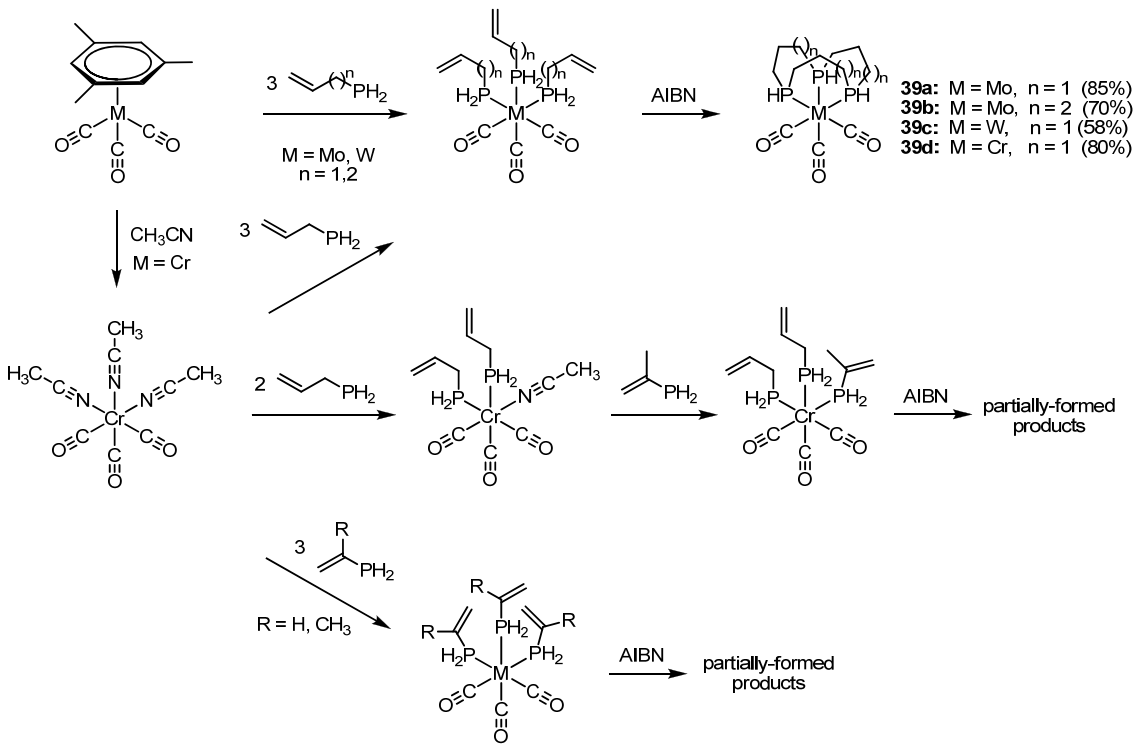

Attempted syntheses of nine-membered macrocycles by template macrocyclizations of vinylphosphine or 2-propenylphosphine were unsuccessful, instead giving oligomeric or polymeric products. Attempts at forming 10 and 11-membered macrocycles using mixed-phosphine templates (formed by first reacting $Cr(CO)_3(MeCN)_3$ with two equivalents of a phosphine, followed by one equivalent of a second phosphine) were also unsuccessful. This may be due to unfavorable ring sizes of these smaller macrocycles but is more likely due to inherent differences in reactivity between vinylphosphines and allyl/butenylphosphines.

Derivatives of **39** were synthesized by alkylation of the secondary phosphine groups, either with alkyl halides to form **40a-e** or by radical addition of allyl-functionalized compounds to form **41** (Scheme 20).[73,74] In addition, the secondary phosphine groups could be converted to halophosphine groups by reaction with CX_4 and

Et_3N.[75] This reaction was significantly faster than that reported for free secondary phosphines, suggesting that coordination to the metal template activates the ligands toward this reaction. Halophosphines **42a** and **42b** were then converted to arylphosphine **43** by treatment with arylcopper reagents.

Scheme 20. Alkylated derivatives of P3 macrocyclic complexes.

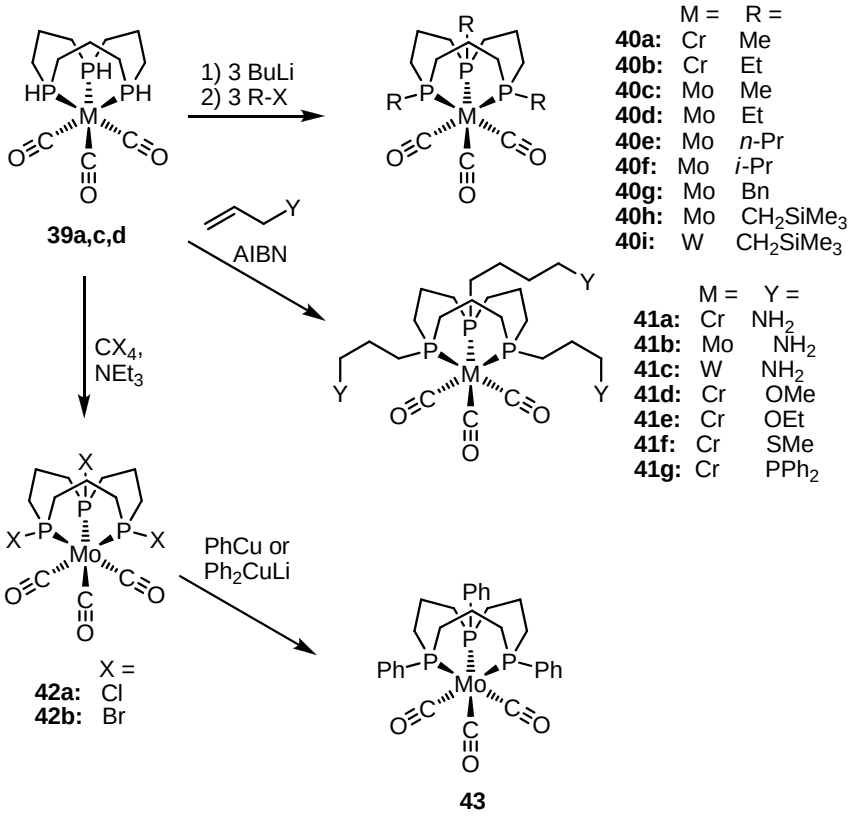

As mentioned above, the Group 6 carbonyl templates could not be used to synthesize P3 macrocycles with rings of fewer than 12 atoms. Instead, Edwards and colleagues used an iron piano stool template to couple 1,2-bis(phosphino)ethane and trivinylphosphine, forming the nine-membered P3 macrocycle **45** (Scheme 21).[76] This and other iron piano stool complexes have proven to be the most versatile templates for

the synthesis of P3 macrocycles, with variations in the cyclopentadienyl ring, macrocycle ring size, and substituent groups, generating a myriad of triphosphine macrocycles. A plethora of nine-membered macrocycles **47a-j** were synthesized, with the macrocyclizations occurring via Michael-type reactions using KO*t*-Bu instead of radical hydrophosphinations.[77] Nine-membered benzo-fused macrocycles **51** were synthesized by the templated macrocyclization of 1,2-bis(phosphino)benzene (BPB) or 1,2-bis(phosphino)-3-anisole,[78] and the dibenzo-fused macrocycle **55** was synthesized by nucleophilic aromatic substitution of $PhPH_2$ on an *o*-fluorophenyl bidentate phosphine.[79] 12-membered macrocycles **53a,b** were synthesized in moderate yield from the templated trimerization of allylphosphine**.**[80] Strangely, attempted synthesis of an 11-membered macrocycle by the templated coupling of BPE with tri(allyl)phosphine actually generated the 10-membered macrocycle **49** instead.[81] A symmetric 10-membered macrocycle, analogous to **45**, was recently synthesized using the Michael-type addition of trivinylphosphine to 1,3-bis(phosphino)propane. [82] A myriad of derivatives were synthesized by hydrogenation and/or alkylation of these macrocycles.

Scheme 21. Synthesis of P3 macrocycles on iron piano-stool templates.

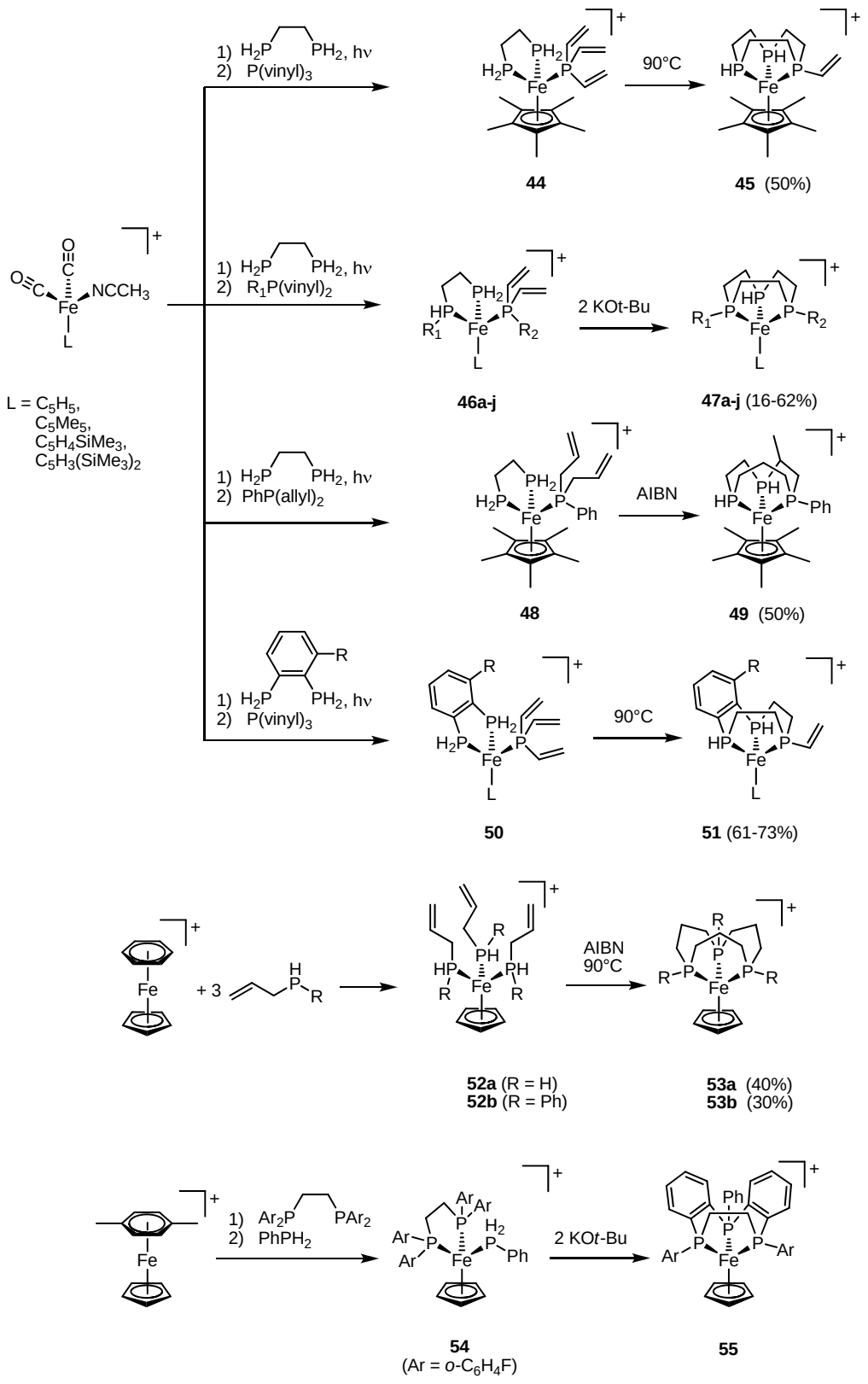

Gladysz et al. synthesized an especially large, 45-membered P3 macrocycle by using ring-closing metathesis of 3 equiv $PhP((CH_2)_6CH{=}CH_2)_2$ on a *fac*-$W(CO)_3$ template (Scheme 22).[83] This reaction is an excellent illustration of a template synthesis favoring a macrocycle over polymeric or small-ring products. Such a large macrocycle would be essentially impossible to form in a cyclocondensation reaction. The success of this reaction suggests that ring-closing metathesis might be used to form smaller macrocyclic phosphines; however, this reactivity has not yet been reported.

Scheme 22. Synthesis of a 45-membered triphosphorus macrocycle.

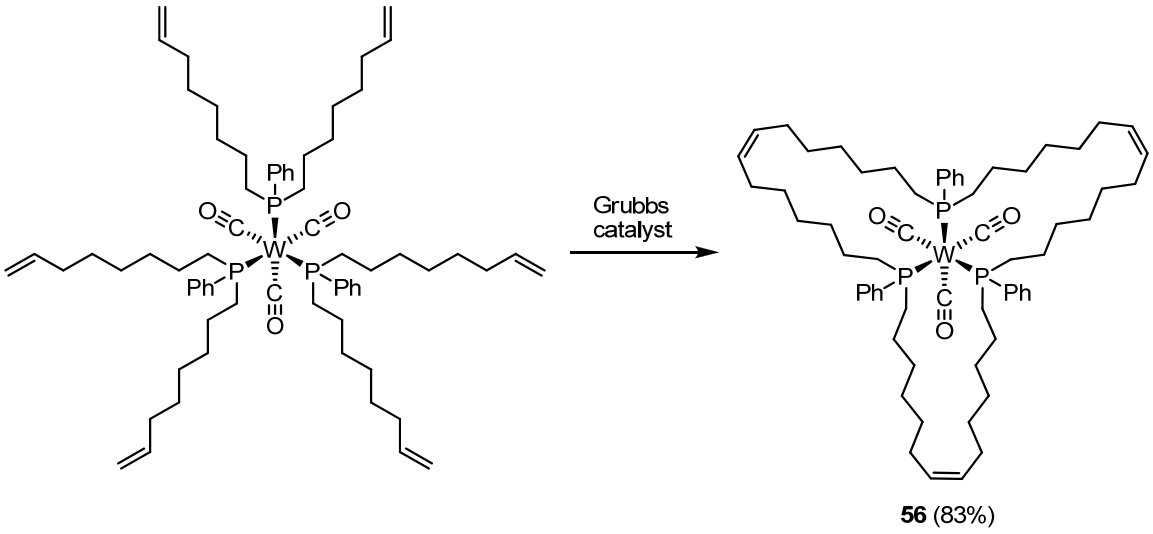

56 (83%)

Although they are not technically within the scope of this review, P3 and P6 macrocycles with silicon backbones have been made by a template synthesis (Scheme 23).[84] The 9-membered P3 macrocycle **57** was synthesized by coordinating *n*-hexylphosphine on a *fac*-$Mo(CO)_3$ template, followed by treatment with *n*-BuLi, then $Me_2Si_2Cl_2$, and then a second treatment with *n*-BuLi. Similarly, a 12-membered P6

macrocycles **59a,b** were synthesized by reacting the cyclic P3Si3 ligand **54** with copper triflate or silver triflate.

Scheme 23. Template syntheses of silane-based phosphorus macrocycles.

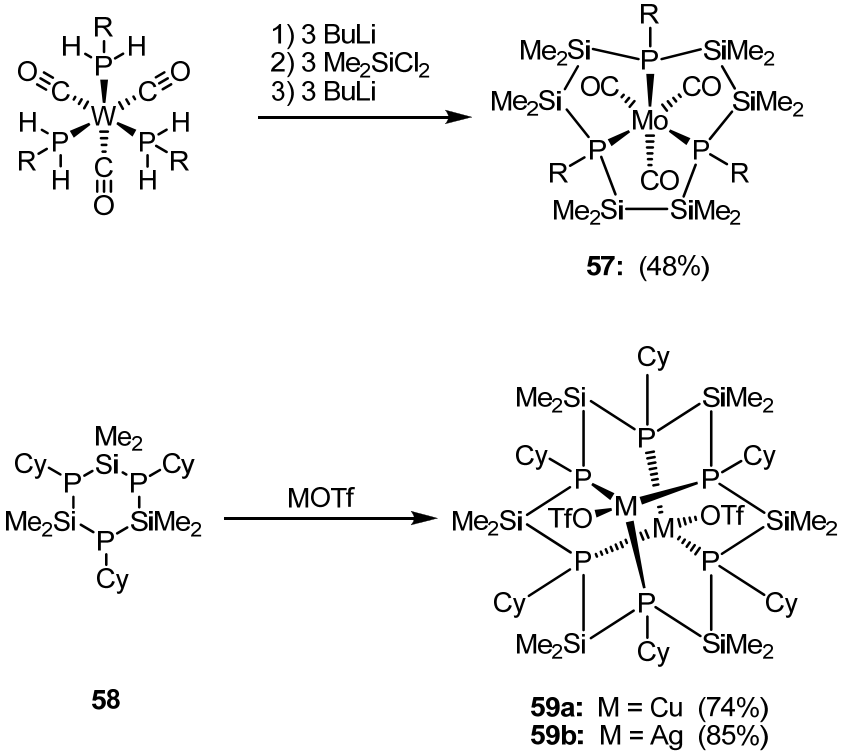

1.2.2.2. Tetraphosphine Macrocycles

In 1977, only two years after the first phosphine macrocycles were synthesized by cycloaddition, DelDonno and Rosen synthesized a macrocyclic tetraphosphine ligand around a square-planar nickel(II) template (Scheme 24).[85,86] They coordinated an open-chain tetraphosphine ligand around Ni(II) and closed the macrocycle with dibromo-*o*-xylene under basic conditions, forming **60** in 52% yield. This macrocyclization did not work with 1,3-dibromopropane, even though methyl iodide was found to alkylate the complex. The failure to react with 1,3-dibromopropane may be

because 1,3-dibromopropane has the potential to undergo elimination under basic conditions and may escape as allyl bromide (b.p. 71°C) over the course of the reaction.

Scheme 24. DelDonno and Rosen's templated macrocyclization.

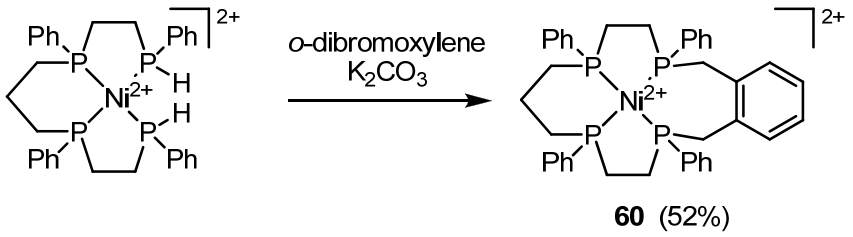

60 (52%)

A similar macrocyclization was performed by the Stelzer group, who reacted two equivalents of dichloro-*o*-xylene with $[Pd(MMPE)_2]Cl_2$ to give the 16-membered P4 macrocycle **61** in 97% yield (Scheme 25).[87] In contrast to the synthesis of **60**, which took 48 h to reach completion, formation of **61** was complete after reacting for 1 hour at room temperature.[i] The structure of the macrocycle was confirmed by x-ray crystallography. The $[Pd(MMPE)_2]^{2+}$ template was cyclized with *cis*-2-butene and isobutene linkers to form macrocyclic complexes **62** and **63**.[16] Under the same reaction conditions, saturated linkers (1,3-dichloropropane and 1,4-dichlorobutane) did not react. Instead, the saturated macrocycle **63** was obtained by reduction of **61** with H_2 and Raney nickel.

[i] This synthesis is deceptively appealing due to the small number of steps; however, the starting ligand MMPE is not a commercially-available reagent and requires four synthetic steps from commercially-available starting materials, as well as an air-free fractional vacuum distillation to purify the final ligand.

Scheme 25. Palladium-templated tetraphosphine macrocycle syntheses.

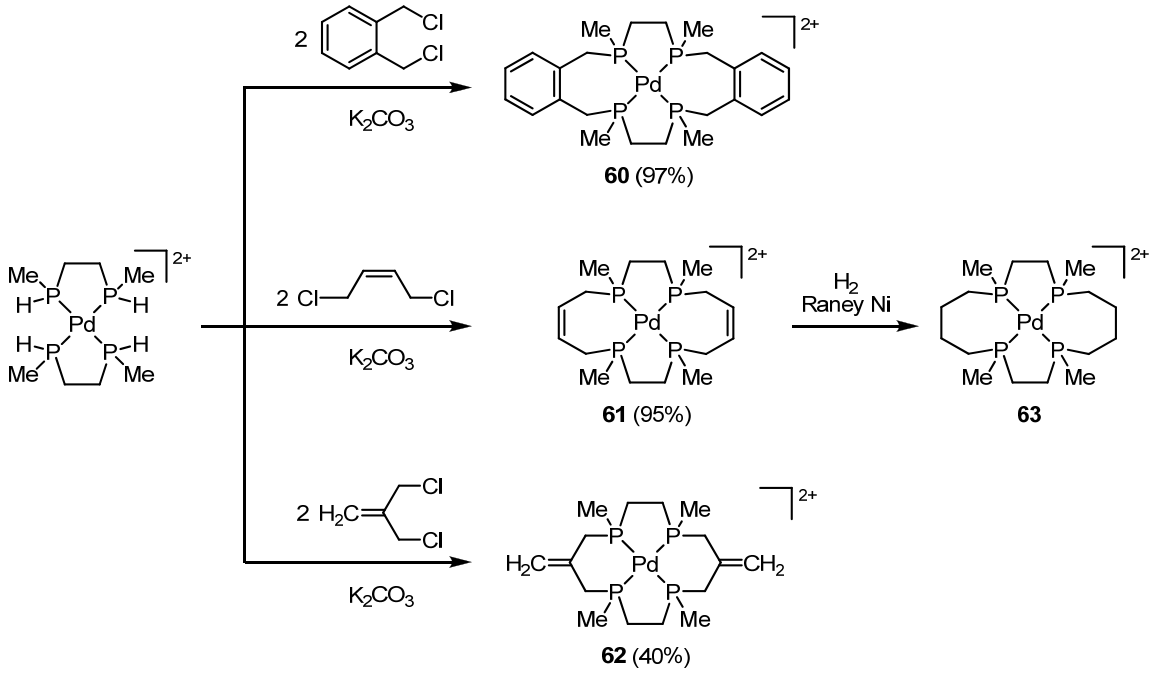

Complexes **61-63** were characterized by NMR spectroscopy and FAB mass spectrometry; however, it should be noted that neither of these techniques can conclusively confirm the macrocyclic ligand structure in these complexes. For templated 2:2 macrocyclizations, two possible ring-closing reactions are possible: linking *between* the phosphines to form the macrocycle or linking *aross* each phosphine to form two small-ring double-chelate ligands (Scheme 26). Both of these products have the same molecular weight, and there are is no spectroscopic method that can definitively tell one of these possibilities from the other.

Scheme 26. Possible products from 2:2 cyclizations of templated phosphines.

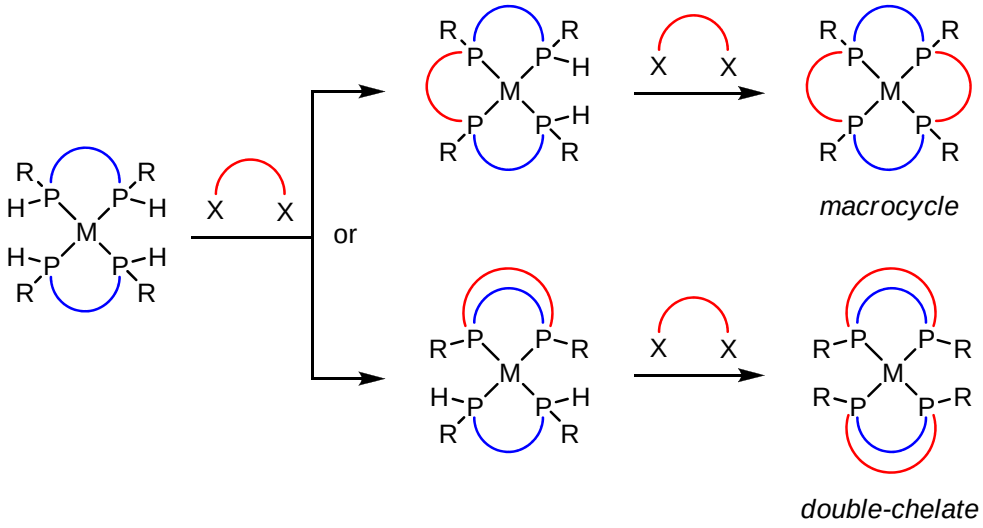

Mizuta et al. formed macrocyclic complexes **6a,b** by reacting 1,3-dibromopropane with $[Pd(MMPE)_2]^{2+}$ and $[Pt(MMPE)_2]^{2+}$ (Scheme 27). The macrocycles were characterized by x-ray diffraction and by ^{31}P NMR spectroscopy, where they displayed sharp singlets indicating highly symmetric macrocycles. However, the reactions took 4 days, yields were very low (10%), and preparative-scale GPC was required in order to separate these complexes from their by-products.[88] The uncharacterized by-products, whose ^{31}P NMR spectra showed multiple unresolved peaks, were speculated to be ill-formed oligomers, but it is also possible they may have been less-symmetric stereoisomers of the macrocycles.

Scheme 27. Mizuta's Pd and Pt-templated P4 macrocycles.

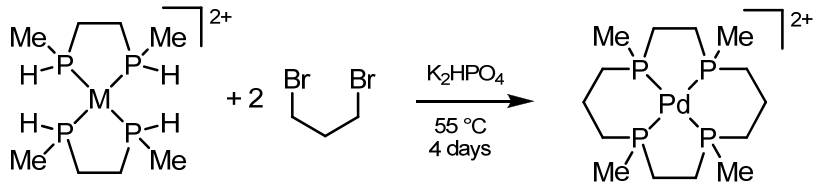

65a: M = Pd (10%)
65b: M = Pt (10%)

The Stelzer group synthesized hydroxyl-functionalized macrocycles by reacting $[M(MMPE)_2]^{2+}$ (M = Ni or Pd) templates with α,ω-dicarbonyl linkers to form 14-membered P4 macrocycles **66** and **67** with hydroxyl groups attached to the backbone (Scheme 28).[89,90] Both acetylacetone and malonaldehyde (added as the bis(dimethyl) acetal) gave macrocycles in high yield. These macrocycles contain hydroxyl groups on C1 and C3 of the three-carbon bridge. Macrocycles with vicinal hydroxyl groups on the two-carbon bridge were also synthesized, using $[Pd(MMPP)_2]^{2+}$ as a template and either 2,3-butanedione or benzyl as linking agents. The structures of the macrocyclic complexes were confirmed by X-ray crystallography.

Scheme 28. 14-membered hydroxyl-functionalized macrocycles.

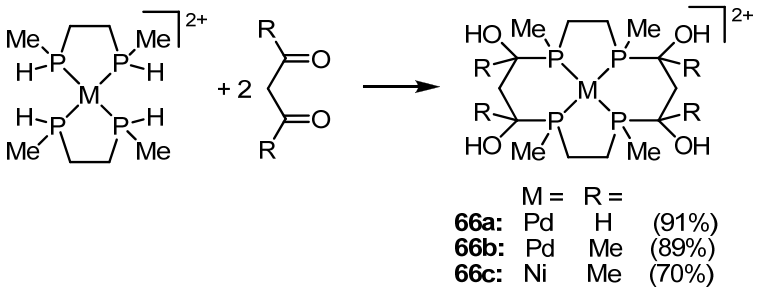

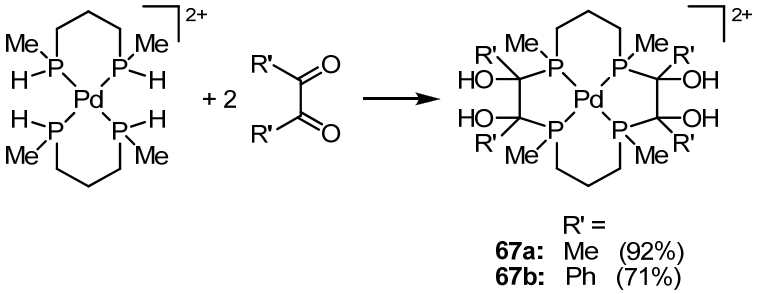

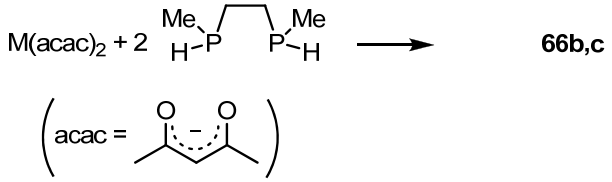

Whereas alkyl dihalide linkers require basic conditions to undergo cyclization, these reactions occurred under neutral or even acidic conditions. The presence of the four hydroxyl groups makes these ligands some of the few examples of hydrophilic phosphine macrocycles (although only complex **66c** was reported to be water-soluble). However, one disadvantage of the hydroxyl groups is that the carbons attached to them are chiral. This creates four chiral carbons in addition to the four chiral phosphorus atoms, and because the synthesis of these macrocycles was not stereochemically controlled, many stereoisomers formed upon macrocyclization.

The nickel templates reacted more slowly than the palladium templates (requiring three days to reach completion instead of 12 hours). H/D exchange experiments showed that the P-H bonds on the Ni templates are less acidic than those on the Pd templates. This suggests that the mechanism for alkylation of coordinated phosphines begins by deprotonation of the phosphine, followed by attack of the coordinated phosphido ligand on a carbon electrophile. The metal template not only controls the stoichiometry of the reactants, but also activates the secondary phosphines toward reaction with the electrophilic carbonyl groups.

Macrocycles **66b** and **66c** was also synthesized by reacting free MMPE with $M(acac)_2$ complexes, followed by protonation with dilute HCl. This reaction combines formation of the template and macrocyclization in a single step, by introducing the linker reagent as a weak ligand coordinated to the metal, which is displaced by the phosphine to form the template and whichthen reacts with the template to form the macrocycle.

Twelve-membered and 16-membered macrocycles were inaccessible by this route. This finding suggests that a 14-membered macrocycle may be the ideal ring size to fit around a square-planar transition metal. Although macrocycle size has not yet been systematically studied for phosphine macrocycles, 14-membered macrocyclic amines form more stable Ni(II) complexes than 12- or 16-membered macrocycles,[11] which may also hold true for phosphine macrocycles.

The Stelzer group used a 1:1 templated synthesis to make a series of 14-, 15-, and 16-membered macrocyclic complexes, **67a-k**, by coordination of one α,ω-acetal-functionalized bisphosphine around a square-planar template then binding this complex to a secondary bisphosphine (MMPE or MMPP) (Scheme 29).[91] Subsequent deprotection

of the acetal with H^+ generates the carbonyl groups *in situ*, which react with the secondary phosphine to form the macrocycle in high yields. This reaction can be considered a 1:1 macrocyclization. Reaction times averaged 70 hours, and depended on the metal template (Pd and Pt reacted faster than Ni), as well as the nature of the carbonyl group (aldehydes reacted faster than ketones).

Scheme 29. Templated syntheses of 14, 15, and 16-membered P4 macrocycles.

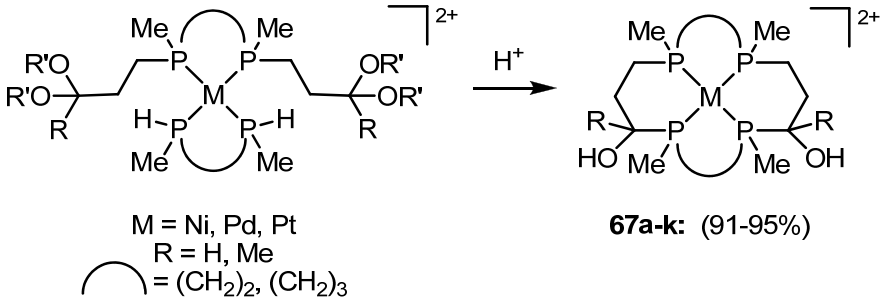

Each of the routes outlined in Schemes 23-27 involve the linking of two bidentate phosphine ligands to form a macrocycle. In 1992, Stelzer et al. synthesized a series of 14-membered macrocyclic complexes **68a-e** containing adjacent 5 and 6-membered rings by the templated linkage of a tridentate phosphine with divinyl-functionalized monodentate phosphorus ligands (Scheme 30).[92,93] The reactions occurred within 48 h in refluxing dichloromethane, and resulted in >90% yields for all but one of the macrocycles. Two of these macrocycles, which contain secondary phosphine groups, were further functionalized by hydrophosphination with methyl acrylate.

Scheme 30. Synthesis of macrocycles with adjacent 5 and 6-membered chelate rings.

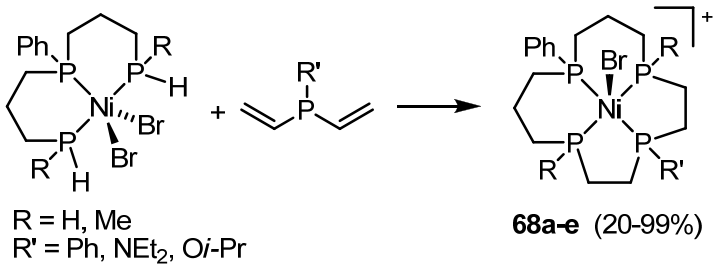

Most template syntheses of tetraphosphine macrocycles occur around d^8 metals such as Ni(II) or Pd(II) because of the preferred square-planar ML_4 or sometimes square-pyramidal ML_4X coordination geometries.. Such geometries place the templated precursor ligand in the ideal geometry for macrocyclization, with the reactive phosphines adjacent to each other. However, this geometry is not necessarily required for a macrocyclization template. Two interesting macrocycle structures were synthesized around a copper(I) center (Scheme 31).[94] Reaction of $Cu(BPB)_2OTf$ (BPB = *o*-bisphosphinobenzene) with 1,3-dibromopropane and KO*t*-Bu, followed by demetallation with excess cyanide, gave a mixture of products that were separated by HPLC. One of the isolated fractions, when analyzed by mass spectrometry, contained a peak corresponding to macrocycles **69** and/or **70** (8% yield). The presence of two signals in the ^{31}P NMR spectrum indicated that both of these isomers were present. These macrocycles may have been generated by linking 1,3-dibromopropane between the two BPB ligands while templated to the copper center, although the authors suggested a bis(phosphetane) intermediate, which then dimerizes to give the macrocyclic products. Although neither of these macrocycles was fully characterized, they are still interesting in

that each represents a unique structure type: a doubly-bridged "reinforced" macrocycle for **69** and a "cage-type" macrocycle for **70**.

Scheme 31. Wild's Cu(I)-templated phosphine macrocycle synthesis.

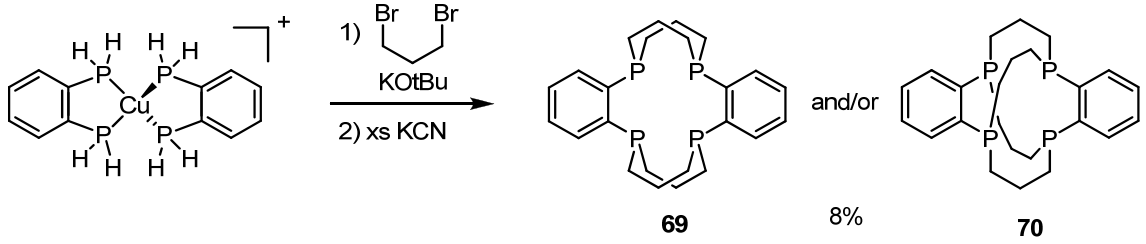

Cu(I) was used in one other case as a template in a phosphine macrocycle synthesis. Reaction of $[Cu(MPPE)_2]^+$ with 1,3-dibromopropane or *o*-dibromoxylene gave macrocyclic complexes **71** and **72** (Scheme 32).[17] The macrocyclic structures were confirmed by demetallation and characterization of the corresponding macrocyclic phosphine oxides by mass spectrometry. For more details, see Section 1.4.

Scheme 32. Cu(I)-templated phosphine macrocycles.

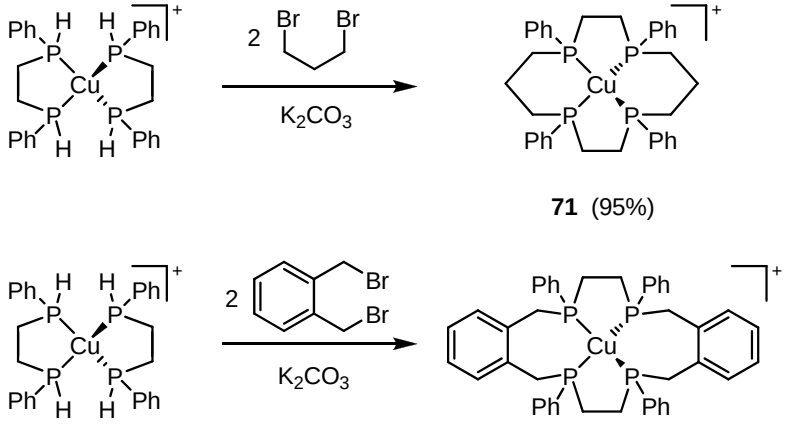

1.2.2.3. Larger Macrocycles

Although P3 and P4 macrocycles have been the primary synthetic targets in phosphine macrocycle syntheses, an impressive 36-membered P12 macrocycle was recently reported to result from a hexametallic "golden wheel" template.[95] As shown in Scheme 33, $PhP(vinyl)_2AuCl$ was reacted with benzenehexathiol to generate template **73** in good yield. Molecule **73** then underwent AIBN-initiated hydrophosphination with excess phenylphosphine to generate the macrocyclic complex **74**. This compound was characterized by ^{31}P NMR spectroscopy and ESI-MS, which was reported as a weak signal at +3062 amu. However, the actual molecular mass of **74** is +3078 amu, and there is no reasonable 16 amu fragment that can be lost from this compound. The macrocyclic structure of **74** should therefore be regarded with care.

Scheme 33. Template synthesis of a 36-membered P12 macrocycle.

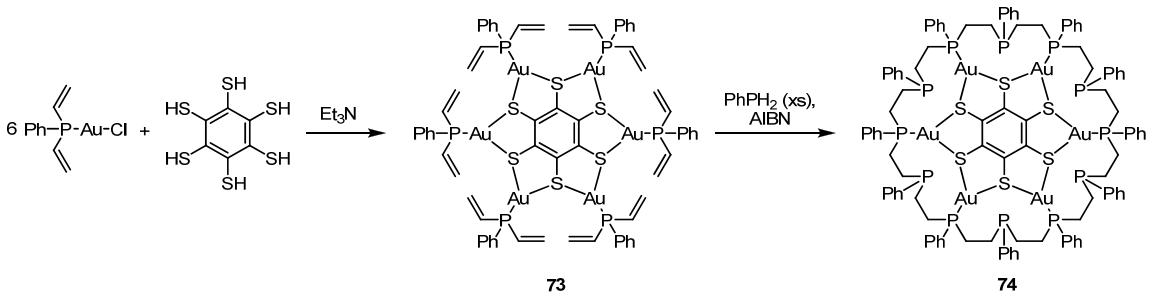

1.3. Coordination Chemistry of Macrocyclic Phosphine Ligands

1.3.1. Triphosphine Macrocycles

Most triphosphine macrocycles synthesized to date are 9- to 12-membered, which is too small to fully encircle a transition metal ion. Because of their small size, these ligands act exclusively as facially-coordinating tridentate ligands. For example,

macrocycle **8** was coordinated to $Mo(CO)_3$ and Rh(norbornadiene) to form complexes **75** and **76** (Figure 5).[32]

Figure 5. Facially-coordinating triphosphine macrocycles.

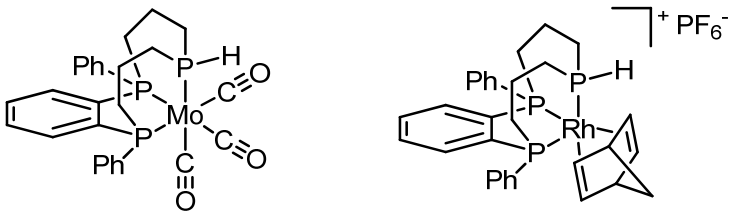

75 **76**

Helm's nine-membered P3 macrocycles **30a,b** coordinate facially to $Mo(CO)_3$ to form complex **77** (Scheme 34).[56] The *syn-anti* isomer **30b** is the major isomer of this ligand, which is not geometrically situated to coordinate facially. Surprisingly, though, both the *syn-syn* and *syn-anti* isomers reacted to form **77**, suggesting that isomer **30b** isomerizes to **30a** upon coordination.

Scheme 34. Coordination of Helm's 9-membered P3 macrocycle.

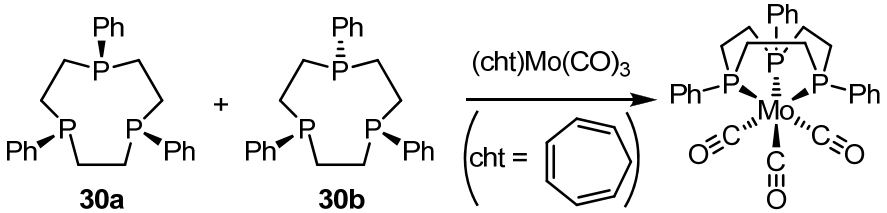

30a **30b** **77** (68%)

Mizuta's ferrocene-bridged P3 macrocycle **33** was coordinated to AgOTf to form complex **78** (Scheme 35) and its crystal structure was obtained. In addition to the

tridentate ligand, the triflate counterion is also coordinated. Like **34**, both the all-*syn* and *syn-anti* isomers of **33** reacted with Ag^+ to give the same product, suggesting that **33b** (the *syn-anti* isomer) undergoes inversion to form **78**.

Scheme 35. Coordination chemistry of the ferrocene-bridged P3 macrocycle.

33a,b **78**

In addition to their template syntheses on Cr, Mo, W, and Fe templates, 12-membered P3 macrocycles have been coordinated to a variety of early transition metal halides ($TiCl_3$, VCl_3, $NbCl_3$ and $NbCl_4$) (Figure 6),[96] although the Nb complexes were unstable at room temperature. The geometry of the $TiCl_3P_3$ and VCl_3P_3 complexes **79a-c** were confirmed by X-ray crystallography. The complexes in Figure 6 are excellent (if only qualitative) examples of the macrocyclic effect, as such complexes are usually only stable at low temperature and dissociate a phosphine ligand to form MCl_3P_2 complexes. Also, exposure of a solution of **79b** to air preferentially oxidized the vanadium instead of the phosphine ligand, forming **80a**. This is the first example of an octahedral vanadyl-phosphine complex.

Figure 6. Complexes of 12-membered P3 macrocycles.

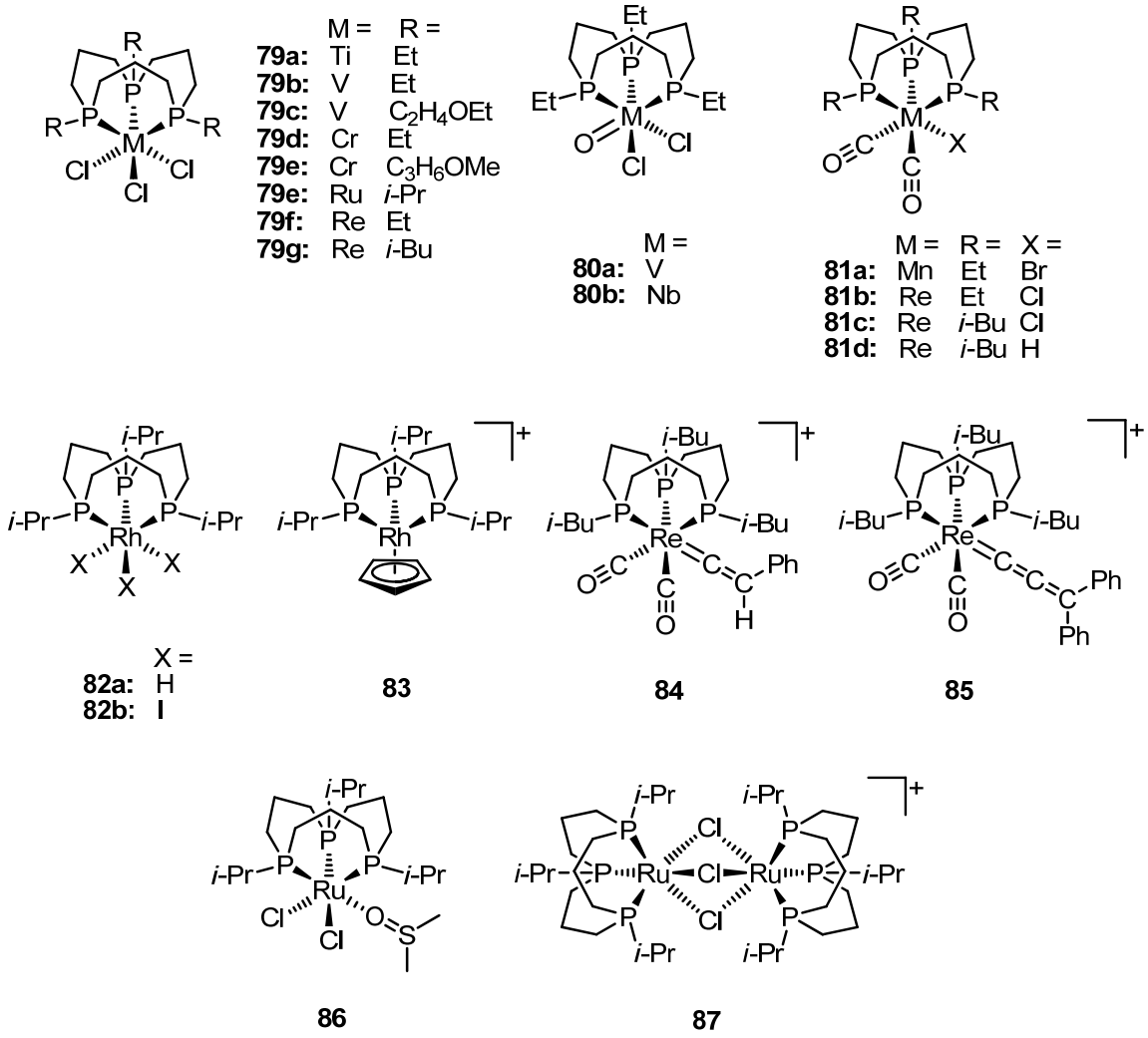

$CrCl_3$ complexes **79d** and **79e** were also synthesized; however, they were formed by oxidation of the Cr^0 complexes **40b** and **41d** with Cl_2. Strangely, attempts to abstract the halides and induce coordination of the ether arms of **79e** were unsuccessful.

Macrocyclic P3 complexes of Ru(II), Rh(I), Mn(I), Re(III), and Re(I) have also been synthesized.[97] In the case of the Re(I) complex **81c**, the chloro ligand could be replaced by hydride, vinylidene, or cumulene ligands. Mn(I), Re(I), and Ru(II)

complexes **81a-c** and **86** were found to be catalysts for ring opening metathesis polymerization (ROMP) when treated with $EtAlCl_2$, with **81b** being especially active.

1.3.2. Tetraphosphine Macrocycles

As reviewed in Section 1.2, tetraphosphine macrocycles of various sizes have been synthesized by either cyclocondensation reactions or template syntheses. The macrocycles that are formed around metal templates are difficult or even impossible to remove from the metal (see Section 1.4) so the coordination chemistry of tetraphosphine macrocycles has not been thoroughly studied.

Macrocycle **19** was coordinated to various Mn(II) salts, forming octahedral complexes **88a-d** (Scheme 36).[43] These complexes contain alternating five and seven-membered chelate rings, with *cis*-alkene groups in the seven-membered rings. It is assumed that these complexes exhibit *trans*-octahedral geometries, although no data are reported to confirm this. These complexes are more air-stable than most MnX_2P_4 complexes because of the macrocyclic effect.

Scheme 36. Manganese complexes of macrocycle **19**.

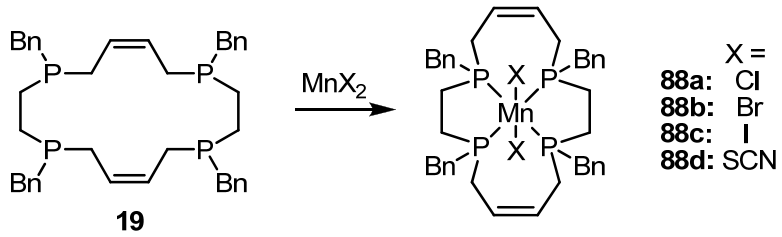

Ciampolini's 18-membered crown ether type mixed-donor macrocycles **9-11** showed interesting coordination chemistry with cobalt and nickel; the complexes acted as tetradentate, pentadentate, or hexadentate ligands depending on the metal, the identity of

the non-phosphorus donors, and the presence of auxiliary ligands such as chloride or solvent (Figure 7).[33-36,98] Tetradentate and pentadentate Co(II) complexes of **9** were characterized (**89a** and **89b**, respectively), as well as two different hexadentate complexes **89c**,**d**. These examples illustrate that the coordination behavior can vary widely between different stereoisomers of macrocyclic phosphine ligands. As expected, P4O2 macrocycles **9** and **11** acted as tetradentate ligands to Ni(II), forming square-planar complex **90**. The P4S2 ligand **10** bonded to Ni(II) as a hexacoordinate ligand, forming a highly distorted octahedral complex **91** with the phosphorus donors in the equatorial positions and the sulfur donors in the axial positions. The Ni-S bonds are quite long (2.94 Å), indicating a weak interaction.

Figure 7. Coordination complexes of P4X2 macrocycles **9**-**11**.

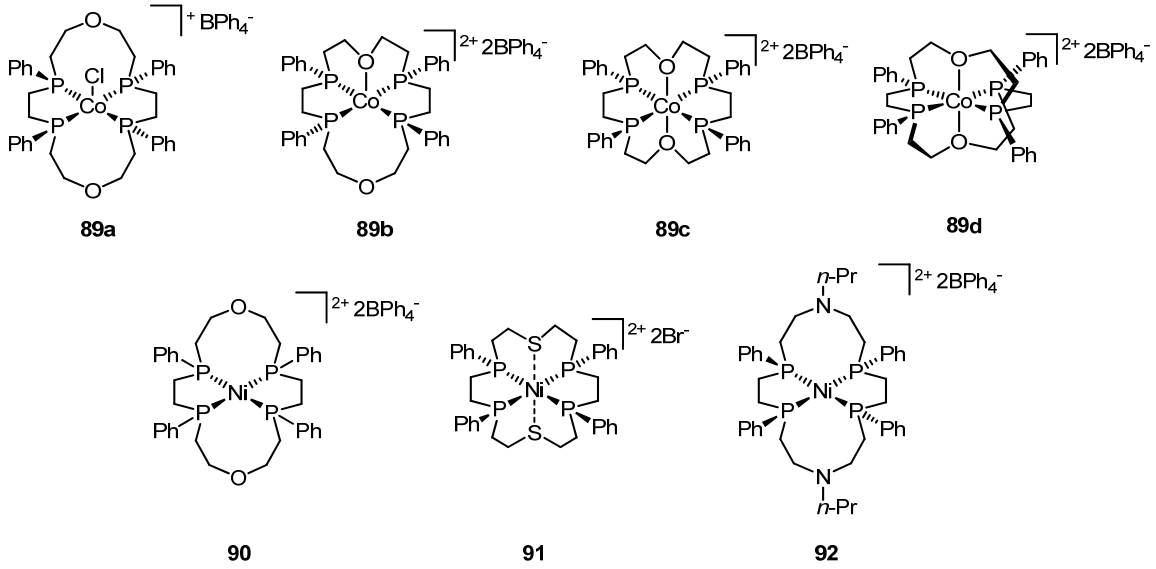

Even when the macrocycle contains only phosphorus donors, the stereochemistry of the ligand can influence the coordination behavior of the metal center. Two isomers of Stelzer's α-hydroxyl-functionalized macrocyclic Pd complex **66b** were isolated, and their

crystal structures obtained (Figure 8).[89,90] Interestingly, isomer **A** (*R,S,S,R*) crystallized as a square planar $[PdP_4]^{2+}$ complex, while isomer **B** (*R,S,R,S*) crystallized as a square-pyramidal $[PdP_4Cl]^{+}$ complex, with the axial chloro ligand *syn* to the methyl groups. The Pd-Cl bond is especially long (2.831 Å vs. normal bond distances of 2.2-2.4 Å), and dissociates in solution. The authors speculated that the all-*syn* configurations of the methyl substituents (arising from *R,S,R,S* stereochemistries of the phosphines) force the Pd ion slightly out of the macrocyclic plane, allowing access to a fifth coordination site.

Figure 8. Solid-state structures of macrocyclic PdP4 complexes.

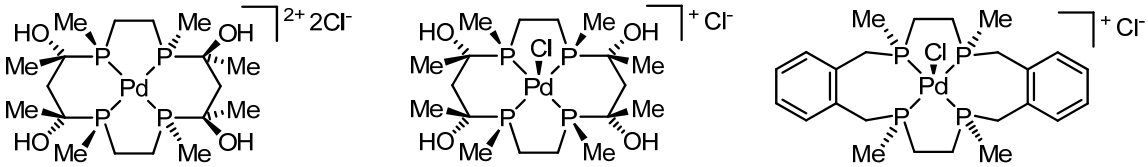

The 16-membered *o*-xylene-bridged Pd-P4 macrocycle **60** also crystallized as a square-pyramidal $[PdP_4Cl]^{+}$ complex.[87] Again, the macrocyclic phosphine was the (*R,S,R,S*) isomer, with all methyl groups *syn* to each other. However, in this case the chloride ligand coordinated on the *opposite* side of the methyl groups. This suggests that the explanation for the 5-coordinate geometry of complex **66b** does not extend to other systems.

Because no thermodynamic studies of macrocyclic phosphine complexes have been conducted, the ideal ring size for a macrocyclic P4 ligand is not known. In lieu of thermodynamic data, examination of crystal structures may yield some clues to which ring size will be the best fit. In both isomers of **66b**, the bite angles of the five-

membered chelate rings are slightly less than 90° (86.2-87.6°), while the bite angles of the 6-membered rings are slightly more than 90° (92.8-93.2°). This suggests that a P4 macrocycle with only five-membered chelate rings (a 12-membered ring) would not be large enough to fit around a transition metal ion. Instead, a combination of five and six-membered rings (or perhaps all six-membered rings) should be more ideal for a tetraphosphorus macrocycle. Alternating five- and six-membered chelate rings, formed from phosphines with two- and three-carbon spacers, approximately supplement each other, allowing a planar arrangement of the four phosphorus atoms around the metal center. Complex **60** has a 16-membered macrocycle, with alternating five-membered and seven-membered chelate rings. The five-membered bite angles are about 85°, whereas the seven-membered rings' bite angles are around 95° (thus supplementing each other). However, seven-membered metallacycles are usually less stable than six-membered ones, as will be discussed in Section 1.4.

The 10-membered tetraphosphole macrocycle **22a** is too small to fully encircle a transition metal ion.[46] Instead, it coordinates to $Mo(CO)_4$ as a bidentate ligand, yielding compound **93** (Scheme 37). The ligand is twisted into a boat-type configuration, with alternating phosphole groups chelating to a single Mo center. The ligand can coordinate to a second Mo center through the other two phosphole groups, generating the bimetallic complex **94**. The structures of both of these complexes were confirmed by X-ray crystallography.

Scheme 37. Coordination chemistry of the 10-membered phosphole macrocycle **22a**.

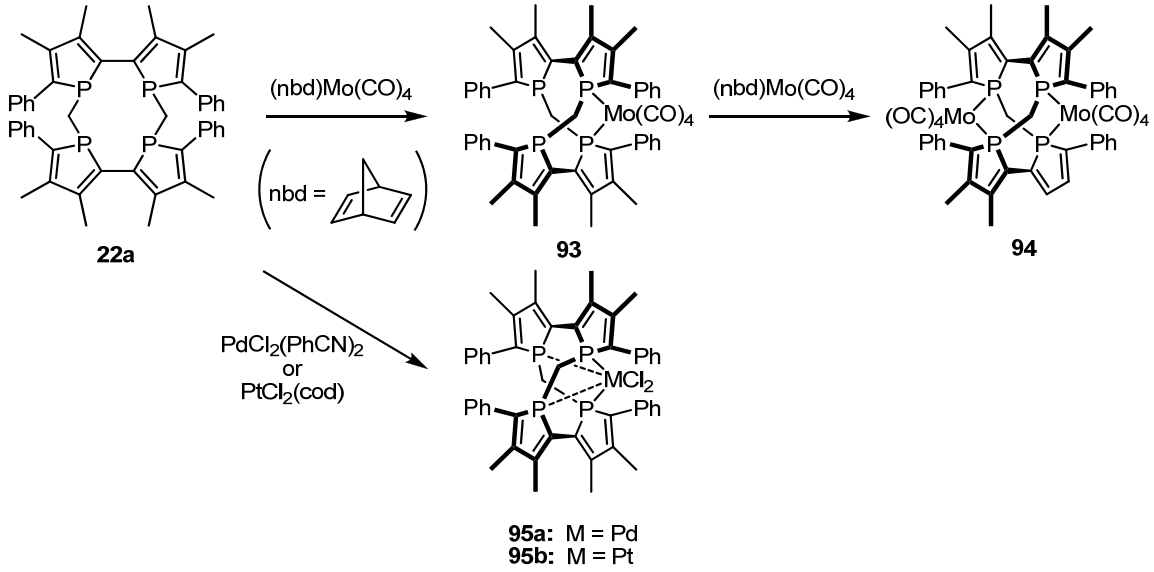

Pd(II) and Pt(II) complexes of ligand **22a** were also synthesized (compounds **95a,b**).[99] As with the Mo complexes, alternating phosphole groups are coordinated to the metal center. X-ray crystallography confirmed the chelation of the metal by alternating phosphole groups, and also suggested some degree of interaction between the metal and the non-coordinating phospholes.

A mixture of macrocycle **22a** and $Pd(OAc)_2$ was tested for catalytic activity in the Stille and Heck couplings, where it showed comparable catalytic activity to $Pd(OAc)_2$ + tri(2-furyl)phosphine, but with much longer catalytic lifetimes. In addition, the system did not precipitate Pd^0 over time, and remained active when additional reactants were introduced. The extended lifetime of the catalyst is presumably caused by increased stability of the macrocyclic complex. However, because the macrocycle does not actually surround the metal and only acts as a bidentate ligand, this should not be regarded as a true "macrocyclic effect", but more accurately as a reinforced chelate

effect. This is the only reported application of a macrocyclic tetraphosphine complex, *ironically as a bidentate ligand!*

Phosphinine macrocycles **23-27** were synthesized with the expectation that they would stabilize low oxidation states of metals, because phosphinines are good π-acceptor ligands, similar to CO.[100] W, Ir, and Rh complexes **96, 97a**, and **97b** (Figure 9) were prepared in high yield and characterized crystallographically.[48] In addition, a rare Au(I) macrocyclic complex (**98**) was synthesized and its redox properties studied.[101] The metal was reduced electrochemically or with sodium naphthalenide. The resulting Au(0) complex was unstable above -20 °C, whereupon it decomposed to free ligand and colloidal gold. Still, this is a rare example of a monomeric Au(0) complex, and it is more stable than Au(0) carbonyl complexes, which are only stable below 77 K.[102]

Figure 9. Phosphinine macrocycle complexes.

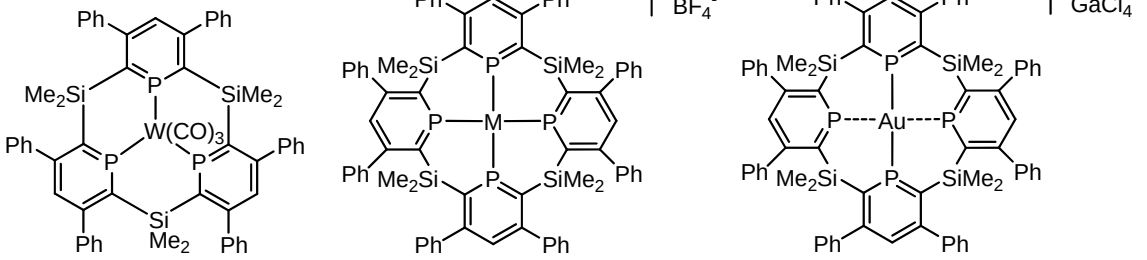

96 **97a:** M = Rh **97b:** M = Ir **98**

1.4. Demetallation of Macrocyclic Phosphine Complexes

As described above, template syntheses can allow for high-yield macrocyclization steps by coordinating the phosphine precursors around the transition metal, followed by linking these phosphines to form the macrocyclic ligand which is already coordinated to

the metal. In order to extend the coordination chemistry of macrocyclic phosphine ligands, it would be useful to be able to replace the template metal with different transition metal ions. This is the major drawback of template syntheses: because of the macrocyclic effect, macrocyclic phosphines are more difficult to remove from their complexes than other ligands. Indeed, it is often difficult or impossible to demetallate macrocyclic phosphine complexes.

1.4.1. Triphosphine Macrocycles

As discussed in Section 1.3.1, triphosphine macrocycles do not surround a metal but instead act as facially-coordinating ligands. Because the metal is not surrounded by the ligand, stepwise removal of each donor atom should be easier for tridentate macrocycles than for tetradentate macrocycles. Indeed, many P3 macrocycles can be removed from their complexes, although harsh conditions are often necessary.

Norman's *fac*-$Mo(CO)P_3$ complexes **39a-d** did not demetallate, even upon treatment with cyanide.[70,71] Follow-up studies by the Edwards group showed that these complexes can, however, be converted into complexes thatallow dissociation of the phosphine. For example, the W and Mo complexes **39** and **40** undergo oxidative addition with halogens, followed by loss of CO after standing for a few days in dichloromethane (Scheme 38).[103] Treatment of **99** with NaOH in ethanol liberated the macrocyclic phosphine ligands **100a-d**, which were isolated and fully characterized.[104,105] The x-ray crystal structure of **100b** confirmed the all-*syn* stereochemistry (all lone pairs on the same side of the macrocycle), as would be expected for a facially coordinating tridentate ligand. Comparison of this crystal structure to that of its Mo complex shows that the

macrocycle contracts upon coordination and might be large enough to facially coordinate much larger metal ions.

Scheme 38. Demetallation of macrocyclic $MP_3(CO)_3$ complexes.

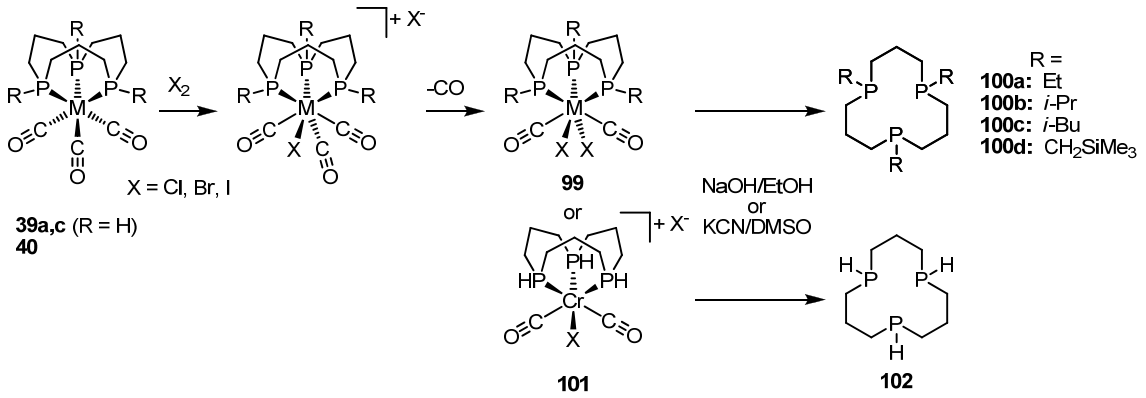

Strangely, Mo and W complexes of the secondary triphosphine macrocycle **102** did not liberate the phosphine from the metals. Instead, the analogous Cr complex **101** was prepared, which did liberate the phosphine, although the yields of this demetallation were lower (40% vs. 60-90%).

Edwards' macrocyclic piano-stool complexes were demetallated in high yield by digestion of the metal complex with Na/NH_3 to release the free macrocycles **103a,b** (Scheme 39).[80] These free ligands were then coordinated to other first-row transition metals (see Section 1.3.1). *These are the only examples where macrocyclic phosphine ligands have been synthesized around one transition metal, demetallated, then transferred to other metals.*[96] The 9-membered macrocycle on complex **104** (synthesized by alkylation of **47b** (R_1 = H, R_2 = vinyl), followed by hydrogenation of the vinyl group) was oxidatively demetallated with Br_2 or H_2O_2.[77]

Scheme 39. Demetallation of macrocyclic iron piano-stool complexes.

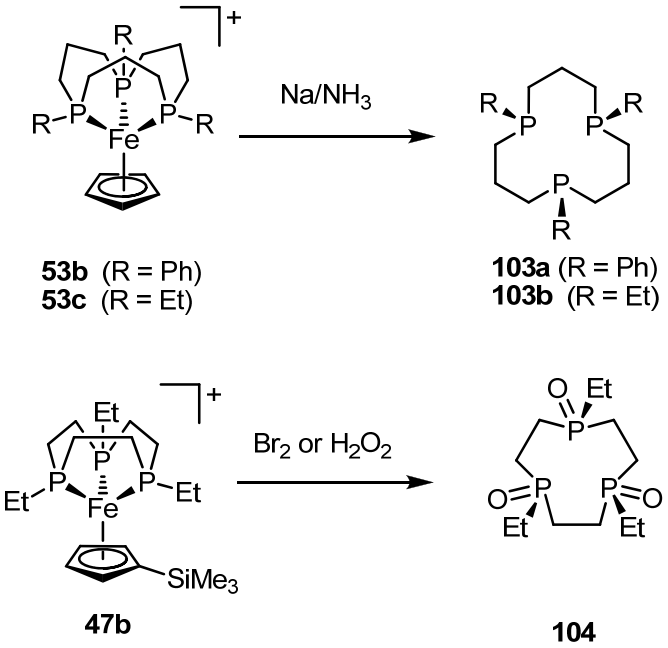

1.4.2. Tetraphosphine Macrocycles

The success of demetallations of tetraphosphine macrocycles seem to depend on the size of the chelate rings present on the ligand. Complex **60**, containing five, six, and seven-membered chelate rings, was demetallated by treatment with aqueous NaCN (Scheme 40).[86] Also, complex **61**, with alternating five and seven-membered metallacycles, was quickly demetallated by heating with excess cyanide.[87] In contrast, complexes **66** and **67**, featuring only five- and six-membered rings, could not be demetallated with cyanide. Instead, the macrocyclic complex either resisted demetallation completely or the macrocycle fell apart, releasing the precursor phosphine MMPE from the template.[90,91] Seven-membered chelate rings are less stable than five- or six-membered rings so it is likely that complexes **60** and **61** are less stable than **66** and

67, which allows them to be demetallated with cyanide. It is not known whether this result is a thermodynamic or kinetic effect.

Scheme 40. Demetallation reactions of tetraphosphine macrocycles with cyanide.

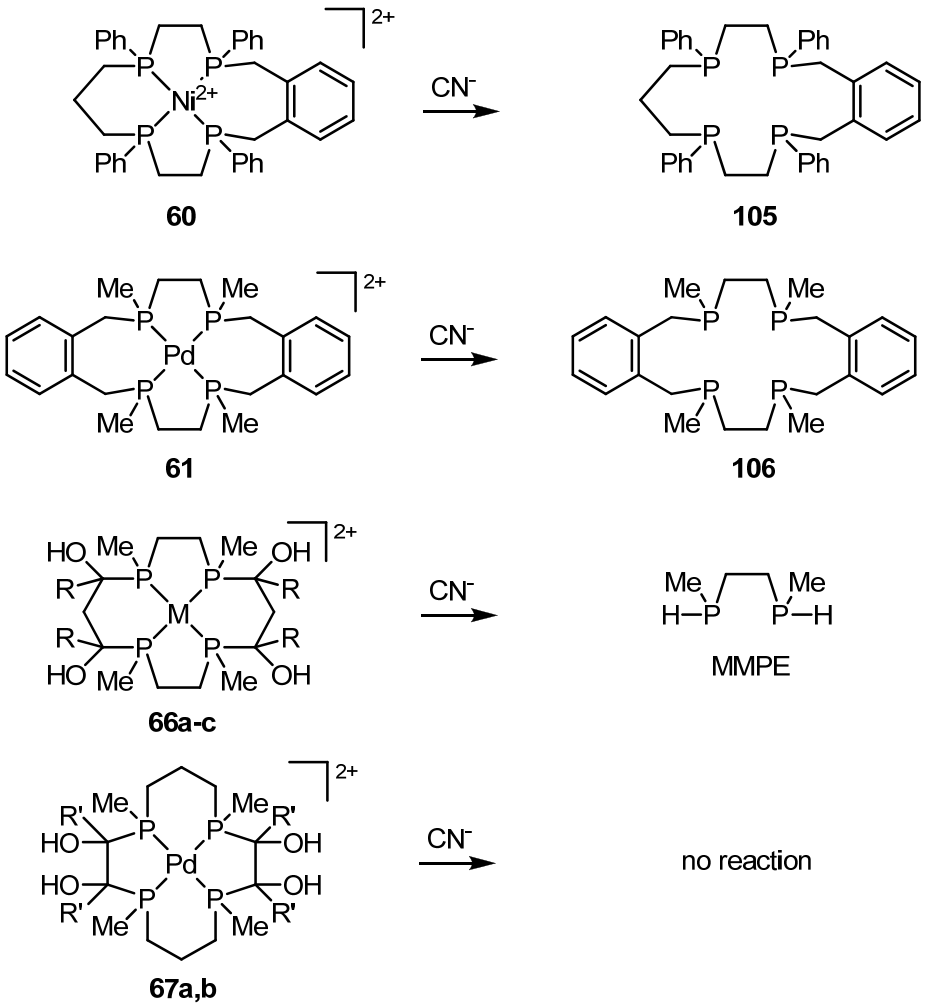

60 **105**

61 **106**

66a-c

67a,b

Although the 14-membered macrocycles above could not be demetallated, copper(I) complexes of the *reinforced* 14-membered macrocycles **69** and **70** were successfully demetallated by treatment with cyanide (Scheme 31). In fact, the macrocyclic complexes were not even isolated in this case. Complex **71**, another 14-membered

macrocyclic copper complex, was demetallated by treatment with H_2S in basified ethanol and air, which precipitated Cu_2S and oxidized the ligand to phosphine oxide **107**, which was reduced to phosphine **108** by reduction in neat phenylsilane (Scheme 41). Complex **72** was also demetallated in this manner to release macrocyclic phosphine oxide **109**.

Scheme 41. Oxidative demetallation of macrocyclic Cu(I) phosphine complexes.

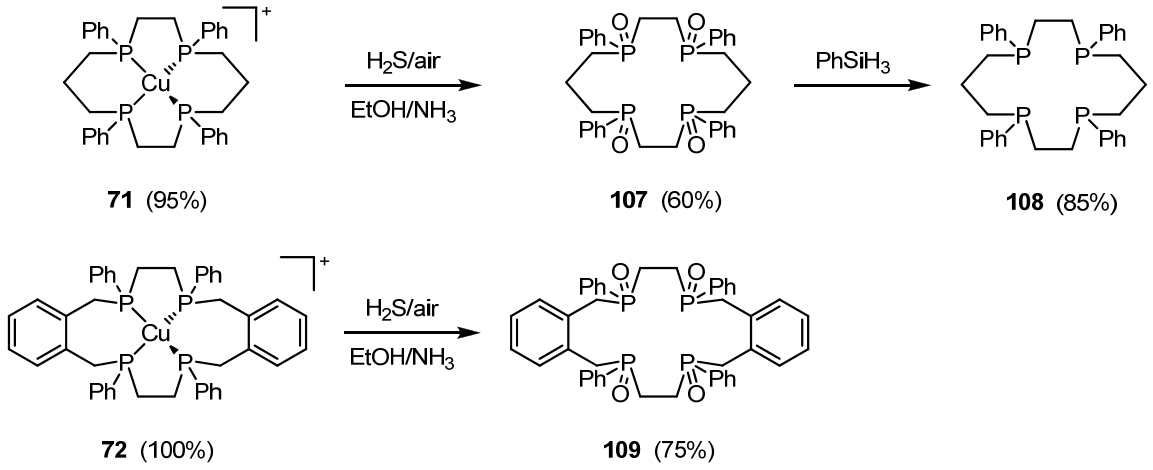

The demetallation of macrocyclic Cu(I) complexes **69-71** contrasts with the inability to successfully demetallate complexes **66** and **67**. This result may be attributable to the differences in the coordination geometries of the metals. The d^8 metals Ni(II), Pd(II), and Pt(II) favor square-planar (or sometimes square-pyramidal) geometries, with P-M-P angles of ~90°. This geometry facilitates coordination of the five- and six-membered chelate rings with minimal ring strain. In contrast, d^{10} Cu(I) favors a tetrahedral geometry, with ideal P-M-P angles of 109°. This geometry strains the chelate rings, resulting in weaker binding to the metal, and thus easier demetallation. Unfortunately, for now, this explanation is only hypothetical. Hopefully, further structural studies on macrocyclic copper-phosphine complexes will give data on bond

angles and ring strain in these complexes, and the reasons for any instabilities will become clearer.

1.5. Summary

It has been over 35 years since the first macrocyclic phosphine ligands were made. Because these ligands promise to be strongly coordinating, , many strategies have been designed for their synthesis. However, only a handful of synthetic methods have shown broad applicability in terms of the ring sizes, functional groups, and metal complexes that can be obtained. Still fewer of the resulting complexes have found use in their intended applications.

The main challenges in phosphine macrocycle synthesis are: a) selectivity of the desired ring size over smaller rings or larger oligomers, b) control over stereochemistry, and c) characterization, including confirmation that the ligand is indeed macrocyclic. Facially-coordinating triphosphorus macrocycles have seen the most success in all of these areas, as well as in their subsequent functionalization, demetallation, and/or coordination to a variety of transition metals. Tetraphosphine macrocycles, on the other hand, are still primitive in these respects. Of the handful of synthetic methods that have been developed, none has allowed for more than a few variations thus far. Only four metals: Ni(II), Pd(II), Pt(II), and Cu(I), have been coordinated to tetradentate phosphine macrocycles, and these have been formed almost exclusively by template syntheses of the macrocycles around that particular metal. Moreover, these ligands bind so strongly to the template metal that their removal from the metal is difficult or even impossible. These difficulties have hampered the development of macrocyclic tetradentate phosphine

ligands and have so far prevented their use in applications such as catalysis or radiopharmaceuticals.

1.6. Bridge

This chapter has reviewed the current status of macrocyclic phosphine ligands in the literature, including their synthesis, coordination chemistry, and demetallation of macrocyclic phosphine complexes. Chapter II will detail the synthesis of two water-soluble bidentate phosphines and investigation of their coordination chemistry with iron(II), in attempts to use these complexes as templates for the synthesis of new water-soluble, macrocyclic iron(II) phosphine complexes for the purposes of separating nitrogen (N_2) from natural gas.

This dissertation includes previously published and unpublished co-authored material. Chapter 2 contains experimental work performed by Ian J. Doxsee, and crystal structures solved by Lev N. Zakharov. Parts of Chapter 3 have been previously published in Swor, C. D.; Zakharov, L. N.; Tyler, D. R. *J. Org. Chem*. **2010**, *75*, 6977-6979. Parts of Chapter 4 have been prepared for Swor, C. D.; Hanson, K. R.; Zakharov, L. N.; Tyler, D. R. *Inorg. Chem*. **2011**, *manuscript submitted.* In addition, some experimental work in Chapter 5 was performed by Andrew Hughett, and crystal structures were solved by Lev N. Zakharov.

CHAPTER II

SYNTHESIS OF WATER SOLUBLE SECONDARY PHOSPHINE LIGANDS AND THEIR IRON(II) COMPLEXES

Some of the experimental work presented in this chapter was performed by Ian J. Doxsee. Crystal structure determinations were performed by Lev N. Zakharov.

2.1. Introduction

Natural gas currently supplies one quarter of the energy used in the United States.[1] In addition, natural gas is currently the primary source for H_2, a major commodity chemical and proposed fuel of the future. The United States produces most of its natural gas domestically; however, approximately 15% of domestic natural gas resources are contaminated with high levels of dinitrogen (N_2).[2-4] Since N_2 is a nonflammable gas, its presence in natural gas lowers the energy content per unit volume, limiting the gas's use as a fuel. The maximum N_2 content for pipeline-quality natural gas is 4%, but high-nitrogen natural gas deposits can be up to 86% N_2.[5] Unlike other impurities such as water, carbon dioxide, and hydrogen sulfide, N_2 is difficult to separate

from natural gas because of its chemical inertness and similar physical properties to methane, the major component of natural gas.

The most commonly used method of removing nitrogen from natural gas is cryogenic distillation, which separates N_2 from methane (CH_4) based on their different boiling points (77 K vs. 112 K, respectively).[6] However, this method is very energy-intensive, and is only economical for very large natural gas deposits. Pressure-swing-adsorption technologies have also been developed, using materials that selectively absorb one gas over the other. Common materials for pressure-swing adsorption are activated carbon and molecular sieves. Recent innovations include Nitrosep^{TM}, which uses polymeric membranes,[7] and "Molecular Gate" technology, which uses highly-selective titanium silicate molecular sieves which can separate N_2 from CH_4 based on the small difference in size between the two molecules (3.6 Å vs. 3.8 Å, respectively).[8]

Another approach to separating nitrogen from methane involves nitrogen's ability to bind as a ligand to transition metal complexes. Our lab has synthesized water-soluble iron(II) phosphine complexes which are capable of reversibly binding N_2 via pressure-swing absorption (Scheme 1), and can reduce N_2 to NH_3 at ambient temperature and pressure.[9,10] Currently, these complexes employ water-soluble bidentate phosphine ligands such as 1,2-bis(di(methoxypropyl)phosphino)ethane (DMeOPrPE). Water is chosen as the solvent not only because of its benign nature, but also because of the low inherent solubility of either N_2 or CH_4 in water. Unfortunately, the nitrogen-binding complexes degrade in water (Scheme 2).[11] For example, when $Fe(DMeOPrPE)_2Cl_2$ (**1**) is dissolved in water, a water molecule substitutes for one of the chloro ligands, followed by dissociation of the phosphine ligands and the ultimate formation of the inert

homoleptic complex $[Fe(DMeOPrPE)_3]^{2+}$ (**2**).

Scheme 1. Pressure-swing absorption using water-soluble iron complexes.

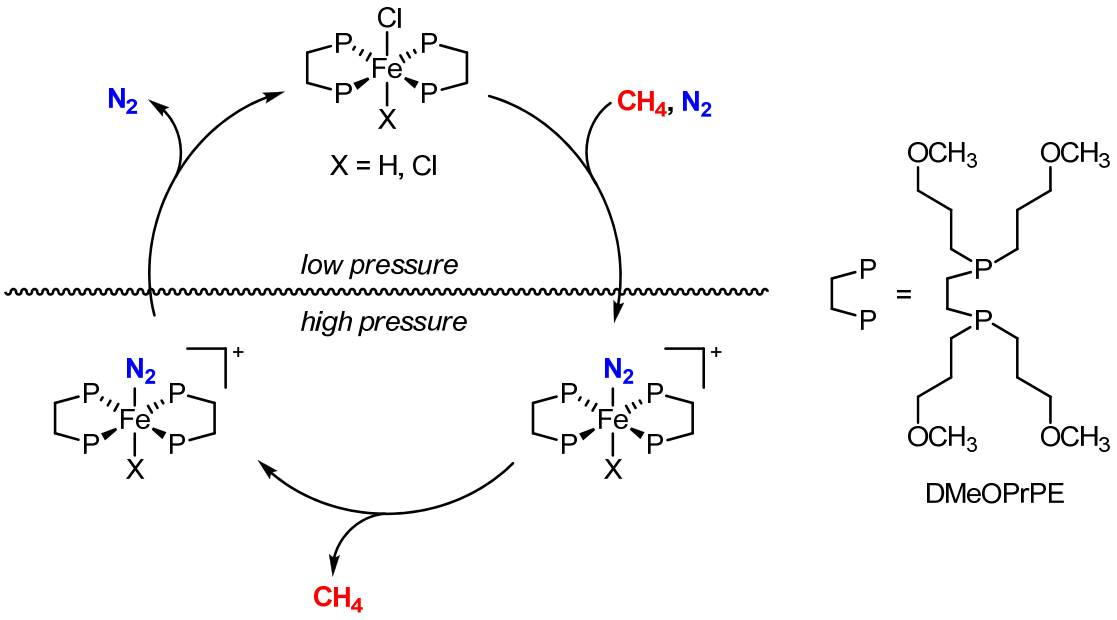

Scheme 2. Decomposition of $Fe(DMeOPrPE)_2Cl_2$ in aqueous solution.

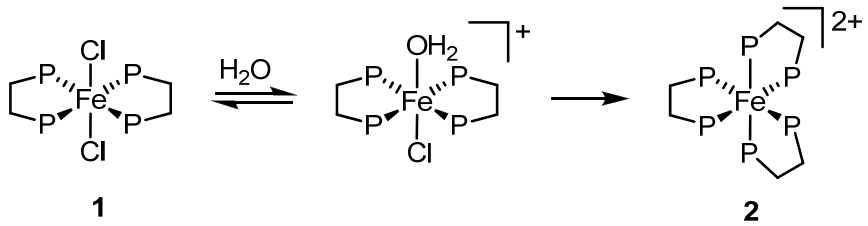

In order to inhibit this degradation pathway, we are attempting to synthesize a macrocyclic version of DMeOPrPE, which will bind to the iron atom more strongly and cannot decompose into the homoleptic complex **2**. Macrocyclic phosphine ligands have long been sought as a means to stabilize useful complexes for applications in catalysis,[12-15] radiopharmaceuticals[16], and nuclear waste processing (as phosphine oxides).[17] The

increased binding stability of macrocyclic ligands over analogous monodentate, bidentate, or open-chain multidentate ligands is attributed to the *macrocyclic effect*, where the presence of a continuous covalently-bonded ring pre-organizes the macrocyclic ligand into a geometry that is more suited to binding to a metal.[18-21]

In practice, macrocyclic phosphines are most successfully synthesized using a *template synthesis*, where one or more reactive phosphines are coordinated to a metal ion, followed by treatment with a difunctional linking reagent (usually a carbon electrophile) to form the macrocycle. For tetradentate phosphine macrocycles, the most successful applications of this strategy involve templating a bidentate or tetradentate secondary phosphine to a d^8 transition metal such as Ni(II) or Pd(II) to generate a square-planar template complex, which is then reacted with an α-ω-di(alkyl halide)[22] or dicarbonyl[23] bridging agent. Unfortunately, the resulting complexes are invariably difficult or even impossible to demetallate, limiting the range of transition metals which can be used in macrocyclic ligands synthesized in this manner.

In our attempts to synthesize a macrocyclic iron-phosphine complex, we hypothesized that we might be able to use *trans*-octahedral Fe(II) in place of the standard square-planar d^8 metal macrocyclization template (Scheme 3). Toward this end, we have synthesized new water-soluble secondary bidentate phosphines, which are reported here. We also report the coordination behavior of these phosphines, as well as the hydrophobic secondary phosphines MPPE and MPPP, with iron(II). Finally, we discuss our attempts to form macrocyclic complexes via various alkylation methods.

Scheme 3. Planned template synthesis of a macrocyclic iron(II)-phosphine complex.

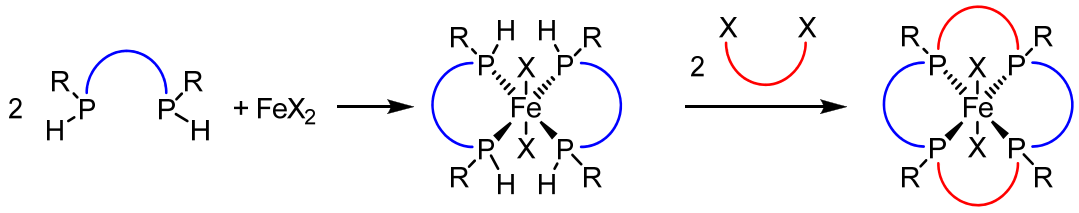

2.2. Experimental

2.2.1. Materials and Reagents

Unless otherwise noted, all manipulations were conducted under an N_2 atmosphere, using standard Schlenk and/or glovebox techniques. BPE and MPPP were purchased from Strem, Inc. 1-chloro-3-methoxypropane was purchased from AK Scientific, Inc. MPPE was synthesized according to a literature procedure.[24] *Safety note: All phosphines used in this work are highly toxic, pyrophoric, and malodorous. These compounds must be handled in a glovebox or a well-ventilated fume hood, using strict air-free techniques.* HPLC-grade THF, hexanes, and acetonitrile (Burdick and Jackson) were dried and deoxygenated by passing them through commercial columns of CuO and alumina under argon.

2.2.2. Instrumentation

^{31}P and ^{1}H NMR spectra were recorded on either a Varian Unity/Inova 300 spectrometer operating at a frequency of 299.94 MHz (^{1}H) or 121.42 MHz (^{31}P), or on a Varian Unity/Inova 500 spectrometer operating at a frequency of 500.62 MHz (^{1}H) or 202.45 MHz (^{31}P). ^{31}P chemical shifts were referenced to 1% H_3PO_4 in D_2O. Mass spectra were obtained on a Thermo LCDecaXP mass spectrometer using direct injection.

2.2.3. X-ray Crystallography

Diffraction intensities for *cis*-Fe(MPPP)$_2$Cl$_2$ (**8**) and *trans*-[Fe(MPPP)$_2$(CH$_3$CN)$_2$](PF$_6$)$_2$ (**12**) were collected at 173(2) K on a Bruker Apex CCD diffractometer using MoKα radiation λ= 0.71073 Å.[25] Space groups were determined based on systematic absences (**8**) and intensity statistics (**12**). Absorption corrections were applied by SADABS.[26] Structures were solved by direct methods and Fourier techniques and refined on F^2 using full matrix least-squares procedures. All non-H atoms were refined with anisotropic thermal parameters. All H atoms in **12** and the H atoms coordinated to the P atoms in **8** were found on the residual density maps and refined with isotropic thermal parameters. Other H atoms in **8** were treated in the calculated positions in a rigid group model. A solvent CH$_3$CN molecule in **12** which is not involved in coordination of the Fe atom is disordered over two positions related by an inversion center. Atoms H in this disordered solvent molecule were not taken into consideration in the refinement. The Flack parameter for **8** is 0.08(2); the given structure of **8** corresponds to an absolute configuration of the compound. All calculations were performed by the Bruker SHELXTL (v. 6.10) package.[27]

Crystal data for *cis*-Fe(MPPP)$_2$Cl$_2$ (8). $C_{30}H_{36}Cl_2FeP_4$, M = 647.22, 0.20 x 0.10 x 0.04 mm, T = 173(2) K, monoclinic, space group $P2_1$, a = 9.194(2) Å, b = 16.406(4) Å, c = 10.500(3) Å, β = 111.439(4)°, V = 1474.3(7) Å^3, Z = 2, Z'= 1, D_c = 1.458 Mg/m^3, μ = 0.930 mm^{-1}, F(000) = 672, $2\theta_{max}$ = 52.00°, 12433 reflections, 5700 independent reflections [R_{int} = 0.0412], R1 = 0.0460, wR2 = 0.0918 and GOF = 1.038 for 4933 reflections (350 parameters) with $I>2\sigma(I)$, R1 = 0.0578, wR2 = 0.0987 and GOF = 1.038 for all 5700 reflections, max/min residual electron density +0.752/-0.388 eÅ^3.

Crystal data for *trans*-[Fe(MPPP)$_2$(CH$_3$CN)$_2$](PF$_6$)$_2$ (12). $C_{36}H_{45}F_{12}FeN_3P_6$, M = 989.42, 0.37 x 0.16 x 0.04 mm, T = 173(2) K, triclinic, space group *P*-1, a = 9.7075(8) Å, b = 10.7282(8) Å, c = 11.8667(9) Å, α = 96.927(1)°, β = 94.820(1)°, γ = 115.671(1)°, V = 1092.83(15) Å^3, Z = 1, Z'=0.5, D_c = 1.503 Mg/m^3, μ = 0.647 mm^{-1}, F(000) = 506, $2\theta_{max}$ = 54.00°, 12344 reflections, 4732 independent reflections [R_{int} = 0.0161], R1 = 0.0362, wR2 = 0.0969 and GOF = 1.064 for 4297 reflections (358 parameters) with $I>2\sigma(I)$, R1 = 0.0400, wR2 = 0.1004 and GOF = 1.064 for all 4732 reflections, max/min residual electron density +0.413/-0.462 eÅ^3.

2.2.4. Methods

Synthesis of 1,2-bis(methoxypropylphosphino)ethane, MeOPrPE. 1,2-bisphosphinoethane (2.26 g, 24.0 mmol) was dissolved in 15 mL hexanes and cooled to -78 °C. 30.0 mL of 1.6 M *n*-butyllithium (48.0 mmol) was added dropwise over the course of 1 h, turning the reaction mixture yellow. The mixture was stirred for 15 min at -78 °C, then 1-chloro-3-methoxypropane (5.50 g, 50.6 mmol) was added dropwise, resulting in a loss of the yellow color. The mixture was allowed to warm to room temperature overnight, then filtered through a frit and the solid rinsed with hexanes. The solvent was then removed under reduced pressure, and the crude product was purified via fractional vacuum distillation (160-170 °C at 0.1 torr), yielding 5.02 g (88%) of a colorless liquid. ^{31}P NMR ($CDCl_3$): δ -59.5 (d, J_{P-H} = 202 Hz). ^{1}H NMR ($CDCl_3$): δ 1.3-1.9 (m, 12H), 3.19 (d, 2H, P*H*), 3.34 (s, 6H, OC*H*$_3$), 3.52 (t, 4H, C*H*$_2$OCH$_3$) ^{13}C{^{1}H} NMR ($CDCl_3$): δ 16.6, 19.1, 28.3, 58.6, 73.0.

Synthesis of 1,3-bis(methoxypropylphosphino)propane, MeOPrPP. The same procedure was followed as for the synthesis of MeOPrPE, using 1,3-bisphosphinopropane

(2.12 g, 19.6 mmol). Yield: 4.95 g (80%) of a colorless liquid. ^{31}P NMR ($CDCl_3$): δ –69.9 (d, J_{P-H} = 202 Hz). ^{1}H NMR ($CDCl_3$): δ 1.4-2.0 p, (m, 14H), 3.13 (d, 2H, P*H*), 3.35 (s, 6H, OC*H*$_3$), 3.42 (t, 4H, C*H*$_2$OCH$_3$) ^{13}C{^{1}H} NMR ($CDCl_3$): δ 16.7, 21.8, 27.1, 28.4, 58.6, 73.2.

General Procedure for the Preparation of Complexes 5 and 6. 2 equiv of the appropriate phosphine were dissolved in THF and added to a THF solution $FeCl_2 \cdot 4H_2O$, immediately giving a deep red solution. The reaction was stirred for 1 h, then the solvent was removed under reduced pressure and the product dried under vacuum overnight.

***cis*-Fe(MeOPrPE)$_2$Cl$_2$ (5).** Used 0.592 g MeOPrPE (2.48 mmol) and 0.250 g $FeCl_2 \cdot 4H_2O$ (1.25 mmol) gave 0.606 g (81%) of a deep red amorphous solid. ^{31}P NMR (THF): δ +45 to +85 ppm (m). ESI-MS: 567 amu ([m-Cl]$^+$).

***cis*-Fe(MeOPrPP)$_2$Cl$_2$ (6).** Used 0.604 g MeOPrPP (2.39 mmol) and 0.2433 g $FeCl_2 \cdot 4H_2O$ (1.22 mmol) gave 0.640 g (85%) of a deep red amorphous solid. ^{31}P NMR (THF): δ +10 to +50 ppm (m). ESI-MS: 595 amu ([m-Cl]$^+$).

General Procedure for the Preparation of Complexes 7 and 8. 2 equiv of the appropriate phosphine were dissolved in THF and added to a THF solution $FeCl_2 \cdot 4H_2O$, immediately giving a deep red solution which precipitated some of the product as a purple solid. The reaction was stirred for 1 h, and the remaining product was precipitated with hexanes, collected by filtration, and dried under vacuum overnight.

***cis*-Fe(MPPE)$_2$Cl$_2$ (7).** Used 0.589 g MPPE (2.39 mmol) and 0.238 g $FeCl_2 \cdot 4H_2O$ (1.20 mmol). Yield: 0.532 g (72%) of a purple solid. ^{31}P{^{1}H} NMR ($CDCl_3$): ^{31}P{^{1}H} NMR ($CDCl_3$): δ + 40-120 (br) ESI-MS: 583 amu ([m-Cl]$^+$).

***cis*-Fe(MPPP)$_2$Cl$_2$ (8).** Used 0.570 g MPPP (2.19 mmol) and 0.218 g $FeCl_2 \cdot 4H_2O$

(1.10 mmol). Yield: 0.5249 g (74%) of a purple solid. $^{31}P\{^{1}H\}$ NMR ($CDCl_3$): δ +26 to 50 ppm (m). ESI-MS: 611 amu ($[m\text{-}Cl]^{+}$). Single crystals suitable for x-ray diffraction were grown by vapor diffusion of hexanes into a THF solution over the course of 1 month.

General Procedure for the Preparation of Complexes 9-12. The *cis*-Fe(bisphosphine)Cl_2 complex was dissolved in 10mL MeCN, giving a dark orange solution. Addition of 2 equiv NaOTf in 5 mL MeCN resulted in a lightening of the solution within minutes, and formed a white precipitate (NaCl). After stirring for 1h, the reaction mixture was filtered. The solvent was removed under reduced pressure and the product was dried under vacuum overnight.

Synthesis of *trans*-[Fe(MeOPrPE)$_2$(CH$_3$CN)$_2$](OTf)$_2$ (9). Used 0.507 g **5** (0.840 mmol) and 0.311 g NaOTf (1.80 mmol). Yield: 0.465 g (73%) of an orange viscous oil. $^{31}P\{^{1}H\}$ NMR (CD_3CN): δ +40 to +70 ppm (m).

Synthesis of *trans*-[Fe(MeOPrPP)$_2$(CH$_3$CN)$_2$](OTf)$_2$. Used 1.46 g **6** (2.31 mmol) and 0.797 g NaOTf (4.64 mmol). Yield: 1.477 g (68%) of an orange amorphous solid. $^{31}P\{^{1}H\}$ NMR (CD_3CN): δ +8 to +28 ppm (m).

Synthesis of *trans*-[Fe(MPPE)$_2$(CH$_3$CN)$_2$](PF$_6$)$_2$. Used 0.273 g **7** (0.441 mmol) and 0.148 g $NaPF_6$ (0.881 mmol). Yield: 0.282 g (70%) of an orange crystalline solid. $^{31}P\{^{1}H\}$ NMR (CD_3CN): δ +30 to +80 ppm (m).

Synthesis of *trans*-[Fe(MPPP)$_2$(CH$_3$CN)$_2$](PF$_6$)$_2$. Used 0.292 g **8** (0.451 mmol) and 0.155 g $NaPF_6$ (0.922 mmol). Yield: 0.399 g (93%) of an orange crystalline solid. $^{31}P\{^{1}H\}$ NMR (CD_3CN): δ +25 to +47 ppm (m). Single crystals suitable for X-ray diffraction were grown by slow evaporation of an acetonitrile solution over the course of three months.

2.3. Results

2.3.1. Synthesis of MeOPrPE and MeOPrPP

The water-soluble secondary bisphosphine 1,2-bis(methoxypropylphosphino)-ethane (MeOPrPE, **3**) was synthesized by deprotonation of 1,2-bisphosphinoethane with 2 equiv *n*-butyllithium, followed by alkylation with exactly two equivalents of 1-chloro-3-methoxypropane (Scheme 4). The product, a secondary bis(phosphine), was identified by $^{31}P\{^{1}H\}$ NMR spectroscopy as a singlet at -64.8 ppm, which splits into a doublet ($J_{P\text{-}H}$ = 202 Hz) in the proton-coupled spectrum. Even under carefully-controlled conditions at reduced temperature (-78 °C) and using precisely 2 eq. butyllithium and MeOPrCl, a small amount of over-alkylated and under-alkylated by-products are generated, in up to 10% as determined by ^{31}P NMR. Fortunately, because of the mass of the methoxypropyl group, these products are sufficiently different in molecular weight as to be separated by fractional vacuum distillation, giving pure MeOPrPE in 88% yield. The analogous three-carbon bridged phosphine 1,3-bis(methoxypropylphosphino)propane (MeOPrPP, **4**) was synthesized and purified in the same manner (80% yield). MeOPrPE and MeOPrPP are both clear, colorless viscous liquids. The ambiphilic methoxypropyl functional group causes these compounds to be miscible in a wide range of solvents, from water to hexanes. To our knowledge, these are the first examples of hydrophilic secondary phosphines. Smaller secondary bisphosphines, such as bis(methylphosphino)ethane (MMPE) can also be generated in this fashion (using methyl iodide as the alkylating agent), however the over- and under-alkylated products are too similar in molecular weight to be effectively separated from the desired product by distillation.

Scheme 4. Synthesis of MeOPrPE and MeOPrPP.

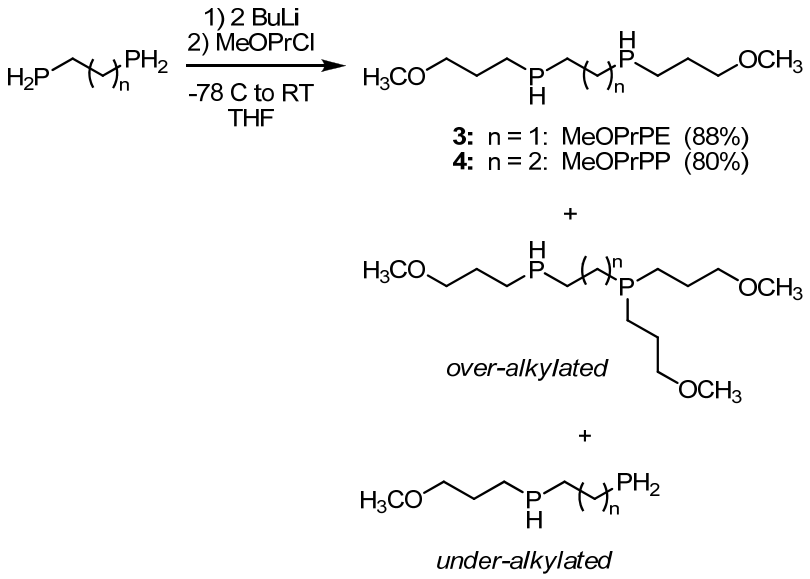

2.3.2. Reaction of Secondary Bisphosphines with $FeCl_2$

In an attempt to synthesize reactive templates for macrocyclic iron-phosphine complexes, MeOPrPE and MeOPrPP were each reacted with $FeCl_2 \cdot 4H_2O$. Addition of 2 eq. **3** or **4** to $FeCl_2 \cdot 4H_2O$ in THF immediately gives complex **5** or **6** as a deep reddish-purple product (Scheme 5). The $^{31}P\{^1H\}$ NMR spectra of these complexes showed a complicated series of peaks, which could not be fully interpreted. A number of $FeCl_2P_4$ complexes have been synthesized previously, by us and others (see Section 2.4). In all cases, the *trans* complexes are colored green, while the *cis* complexes are red or purple. Based on this, it can be assumed that the geometry of these complexes are *cis*-octahedral. Because of the flexible methoxypropyl substituents on these complexes, both **5** and **6** are viscous oils at room temperature, and repeated attempts at crystallization were unsuccessful.

Scheme 5. Synthesis of *cis*-Fe(bisphosphine)$_2$Cl$_2$ complexes.

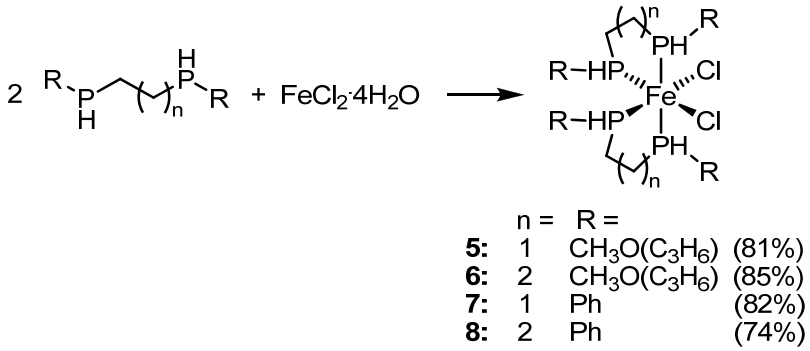

	n =	R =	
5:	1	$CH_3O(C_3H_6)$	(81%)
6:	2	$CH_3O(C_3H_6)$	(85%)
7:	1	Ph	(82%)
8:	2	Ph	(74%)

In order to confirm the *cis*-octahedral geometry of complexes **5** and **6**, $FeCl_2 \cdot 4H_2O$ was also reacted with the hydrophobic secondary phosphines 1,2-bis-(phenylphosphino)ethane (MPPE) and 1,3-bis(phenylphosphino)propane (MPPP). Both MPPE and MPPP immediately reacted with $FeCl_2 \cdot 4H_2O$ to form complexes **7** and **8** as reddish-purple products. Single crystals of **8** were grown and analyzed via X-ray crystallography (Figure 2), which confirms the *cis*-octahedral geometry of the complex. THe MPPP ligands are of *R,R* and *S,S* stereochemistry, and are coordinated to the iron in a Λ (left-handed twist) fashion. The space group is $P2_1$, meaning that the crystal is enantiopure. Each six-membered metallacycle is situated in a chair conformation. The bite angles for the MPPP ligands are 91.09(5)° (*R,R*) and 88.81(5)° (*S,S*). The chloro ligands and the phosphorus atoms *trans* to them are almost exactly coplanar with the central iron atom (sum of L-M-L angles = 359.9(1)°), and thus can be considered an equatorial plane. One of the axial phosphines (P2) is nearly orthogonal to the equatorial plane, while the other (P3) is tilted about 10° towards the chloro ligands.

Figure 1. ORTEP plot of *cis*-Fe(MPPP)$_2$Cl$_2$ (**8**). Ellipsoids are drawn at 50% probability. C-H hydrogen atoms have been omitted for clarity.

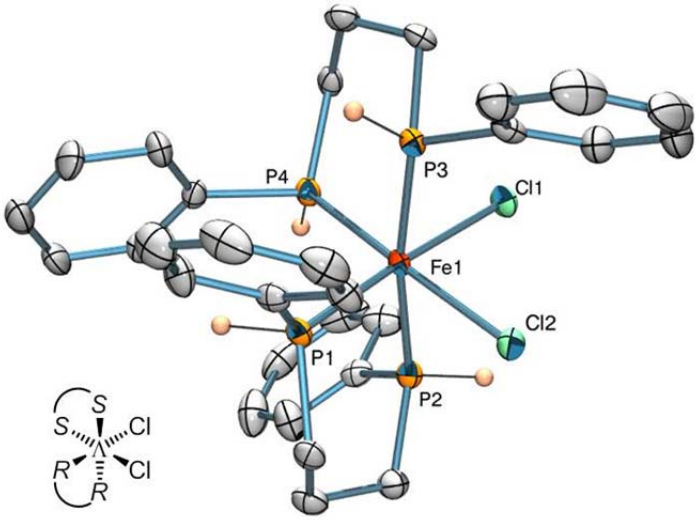

Table 1. Selected bond lengths (Å) and angles (°) for *cis*-FeCl$_2$(MPPP)$_2$ (**8**).[a]

Fe(1)-P(1)	2.2009(13)	P(2)-Fe(1)-Cl(1)	85.16(5)
Fe(1)-P(2)	2.2517(14)	P(3)-Fe(1)-Cl(1)	87.86(5)
Fe(1)-P(3)	2.2455(14)	P(4)-Fe(1)-Cl(1)	85.68(5)
Fe(1)-P(4)	2.1918(14)	P(1)-Fe(1)-Cl(2)	87.44(5)
Fe(1)-Cl(1)	2.3780(13)	P(2)-Fe(1)-Cl(2)	81.29(5)
Fe(1)-Cl(2)	2.3710(13)	P(3)-Fe(1)-Cl(2)	92.87(5)
P(1)-Fe(1)-P(2)	91.09(5)	Cl(1)-Fe(1)-Cl(2)	90.72(4)
P(3)-Fe(1)-P(4)	88.81(5)	P(1)-Fe(1)-Cl(1)	176.05(5)
P(1)-Fe(1)-P(3)	95.73(5)	P(4)-Fe(1)-Cl(2)	175.97(5)
P(1)-Fe(1)-P(4)	96.04(5)	P(2)-Fe(1)-P(3)	170.83(5)
P(2)-Fe(1)-P(4)	96.57(5)		

Because of the chirality of the secondary phosphine groups on these complexes, as well as the twist chirality of the *cis*-octahedral metal center, these complexes can exist as a mixture of up to 7 diastereomeric pairs of enantiomers (Figure 2). Only three of these pairs are sufficiently symmetric to give rise to a simple A_2B_2 pattern (two triplets) in the ^{31}P NMR spectrum. The rest of the isomers are of such low symmetry that all phosphorus atoms are magnetically inequivalent, and couple as 4-spin sytems, resulting in a very complicated ^{31}P NMR spectrum for each of these complexes. Indeed, the ^{31}P NMR spectra of all of these complexes exhibit multiple peaks which cannot be structurally interpreted. None of these spectra change upon heating or cooling, indicating that these isomers are diamagnetic (no spin crossover) at room temperature.

Figure 2. Possible stereoisomers of *cis*-$FeCl_2$(bisphosphine)$_2$ complexes.

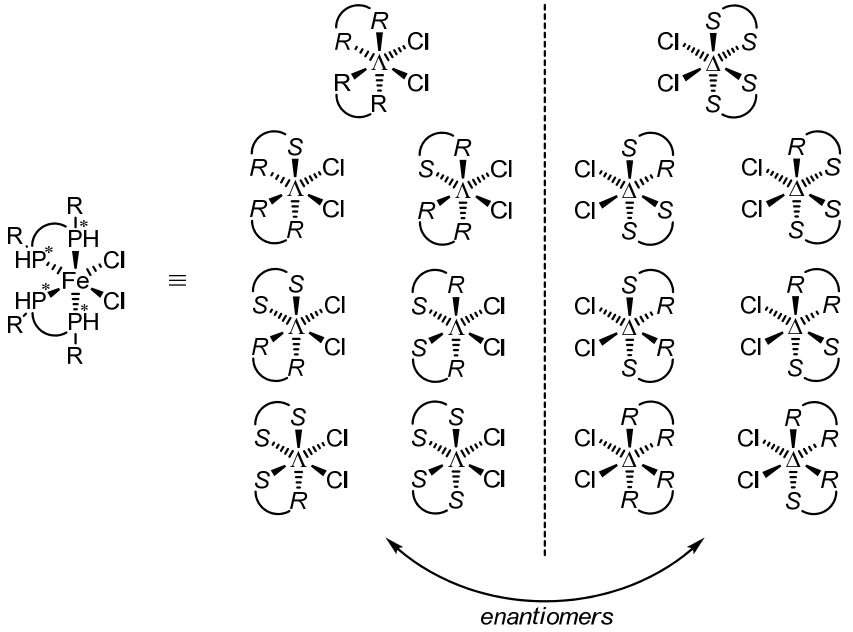

In a few attempts, the reaction of MPPE with $FeCl_2 \cdot 4H_2O$ in THF gave a bright

green precipitate as the major product. $^{31}P\{^{1}H\}$ NMR of a freshly prepared $CDCl_3$ solution revealed a sharp singlet at +71.2 ppm as the major peak ($J_{P\text{-}H}$ = 325 Hz in the proton-coupled spectrum), which indicates that the major product is a highly-symmetric isomer of *trans*-$Fe(MPPE)_2Cl_2$. This product is only soluble in dichloromethane and chloroform, and isomerizes rapidly to the *cis*-octahedral product in both solvents. Unfortunately, this result could not reliably be reproduced, and repeated attempts at optimizing the reaction conditions to favor the *trans* product were unsuccessful.

2.3.3. Synthesis of trans-[Fe(bisphosphine)$_2$(MeCN)$_2$]$^{2+}$ Complexes

As mentioned before, the majority of templates for the synthesis of macrocyclic phosphines are square-planar d^8 metals, coordinated by two bidentate secondary phosphines. Our hypothesis was that *trans*-octahedral iron-phosphine complexes could also be used as templates for macrocyclic iron-phosphine complexes. In order to convert the *cis*-$FeCl_2P_4$ complexes to *trans*-octahedral complexes, the chloro ligands were substituted for less π–donating ligands so that they would be less likely to coordinate *trans* to the secondary phosphines (see Section 2.4). Acetonitrile was chosen as the new ligand, because of its slightly π–accepting nature, ease of substitution, and weak coordination, such that it could potentially be replaced by other ligands later in the synthesis. For each complex, the reaction was carried out by dissolving the complex in acetonitrile, resulting in a color change from purple to red-orange. Addition of 2 equiv NaX (where X is the weakly-coordinating anion OTf^- or PF_6^-) resulted in a lightening of the orange color, as well as the formation of a white precipitate (NaCl). The color change upon addition of NaX suggests that the $FeP_4(MeCN)_2^{2+}$ complexes **8-12** are partially formed upon dissolution in MeCN, but a chloride abstractor such as NaCl is required to

drive the reaction to completion (Scheme 6).

Scheme 6. Synthesis of *trans*-[Fe(bisphosphine)$_2$(MeCN)$_2$]$^{2+}$ complexes.

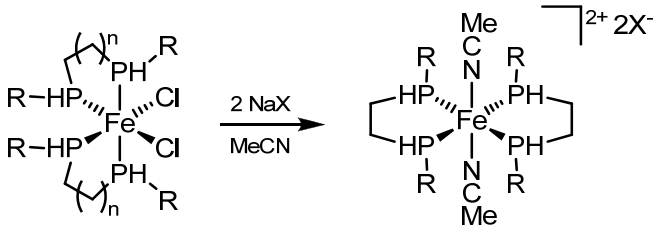

	n =	R =	X =	
9:	1	$CH_3O(C_3H_6)$	OTf	(73%)
10:	2	$CH_3O(C_3H_6)$	OTf	(68%)
11:	1	Ph	PF_6	(70%)
12:	2	Ph	PF_6	(93%)

As with the *cis*-$FeCl_2P_4$ complexes, the lack of stereospecificity in the ligands results in multiple isomers of $[FeP_4(MeCN)_2]^{2+}$ complexes **8-12** (Figure 3). For *trans*-$[FeP_4(MeCN)_2]^{2+}$, seven stereoisomers are possible, consisting of two pairs of enantiomers and three *meso* isomers. Of these, the only the all-*R* and all-*S* isomers are of sufficient symmetry to display a singlet in the ^{31}P NMR spectrum, which is typically observed for more symmetric *trans*-FeX_2P_4 complexes. The rest of the isomers are A_2B_2 systems at best, and four-spin systems at worst. Indeed, the ^{31}P spectrum of each of these complexes is complicated to the point that structural information cannot be obtained.

Figure 3. Possible stereoisomers of *trans*-$[FeP_4(MeCN)_2]^{2+}$.

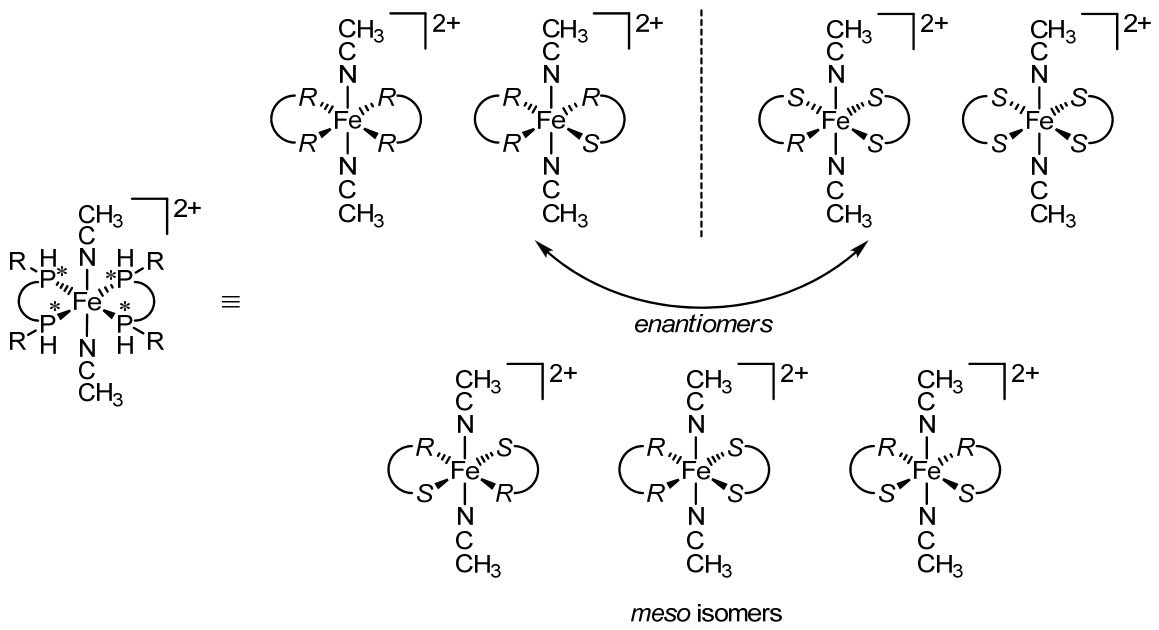

In order to confirm the *trans* geometry of these complexes, single crystals of *trans*-$[Fe(MPPP)_2(MeCN)_2](PF_6)_2$ (**12**) were grown and analyzed by x-ray diffraction (Figure 4). The complex is indeed *trans*-octahedral, and is C_i symmetric, with both MPPP ligands lying exactly in the equatorial plane. The stereochemistry of both MPPP ligands is *R*,*R*. Each six-membered metallacycle is situated in a chair conformation. The bite angles for the MPPP ligands are 87.83(2)°. The axially-coordinated acetonitrile ligands are almost exactly orthogonal to the equatorial plane. One non-coordinated, disordered acetonitrile molecule is present as a solvent of crystallization.

Table 2. Selected bond lengths (Å) and angles (°) for *trans*-$[Fe(MPPP)_2(MeCN)_2](PF_6)_2$.

Fe(1)-P(1)	2.2687(5)	P(1)-Fe(1)-P(2)	87.83(2)
Fe(1)-P(2)	2.2686(5)	P(1)-Fe(1)-N(1)	89.30(5)
Fe(1)-N(1)	1.913(2)	P(2)-Fe(1)-N(1)	88.45(5)

Figure 4. ORTEP plot of the cation in *trans*-[Fe(MPPP)$_2$(MeCN)$_2$](PF$_6$)$_2$. Ellipsoids are drawn at 50% probability. C-H hydrogen atoms have been omitted for clarity.

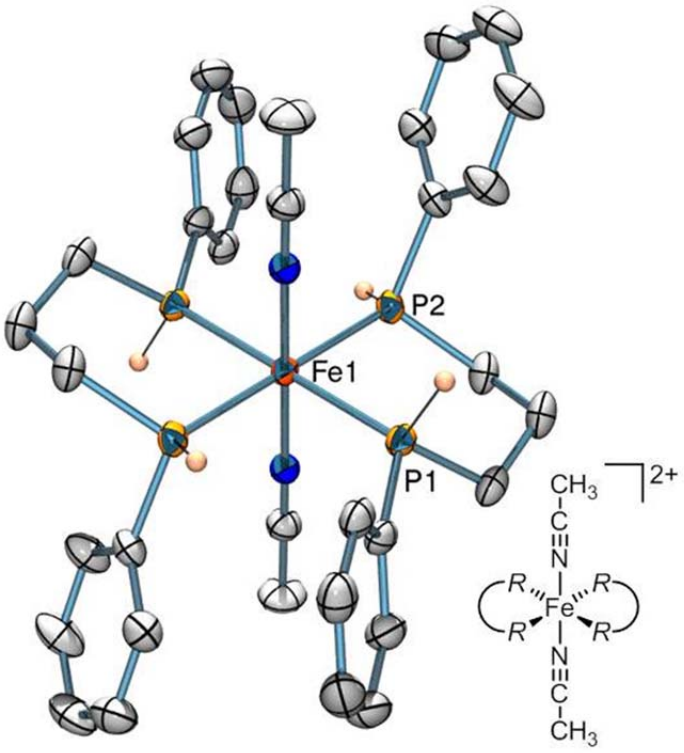

2.3.4. Attempts at Macrocyclization

Metal-templated macrocyclizations of secondary phosphines have been dominated by two routes: 1) alkylation with an α,ω-dihalide under basic conditions, using K_2CO_3 or KO*t*-Bu as a base, and 2) reaction with an α,ω-dialdehyde or diketone, forming hydroxymethylphosphine linkages. In the second route, the reaction may be run in the presence of a weak acid, such as in the case where malonaldehyde is used as the bridging agent. Malonaldehyde is an unstable compound whose most stable form is the mono-enol tautomer, and this configuration readily self-polymerizes via the aldol reaction. Because of this, malonaldehyde is added as the bis(dimethyl) acetal, which is deprotected *in situ* by catalytic H^+.

Both the *cis*-Fe(bisphosphosphine)$_2$Cl$_2$ and *trans*-[Fe(bisphosphosphine)$_2$-

$(MeCN)_2]^{2+}$ complexes were treated with various carbon electrophiles under similar conditions to the previous literature methods, and the reactions were monitored by ^{31}P NMR. However, no changes in the ^{31}P NMR spectra were observed after 2 weeks at reflux, indicating that these complexes did not react under normal macrocyclization conditions. Attempts at using a stronger base such as DBU or Proton Sponge instead of K_2CO_3 or KO*t*-Bu were also innefective, and even stronger bases such as *n*-butyllithium resulted in decomposition of the complexes. Reactions with more reactive carbon electrophiles (neopentylene bis(triflate), bromomaleic anhydride and dimethylmalonyl dichloride) were also unsuccessful.

2.4. Discussion

2.4.1. cis- *vs.* trans-*Octahedral Coordination*

The propensity of previously-reported phosphines to form *cis*- or *trans*-$FeCl_2P_4$ complexes is unclear. Most hydrophobic bidentate phosphines form *trans*-octahedral complexes,[28-34] whereas water-soluble bidentate phosphines bearing hydroxyl substituents may form *cis* or *trans* complexes, depending on the solvent.[9] A few tetradentate phosphines favor the formation of *cis*-octahedral complexes, due to geometric constraints that disfavor formation of the *trans*-octahedral geometry.[35,36] Until this work only one bidentate phosphine has been reported which exclusively favors a *cis*-$FeCl_2P_4$ geometry: 1,2-diphospholanoethane (Figure 5).[37] In this case, it was proposed that the size and rigidity of the phospholane heterocycles might cause increased steric hindrance in the *trans* conformation, so the *cis* conformation would be favored. However, since the *trans* isomer was not observed, this explanation is only speculative.

Figure 5. 1,2-diphospholanoethane.

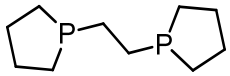

All four ligands in the current study form *cis*-octahedral complexes when coordinated to $FeCl_2$. These ligands differ from each other in terms of chelate ring size (five- or six-membered), hydrophilicity, and electron-donating ability of the pendant groups (hydrophilic, electron-donating methoxypropyl groups versus hydrophobic, electron-withdrawing phenyl groups). The one feature common to all four of these ligands is that they are *secondary* phosphines. This suggests that secondary bidentate phosphines favor the formation of *cis*-octahedral complexes with $FeCl_2$.

We propose that the tendency of these ligands to form *cis*-octahedral complexes is attributed to electronic factors. Electronically, secondary phosphines are stronger π-acceptors than comparable tertiary aryl or alkylphosphines.[38] This should result in an increased preference for binding *trans* to the π-donating chloride ligands, in order to maximize the synergistic π -bonding between the *trans* ligands. This synergistic π -bonding stabilizes the *cis*-octahedral complex relative to the *trans*-octahedral complex, and may account for the preference of a *cis* geometry in these complexes. Analysis of the Fe-P bond lengths in *cis*-$Fe(MPPP)_2Cl_2$ (**8**) suggests that this is the case. The average Fe-P bond length of the equatorial bonds is 2.1964(19) Å, versus 2.249(2) Å for the axial bonds. The shorter bond length of the equatorial Fe-P bonds indicates increased synergistic π-effects for the phosphines situated *trans* to the chloride. This effect is also seen in the lengthening of the equatorial phosphines' P-H bond lengths (avg. 1.37(6) Å for the equatorial phosphines vs. 1.27(7) Å for the axial phosphines). The P-C bond

lengths are also slightly longer for the equatorial positions, but are within the uncertainty of the measurements.

Comparison of Fe-P, P-H, and P-C bond lengths between *cis*-$Fe(MPPP)_2Cl_2$ (**8**) and *trans*-$[Fe(MPPP)_2(MeCN)_2]^{2+}$ (**12**) (Table 3) confirms the the presence of a π-synergistic effect between the chloride ligands and the secondary phosphine ligands in **8**. First, all Fe-P bonds are shorter in **8** than in **12**, especially the equatorial Fe-P bonds that are *trans* to the pi-donating chloro ligands, indicating increasing bond order of the Fe-P bonds. The P-H bonds of the equatorial ligands are also lengthened due to increased electron-donation into the P-H σ* orbitals. In the same manner, all of the P-C bonds are lengthened in **8** relative to **12**, although the P-C bonds of the equatorial phsophines are not always longer than those of the axial phosphines. This may be due to steric crowding of the axial phenyl groups. Nevertheless, all of the crystal structure evidence is consistent with the synergistic π-donation / π-acceptance between the chloro ligands and the secondary phosphines, which is maximized when the $FeCl_2P_4$ complex is in the *cis*-octahedral geometry.

Table 3. Comparison of bond lengths in *trans*-$[Fe(MPPP)_2(MeCN)_2]^{2+}$ and *cis*-$Fe(MPPP)_2Cl_2$.

	trans-$Fe(MPPP)_2(MECN)_2(PF_6)_2$	*cis*-$FeCl_2(MPPP)_2$	
		equatorial	axial
Fe-P	2.2687(7)	2.196(2)	2.249(2)
P-H	1.29(3)	1.37(6)	1.27(7)
P-C(bridge)	1.832(3)	1.841(6)	1.837(7)
P-Ph	1.819(3)	1.825(6)	1.828(7)

Figure 6. Summary of π-synergistic effects in secondary phosphine complexes.

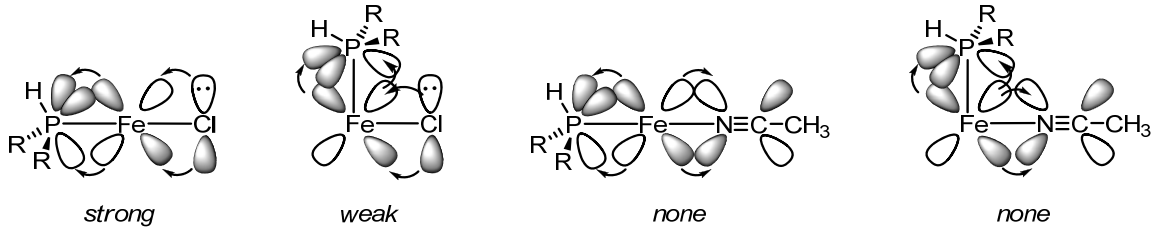

2.4.2. Lack of Reactivity Towards Macrocyclization

Macrocyclic tetraphosphine ligands have previously been synthesized around square-planar d^8 (Ni(II), Pd(II), or Pt(II)), or more rarely, tetrahedral d^{10} (Cu(I)) templates. With both d^8 and d^{10} templates, not only does the metal act as a collection point, placing the phosphines in the correct stoichiometry and geometry for macrocyclizaiton, but the metal also *activates* the phosphines toward alkylation (see Scheme 7).[17,23] This activation is two-fold: 1) coordination to the metal lowers the pK_a of the ligand, making deprotonation easier, and 2) back-donation from the electron-rich metal center destabilizes the lone pair on the deprotonated ligand, increasing its nucleophilicity. The deprotonated phosphido ligand can then nucleophilically attack an electrophilic bridging agent, forming the macrocycle around the metal center.

Scheme 7. Mechanism of alkylation of coordinated phosphines.

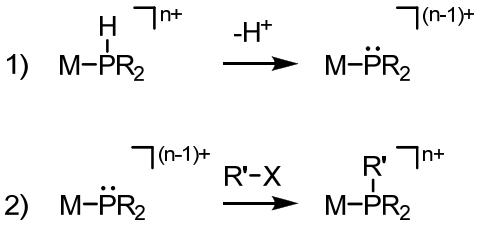

Unlike complexes of d^8 and d^{10} templates, the *cis*-Fe(bisphosphosphine)$_2$Cl$_2$ and *trans*-[Fe(bisphosphosphine)$_2$(MeCN)$_2$]$^{2+}$ complexes are not alkylated under normal macrocyclization conditions. This is most likely because the d^6 iron(II) atom is not as electron-rich as d^8 and d^{10} metals normally used for templates. We propose that the decreased electron density of Fe(II) results in reduced nucleophilicity of the phosphido ligands after deprotonation.

2.5. Conclusion

We have synthesized two new water-soluble secondary bidentate phosphines as precursors to water-soluble phosphine macrocycles. In attempts to form phosphine macrocycles around an Fe(II) template, we have coordinated these ligands, as well as MPPE and MPPP, to $FeCl_2$. In all cases, coordination gives *cis*-Fe(bisphosphine)$_2$Cl$_2$ complexes as opposed to the desired *trans*-octahedral templates. This is due to synergistic π-donation/acceptance between the π -donating chloro ligands and the π -accepting secondary phosphines. This effect is maximized in the *cis*-octahedral geometry, where the chloro ligands occupy positions *trans* to the secondary phosphines. Substitution of the chloro ligands for acetonitrile results in *trans*-[Fe(bisphosphine)$_2$(MeCN)$_2$]$^{2+}$ complexes. Neither these nor the *cis*-Fe(bisphosphine)$_2$Cl$_2$ complexes are reactive toward macrocyclization, likely because the phosphine ligands are insufficiently activated by the d^6 Fe(II) metal.

2.6. Bridge

Chapter II has described the first attempts at synthesizing macrocyclic iron-

phosphine complexes using previously-reported macrocyclization reagents and conditions. Chapter III will describe an unexpected reaction which was discovered while attempting to react these complexes with a different carbon electrophile, bromomaleic anhydride, while using proton sponge as a base.

CHAPTER III

COLORIMETRIC PROTON SPONGES

Some of this work has been previously published and is reproduced with permission from: Swor, C. D.; Zakharov, L. N.; Tyler, D. R. *J. Org. Chem*. **2010**, *75*, 6977-6979.

3.1. Introduction

1,8-dimethylaminonaphthalene, trademarked by Aldrich as Proton Sponge, is a widely used base in organic and inorganic chemistry. It is often chosen due to its high basicity (BH^+ pK_a = 12.34 in H_2O[1] and 18.62 in MeCN[2]) and slow uptake of protons. It is also generally regarded as an innocent, non-nucleophilic and non-coordinating base relative to other amines. However, it has been shown that Proton Sponge (PS) can sometimes act as a *carbon* nucleophile in electrophilic aromatic substitution reactions.[3] Due to the electron-donating nature of the amino groups, Proton Sponge (like other anilines) is more reactive than unsubstituted aromatics to typical electrophilic aromatic substitution reactions (nitration,[4,5] Friedel-Crafts acylation,[6] Vilsmeier-Haack reaction,[7] etc.). Reactions with carbon electrophiles are typically slow, except with very exotic and strong electrophiles.[3,8-9]

Maleic anhydrides readily undergo hydrophosphination with secondary

phosphines.[10,11] More specifically, bromomaleic anhydride (BMA) reacts with two equivalents of secondary phosphine, forming unique bisphosphines that can be used as bidentate ligands (Scheme 1).[12] After addition of one equivalent of phosphine, HBr is eliminated, re-forming the double bond and allowing the second equivalent of phosphine to react.

Scheme 1. Reaction of bromomaleic anhydride with a secondary phosphine.

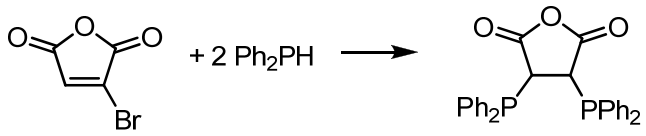

We hypothesized that this reaction might allow us to use bromomaleic anhydride as a linking reagent in the template synthesis of phosphine macrocycles from secondary phosphine complexes (Scheme 2). However, upon attempting this reaction, using PS as a base to neutralize the HBr by-product, we discovered an unanticipated reaction between PS and BMA, which we report here.

Scheme 2. Attempted reaction between bromomaleic anhydride and secondary phosphine complexes.

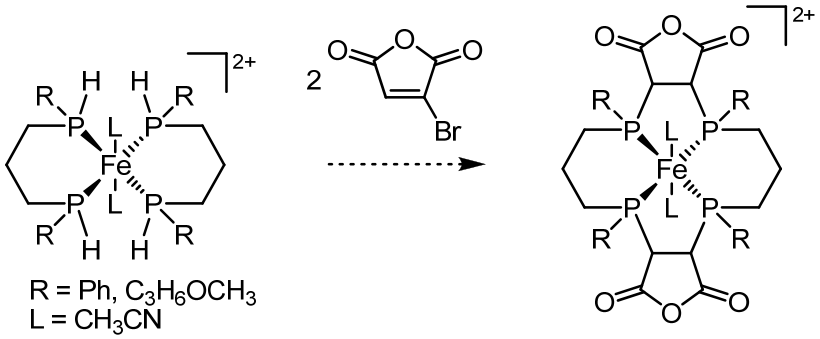

3.2. Experimental

3.2.1. Materials and Instrumentation

All reagents were purchased from Aldrich. Proton Sponge was recrystallized from 95% ethanol. All other reagents were used as received. ^{1}H and ^{13}C NMR spectra were recorded on a Varian Unity/Inova 500 spectrometer operating at a frequency of 500.10 MHz (^{1}H) or 125.77 MHz (^{13}C). Chemical shift values are reported in ppm using $CDCl_3$ as an internal reference. UV-Vis spectroscopy was performed using a Hewlett-Packard 8453 UV-Vis spectrometer. Infrared spectra were obtained on a Nicolet Magna-IR 550 spectrometer.

3.2.2. X-ray Crystallography

X-ray diffraction intensities for MAPS were collected at 173(2) K on a Bruker Apex CCD diffractometer using MoKα radiation λ= 0.71073 Å.[13] The space groups was determined based on systematic absences. The absorption correction was applied by SADABS.[14] The structure was solved by direct methods and Fourier techniques and refined on F^2 using full matrix least-squares procedures. All non-H atoms were refined with anisotropic thermal parameters. H atoms were found from the residual map and refined with isotropic thermal parameters. An absolute configuration could not be determined because the compound is a weak anomalous scatterer. All calculations were performed by the Bruker SHELXTL (v. 6.10) package.[15]

Crystal data for MAPS: $C_{18}H_{18}N_2O_3$, M = 310.34, 0.28 x 0.10 x 0.02 mm, T = 173(2) K, monoclinic, space group $P2_1$, a =7.0429(6) Å, b = 17.4903(16) Å, c = 12.7831(11) Å, β = 96.697(2)°, V = 1963.9(2) Å^3, Z,Z' = 4,2, D_c = 1.318 Mg/m^3, μ = 0.091 mm^{-1}, $F(000)$ = 656, $2\theta_{max}$ = 54.00°, 17571 reflections, 6786 independent

reflections [R_{int} = 0.0362], R1 = 0.0446, wR2 = 0.0747 and GOF = 1.059 for 6786 reflections (559 parameters) with I>2σ(I), R1 = 0.0608, wR2 = 0.0811 and GOF = 1.059 for all reflections, max/min residual electron density +0.156/-0.145 eÅ^3.

3.2.3. Methods

Synthesis of 4-maleicanhydridoproton sponge (MAPS). 1,8-bis(dimethylamino)-naphthalene (954 mg, 0.45 mmol) in 10 mL THF was added to bromomaleic anhydride (393 mg, 0.22 mmol) in 5 mL THF with stirring. Upon mixing, the reaction mixture immediately turned deep red. After stirring for 15 minutes, the solvent was removed under reduced pressure, and the residue was re-dissolved in 50 mL THF and filtered to remove PSHBr. The solvent was removed under reduced pressure, yielding a purple hygroscopic solid (645 mg, 94%): mp 116-127° C, ^{1}H NMR (500 MHz, $CDCl_3$, COSY, NOESY) δ 2.81 (s, 2CH_3), 2.95 (s, 2CH_3), 6.87 (d, J = 8.65 Hz, H2), 6.88 (s, H14), 6.96 (d, J = 7.56 Hz, H7), 7.41 (t, J = 8.01 Hz, H6), 7.58 (d, J = 8.52 Hz, H5), 7.91 (d, J = 8.51 Hz, H3), ^{13}C δ 43.2 (CH_3), 43.3 (CH_3), 109.4 (CH), 112.4 (CH), 115.3, 116.1 (CH), 121.6 (CH), 128.0 (CH), 131.8 (CH), 135.0, 136.2, 146.2, 151.7, 154.8, 165.3, 166.6, IR 2962.5 (m), 1824.4 (m), 1754.9 (s), 1660.0 (s), 801.8 (m). Anal. Calcd. for $C_{18}H_{18}N_2O_3 \cdot 1/3H_2O$: C, 68.34; H, 5.95; N, 8.86, found C, 68.42; H, 6.07; N, 8.95).

pK_a Determination. A series of 3.00 mL samples of 10.15 μM solutions of MAPS in dry acetonitrile were prepared (0.03045 μmol each), and titrated with 0 to 11 10.00 μL aliquots of 2.018 mM PSHCl (0.02018 μmol each) (PSHCl = 1,8-dimethylaminonapthalene hydrochloride, pK_a = 18.62 in MeCN). Samples were allowed to equilibrate for 24 h and UV-Vis spectra were obtained for each sample. The

absorptions of each sample at 521 nm were obtained, and plotted vs. equivalents of PSHCl added. The baseline absorption was calculated by averaging the absorptions of the last four measurements (points 8-11). Points 0-7 were baseline corrected by subtracting out this value, and a linear regression of these values was used to obtain the equivalents of PSHCl required to protonate half of the MAPS (2.57 equivalents). The equilibrium constant *K* was determined by inputting the concentrations into the equation $K = \frac{[\text{PSHCl}][\text{MAPS}]}{[\text{MAPSHCl}][\text{PS}]} = 0.24$. This is the ΔK_a between $MAPSH^+$ and PSH^+. $\Delta pK_a = -\log K_a = 0.62$; so $pK_a(MAPS) = pK_a(PS) - \Delta pK_a = 18.62 - 0.62 = 18.00$.

General procedure for attachment of MAPS to solid supports. MAPS was dissolved in 30 mL toluene and the appropriate amine-functionalized solid support (aminomethylated polystyrene or aminopropyl-functionalized silica) was added. A Dean-Stark trap filled with toluene and a condenser were attached, and the mixture was refluxed overnight. The solid product was filtered and rinsed with toluene until no color leached from the solid (~10x), then dried under vacuum overnight. **MAPS-PS:** IR 1707 cm^{-1}. **MAPS-SiO_2:** IR 1709 cm^{-1}.

Synthesis of $[Fe(DMeOPrPE)_2(H_2)H](BPh_4)^-$ using MAPS-PS. *trans*-$Fe(DMeOPrPE)_2Cl_2$ (0.184 g, 0.207 mmol) and $NaBPh_4$ were dissolved in 10 mL THF/Et_2O in a Fischer-Porter tube containing 0.228 g MAPS-PS (~0.23 mmol). The tube was charged with 45 psig H_2, resulting in a dark brown solution. The reaction was stirred for 19h, then filtered to remove NaCl and MAPS-$PSH^+BPh_4^-$, which was in the form of light brown beads. ^{31}P NMR: +87.6 ppm (s).

3.3. Results and Discussion

3.3.1. Synthesis and Structure of MAPS

While investigating whether bromomaleic anhydride would react with *coordinated* secondary phosphines (i.e. complexes **5-12** in Chapter II), we combined the phosphine complex *trans*-$[Fe(MPPP)_2(MeCN)_2](PF_6)_2$, bromomaleic anhydride, and 2 equiv Proton Sponge to neutralize the HBr by-product. Upon addition of Proton Sponge to the reaction mixture, a deep purple product formed within seconds. Control reactions showed that Proton Sponge and bromomaleic anhydride reacted in the *absence* of the metal complex or the phosphine to generate this new product. Slow evaporation of the reaction solution resulted in deep purple crystals suitable for X-ray diffraction, which were found to be 4-maleicanhydridoproton sponge (MAPS).

Proton Sponge and bromomaleic anhydride react within seconds at room temperature in a variety solvents (chloroform, dichloromethane, acetonitrile, THF) to form MAPS (Scheme 3). This reaction can be viewed as *both* an electrophilic aromatic substitution, with bromomaleic anhydride acting as the electrophile, and as a Michael reaction, with Proton Sponge acting as the nucleophile. Because HBr is a byproduct of this coupling, 2 equiv of proton sponge are needed for the reaction to reach completion. One equivalent couples with BMA, while the other neutralizes HBr. Attempts at using a different base (such as sodium methoxide) to avoid using two equivalents of proton sponge in the reaction were unsuccessful, and resulted in decomposition of the product.

Scheme 3. Coupling of proton sponge and bromomaleic anhydride.

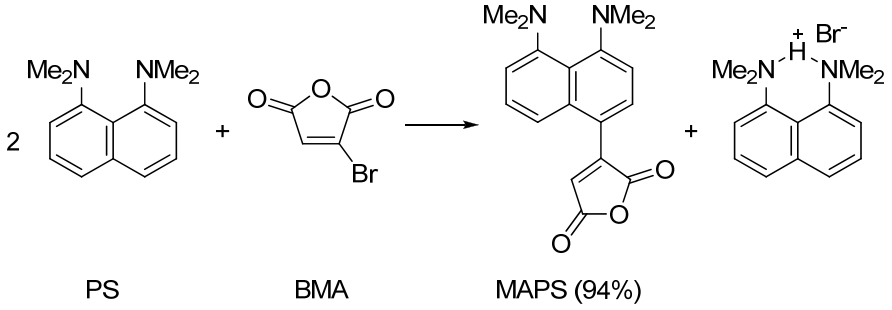

Researchers following the procedure in the Experimental Section for the synthesis of MAPS may wonder why the THF solvent needs to be removed and then reintroduced following the reaction. The PSH^+Br^- byproduct of the reaction is insoluble in THF, which may lead some to conclude that it can be removed by filtration at this point. However, PSH^+Br^- does not quickly precipitate from the THF reaction solution. When the solvent is evaporated under reduced pressure, both products precipitate from solution, but only MAPS redissolves in THF. Thus, from a practical standpoint, it is easier to conduct the reaction in THF, evaporate off the solvent, redissolve the products in THF, and filter than to wait for the PSH^+Br^- byproduct to precipitate from solution.

The HBr byproduct of the reaction is almost entirely neutralized by PS, suggesting that MAPS is a weaker base than PS. To quantify this, the pK_a of MAPS was determined by titration with PSH^+Cl^- in acetonitrile. The pK_a was found to be 18.00, slightly less basic than the parent proton sponge (pKa = 18.62).

X-ray crystallography confirms the structure of MAPS (Figure 1). The unit cell is monoclinic, with two inequivalent molecules per unit cell. The naphthalene rings, and therefore the dimethylamino groups, are twisted, with the first molecule having a Λ (left-handed) twist and the second having a Δ (right-handed) twist. Table 1 lists important

structural parameters. The maleic anhydride ring is twisted 25° out of plane from the naphthalene ring in one of the independent molecules and 27° in the other.

Table 1. Selected structural parameters of MAPS and PS.

Molecule	N-N distance (Å)	C1-C6-C5-C4 torsion angle	Sum of C-N-C angles	N1-C1-C6 (α)	N2-C7-C6 (β)	C1-C6-C7 (γ)	Napthalene-maleic anhydride torsion angle
Λ-MAPS	2.825	16.7° 17.7°	353.5° 348.6°	121.1°	119.9°	123.1°	26.8°
Δ-MAPS	2.832	15.9° 16.8°	350.8° 347.2°	121.1°	120.2°	124.1°	25.0°
PS	2.79	8.9° 10.5°	347.1°	120.1°	120.8°	125.8°	n/a

Figure 1. ORTEP plot of MAPS. The ellipsoids are drawn at 50% probability, and the hydrogen atoms have been omitted for clarity.

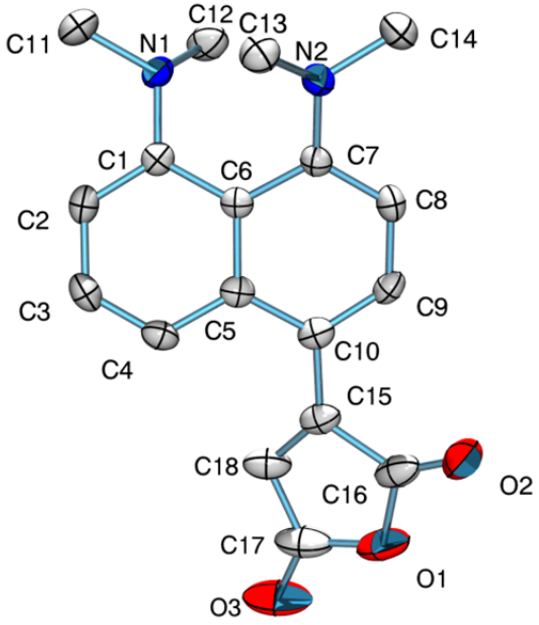

The most important structural parameters of derivatized proton sponges are the orientation of the dialkylamino groups and the planarity of the aromatic system.[16] The naphthalene ring of MAPS is more distorted than PS, with internal (C1-C6-C5-C4) torsion angles of 15.9°-17.7°, vs. 8.9°-10.5° for PS. Thus, the N-N interatomic distances of MAPS are slightly longer than PS at 2.825 and 2.832 Å (vs. 2.79 Å for PS).[17] On the basis of the torsion angle θ between the nitrogen lone pairs and the naphthalene ring plane, the four nitrogen lone pairs (in the two independent molecules) are between 68% and 77% conjugated to the aromatic ring. (These percentages were calculated using the equation $M = M_0 \cos^2 \theta$ where M is the percent conjugation.[16]) This is more conjugated than PS (59%), and is consistent with the decreased basicity of MAPS compared to PS.[18] (The decreased basicity is due to the electron-withdrawing maleic anhydride group, which removes electron density from the amine moieties, causing MAPS to be less basic than proton sponge.) Finally, note that the geometry of each nitrogen atom is slightly more planar than PS, with C-N-C angles totaling 347.2° to 353.5° (vs 347.1° for PS).

Although the reaction of PS and bromomaleic anhydride was unanticipated, similar reactivity has previously been seen with other tertiary anilines and activated alkenes. For example, tertiary anilines are known to act as carbon nucleophiles toward tetracyanoethylene[19] as well as halogenated maleic anhydrides and maleimides.[20,21] Note, however, that this type of reactivity has not previously been observed for Proton Sponge, even though it has been reacted before in the presence of tetracyanoethylene.[22]

3.3.2. Color and Solvatochromism

In solution, MAPS exhibits solvatochromism, ranging from orange in hexanes to purple in chloroform. Table 2 lists λ_{max} values and the extinction coefficients in various

solvents. MAPS exhibits positive solvatochromism in halogen-free solvents, with λ_{max} correlating with Reichardt's E_T^{30} polarity parameter.[23] Positive solvatochromism has been observed for other substituted proton sponges in their free base and/or protonated forms.[24-25] However, MAPS remains purple in chloroform (λ_{max} = 536 nm) and dichloromethane, even though these solvents are *less* polar than acetonitrile (λ_{max} = 521 nm). The apparently anomalous λ_{max} values in these two solvents may be due to their hydrogen-bonding ability, as indicated by their large σ values.[26]

Figure 2. UV-Vis spectra of MAPS in various solvents.

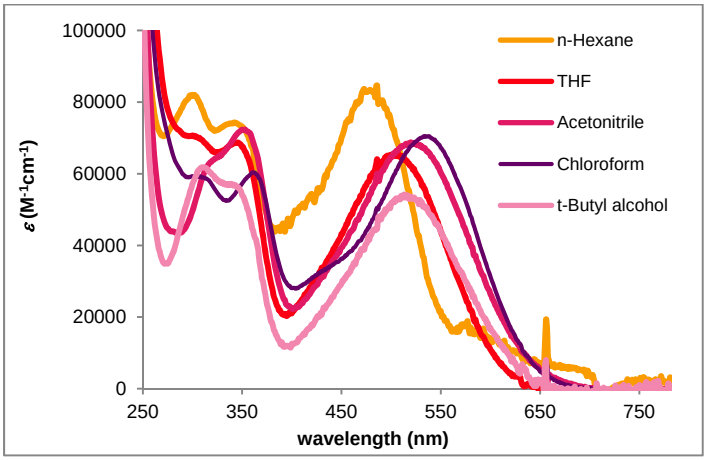

Table 2. UV-Vis spectral data in various solvents.

Solvent	$E_T(30)$	Color	λ_{max}	ε ($M^{-1}cm^{-1}$)
n-Hexane	31	Orange	480	83200
THF	37	Red	504	65200
t-Butyl alcohol	43	Red	516	53700
Acetonitrile	46	Red	521	68500
Chloroform	35	Purple	536	70300

The deep color of the neutral compound is presumably due to the presence of conjugated electron-donor (amine) and electron-acceptor (anhydride) groups on the molecule. The standard interpretation[27,28] is that excitation by visible light causes the nitrogen lone pair to donate via conjugation to the maleic anhydride moiety. Protonation of the nitrogen atoms should prevent this mode of excitation. In fact, MAPS can be protonated in wet acetonitrile by glacial acetic acid, resulting in a loss of color. When PS is added to the acetonitrile solution of protonated MAPS, the compound is deprotonated and color is restored (Scheme 4).

Scheme 4. Acid-base switchable colorimetric behavior in acetonitrile.

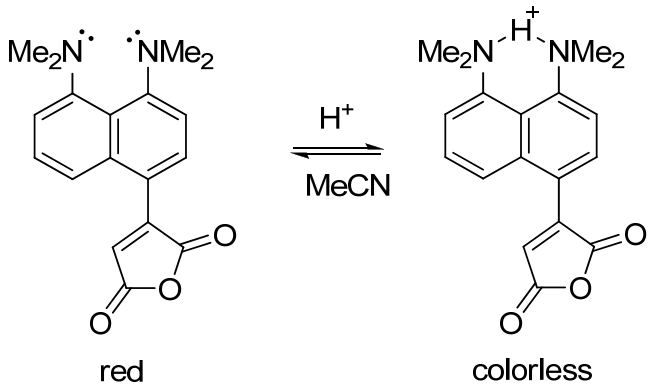

MAPS quickly loses its color when dissolved in methanol, and slowly when dissolved in ethanol, but remains deeply colored for weeks in *t*-butyl alcohol. The color changes in methanol and ethanol are reversible; when the solvent is removed under reduced pressure, the purple color is restored. This indicates that MAPS may be protonated by these solvents; however it is also possible that MAPS undergoes reversible alcoholysis in these solvents. ^{1}H NMR of MAPS in perdeuterated MeOH and EtOH was

attempted in order to determine the nature of the reaction between MAPS and alcohols, but identification of the product was unsuccessful.

3.3.3. Attachment of MAPS to Solid Supports

Often the most difficult task of synthetic organic and inorganic chemistry is separation of a desired synthetic product from excess reagents and by-products. When PS is used as a base, its by-products are salts of the form PSH^+X^-, where X may be one of a variety of anions (halides, weakly coordinating anions, etc.) Often these salts are especially difficult to separate from the reaction mixture, due to their high solubility in organic solvents. A solid-supported proton sponge would offer the advantages of a strong but otherwise mild organic base, without the problem of separating its highly-soluble conjugate acid.

Maleic anhydrides can undergo condensation reactions with primary amines to form maleimides. In an attempt to synthesize solid-supported proton sponges, it was realized that this reaction might allow MAPS to be easily tethered to commercially available amine-functionalized solid supports (Scheme 5).

Scheme 5. Attachment of MAPS to solid supports.

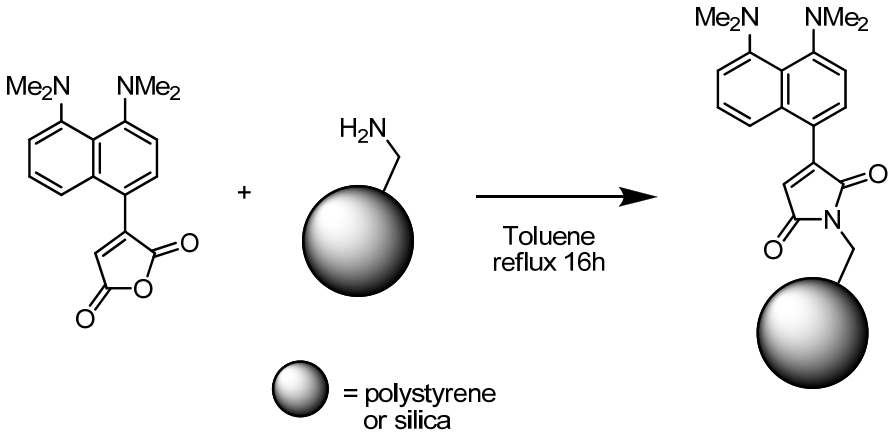

To accomplish this reaction, aminomethyl-functionalized polystyrene beads and aminopropyl-functionalized silica gel were refluxed with a solution of MAPS in toluene. After 16 h, visual examination of the reaction mixtures revealed that a significant amount of color had been absorbed onto the solid supports (although some color remained in solution). The functionalized solids were filtered and rinsed with toluene until no color leached into the rinse solvent, then the solids were dried under vacuum overnight. Covalent tethering of MAPS to the solid supports was confirmed by FTIR spectroscopy, which showed carbonyl stretches at 1707 cm^{-1} for MAPS-functionalized polystyrene (MAPS-PS) and 1709 cm^{-1} for MAPS-functionalized silica (MAPS-SiO_2) (Figure 3). These stretches are indicative of maleimide carbonyl groups, whereas the carbonyl stretch for the maleic anhydride group on MAPS is 1755 cm^{-1}. The mass of MAPS-PS increased 41%, corresponding to a loading of 1.0 mmol MAPS per gram of the polystyrene support.

Figure 3. Infrared spectra of MAPS and solid-supported proton sponges.

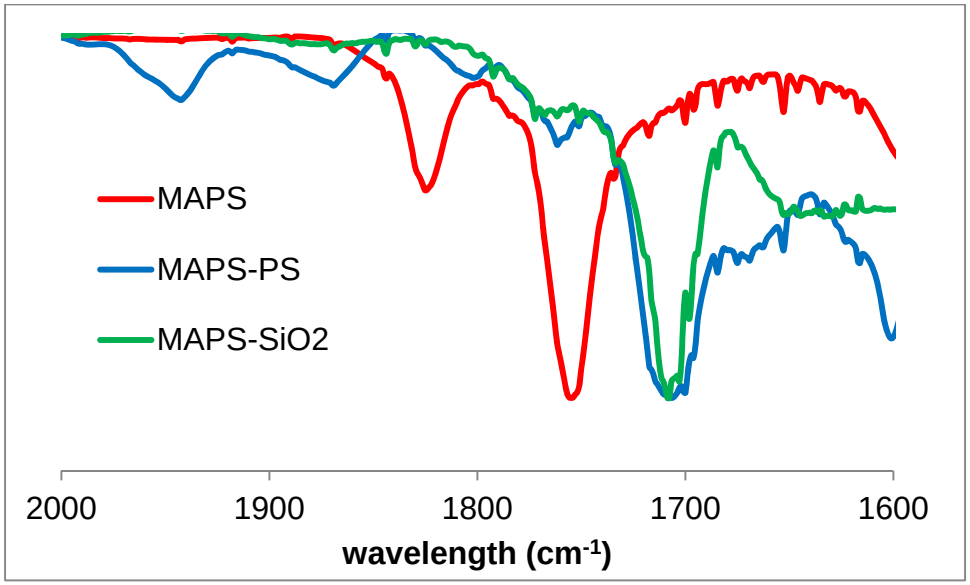

3.3.4. Reversible Acid-Base Behavior of Solid-Supported Proton Sponges

In order to test the utility of the solid-supported proton sponges, MAPS-PS and MAPS-SiO_2 were treated with 1M HCl in ether. The deep reddish-purple solids immediately lost most of the color, turning tan within a few seconds. Addition of a solution of Proton Sponge in acetonitrile to these solids quickly restored the color, indicating that the solid-supported proton sponges are slightly less basic than the parent Proton Sponge. Both PS-MPS and PS-SiO_2 could be reversibly protonated/deprotonated at least 3 times with little loss of color.

3.3.5. Use of Solid-Supported Proton Sponge as a Base

In order to demonstrate the utility of the solid-supported proton sponge as a laboratory reagent, MAPS-PS was used in place of (molecular) Proton Sponge in the synthesis of $[Fe(DMeOPrPE)_2(H_2)H](BPh_4)$. This complex is typically synthesized from *trans*-$Fe(DMeOPrPE)_2Cl_2$ by treatment with $NaBPh_4$ (a halide abstractor) and Proton Sponge under a pressurized atmosphere of H_2 (Scheme 6). Often, this product and successive iron complexes are contaminated with $PSH^+BPh_4^-$, which is difficult to separate from the product due to its high solubiltity. The presence of this byproduct requires its removal by trituration to obtain a solid product, and has resulted in numerous inadvertent crystal structures of this salt by our lab! Reaction of $Fe(DMeOPrPE)_2Cl_2$ with H_2, $NaBPh_4$, and MAPS-PS led to the formation of $[Fe(DMeOPrPE)_2(H_2)H](BPh_4)$ in high yield, demonstrating that MAPS-PS can be used as a base in the place of Proton Sponge. Also, ^{31}P NMR spectroscopy showed that the reaction solution was free of the phosphorus-containing impurities which are normally present in this crude product.

Scheme 6. Synthesis of $[Fe(DMeOPrPE)_2(H_2)H](BPh_4)$.

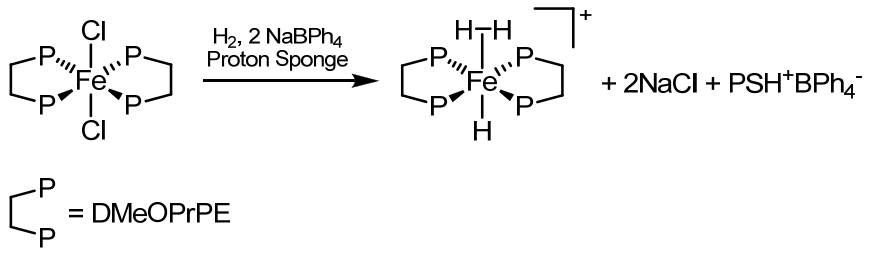

Two previous reports of solid-supported proton sponges have been published in the literature,[29,30] including silica-supported proton sponge that is an efficient base catalyst for the Knoevenagel and Claisen-Schmidt condensations. This solid-supported catalyst is more active than the parent Proton Sponge because of the polar environment of the silica support, and can be recycled up to three times with little loss of activity. However, both of the previously-reported solid-supported proton sponges required four synthetic steps, with most of the steps requiring harsh reagents and/or high temperatures.

3.3.6. Attempted Functionalization of Chitosan

Functionalization of the "green" polymer chitosan with MAPS was also attempted. Chitosan is a primary amine-functionalized biopolymer, most commonly produced by the de-acetylation of chitin (the biopolymer that makes up crab, shrimp, and insect shells), which is a waste product of the seafood industry. The low cost of chitosan, along with its polarity and solubilty properties (it is only soluble in aqueous acid), have made chitosan an attractive substrate for solid-supported reagents and catalysts.[31]

The amine group on chitosan is commonly protected by reaction with phthalic anhydride in DMF to form a phthalimide,[32] which is a similar reaction to the condensation of MAPS with amine-functionalized polystyrene and silica. Refluxing chitosan with a solution of MAPS in DMF did lead to a deep coloration of the chitosan;

unfortunately, treatment of this product with H^+ did not produce a color change, indicating that MAPS was not successfully tethered to chitosan. Note that chitosan contains many primary and secondary alcohol groups, so MAPS may be reacting with chitosan in a similar way to its reaction with methanol and ethanol.

3.4. Conclusions

Proton sponge and bromomaleic anhydride react quickly, via an electrophilic aromatic substitution / Michael addition, to produce MAPS in high yield. Due to the conjugated donor/acceptor moieties on the molecule, MAPS is deeply colored, and is highly solvatochromic. The basicity of MAPS is slightly weaker than the parent Proton Sponge, and protonation of MAPS disrupts the donor/acceptor network, resulting in a loss of color. Thus, MAPS acts as a colorimetric version of a proton sponge.

The presence of the maleic anhydride group allows MAPS to be tethered to primary amine-functionalized solid supports by means of a condensation reaction to form a maleimide. These products are one of a few examples of solid-supported proton sponges, and can be prepared in two simple steps from commercially-available materials. This reagent acts as an insoluble, strong, but otherwise non-reactive base, whose by-products can be separated from a reaction mixture by simple filtration, regenerated with a stronger base, and re-used. In addition, the colorimetric response upon protonation/deprotonation gives the researcher a visual cue when the reagent is spent and needs to be regenerated.

3.5. Bridge

This chapter has explored a unique reaction between Proton Sponge and bromomaleic anhydride, discovered while attempting to use bromomaleic anhydride as a linking agent in the synthesis of macrocyclic phosphines around an iron(II) template (see Chapter II). Not only is this an interesting reaction in itself, but the fact that bromomaleic anhydride *does* react as an electrophile toward Proton Sponge but *not* with the iron(II)-phosphine template complexes illustrates the lack of nucleophilicity of these templates toward alkylation. Chapter IV describes another attempt to synthesize macrocyclic phosphine complexes, using the phosphorus Mannich reaction between amines and the bidentate hydroxymethylphosphine DHMPE, around an iron(II) template.

CHAPTER IV

REACTIONS OF COORDINATED HYDROXYMETHYLPHOSPHINES WITH NH-FUNCTIONAL AMINES: INVESTIGATION OF THE PHOSPHORUS MANNICH REACTION

Some of this work has been previously published and is reproduced with permission from: Swor, C. D.; Hanson, K. R.; Zakharov, L. N.; Tyler, D. R. *Inorg. Chem*. **2011**, *manuscript submitted.*

4.1. Introduction

Water-soluble phosphines are useful ligands for aqueous catalysis, aqueous/organic biphasic catalysis,[1-7] biochemical[8] and medicinal applications,[4,9-13] and electroless metal plating.[14] Of the water-soluble phosphines, hydroxymethylphosphines ($R_nP(CH_2OH)_{3-n}$) are especially attractive because of their easy preparation from PH-functional phosphines (or PH_3) and formaldehyde (eq 1).[15-21] The hydroxymethyl-phosphine ligands are easily functionalized by using the phosphorus Mannich-type reaction with NH-functional amines (eq 2).[22-31] Phosphine ligands with ancillary amino groups are useful because they can provide basicity in the secondary coordination sphere

of metal complexes and because complexes with such ligands can activate small molecule substrates as both Lewis acids and Lewis bases.[32-41] It is interesting to note that the aminomethylphosphines generated by these reactions are generally air-stable, a rare trait among phosphine ligands.

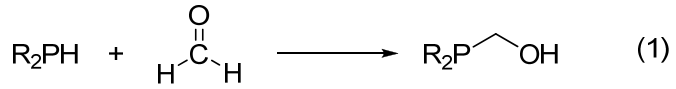

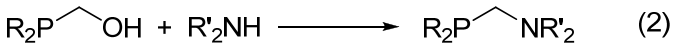

A useful property of hydroxymethylphosphines is their ability to self-assemble into multidentate ligands when combined with the appropriate primary amines (or ammonia) and a suitable metal template (Scheme 1). This property was first discovered by Jeffery in 2000[42] while investigating a red coloration obtained when aqueous solutions of $(P(CH_2OH)_4)_2SO_4$ (a biocide) were added to oil deposits containing FeS. Such self-assembly has been further developed by Burrows.[43,44] The self-assembled molecules are presumed to be generated by a series of Mannich-type reactions between hydroxymethylphosphines and ammonia. We hypothesized that if this process could be better understood and harnessed then it could lead to a variety of easily synthesized polyphosphine ligands and their complexes, including macrocyclic phosphine complexes (eq 3). In this paper, we report the results of our investigation on the phosphorus Mannich reaction using a) Ph_2PCH_2OH, b) the water-soluble 1,2-bis(dihydroxymethyl-phosphino)ethane ligand (DHMPE, Figure 1), and c) metal complexes of DHMPE. In addition to demonstrating the synthetic possibilities and limitations of the phosphorus Mannich reaction, the results have implications for the mechanism of the reaction. These mechanistic aspects are discussed herein as well.

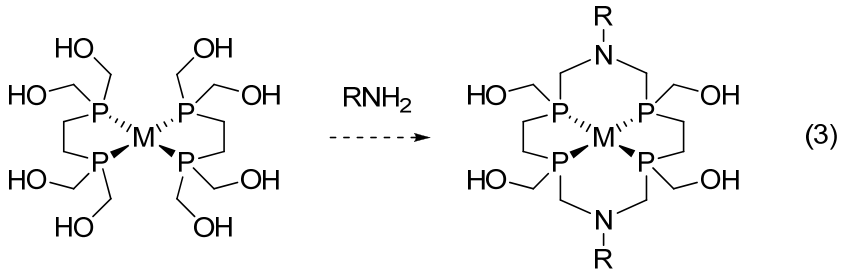

Figure 1. 1,2-bis(dihydroxymethylphosphino)ethane, DHMPE.

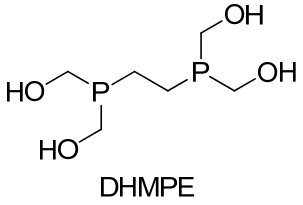

Scheme 1. Self-assembling metal-phosphine complexes generated via the phosphorus Mannich reaction.

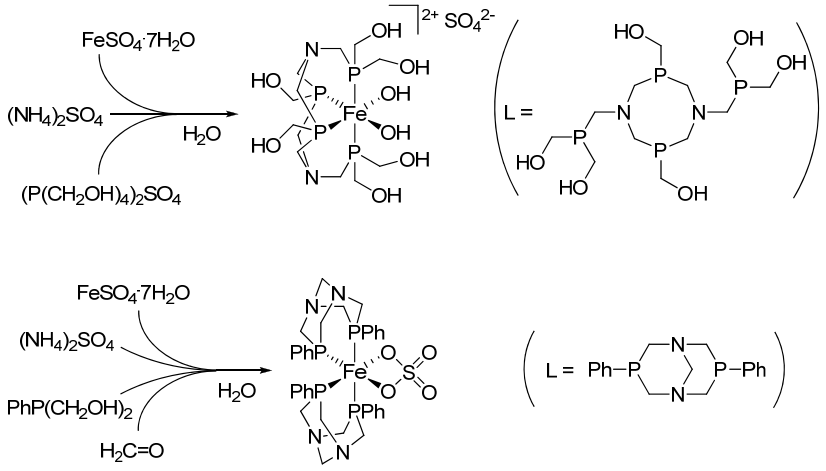

4.2. Experimental

4.2.1. Materials and Instrumentation

Unless otherwise noted, all experimental procedures were performed under inert (N_2) atmosphere, using standard Schlenk and glovebox techniques. DHMPE,[20]

Ph_2PCH_2OH,[45] $Ph_2PCH_2OH \cdot 2BH_3$,[46] $RuCl_2(DHMPE)_2$,[47] and $Ni(DHMPE)_2Cl_2$[20] were prepared via previously published methods. NMR spectra were obtained on a Varian/Unity 300 or Varian/Unity 500 NMR spectrometer. Mass spectra were obtained using a Thermo Finnigan LCQ Deca XP Plus ESI Mass Spectrometer. Elemental analyses were performed by Robertson Microlit Laboratories.

4.2.2. X-ray Crystallography

Diffraction intensities were collected at 173(2) K on a Bruker Apex CCD diffractometer using MoKα radiation λ= 0.71073 Å.[48] Space groups were determined based on systematic absences. Absorption corrections were applied by SADABS.[49] Structures were solved by direct methods and Fourier techniques and refined on F^2 using full matrix least-squares procedures. All non-H atoms were refined with anisotropic thermal parameters. H atoms in both structures were found on the residual density maps and refined with isotropic thermal parameters. All calculations were performed by the Bruker SHELXTL (v. 6.10) package.[50]

Crystallographic Data for *trans*-Fe(DHMPE)$_2$Cl$_2$. $C_{24}H_{64}Cl_4Fe_2O_{16}P_8$, M = 1110.01, 0.09 x 0.07 x 0.04 mm, T = 173(2) K, monoclinic, space group $P2_1/n$, a = 7.7855(4) Å, b = 13.0809(7) Å, c = 10.4136(6) Å, β = 92.393(1)°, V = 1059.61(10) Å^3, Z = 1, Z'=0.25, D_c = 1.740 Mg/m^3, μ = 1.303 mm^{-1}, $F(000)$ = 756, $2\theta_{max}$ = 54.00°, 11961 reflections, 2428 independent reflections [R_{int} = 0.0494], R1 = 0.0355, wR2 = 0.0729 and GOF = 1.073 for 1974 reflections (188 parameters) with $I>2\sigma(I)$, R1 = 0.0500, wR2 = 0.0800 and GOF = 1.073 for all 2428 reflections, max/min residual electron density +0.477/-0.290 eÅ^3.

Crystallographic Data for DHMPE·2BH$_3$. $C_6H_{22}B_2O_4P_2$, M = 241.80, 0.27 x 0.12 x 0.02 mm, T = 173(2) K, monoclinic, space group $C2/c$, a = 18.092(3) Å,

b = 6.2042(11) Å, c = 11.757(2) Å, β = 100.688(3)°, V = 1296.8(4) Å^3, Z = 4, Z'=0.5, D_c = 1.238 Mg/m^3, μ = 0.323 mm^{-1}, F(000) = 520, $2\theta_{max}$ = 54.00°, 6768 reflections, 1408 independent reflections [R_{int} = 0.0549], R1 = 0.0484, wR2 = 0.1126 and GOF = 1.058 for 1138 reflections (108 parameters) with $I>2\sigma(I)$, R1 = 0.0631, wR2 = 0.1224 and GOF = 1.058 for all 1408 reflections, max/min residual electron density +1.153/-0.301 eÅ^3.

4.2.3. Methods

Synthesis of *trans*-Fe(DHMPE)$_2$Cl$_2$. A solution of 0.82 g (4.12 mmol) $FeCl_2 \cdot 4H_2O$ in 60 mL of ethanol was added to a solution of 1.77 g (8.27 mmol) DHMPE in 100 mL ethanol, giving an immediate dark green solution. After stirring for a few minutes, a bright green precipitate formed. When the precipitate was allowed to settle, a pale red solution was present. The solid was filtered through a glass frit, rinsed with ethanol, and dried under vacuum overnight. Yield 2.13 g (93%). $^{31}P\{^1H\}$ NMR (solvent): δ 73.2 (s). ^1H NMR (d6-DMSO): δ 2.40 (s, 4H, PCH_2CH_2P), 4.20 (m, 8H, PCH_2OH)), 4.87 (s, 4H, CH_2OH). $^{13}C\{^1H\}$ NMR (d6-DMSO): δ 17.4 (s, PCH$_2$$CH_2$P), 56.1 (s, P$CH_2$OH). Anal. Calcd. for $C_{12}H_{32}C_{l2}FeO_8P_4$: C, 25.97; H, 5.81. Found: C, 26.23; H, 5.90. Single crystals suitable for X-ray diffraction were grown by removing an aliquot of the reaction mixture and allowing the product to quiescently precipitate overnight.

Synthesis of DHMPE·2BH$_3$. 2.5 mL of 2M BH_3Me_2S in THF (5.0 mmol) was added to a suspension of DHMPE (0.500 g, 2.34 mmol) in 30 mL THF. The mixture was stirred vigorously under nitrogen for 30 minutes. The solvent was removed under reduced pressure, and the product was recrystallized in air from 95% EtOH. The white microcrystalline solid was dried under vacuum. Yield: 0.352 g (62%). $^{31}P\{^1H\}$ NMR

(solvent): δ 21.3 (br). ^{1}H NMR (D_2O): δ 0.6 (q, 3H, B*H*$_3$), 1.92 (d, 4H,PC*H*$_2$C*H*$_2$P) , 4.05 (s, 8H,PC*H*$_2$OH). ^{13}C{^{1}H} NMR (d6-DMSO): δ 11.1 (d, P*C*H$_2$*C*H$_2$P), 54.2 (d, P*C*H$_2$OH). ^{11}B NMR (D_2O): δ -42.0 (s). Anal. Calcd. for $C_6H_{22}B_2O_4P_4$: C, 29.80; H, 9.17. Found: C, 29.97; H, 9.17. Single crystals suitable for x-ray crystallographic analysis were grown by evaporating an ethanolic solution in air overnight.

Reaction of $FeCl_2(DHMPE)_2$ with butylamine. To a suspension of $FeCl_2(DHMPE)_2$ in saturated NaCl was added BuNH2 (10 equiv) dropwise. As the amine was added, the solid $FeCl_2(DHMPE)_2$ dissolved, forming a dark red solution. 10 equiv of $BuNH_2$ were required to fully dissolve the complex. Over the course of 20 minutes, the color of the solution changed from maroon to orange. ^{31}P{^{1}H} NM: δ 93.3 (s). ESI-MS: +733 ($FeCl(DHMPE)_3^{+}$). The same reactivity was observed when 1% NaOH was used instead of $BuNH_2$.

Attempted reactions of Ru and Ni DHMPE complexes with butylamine. 8 equiv $BuNH_2$ was added to the DHMPE complex in absolute ethanol. The mixture was refluxed for 2 weeks with stirring. Periodically, aliquots were removed and analyzed by ^{31}P NMR spectroscopy. In all cases, no reaction was observed and the original complex remained intact.

Reactions of *trans*-$Fe(DHMPE)_2Cl_2$ in water. DHMPE (0.1072 g, 0.500 mmol) in 10 mL H_2O was added to a sample of *trans*-$Fe(DHMPE)_2Cl_2$ (0.2725 g, 0.491 mmol) with stirring. As the complex dissolved, the solution turned maroon, then slowly turned orange over 20 minutes. After 24 hours, the color of the solution stabilized as yellow-orange. ^{31}P{^{1}H} NMR revealed a series of peaks at aa.a-bb.b ppm, including a sharp singlet at + 93.3 ppm $(Fe(DHMPE)_3)^{2+}$.

Reaction of *trans*-$Fe(DHMPE)_2Cl_2$ with *n*-butylamine. *n*-$BuNH_2$ (0.56g, 7.6

mmol) was slowly added dropwise to a suspension of *trans*-$Fe(DHMPE)_2Cl_2$ (0.5165 g, 0.906 mmol) in 30 mL NaCl-saturated H_2O under heavy stirring. With the first drops, the supernatant turned maroon. After stirring for 5 minutes, no more undissolved *trans*-$Fe(DHMPE)_2Cl_2$, and the solution turned orange within 20 minutes.

Reactions of phosphines and phosphine-boranes with diethylamine. The phosphine or phosphine-borane was dissolved in d4-methanol (DHMPE and $DHMPE{\cdot}2BH_3$) or d6-ethanol (Ph_2PCH_2OH and $Ph_2PCH_2OH{\cdot}2BH_3$)**.** 1 equiv. of diethylaminewas added, and conversion to the aminomethylphosphine was monitored via ^1H NMR by following the appearance of PCH_2N methylene signals (2.9-3.1 ppm), which are significantly different than the PCH_2OH methylene signals (3.8-4.1 ppm). Conversion was also monitored by ^{31}P NMR , but as ^{31}P signals are not reliable for integration, the reaction progress was quantified via ^1H NMR.

4.3. Results

4.3.1. Synthesis of trans-$Fe(DHMPE)_2Cl_2$

The reaction of 2 equiv of 1,2-bis(dihydroxymethylphosphino)ethane (DHMPE) with 1 equiv of $FeCl_2{\cdot}4H_2O$ in THF gave, within seconds, a deep green solution. After stirring for five minutes longer, a lime-green solid precipitated, leaving behind a pale red solution. The solid is insoluble in all but strongly hydrogen-bond-accepting solvents (pyridine, DMF, and DMSO), and spectroscopic and X-ray analysis showed it to be *trans*-$Fe(DHMPE)_2Cl_2$ (eq. 4). The $^{31}P\{^1H\}$ NMR spectrum in DMSO showed a single sharp peak at +73.2 ppm, indicative of a *trans*-$FeCl_2P_4$ coordination geometry in the complex. Crystals suitable for X-ray diffraction were grown by removing an aliquot of the reaction mixture immediately after mixing the reactants and allowing the product to

quiescently precipitate from solution. X-ray crystallography confirmed the structure as *trans*-Fe(DHMPE)$_2$Cl$_2$ (Figure 2). The coordination geometry is pseudo-octahedral, with the iron and equatorial phosphines exactly coplanar, and the molecule is centrosymmetric (C_i symmetry). The chelate angle of the DHMPE ligand is 84.5°, and the axial chloride ligands are tilted 3.2° from orthogonal to the equatorial plane.

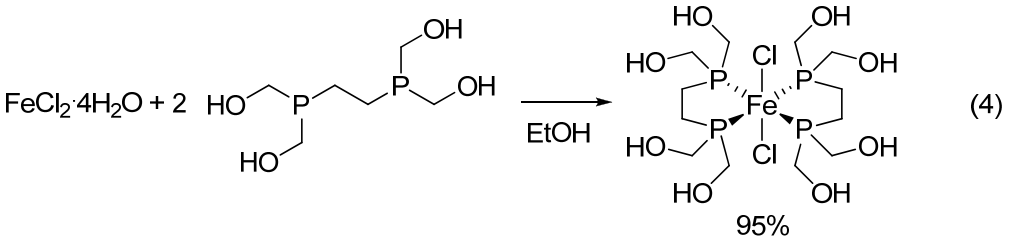

(4)

Two intramolecular hydrogen bonds are present in the molecule: an OH···O bond between two hydroxymethyl groups attached to the same phosphorus atom, and an OH···Cl hydrogen bond between each chloro ligand and one of the hydroxyl groups on the other phosphorus atom. In addition, examination of the crystal packing revealed three intermolecular hydrogen bonds (Figure 3), two of which are OH···O hydrogen bonds and one of which is an (admittedly weak) OH···Cl bond. These hydrogen bonds form an extended, three-dimensional hydrogen-bonding network in the crystal structure, which may account for the product's insolubility all but the most strongly hydrogen-bond-accepting organic solvents.

Figure 2. ORTEP plot of *trans*-Fe(DHMPE)$_2$Cl$_2$, showing intramolecular hydrogen bonds. Ellipsoids are drawn at 50% probability. Some hydrogen atoms have been omitted for clarity.

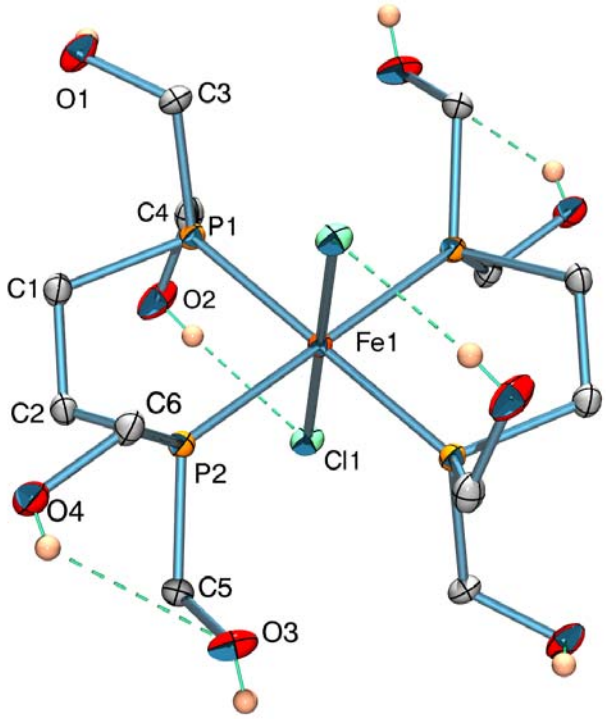

Figure 3. Packing of *trans*-Fe(DHMPE)$_2$Cl$_2$, showing the three-dimensional hydrogen-bonded network.

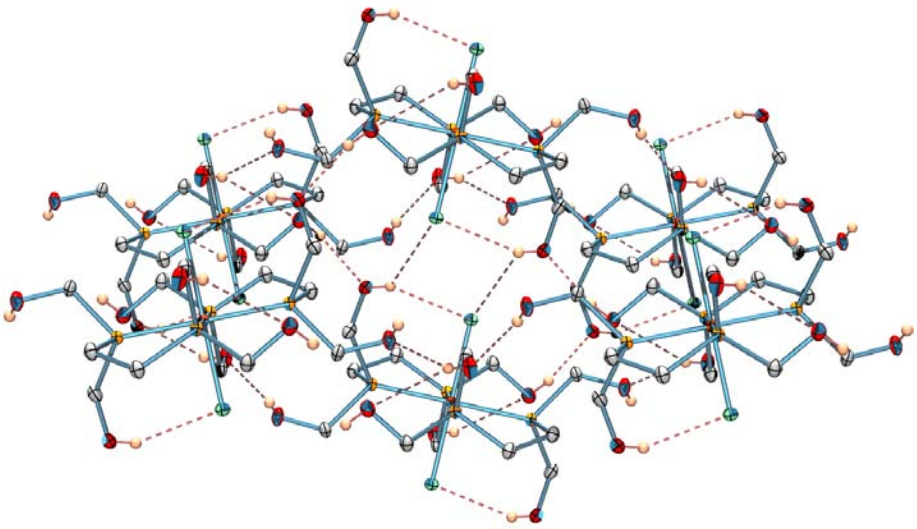

Table 1. Selected bond lengths (Å) and angles (°) for *trans*-$Fe(DHMPE)_2Cl_2$.

Fe(1)—P(1)	2.2486(6)	P(1)—Fe(1)—P(2)	84.48(2)
Fe(1)—P(2)	2.2311(6)	P(1)—Fe(1)—Cl(1)	89.27(2)
Fe(1)—Cl(1)	2.3624(6)	P(2)—Fe(1)—Cl(1)	86.93(2)

Table 2. Bond distances and angles for hydrogen bonds in *trans*-$Fe(DHMPE)_2Cl_2$.

	X-H---Y distance (Å)	X----Y distance (Å)	X-H---Y angle (°)	Strength
O(4)-H···O(3) (intramolecular)	2.758	3.135	122.1	Weak
O(2)-H···Cl(1) (intramolecular)	2.415	3.036	152.0	Weak
O(3)-H···O(2) (intermolecular)	1.944	2.673	167.0	Moderate
O(1)-H···O(4) (intermolecular)	2.123	2.731	167.5	Moderate
O(1)-H···O(4) (intermolecular)	2.169	2.733	111.8	Weak
O(2)-H···Cl(1) (intermolecular)	3.113	3.502	119.6	Weak

4.3.2. Reactivity of DHMPE Complexes with Primary Amines

The Mannich-type reaction between hydroxymethylphosphines and amines can be used to generate *cis*-octahedral iron complexes with self-assembling tetradentate phosphine ligands.[42-44] This type of reactivity suggested that macrocyclic phosphines might be synthesized by reacting $FeCl_2(DHMPE)_2$ with the appropriate primary amine, as shown in eq 3. To this end, $FeCl_2(DHMPE)_2$ was reacted with a variety of amines in a range of solvents. In most cases, ill-defined products were formed, which contained no

nitrogen according to elemental analyses. One exception, however, was the reaction between *n*-butylamine and a suspension of $FeCl_2(DHMPE)_2$ in saturated aqueous NaCl. The reaction mixture turned maroon within seconds, then to orange within 10 minutes. At least 8 equivalents of $BuNH_2$ were needed for the reaction to reach completion; undissolved $FeCl_2(DHMPE)_2$ was observed with any amount less than 8 equivalents. After the reaction was complete, ^{31}P NMR spectroscopy of the reaction solution showed a singlet at +93.3 ppm, indicative of a highly symmetric iron phosphine complex. ^{1}H NMR of the isolated product revealed the presence of butylammonium, indicating that the butylamine had acted as a base in the reaction. A control reaction, carried out by adding two drops of 10% NaOH to a suspension of $FeCl_2(DHMPE)_2$, gave the same product as the reaction with *n*-butylamine (Scheme 2).

Scheme 2. Reaction of *trans*-$Fe(DHMPE)_2Cl_2$ with amines or hydroxide.

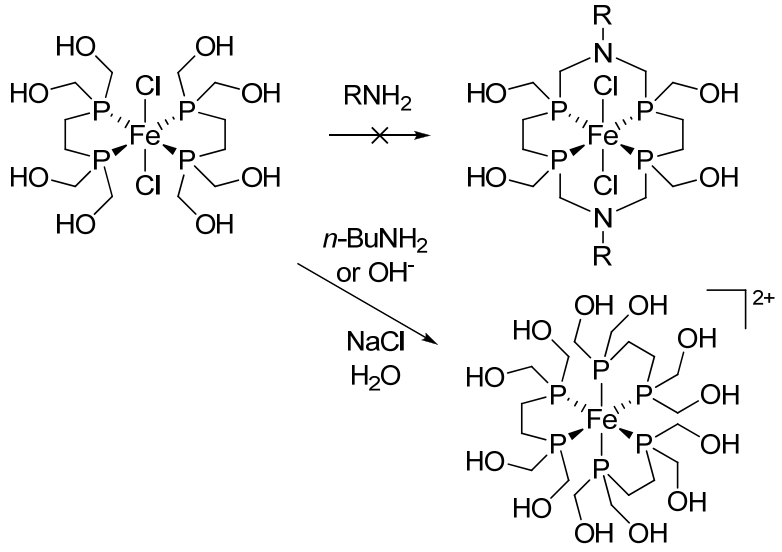

ESI-MS of the complex in MeOH showed a peak at +733 amu, which is consistent with the mass and isotope pattern of $[FeCl(DHMPE)_3]^+$. This evidence

indicates that the singlet at +93 ppm in the ^{31}P NMR is the highly symmetric cation $Fe(DHMPE)_3^{2+}$.

The phosphorus Mannich reaction was also attempted on $Ni(DHMPE)_2Cl_2$[20] and *trans*-$Ru(DHMPE)_2Cl_2$,[47] both previously reported complexes. The complexes were refluxed with *n*-butylamine in either water or absolute ethanol, and the reactions were monitored by ^{31}P NMR. In both cases, the complexes showed no reactivity towards the amine, even after weeks under reflux (Scheme 3).

Scheme 3. Summary of reactions of DHMPE complexes with primary amines.

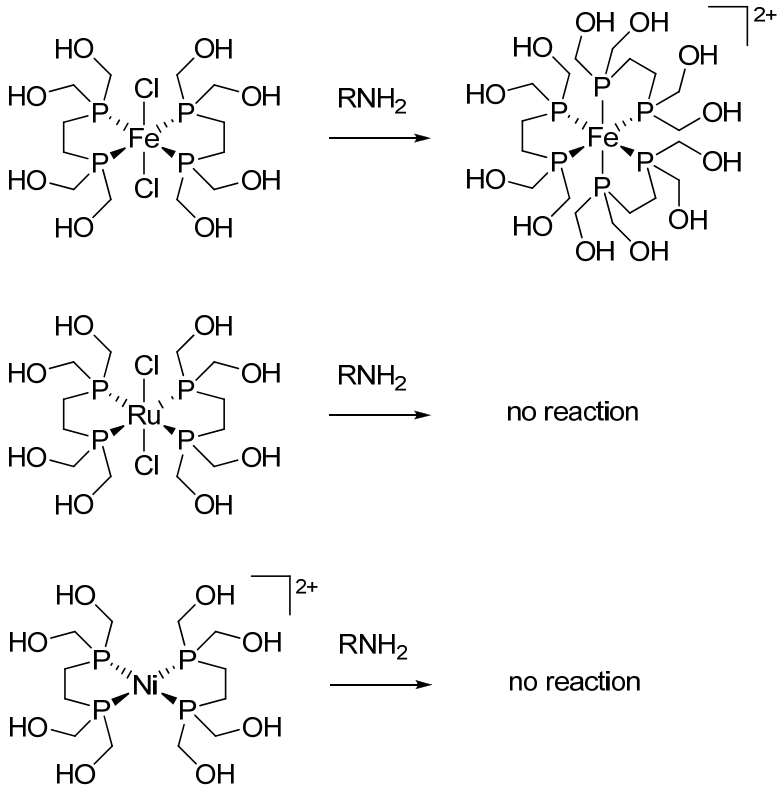

4.3.3. Synthesis and Mannich Reactivity of Borane-Protected Phosphines

To understand the absence of reactivity of hydroxymethylphosphine complexes toward the phosphorus Mannich reaction, the reactions of free and borane-protected

hydroxymethyl-phosphines with secondary amines were studied. The phosphine-borane adduct of DHMPE, as well as the adduct of diphenyl(hydroxymethyl)phosphine, Ph_2PCH_2OH were chosen as substrates for this study. (The Ph_2PCH_2OH ligand was chosen because it would react in a simple 1:1 stoichiometry with secondary amines.) The phosphine-borane adducts were prepared by reaction of each phosphine with stoichiometric quantities of borane-dimethylsulfide. $Ph_2PCH_2OH \cdot BH_3$ has previously been reported,[46] but DHMPE$\cdot 2BH_3$ is new. After treatment of DHMPE with $BH_3 \cdot Me_2S$, ^{31}P NMR of the initial reaction mixture showed two broad signals at +1.6 ppm and +25.6 ppm, of roughly equal intensity. The peak at +25.6 ppm corresponds to DHMPE$\cdot 2BH_3$; presumably the peak at +1.6 ppm corresponds to the singly-protected DHMPE$\cdot BH_3$. After evaporation of the solvent, only the +25.6 ppm peak was present. DHMPE$\cdot 2BH_3$ is air stable as a solid for up to two weeks. Single crystals of DHMPE$\cdot 2BH_3$ were grown by allowing a solution of the compound in ethanol to evaporate overnight. X-ray crystallography showed that the molecule is centrosymmetric (C_i symmetry; Figure 4). The P-B bond is 1.907 Å, an intermediate length for a phosphine-borane bond.[51] Like $FeCl_2(DHMPE)_2$, DHMPE$\cdot 2BH_3$ contains an extended intermolecular hydrogen-bonded network; however, in this case, the network is two-dimensional (Figure 5).

Figure 4. ORTEP plot of DHMPE·2BH_3. Ellipsoids are drawn at 50% probability. Some hydrogen atoms have been omitted for clarity.

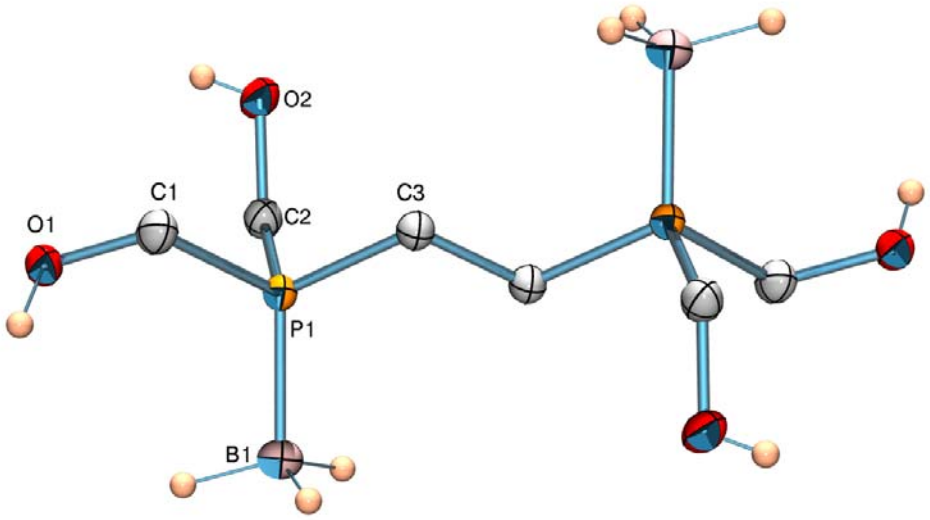

Figure 5. Packing of DHMPE·2BH_3 showing the two-dimensional hydrogen-bonded network.

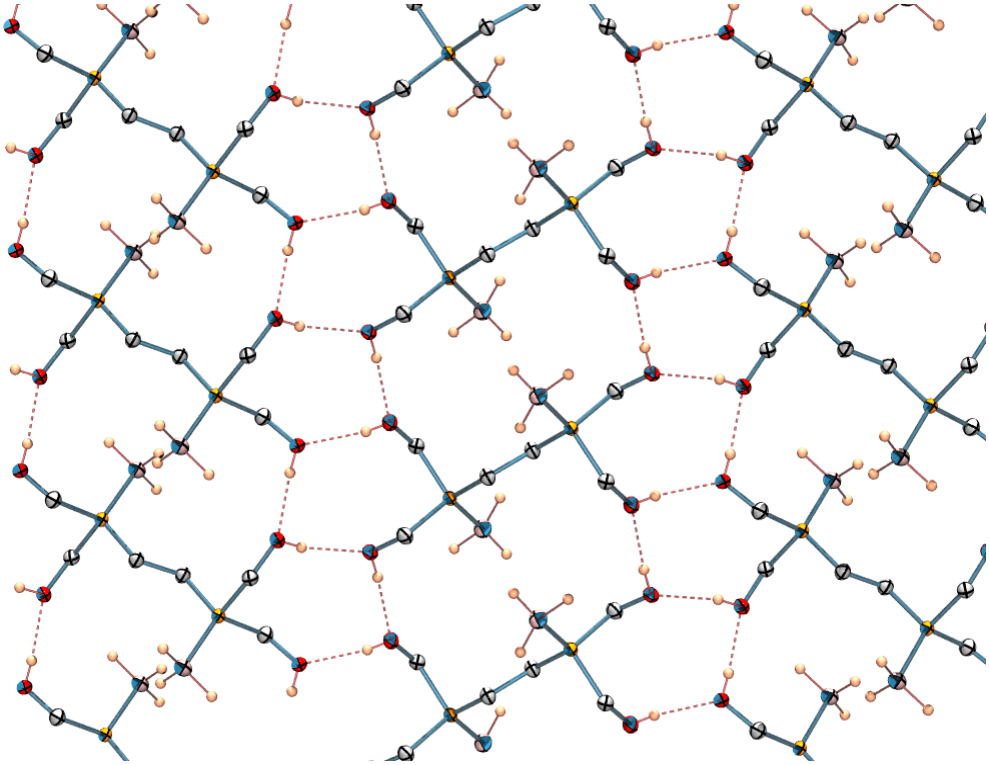

Table 3. Bond distances and angles for hydrogen bonds in DHMPE·$2BH_3$.

	X-H---Y distance (Å)	X----Y distance (Å)	X-H---Y angle	Strength
O(1)-H···O(2)	1.902	2.674	174.71	Moderate
O(2)-H···O(1)	1.988	2.687	167.30	Moderate

In order to study the phosphorus Mannich reaction of free and coordinated phosphines, NMR-scale reactions of Et_2NH with Ph_2PCH_2OH or DHMPE were carried out, as were reactions with the corresponding phosphine-boranes. The reactions were monitored by ^1H and ^{31}P NMR. DHMPE reacted with 1.2 equiv Et_2NH to generate various partially Mannich-reacted products, which were formed over the course of 8 h. In a separate experiment, treatment of DHMPE with 4 equiv Et_2NH resulted in complete conversion to $(Et_2NCH_2)_2PCH_2CH_2P(CH_2NEt_2)_2$. In the case of Ph_2PCH_2OH, the reaction proceeded over the course of 36 h to give $Ph_2PCH_2NEt_2$ (Figure 6).[i] In the case of $Ph_2PCH_2OH·BH_3$, the only product was $Ph_2PCH_2NEt_2$, apparently formed by deprotection of a small amount of the starting material. Over time, more $Ph_2PCH_2NEt_2$ was slowly formed, presumably due to continuing slow deprotection of the starting material, which was then able to react with the amine. It is important to note, however, that the Mannich-reacted phosphine-borane $Ph_2PCH_2NEt_2·BH_3$ was not observed. Likewise, DHMPE·$2BH_3$ showed no reaction after 2 days. These results are summarized in Scheme 4. The conclusion from these experiments is that the phosphine-borane adducts do not undergo the Mannich reaction with amines and that any Mannich-type

[i] Note that both $Ph_2PCH_2NEt_2$ and $(Et_2NCH_2)_2PCH_2CH_2P(CH_2NEt_2)_2$ have been previously reported[52,53]; however, they were previously synthesized by adding formaldehyde and Et_2NH to the primary or secondary phosphine in a single synthetic step.

product results from deprotection of the phosphine-borane.

Figure 6. Phosphorus Mannich reaction kinetic study.

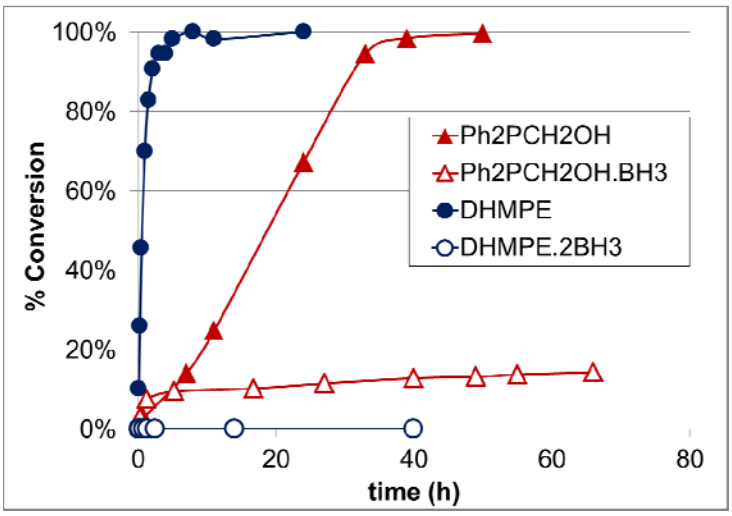

Scheme 4. Reactions of hydroxymethylphosphines with diethylamine.

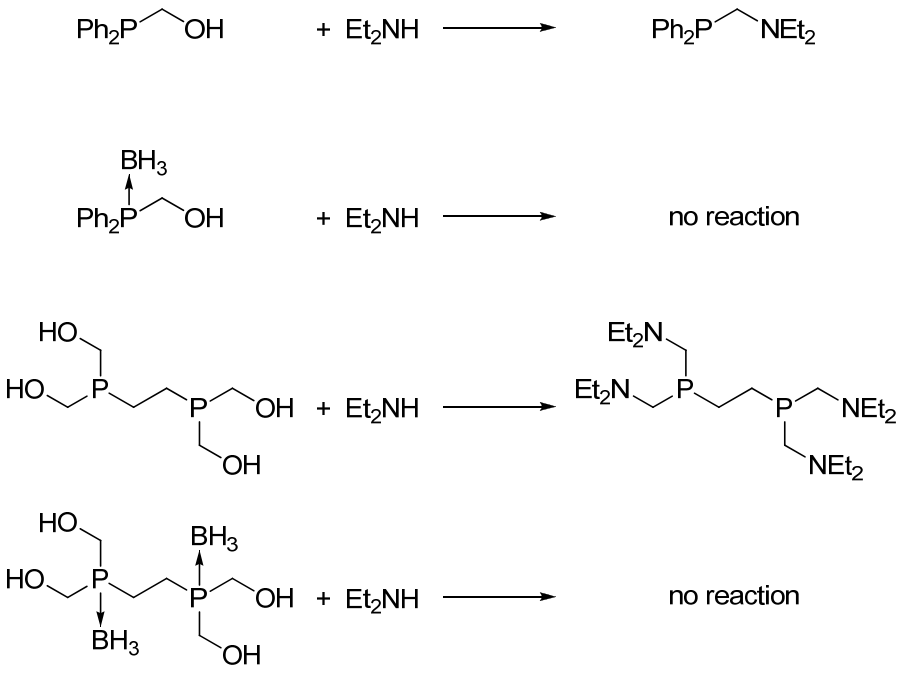

4.3.4. Aqueous Reactivity of $Fe(DHMPE)_2Cl_2$

Previous studies of $FeCl_2$ complexes containing the hydrophilic phosphine ligand DMeOPrPE (DMeOPrPE = 1,2-bis(dimethoxypropylphosphino)ethane)[54] showed that when green *trans*-$FeCl_2(DMeOPrPE)_2$ is added to water it initially transforms into the purple *trans*-$[Fe(DMeOPrPE)_2(H_2O)Cl]$ complex, then slowly decomposes into the orange homoleptic complex $[Fe(DMeOPrPE)_3]^{2+}$. Similarly, when solid *trans*-$Fe(DHMPE)_2Cl_2$ is added to water, a purple solution forms immediately, which changes to orange over the course of a few minutes. The expected decomposition product, $[Fe(DHMPE)_3]^{2+}$, should appear as a singlet in the ^{31}P NMR spectrum; however, the actual spectrum revealed a sharp singlet at +93ppm, along with a complicated mixture of peaks over a wide range of chemical shifts. Because there are only two equivalents of DHMPE in the starting complex, whereas the final complex requires three equivalents, the initial assumption was that an extra equivalent of DHMPE ligand might allow complete conversion to this complex. However, addition of *trans*-$Fe(DHMPE)_2Cl_2$ to an aqueous solution containing 1.5 equiv DHMPE yielded the same set of peaks in the ^{31}P NMR spectrum as in the absence of additional DHMPE. (Uncoordinated DHMPE was observed in the ^{31}P NMR spectrum, of course.)[ii]

ESI-MS of the solution from the addition of *trans*-$Fe(DHMPE)_2Cl_2$ to water revealed at least four sets of peaks.[iii] The first is m/z = 667, with an isotope pattern

---

[ii] Homoleptic iron(II) tris(bisphosphine) complexes have been prepared previously[55,56]; however, they usually require excess phosphine and the absence of competing ligands for complete conversion. Only in the case of DMeOPrPE does the homoleptic iron complex ($[Fe(DMeOPrPE)_3]^{2+}$) form exclusively when dissolved in water. As was previously observed, decomposition of $FeCl_2(DHMPE)_2$ in water is inhibited by the addition of chloride, and the complex is stable (although not soluble) in a saturated NaCl solution.

[iii] Although the homoleptic complex $[Fe(DHMPE)_3]^{2+}$ is not easily visible in the full spectrum, a zoomed-in scan confirms the presence of a peak at m/z = 348.7, with the correct isotope pattern for this complex (see Appendix C).

matching the formula $[C_{17}H_{45}FeO_{11}P_6]^+$. This formula is one carbon, one oxygen, three hydrogens, and one positive charge less than $[Fe(DHMPE)_3]^{2+}$. This species corresponds to $[Fe(DHMPE)_2((HOCH_2)_2PCH_2CH_2PCH_2OH)]^+$ (see the complex at m/z = 667 in Figure 7), which results from a loss of one of the hydroxymethyl arms on one of the DHMPE ligands. Presumably, this arm is not lost as $HOCH_2^+$ but rather as a molecule of formaldehyde and a proton.

Figure 7. ESI-MS of the decomposition of *trans*-$Fe(DHMPE)_2Cl_2$ in an aqueous solution containing excess DHMPE.

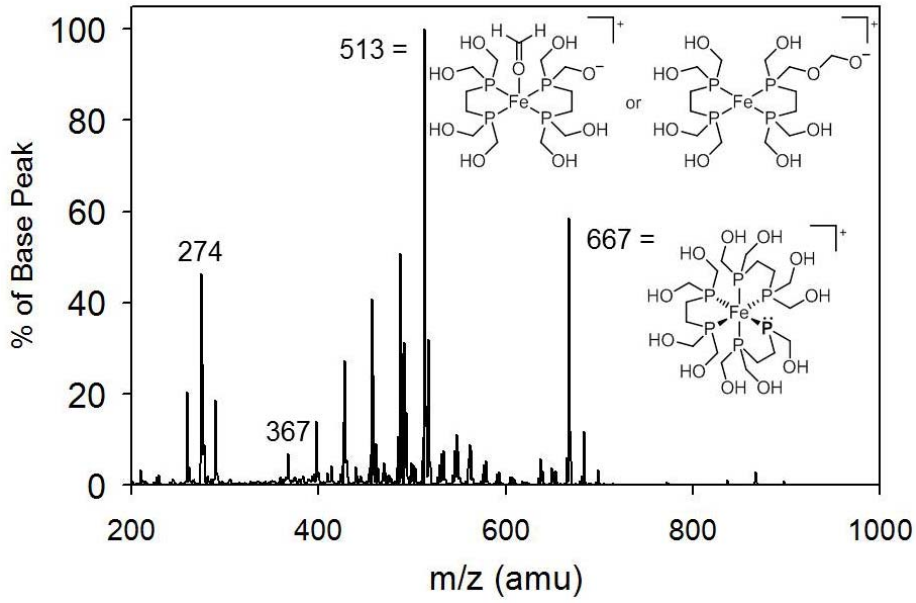

The second species is at m/z = 513 amu, which matches the formula $[C_{13}H_{33}FeO_9P_4]^+$. This species corresponds to $[Fe(DHMPE)_2(CH_2O)(-H)]^+$. Because of the low coordination number of this complex, the CH_2O may be present as coordinated formaldehyde; however, because formaldehyde is known to polymerize in water, it may also be added to the deprotonated oxymethyl group to form an oxymethoxymethyl group (see Figure 7).

A series of lower molecular weight peaks were present between m/z = 367 and 517 amu, each with mass differences of 30 amu. These correspond to fragments of $[Fe(DHMPE)_3]^{2+}$, with successive losses of between 6 and 11 formaldehyde molecules, as well as a proton.

The final series of peaks is found at m/z = 259, 274, and 289. The isotope patterns of these peaks indicate that they are +2 cations. Thus, the molecular weights of these species are 518, 548, and 578 amu. These masses correspond to fragments of $[Fe(DHMPE)_3]^{2+}$ with losses of 4, 5, and 6 CH_2O fragments.

All of these species indicate that in aqueous solution, the coordinated DHMPE ligand may lose one or more of its hydroxymethyl arms and that the resulting ligands are not fully protonated (Scheme 5). This observation suggests that elimination of formaldehyde from hydroxymethylphosphines is not inhibited upon coordination with a transition metal.

Scheme 5. Behavior of *trans*-$Fe(DHMPE)_2Cl_2$ in water.

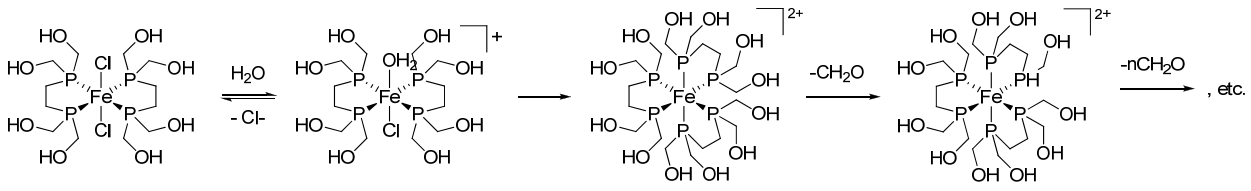

4.4. Discussion

The classical Mannich reaction (Scheme 6) is the reaction between an amine, an aldehyde (typically formaldehyde), and a nucleophile.[57] The amine and aldehyde are typically introduced first. They react to form a transient hydroxymethylamine, which is unstable and readily dehydrates to form a stable, isolable iminium ion. In the second

step, the nucleophile (the "Mannich substrate") is added, which attacks the iminium carbon to yield the product, which is known as a Mannich base. The Mannich substrate is often an enolized carbonyl compound; however, other nucleophiles such as amines and even phosphines can act as Mannich substrates.

Scheme 6. The (classical) Mannich reaction.

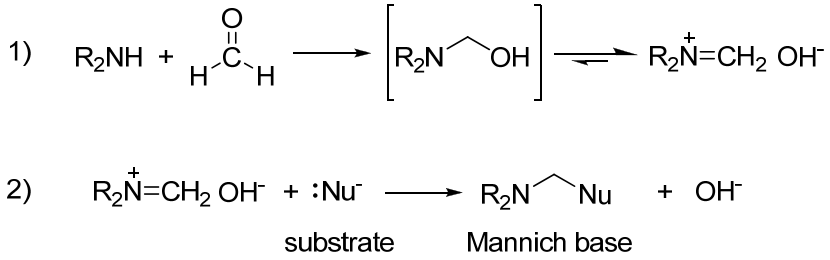

The *phosphorus* analog of the Mannich reaction involves the condensation of a hydroxymethyl-functionalized phosphine ($R_nP(CH_2OH)_{3-n}$) with an NH-functional amine (Scheme 7). The hydroxymethylphosphine starting material is typically synthesized from a PH-functional phosphine and formaldehyde. In contrast to hydroxymethylamines, hydroxymethyl-phosphines are stable and isolable.[iv]

[iv] Note that in practice the three reactants: NH-amine, formaldehyde, and PH-phosphine, can be added in *any* order to form the $R_2P\text{-}CH_2\text{-}NR'_2$ product, including in a one-pot reaction. This discussion is limited to reactions in which the hydroxymethylphosphine and amine are reacted directly.

Scheme 7. The phosphorus Mannich reaction. The classical Mannich reaction is shown for comparison.

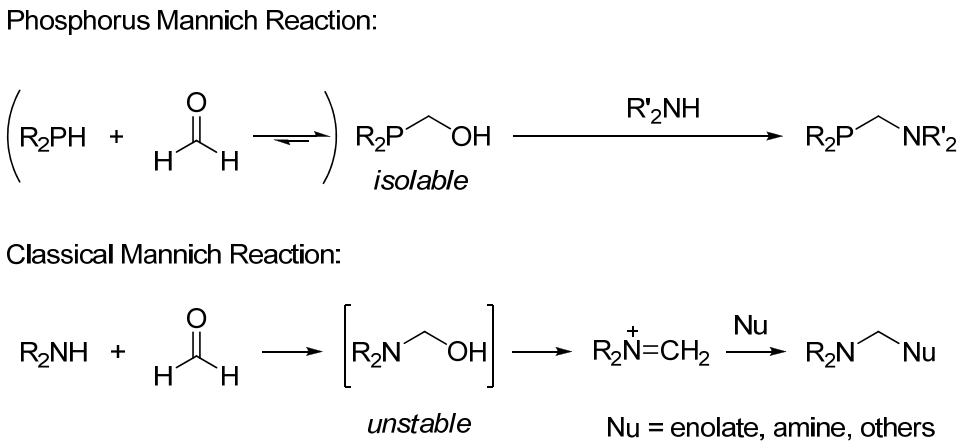

Although the phosphorus Mannich reaction is, on paper, analogous to the classical Mannich reaction, the mechanism has not been fully investigated. Specifically, the mechanism of the formal substitution of OH by NR_2 is unknown. It has been suggested that the reaction proceeds by decomposition of the hydroxymethylphosphine, generating a secondary phosphine and formaldehyde, followed by the standard Mannich pathway (Scheme 8).[25,58] This suggestion is supported by the observation that hydroxymethylphosphines are in equilibrium with secondary phosphine and formaldehyde. However, no other evidence for this mechanism has been reported in the literature.

Scheme 8. Previously-proposed mechanism for the phosphorus Mannich reaction (Mechanism A). The protonation and deprotonation steps are omitted for clarity.

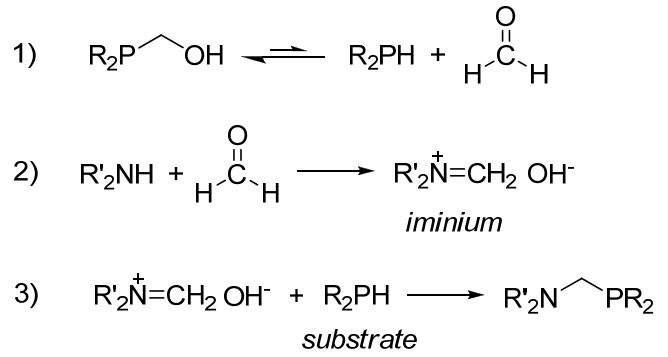

Although the phosphorus Mannich reaction typically occurs within hours at room temperature, none of the metal-DHMPE complexes studied in this paper reacted even after weeks at elevated temperatures (Scheme 3). This is especially surprising for the case of *trans*-$Fe(DHMPE)_2Cl_2$, which was observed to lose formaldehyde in aqueous solution (Step 1 of Mechanism A). Instead, the amine reacted as a base, dissolving the complex and causing it to decompose into $Fe(DHMPE)_3^{2+}$, but no phosphorus Mannich reaction occurred.

The currently-accepted mechanism shown in Scheme 8 (Mechanism A) does not match the observation that the Fe-DHMPE complexes *do* eliminate formaldehyde, but do not react with primary amines. To further investigate this reaction, the reactions of free and borane-protected hydroxymethylphosphines with secondary amines were investigated. In the borane-protected phosphines, the phosphorus lone pair is sequestered and prevented from participating in any further reactivity. BH_3 was chosen, as opposed to a transition metal complex, because of its small size and the inertness of the P-B bond. Also, secondary phosphine-boranes are known to react with aldehydes to form α-hydroxyphosphine-boranes.[46,59] This reaction is the microscopic reverse of the

first step in the proposed phosphorus Mannich reaction mechanism, so borane coordination should not prevent step 1 of Mechanism A. In addition, PH-functional phosphonates are known to react with imines under acidic conditions, indicating that Step 3 of this mechanism also does not require a free phosphorus lone pair.[60] Thus, if Mechanism A is correct, the rate of the reaction between R_2PCH_2OH and R'_2NH should be similar for phosphines and phosphine-boranes. However, if the phosphine lone pair is needed in the reaction mechanism, borane coordination will effectively inhibit the reaction. Along with the ligand of interest, DHMPE, Ph_2PCH_2OH was chosen for these studies because of the 1:1 stoichiometry of the Mannich reaction between it and diethylamine.

Experiments showed that coordination of the phosphine to BH_3 does indeed inhibit the phosphorus Mannich reaction (Figure 6). The mechanistic implication of this study is that a phosphine lone electron pair is necessary for the reaction to occur and that the previously proposed mechanism is probably not operating. Instead, an alternative mechanism for the phosphorus Mannich reaction (Mechanism B) is proposed, wherein the hydroxymethylphosphine eliminates hydroxide to form an electrophilic methylenephosphonium ion, followed by nucleophilic attack of the amine is shown in Scheme 9. Note that an unbonded phosphorus lone pair is required to form the P=C π-bond in this mechanism.

Scheme 9. Alternative mechanism for the phosphorus Mannich reaction (Mechanism B).

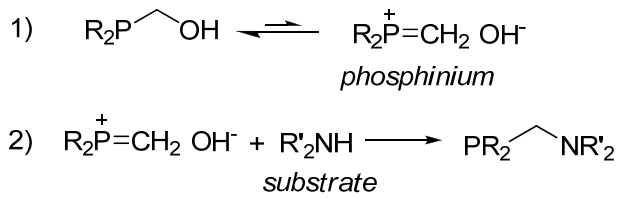

The key difference between Mechanisms A and B is the decomposition of the hydroxymethylphosphine. In Mechanism A, the hydroxymethylphosphine eliminates formaldehyde to re-generate a PH-functional phosphine. In Mechanism B, the hydroxymethylphosphine eliminates hydroxide to form a methylenephosphonium intermediate. In this manner, the hydroxymethyl*phosphine* acts analogously to the hydroxymethyl*amine* in the standard Mannich reaction, and the amine acts as the Mannich substrate. Both species eliminate hydroxide to form electrophilic intermediates, but the equilibrium between hydroxymethylphosphine and methylenephosphonium favors the hydroxymethylphosphine, whereas the equilibrium between hydroxymethylamine and iminium favors the iminium. The possibility of a methylenephosphonium intermediate might have initially been ignored because P=C multiple bonds are typically regarded as unstable. However, methylenephosphonium ions are known and have been generated previously,[61-63] although they are unstable and tend to dimerize.

Pathway 2 is also supported by the previously reported reaction of phosphorus Mannich bases with secondary phosphines to form methylenebisphosphines (R_2P-CH_2-PR'_2; eq 5).[52] The decomposition of the starting material by the microscopic reverse of Pathway 1, generating an iminium and a secondary phosphine, would not lead to the methylenebisphosphine product. However, the microscopic reverse of Pathway 2 would lead to a methylenephosphonium intermediate, which could then undergo nucleophilic attack by the secondary phosphine to generate the observed product. Mannich-type transformations involving methylenephosphonium intermediates are summarized in Scheme 10.

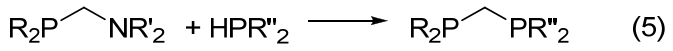

Scheme 10. Summary of phosphorus Mannich transformations via a methylenephosphonium intermediate (Pathway 2).

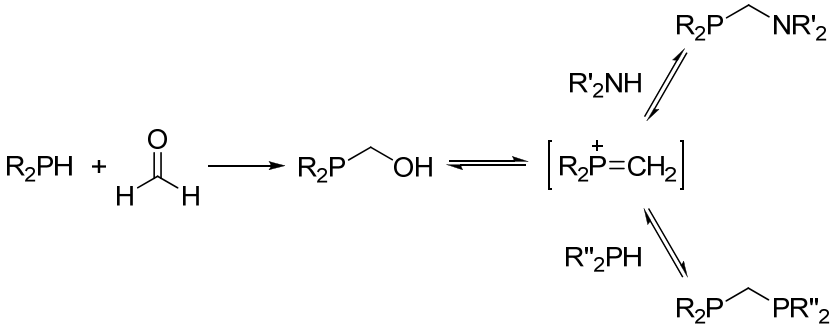

4.5. Conclusions

4.5.1. Implications of the New Mechanism for Self-Assembly Reactions Involving the Phosphorus Mannich Reaction

The experiments reported above indicate that the lone pair of electrons on the phosphorus atom are essential for the occurrence of the phosphorus Mannich reaction. Accordingly, the mechanism in Scheme 9 is proposed, wherein a methylenephosphonium intermediate is generated and then attacked by the amine nucelophile. In light of this new interpretation of the phosphorus Mannich reaction, the self-assembly reactions illustrated in Scheme 1 may occur by a combination of two reactions: a) non-templated reactions between free phosphines and amines, generating multidentate ligands which then coordinate to the metal template, and b) templated reactions on partially-formed multidentate ligands, where one or more phosphorus atom remains coordinated or where one or more metal-phosphine bonds break in order to react with the amine. As with most self-assembly processes, the multistep reactions involved in generating these ligands are most likely in equilibrium with many other Mannich products. The observed self-assembled products may be thermodynamically favored or they may be kinetic "traps",

inert to substitution due to the strong binding of the multidentate ligand, but not necessarily the most thermodynamically stable assembly possible.

4.5. Bridge

This chapter has described attempts at synthesizing macrocyclic iron(II)-phosphine complexes using the phosphorus Mannich reaction between a hydroxymethylphosphine-functionalized template complex and a primary amine. Since these complexes (and indeed all coordinated hydroxymethylphosphines) could not undergo the phosphorus Mannich reaction, we will turned our attention away from iron(II) as a template. Chapter V will explore the synthesis of copper(I) templates of water-soluble phosphines, their reactions with various linker reagents, and the demetallation of the resulting ligands from these complexes.

CHAPTER V

SYNTHESIS AND ALKYLATIONS OF FUNCTIONALIZED COPPER(I) PHOSPHINE COMPLEXES

Initial studies on the acylation reaction were performed by Laquishia Nelson and Andrew Hughett. Crystal structure determinations were performed by Lev N. Zakharov.

5.1. Introduction

As discussed in Chapter I, the most successful preparations of macrocyclic phosphines are by means of template syntheses, where a reactive phosphine (usually a bidentate secondary phosphine) is coordinated to a transition-metal center, then reacted with an electrophilic linking reagent to form the macrocyclic ligand complex. The most common metal ions used for the templates are d^8 metals such as Ni(II), Pd(II), or Pt(II), which typically form square-planar $[MP_4]^{2+}$ complexes. The metal template acts as a collecting point, placing the precursor ligands in the ideal geometry and stoichiometry for the macrocyclization step. In addition to acting as a collecting point, the metal complex also activates the ligand toward alkylation by increasing the acidity of the P-H bond and/or increasing the nucleophilicity of the resulting phosphido ligand (see Chapter II, Scheme 7).[1] Unfortunately, in most cases the resulting macrocyclic ligands bind so

strongly to these metals that removal of the metal from the ligand is difficult, if not impossible.

Our previous studies on iron complexes of bidentate secondary phosphines (Chapter II) showed that for these ligands, octahedral iron(II) suffers from two major drawbacks. First, the coordination of these ligands to $FeCl_2$ generates *cis*-octahedral FeP_4Cl_2 complexes, because of a synergistic π-donation / π-acceptance between the chloro ligands and the secondary phosphine groups, which is maximized when the phosphine is coordinated *trans* to the chloro ligand. This problem of geometry could be overcome by substitution of the chloro ligands with acetonitrile to generate *trans*-octahedral $[FeP_4(MeCN)_2]^{2+}$ complexes, which place the phosphines in the correct geometry for macrocyclization. Unfortunately, neither these complexes nor the *cis*-Fe(bisphosphine)$_2$Cl$_2$ complexes are reactive towards alkylation. This is presumably because of decreased electron-density of the d^6 Fe(II) metal compared to the typical d^8 metals used in most macrocyclizations, which decreases the nucleophilicity of the phosphido ligands after deprotonation.

A few examples of tetraphosphine macrocycles synthesized around d^{10} copper(I) templates have been reported in the literature (see Chapter I, Schemes 29 and 30).[2,3] In addition to being easily alkylated by difunctional alkyl halides, the resulting macrocyclic ligands can be liberated from the Cu(I) metals by treatment with either cyanide[2] or hydrogen sulfide.[3] Demetallation using H_2S was conducted in the presence of oxygen; the copper precipitated from the reaction as Cu_2S, and the ligands were oxidized to the tetra(phosphine oxide), which could be reduced back to the macrocyclic phosphine by treatment with phenylsilane.

In light of these reports, we have attempted to synthesize water-soluble macrocyclic phosphine ligands around Cu(I) templates, in order to eventually demetallate these ligands and coordinate them to Fe(II) (Scheme 1). This chapter reports on the syntheses of the template complexes, their alkylations with various electrophiles, and demetallation of the resulting ligands.

Scheme 1. Planned synthesis of iron(II) phosphine macrocycles from Cu(I) templates.

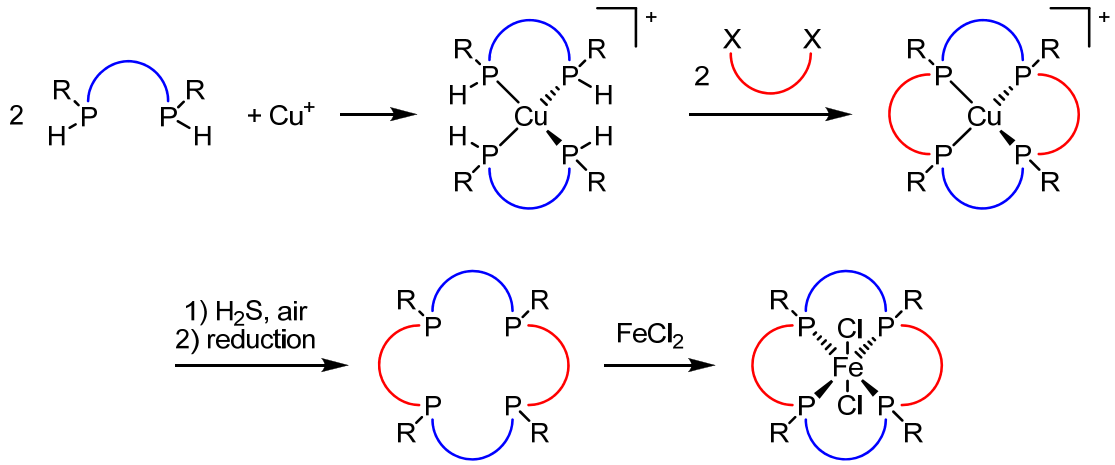

5.2. Experimental

5.2.1. Materials and Instrumentation

Unless otherwise noted, all experimental procedures were performed under inert (N_2) atmosphere, using standard Schlenk and glovebox techniques. Commercially-available reagents were used as received. MPPP was purchased from Strem Chemical Co. MPPE was synthesized according to literature procedures.[4] HPLC-grade THF and MeCN (Burdick and Jackson) were dried and deoxygenated by passing them through commercial columns of CuO, followed by alumina under an argon atmosphere. NMR

spectra were obtained on a Varian Unity/Inova 500 spectrometer operating at a frequency of 500.62 MHz (^{1}H) or 202.45 MHz (^{31}P). ESI mass spectra were obtained using a Thermo Finnigan LCQ Deca XP Plus ESI Mass Spectrometer using THF as the solvent. MALDI mass spectra were obtained using a Waters Q-ToF Premier MALDI/ESI Tandem Mass Spectrometer by evaporating a solution of 2',4',6'-trihydroxyacetophenone (THAP) as the matrix, followed by evaporation of a solution of the analyte in THF.

5.2.2. X-ray Crystallography

Diffraction intensities for $[Cu_2(DHMPE)_4]Cl_2$ were collected at 173(2) K on a Bruker Apex CCD diffractometer using MoKα radiation λ= 0.71073 Å.[5] Space groups were determined based on systematic absences. Absorption corrections were applied by SADABS.[6] The structure was solved by direct methods and Fourier techniques and refined on F^2 using full matrix least-squares procedures. All non-H atoms were refined with anisotropic thermal parameters. The H atoms were treated in calculated positions and refined in a rigid group model, except the H atoms in terminal –OH groups involved in H-bonds which were found on the residual density map and refined with isotropic thermal parameters and with restrictions; the O-H distance of 0.97 Å was used in the refinement as a target for the corresponding O-H bonds. It was found that one of CH_2OH groups in $[Cu_2(DHMPE)_4]Cl_2$ is disordered over two positions in the ratio 0.77/0.23. The H atom at the O atom in this disordered CH_2OH group was refined in the calculated position in a rigid group model. The H atom at the O atom in a solvent CH_3OH molecule was not found and has not been taken into consideration in the refinement. All OH groups in the cation together with the solvent methanol molecule and the Cl anion form in the crystal structure of $[Cu_2(DHMPE)_4]Cl_2$ a network of H-bonds. All calculations were

performed by the Bruker SHELXTL (v. 6.10) package.[7]

Crystallographic Data for $[Cu_2(DHMPE)_4]Cl_2$: $C_{26}H_{72}Cl_2Cu_2O_{18}P_8$, M = 1118.58, 0.16 x 0.14 x 0.03 mm, T = 173(2) K, monoclinic, space group *C*2/*c*, a = 29.353(13) Å, b = 10.653(5) Å, c = 18.737(9) Å, β = 125.771(8)°, V = 4754(4) Å^3, Z = 4, Z'= 0.5, D_c = 1.563 Mg/m^3, μ = 1.340 mm^{-1}, $F(000)$ = 2336, $2\theta_{max}$ = 50.00°, 22316 reflections, 4196 independent reflections [R_{int} = 0.0800], R1 = 0.0427, wR2 = 0.0910 and GOF = 1.025 for 3211 reflections (291 parameters) with $I>2\sigma(I)$, R1 = 0.0630, wR2 = 0.1014 and GOF = 1.025 for all 4196 reflections, max/min residual electron density +0.757/-0.488 eÅ^3.

5.2.3. Methods

General Synthesis of complexes 1-4. 2 equiv secondary bisphosphine and 1 equiv CuCl were dissolved in 8 mL THF and the reaction mixture was stirred for 5 min, then 1 eq NaX (X = PF_6 or BPh_4) in 8 mL THF was added to the copper-phosphine solution. The reaction mixture was stirred for 3 h at RT, precipitating NaCl as a white solid. The mixture was filtered through a celite plug and the solvent was removed under reduced pressure. The crude product was triturated with heptane (**1** and **2**) and/or recrystallized from heptane/THF (**3** and **4**).

$[Cu(MeOPrPE)_2]PF_6$ (1). Used 2.259 g (9.48 mmol) MeOPrPE, 0.471 g (4.76 mmol) CuCl, and 0.803 g (4.78 mmol) $NaPF_6$. Yield: 3.24 g of an off-white viscous oil (99%). ^{31}P: δ -41.1ppm (br). ESI-MS: 539 amu (m+).

$[Cu(MeOPrPP)_2]PF_6$ (2). Used 0.747 g (2.96 mmol) MeOPrPP, 0.147 g (1.46 mmol) CuCl, and 0.245 g (1.46 mmol) $NaPF_6$. Yield: 0.9727 g (93%) of an off-white

viscous oil. ^{31}P: δ -50.5 ppm (br). ESI-MS: 567 amu (m+).

[Cu(MPPE)$_2$]BPh$_4$ (3). Used 0.374 g (1.15 mmol) MPPE, 0.080 g (0.80 mmol) CuCl, and 0.263 g (0.079 mmol) $NaPF_6$. Yield: 0.5287 g (80%) of a white granular solid. ^{31}P: δ -31 ppm (br). ESI-MS: 555 amu (m+).

[Cu(MPPP)$_2$]BPh$_4$ (4). Used 0.673 g MPPP (2.58 mmol), 0.129 g CuCl (1.30 mmol), and 0.420 g $NaBPh_4$ (1.23 mmol). Yield: 0.8737 g (75%) of a white granular solid. ^{31}P: δ -42.1 ppm (br). ESI-MS: 583 amu (m+).

General synthesis of complexes 5-7. 2 equiv 1,3-dibromopropane and 10 eq. K_2CO_3 were added to a solution of the copper template in 10 mL THF. A condenser was attached and the mixture was refluxed until the reaction was complete. Work-up was conducted in air: the reaction mixture was filtered through a celite plug, the solvent was removed under reduced pressure, and the product was dried under vacuum overnight.

5. Used 0.155 g **1** (0.227 mmol), 0.099 g 1,3-dibromopropane (.049 mmol), and 0.308 g K_2CO_3 (2.22 mmol). Yield: 0.973 g (56%) of an off-white viscous liquid. ^{31}P: δ -1.67 ppm (br). ESI-MS: 619 amu (m+).

6. Used 0.251 g **2** (0.352 mmol), 0.149 g 1,3-dibromopropane (0.738 mmol), and 0.559 g K_2CO_3 (4.04 mmol). Yield: 0.1661g of an off-white oil (56%). ESI-MS: 647 amu (m^+)

7. Used 0.301 g (0.334 mmol) **4**, 0.139 g (0.688 mmol)DBE, and 0.464 g (3.36 mmol) K_2CO_3. Yield: 0.214 g (65%) of a white solid. ^{31}P: δ -15 ppm (br). ESI-MS: 663 amu (m+).

Demetallation of Complexes 5-7. The complex was dissolved in 10 mL THF, and added to a solution of 10 eq. NaSH-hydrate in 30 mL absolute EtOH**.** The mixture

was refluxed for 24h, forming Cu_2S as a black precipitate. The reaction mixture was cooled to RT, filtered through a celite plug, then the solvent was removed under reduced pressure, yielding a yellow-brown solid. The product was dissolved in THF and the solution was filtered from the excess NaSH. The crude product was isolated as a brown oil by removal of the solvent under reduced pressure, dissolved in CH_2Cl_2, filtered through a celite plug, then the solvent removed under reduced pressure to yield an off-white product. ^{31}P NMR data for compounds **8-10: 8:** ^{31}P: δ 51.9 ppm (s). **9:** ^{31}P: δ 49.2 ppm (s). **10:** ^{31}P: δ +44.8 ppm (s).

Reduction of compound 8. 8.3 mL of a 2.4 M $LiAlH_4$ solution (20 mmol) in THF was added to a solution of 0.535 g **8** in 8 mL THF. The reaction mixture was refluxed for 5 days, then quenched with 6 mL *i*-PrOH. ^{31}P: δ -26.7 ppm (s).

Synthesis of Complex 11. 0.257 g dimethylmalonyl chloride was added to a solution of 0.661 g **3** (0.756 mmol) in 10 mL THF. Addition of 0.319 g triethylamine (3.16 mmol) led to a yellowing of the solution. The reaction was stirred for 45 minutes, resulting in a deep yellow solution and a white precipitate. The mixture was filtered through a frit (in air) to remove Et_3NHCl, then the solvent was removed under reduced pressure. The crude product was recrystallized from EtOH, yielding 0.261 g of a yellow granular solid (32%). ^{31}P: δ +9 ppm (br). ESI-MS: 747 amu (m+).

Synthesis of $Cu_2(DHMPE)_4Cl$ (12). 0.128 g CuCl (2.34 mmol) was added to a solution of 0.551 g DHMPE (4.67 mmol) in 30 mL MeOH. The reaction was stirred for 1.5 h, and the solvent was removed in vacuo yielding 0.584 g (86%) of a white, air-stable solid. ^{31}P NMR: δ +10.6 ppm (br). ESI-MS: 491 amu (m+).

Synthesis of $Cu_2(DHMPE)_4PF_6$ (14). 0.065 g CuCl (0.66 mmol) was added to a

suspension of 0.270 g DHMPE (1.26 mmol) in 30 mL THF. ^{31}P: δ +10 ppm (br). ESI-MS: 491 amu (m+).

5.3. Results and Discussion

5.3.1. Synthesis of Copper(I) Secondary Phosphine Templates

In order to synthesize Cu(I) templates with water-soluble phosphines, the hydrophilic secondary phosphine ligands MeOPrPE and MeOPrPP were coordinated to Cu(I) by reaction of these ligands with CuCl in THF, and using $NaPF_6$ or as a halide abstractor to form templates **1** and **2** (Scheme 2). Coordination of the phosphines was confirmed by $^{31}P\{^1H\}$ NMR, where the chemical shifts of the uncoordinated phosphines moved ~20 ppm upfield from the free ligands(-41.1 ppm for **1** and -50.5 ppm for **2**). The ^{31}P signals are significantly broadened because of coupling with NMR-active, quadrupolar ^{63}Cu and ^{65}Cu nuclei (both spin 3/2, 69% and 31% abundance, respectively). In some copper-phosphine complexes this broadening can be minimized by obtaining the spectra at high temperature,[8] but the spectra of these complexes do not change between 25 °C and 90 °C. These NMR signals indicate coordination of the phosphines to Cu(I), but do not necessarily confirm the $[CuP_4]^+$ structure. Instead, the $[CuP_4]^+$ structures were confirmed by ESI-MS analysis (**1:** m^+ = 539 amu; **2:** m^+ = 567 amu).

Scheme 2. Syntheses of Cu(I) template complexes.

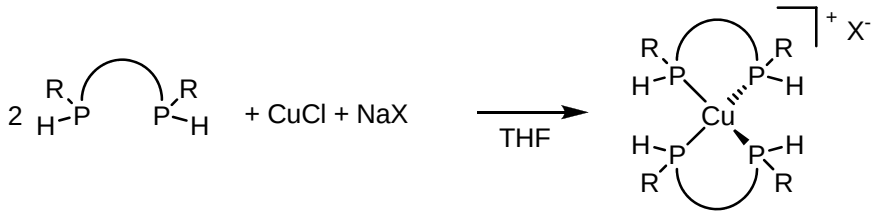

	=	R =	X =	
1:	$(CH_2)_2$	$(CH_2)_3OMe$	PF_6^-	(99%)
2:	$(CH_2)_3$	$(CH_2)_3OMe$	PF_6^-	(93%)
3:	$(CH_2)_2$	Ph	BPh_4^-	(80%)
4:	$(CH_2)_3$	Ph	BPh_4^-	(73%)

Like the Fe(II) complexes of MeOPrPE and MeOPrPP (see Chapter I), both **1** and **2** are isolated as viscous liquids, and repeated attempts at obtaining solid samples or single crystals for X-ray analysis have been unsuccessful. In order to obtain solid products which would be more likely to form X-ray quality crystals, complexes of the hydrophobic ligands MPPE and MPPP were also synthesized, using the $NaBPh_4$ as the halide abstractor to form complexes **3** and **4**. These complexes were also characterized by ^{31}P NMR and ESI-MS, and are indeed isolated as crystalline solids. Although previous reports of such complexes state that they are air-stable, some oxidation of the copper was observed when these products were worked up in air, as evidenced by a blue coloration of the solutions. Therefore, these complexes were handled under inert atmosphere.

The sources of Cu(I) for $[CuP_4]^+$ complexes are typically complexes with weak ligands and a weakly-coordinating anion, such as $Cu(MeCN)_4PF_6$ or $CuOTf{\cdot}C_6H_6$. These complexes are expensive ($7-70/g, $0.02-0.12/mol) compared to simple copper halide salts. Copper-halide starting materials are often avoided because of the possibility that

the halides may remain coordinated as terminal or bridging ligands, forming complexes of various structures such as those shown in Figure 1.[9-14] However, for all the ligands reported herein, the $[CuP_4]^+$ complexes could easily be obtained by reaction with CuCl ($0.07/g, $0.0007/mol) and $NaPF_6$ ($1.88/g, $0.01/mol) or $NaBPh_4$ (($2.67/g, $0.008/mol) as a halide abstractor in one pot. The byproduct of these reactions is NaCl, which can be easily removed from the reaction mixtures by filtration.

Figure 1. Structures of copper(I) halide complexes with bidentate phosphine ligands.

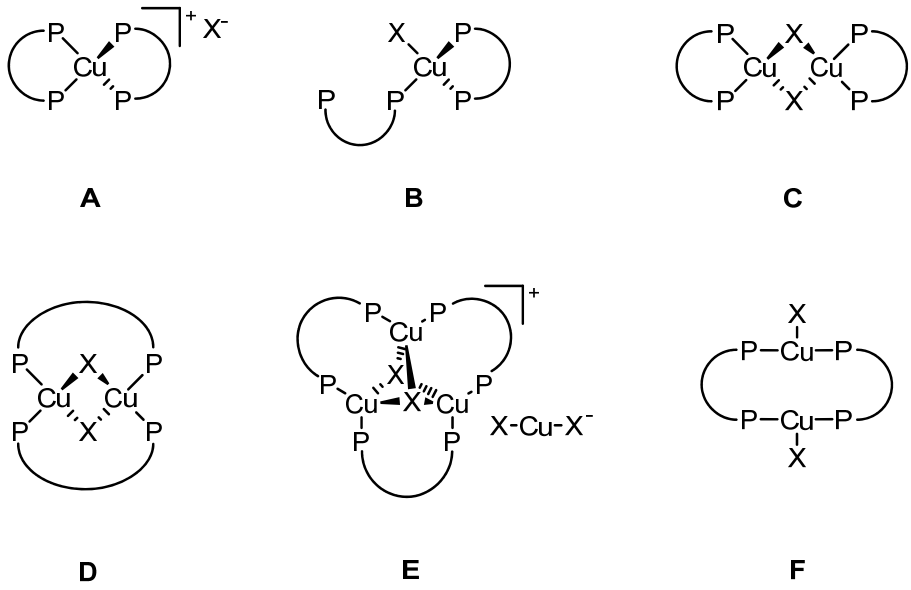

5.3.2. Reactions of Copper Templates with 1,3-Dibromopropane

Complexes **1**, **2**, and **4** reacted with 2 equiv 1,3-dibromopropane in the presence of K_2CO_3 in THF at reflux to form complexes **5-7** (Scheme 3). With complex **4**, the reaction mixture turned yellow soon after heating, indicating deprotonation of the phosphine ligands. After 4 h the yellow color faded, indicating that the reaction was

complete. Alkylation of the coordinated secondary phosphines was confirmed by upfield shifts in the ^{31}P NMR spectra (-15 ppm vs. -41 ppm for **4**). Complexes **1** and **2** were less reactive: no yellow color was observed during the reaction, and alkylation of these templates required 2-3 days to reach completion. This difference in reactivity is attributed to differences in acidity of the coordinated secondary phosphines: the electron-withdrawing phenyl groups in MPPP allow **4** to be more acidic than **1** and **2**, which contain electron-donating methoxylpropyl groups.

Scheme 3. Alkylations of complexes **1-4**.

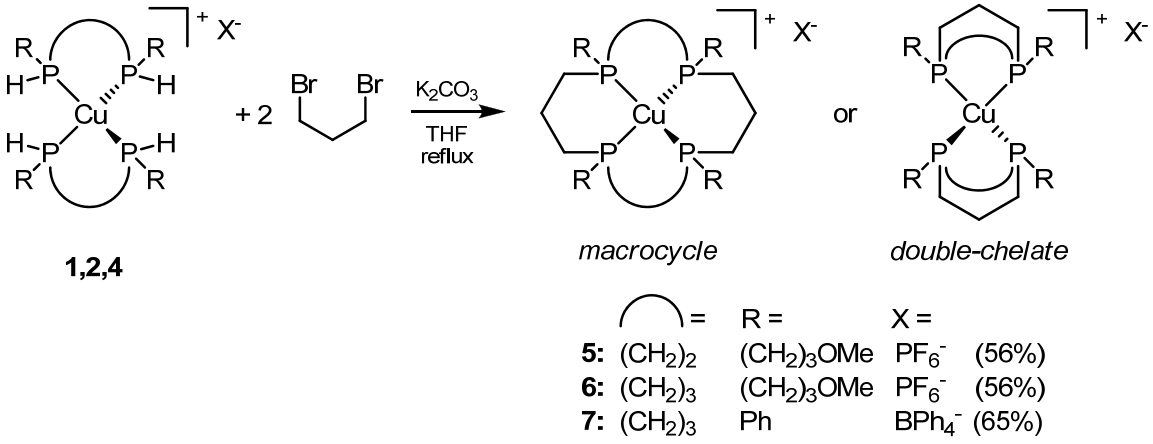

	=	R =	X =	
5:	$(CH_2)_2$	$(CH_2)_3OMe$	PF_6^-	(56%)
6:	$(CH_2)_3$	$(CH_2)_3OMe$	PF_6^-	(56%)
7:	$(CH_2)_3$	Ph	BPh_4^-	(65%)

ESI-MS of complexes **5-7** all show base peaks consistent with the masses of the macrocyclic complexes, indicating complete alkylation with the linking reagents (Table 1). However, this does not conclusively confirm the macrocyclic structures. Instead of 1,3-dibromopropane reacting *between* each bidentate phosphine ligand to form a macrocycle, it may instead bridge *across* an individual ligand to form double-chelate products. These double-chelate complexes are isomers of the macrocyclic complexes, so they cannot be definitively distinguished by mass spectroscopy. Also, spectroscopic

characterization cannot distinguish between these isomers.

Table 1. ESI-MS data for copper(I)-phosphine complexes.

	#	$(CH_2)_n$	R	m+ Formula	m/z (amu)
Templates	**1**	2	$MeO(CH_2)_3$	$[C_{20}H_{48}CuO_4P_4]^+$	539
	2	3	$MeO(CH_2)_3$	$[C_{22}H_{52}CuO_4P_4]^+$	567
	3	2	Ph	$[C_{28}H_{32}CuP_4]^+$	555
	4	3	Ph	$[C_{54}H_{36}CuP_4]^+$	583
Alkylated	**5**	2	$MeO(CH_2)_3$	$[C_{26}H_{56}CuO_4P_4]^+$	619
with	**6**	3	$MeO(CH_2)_3$	$[C_{28}H_{60}CuO_4P_4]^+$	647
$Br(CH_2)_3Br$	**7**	3	Ph	$[C_{36}H_{44}CuP_4]^+$	663
Acylated	**11**	2	Ph	$[C_{38}H_{40}CuO_4P_4]^+$	747

The most common conditions for macrocyclization reactions are refluxing ethanol with excess K_2CO_3 as the base. Initial alkylations of complexes **1-4** were performed according under these conditions, with THF added to increase the solubility of the template complexes. However, thorough analysis of the ESI-MS spectrum of the products from these reactions showed a variety of additional products at m + 40, m + 44, m + 86, and m + 120, as well as various multiples and/or combinations of these added masses (Figure 2). These can be attributed to incomplete reaction of the dibromopropane, resulting in the presence of 3-bromomethyl groups (m + 120),[i] as well as well as three different side-reactions (Scheme 4): 1) elimination of HBr from the bromopropyl group, forming an allyl group (m + 40), 2) formal substitution of ethoxide for bromide, forming an ethoxypropyl group (m + 86), and 3) oxidative coupling of ethanol, forming an ethylphosphinite (m + 44).

[i] These assignments are supported by the isotope patterns of each species: species containing only Cu, C, P, and O display m+2 peaks of ~45% intensity due to the presence of ^{65}Cu, whereas species which also contain Br show m+2 peaks of ~140% intensity due to the presence of either ^{65}Cu or ^{81}Br.

Figure 2. ESI mass spectrum of the reaction products of complex **4** with 1,3-dibromopropane and K_2CO_3 in ethanol/THF. Structures of the partially-alkylated product (623 amu) are shown for reference.

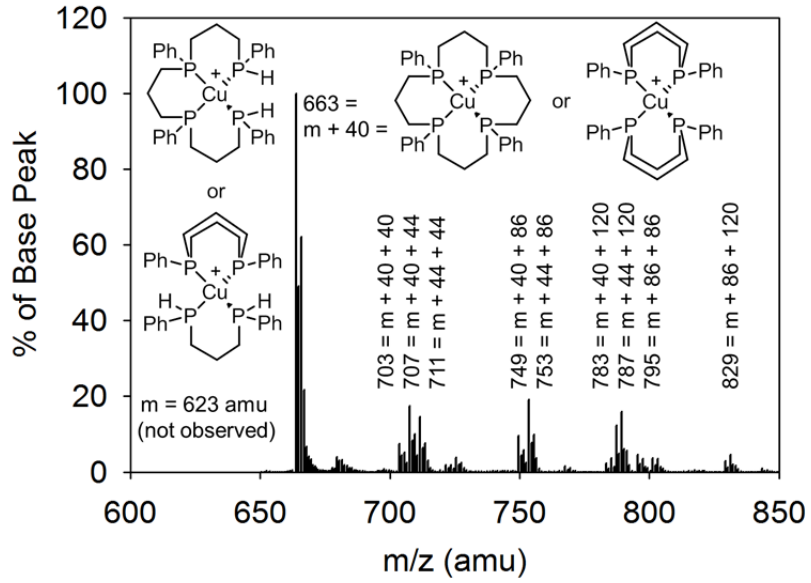

Scheme 4. Summary of side-reactions observed by ESI-MS when alkylations are run in ethanol.

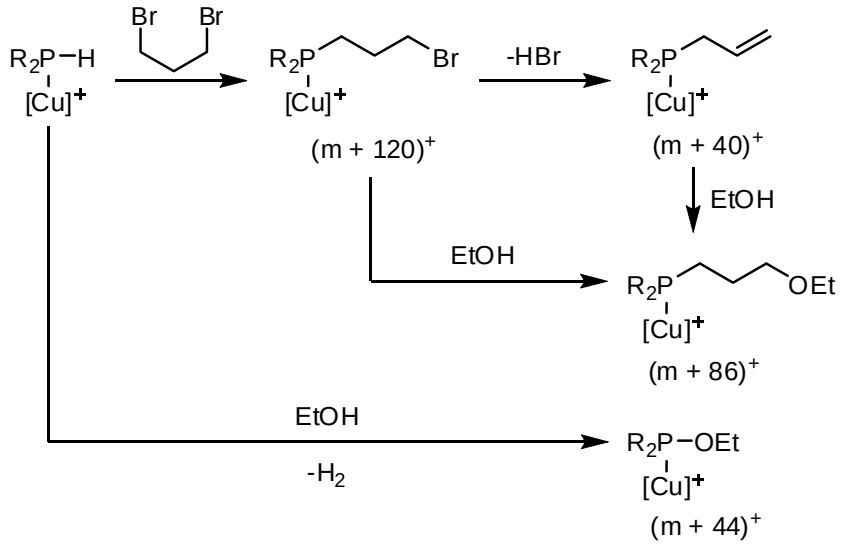

In the cases of partial substitution and/or elimination of HBr, the bromopropyl and allylphosphine groups may still act as linkers for those complexes which still contain

another secondary phosphine group. However, for reactions of the complexes with ethanol (etherification and oxidative coupling), neither of the resulting groups are reactive toward the linking reaction, and the leftover secondary phosphine groups are free to undergo these side reactions as well. When the alkylation reactions were conducted using pure THF as the solvent, these side-products were not observed. Based on these results, it is surprising that nearly all of the previously published template macrocyclizations of tetradentate phosphine macrocycles have used ethanol as the solvent!

5.3.3. Demetallation

In order to remove the metal, complexes **5-7** were refluxed overnight with 10 eq. NaSH-hydrate in ethanol/THF. Demetallation was observed by the formation of Cu_2S as a black precipitate. Oxidation of the ligands was observed by ^{31}P NMR spectroscopy, with the signals shifting significantly downfield (~+35 ppm) and sharpening of the signals, indicating that they were no longer coupled to the quadrupolar Cu nuclei. In most cases, a sharp singlet predominated in the ^{31}P spectrum, indicating that the products are highly symmetric.

Scheme 5. Oxidative demetallation of complexes **5-7**.

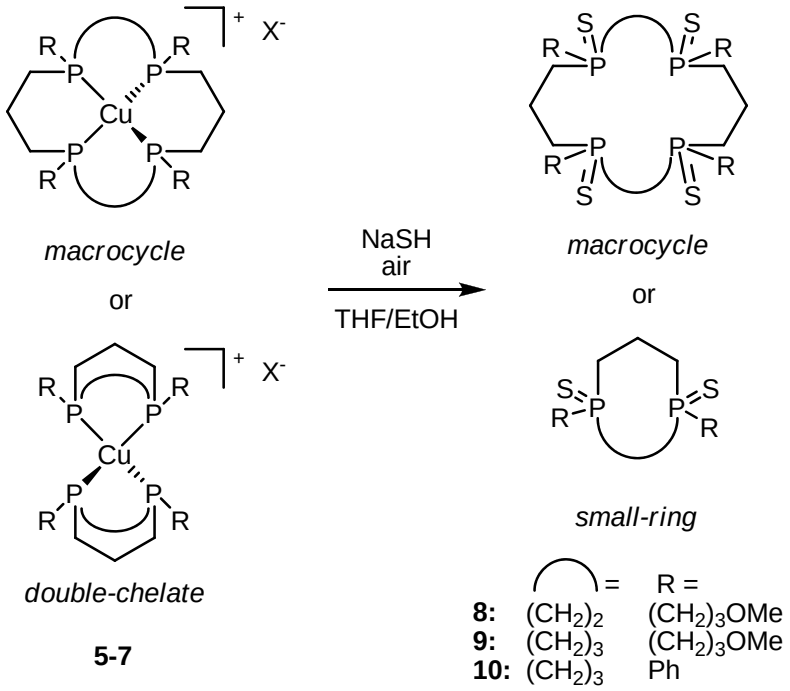

Analysis of the oxidized ligands, including molecular weight determination, is ongoing. In one case, MALDI-MS analysis of compound **8** displayed a series of peaks at m/z = 747, 1089, and 1431 amu (Figure 3). These peaks correspond to two, three, and four molecules of the small-ring phosphine *sulfide* (342 amu), which are ionized by complexation with Cu^{+}, which is presumably present in trace amounts from the demetallation step. Although the peaks at m/z = 747 and 1431 amu may also correspond to one and two equivalents of the *macrocyclic* phosphine sulfide, the observation of the peak at 1089 amu (3 x **8** + Cu^{+}) is definitive evidence for formation of the small-ring product.

Figure 3. MALDI-MS of Compound **8**.

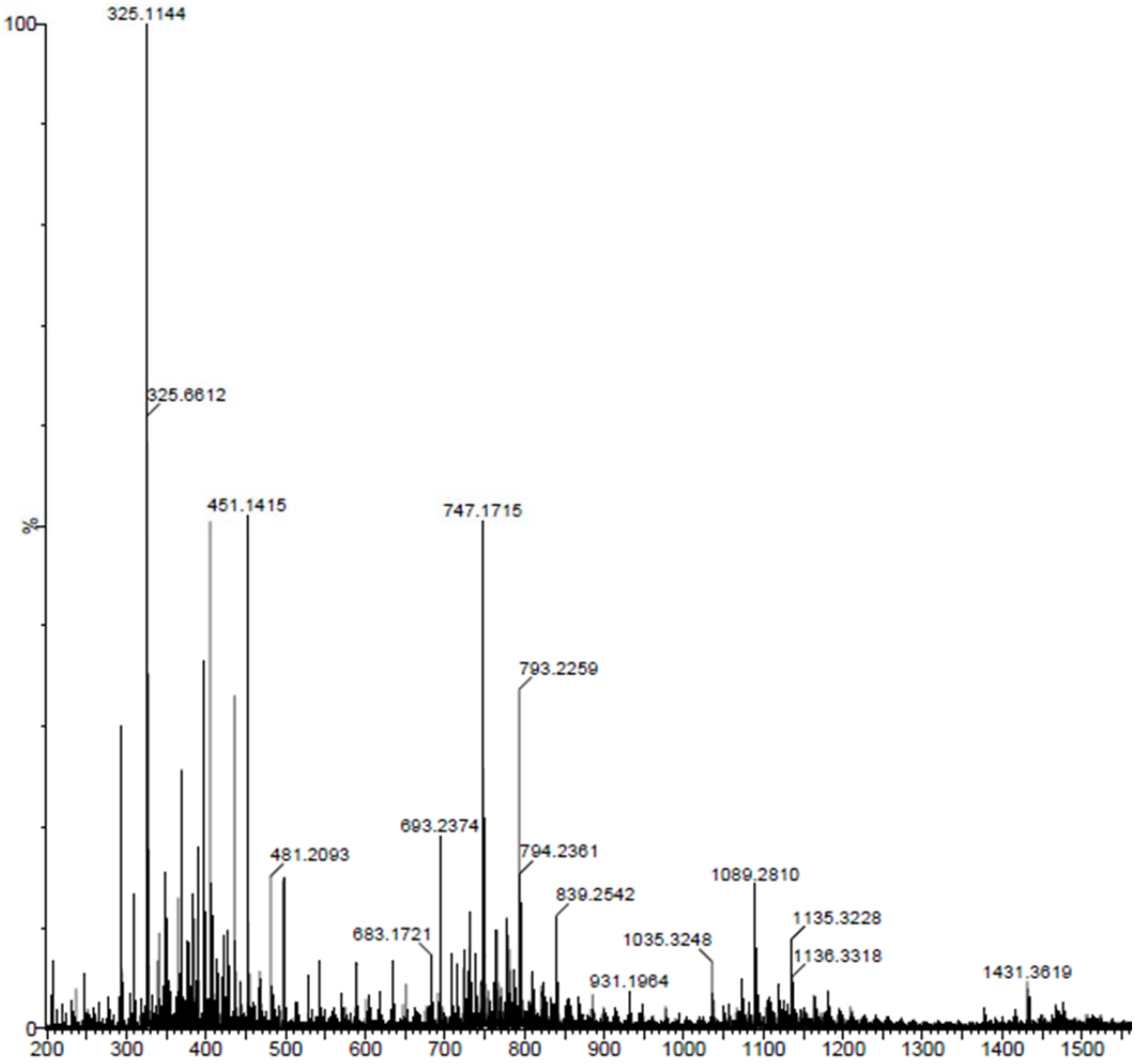

Reduction of the oxidized ligands to phosphines proved difficult, requiring refluxing the compounds with excess $LiAlH_4$ for four days in THF. Contrary to literature reports,[3] phenylsilane proved ineffective as a reducing agent, as did $Li(Et_3BH)$ (Super-Hydride). In an attempt to avoid the need for this reduction step, several attempts at air-free demetallation of the complexes were made. In each attempt, the complexes required at least 5 days to demetallate, and in all but one attempt, the demetallated ligand still

oxidized, presumably reacting with trace oxygen as the reaction proceeded. This suggests that the driving force for demetallation using NaSH is two-fold: precipitation of the copper as Cu_2S, and oxidation of the phosphine ligand. Attempts at inducing metal exchange by reacting complexes **5-7** with excess $FeCl_2$ also proved unsuccessful.

5.3.4. Acylation of Copper Template Complexes

Transition-metal templated macrocyclization reactions are typically slow, requiring hours to days at elevated temperatures to reach completion. In attempts to speed up the macrocycle synthesis, complex **3** was reacted with the difunctional electrophile dimethylmalonyl chloride (eq. 1). Addition of base (triethylamine) caused the reaction mixture to turn deep yellow, indicating the formation of acylphosphine groups. Conversion to complex **11** was complete after 45 minutes at room temperature, indicated by a downfield shift in the ^{31}P NMR spectrum to +9 ppm. The fully-acylated complex was also confirmed by ESI-MS analysis (see Table 1) as the major product.

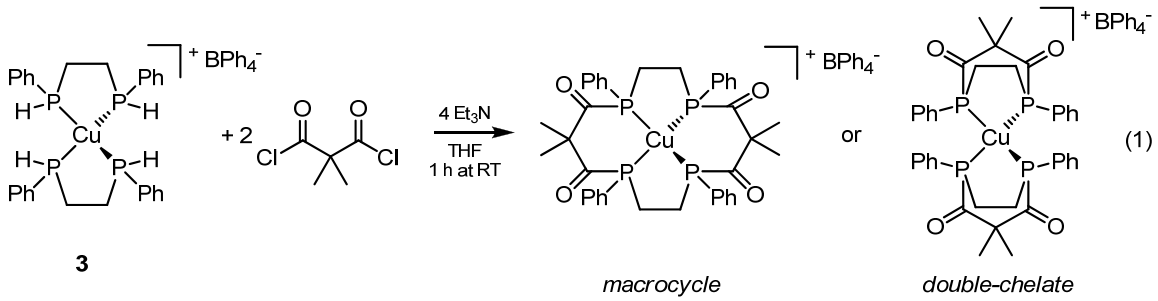

11 (32%)

As with complexes **5-7**, linking of the coordinated phosphines to form **11** can occur in two possible ways: linking *between* the phosphines to form a macrocyclic ligand, or linking *across* the phosphines to form two double-chelate ligands. Because neither of these possibilities can be distinguished from each other except by X-ray crystallography, demetallation of the complex was also attempted so that the molecular weight of the

demetallated ligand could be measured. However, treatment of **7** with NaSH-hydrate resulted in hydrolysis of the acylphosphine groups, as observed by the presence of free MPPP (-45 ppm) in the ^{31}P NMR spectrum. Efforts to demetallate this complex under anhydrous conditions in order to prevent this hydrolysis are ongoing.

5.3.5. Synthesis and Crystal Structure of Cu(DHMPE)$_2$ Complexes

As opposed to the Fe(II) complexes of secondary phosphines presented in Chapter II, secondary phosphine complexes of Cu(I) are reactive toward alkyl halides or acyl chlorides. Because the alkylations of these complexes were so successful, we wondered whether a copper-hydroxymethylphosphine template might also be reactive toward macrocyclization via the phosphorus Mannich reaction, as had been attempted with other templates in Chapter III. In order to explore this, the water-soluble copper phosphine complex $[Cu(DHMPE)_2]^+Cl$ (DHMPE = 1,2-bis(dihydroxymethyl)phosphino-ethane) was prepared.

Copper(I) chloride and DHMPE react in methanol within minutes at room temperature to form $[Cu(DHMPE)_2]Cl$ (compound **12**, eq. 2). The ^{31}P NMR spectrum shows a broad peak at +12 ppm, consistent with coordination of the tertiary phosphine to Cu(I). Like the other copper-phosphine complexes reported herein, the signal is broadened by coupling of the phosphorus nuclei with the quadrupolar copper nuclei and remains broad singlet in D_2O even at 90 °C.

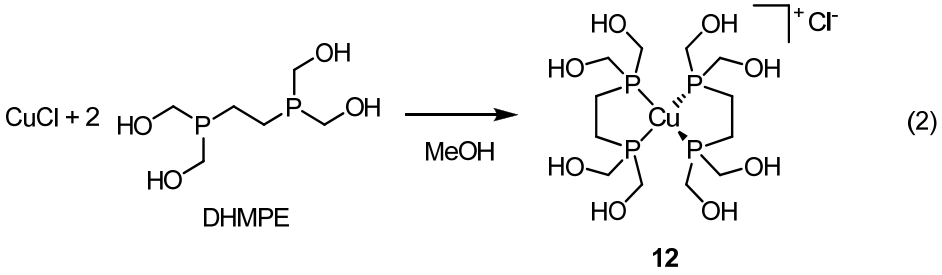

(2)

Slow evaporation of a methanol solution of **12** gave single crystals suitable for x-ray diffraction, which were found to be in the form of a phosphine-bridged dimer, $[Cu_2(DHMPE)_4]Cl_2$ (**13**) (Figure 4). The molecule is centrosymmetric (C_i symmetry), with each copper atom bearing one terminal bidentate phosphine ligand. Two bidentate phosphines bridge between the two copper atoms, forming a 10-membered ring. The bridging ligands are in an extended conformation (P-C-C-P torsion = 166.5(2)°), as opposed to the *gauche* conformation of the terminal phosphine ligands (P-C-C-P torsion = 51.3(3)°). The copper coordination sphere is distorted tetrahedral, with the P1-Cu-P2 (terminal phosphine) plane intersecting the P3-Cu-P4 (bridging phosphines) plane at 87.3°. One of the hydroxymethyl groups in each asymmetric unit (2 per molecule) is disordered. To molecules of methanol Cu dimer are present as solvents of crystallization.

Figure 4. X-ray crystal structure of the cation in $Cu_2(DHMPE)_4Cl_2$ (compound **13**). Ellipsoids are drawn at 50% probability. Nonpolar hydrogen atoms have been omitted for clarity.

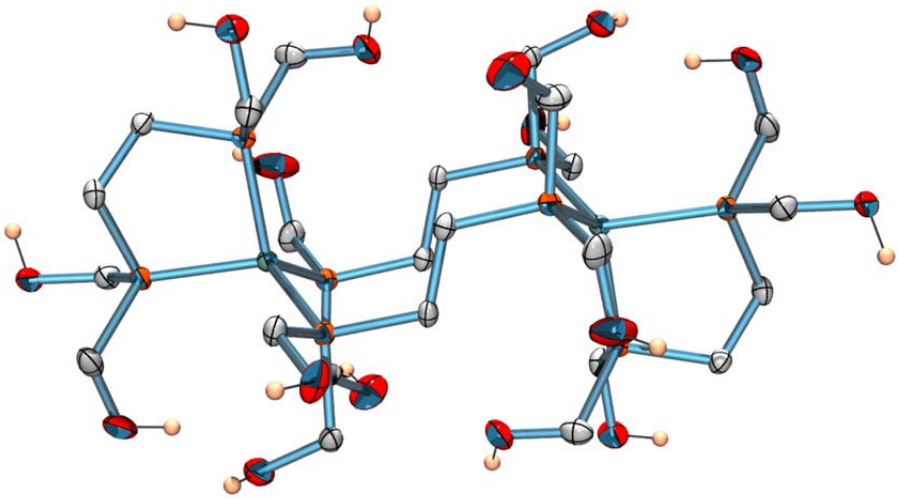

A phosphine-bridged Cu(I) dimer of this type has only been observed once before, in the crystal structure of $[Cu_2(DMPE)_4]BF_4^-$ (**14**; DMPE = 1,2-bis(dimethyl-phosphino)ethane).[8] The analogous monomer, $Cu(DMPE)_2^+$, has also been synthesized and analyzed crystallography, in the presence of the anionic complexes $[Cu(CoCO_4)_2]^-$ and $[CpTi(SCH_2CH_2S)_2]^-$.[1516] The solid-state and solution ^{31}P spectra of this complex are quartets at room temperature, indicating that the solution structure may be the CuP_4^+ monomer or the phosphine-bridged dimer, but the spectra did not have sufficient resolution to differentiate between the two possibilities. It was presumed that interactions with the BF_4^- anion were responsible for dimerization in the solid state; however the exact nature of these interactions was not explained.

The crystal structures of **13** and **14** are strikingly similar (Figure 5). Specifically, the geometries around each metal ion and the conformations of the bridging and terminal ligands are nearly identical in both complexes. Table 2 shows a comparison of bond

lengths, angles, and torsions between the two complexes. A few slight differences are noticeable between the two complexes: all Cu-P bond lengths are slightly shorter in **13**, most P-C bond lengths are shorter (with the exception of the backbone P-C bonds of the bridging phosphines), and the backbone C-C bonds are longer. The tetrahedral geometry is slightly more distorted in **13** than in **14**. The chelate angle of the terminal DHMPE ligand is slightly less than DMPE, as is the P-Cu-P angle between the bridging phosphines. Correspondingly, all other P-Cu-P angles are slightly larger for **13** than for **14**.

Figure 5. Overlayed structures (ball and stick models) of $[Cu_2(DHMPE)_4]^{2+}$ (**13**, blue) and $[Cu_2(DMPE)_4]^{2+}$ (**14**, red).

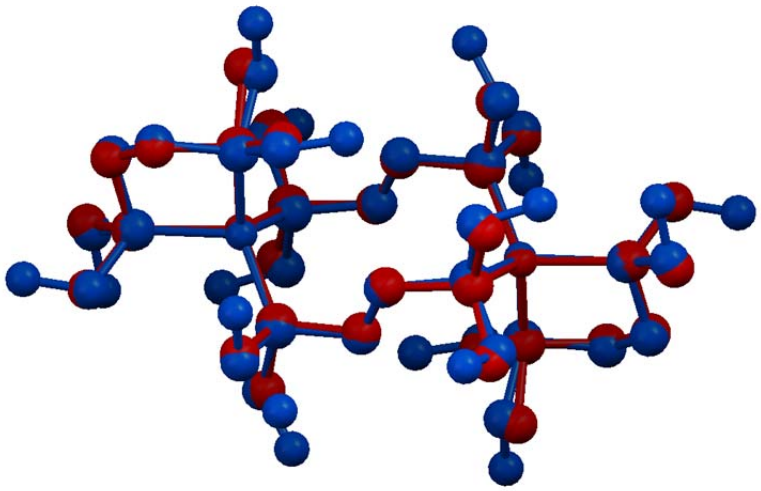

Table 2. Comparison of crystal data for $Cu_2(DHMPE)_4Cl_2$ and $[Cu_2(DMPE)_4](BF_4)_2$.

				13	**14**[8]	Diff.
Ligand				DHMPE	DMPE	
Counterion				Cl^-	BF_4^-	
Crystal System				Monoclinic	Triclinic	
Space Group				C2/c	$P\bar{1}$	
Solvent of Crystallization				MeOH	(none)	
Cu-P Bonds	Terminal		Cu-P1	2.279 (1)	2.289 (1)	0.009
			Cu-P2	2.265 (2)	2.293 (1)	0.028
	Bridging		Cu-P3	2.248 (1)	2.267 (1)	0.018
			Cu-P4	2.259 (1)	2.263 (1)	0.004
P-C Bonds	Terminal	PCCP	P1-C1	1.837 (4)	1.833 (3)	-0.004
			P2-C2	1.832 (4)	1.831 (3)	-0.001
		$P-CH_2X$ (X = H, OH)	P1-C3	1.845 (4)	1.817 (3)	-0.028
			P1-C4	1.839 (4)	1.819 (4)	-0.020
			P2-C5	1.834 (4)	1.822 (4)	-0.012
			P2-C6	1.834 (4)	1.813 (4)	-0.021
	Bridging	PCCP	P3-C7	1.827 (4)	1.835 (2)	0.008
			P4-C8	1.832 (4)	1.839 (2)	0.007
		$P-CH_2X$ (X = H, OH)	P3-C9	1.835 (4)	1.819 (3)	-0.016
			P3-C10	1.845 (4)	1.812 (3)	-0.033
			P4-C11	1.844 (4)	1.813 (4)	-0.031
			P4-C12	1.823 (4)	1.815 (4)	-0.008
C-C Bonds	Terminal		C1-C2	1.537 (5)	1.525 (4)	-0.012
	Bridging		C7-C8	1.527 (5)	1.521 (4)	-0.006
Bond Angles			P1-Cu-P2†	88.59 (4)	89.2 (1)	0.59
			P3-Cu-P4‡	108.29 (4)	110.7 (1)	2.44
			P1-Cu-P3	118.08 (5)	116.9 (1)	-1.21
			P1-Cu-P4	114.03 (4)	113.2 (1)	-0.85
			P2-Cu-P3	112.14 (4)	110.3 (1)	-1.86
			P2-Cu-P4	114.83 (4)	115.1 (1)	0.32
P-C-C-P Torsions		Terminal	P1-C1-C2-P2	51.3 (3)	54.8	3.51
		Bridging	P3-C7-C8-P4	166.5 (2)	168.9	2.39

†Terminal ligand chelate angle. ‡Bridging ligand "chelate angle".

Despite the similar structures of dimers **13** and **14**, the complexes crystallize in very different forms. Not only are the lattices completely different, but the intramolecular forces involved in the packing are also very different. **14**, which contains

the nonpolar ligand DMPE, displays no obvious interactions between the cationic complex and the disordered BF_4^- anion. On the other hand, **13** contains a complex intramolecular hydrogen-bonding network linking molecules of the dimer, methanol, and chloride counterions. This suggests that no particular packing forces or interactions with the anions (other than perhaps packing size matching) can account for formation of the dimer in the solid state.

All other things being equal, dimeric compounds are disfavored over monomers because of the decreased entropy of two particles becoming one. Also, the formation of a flexible ten-membered ring (formed in this case by the two Cu^+ ions and the two bridging phosphines) is entropically disfavored, as opposed to the formation of stable five-membered chelate rings. However, inspection of the dimeric structure of **13** reveals two conformational advantages of the dimeric form over a $[CuP_4]^+$ monomer. First, the terminal phosphines have a small (<90°) chelate angle, which is significantly less than the 109.5° L-M-L angle of a perfectly tetrahedral complex. Formation of the phosphine-bridged dimer removes one of these strained chelate rings, allowing for less distortion of the tetrahedral coordination geometry. Indeed, the P-Cu-P angle between the bridging ligands is 108.29(4)°, much closer to the ideal angle for a tetrahedral complex. Second, the bridging phosphine ligands are in a fully extended conformation, with favorable[17] *anti* P-C-C-P torsion angles (166.5(2)°), as opposed to the energetically disfavored *gauche* conformation of the terminal bridging ligand (P-C-C-P angle = 51.3(3)°). These factors, along with possible intermolecular and crystal packing interactions (strength of the hydrogen-bonding network, etc.), accumulate to favor crystallization of the dimer over the monomer.

Because NMR spectroscopy does not provide sufficient information to fully characterize the solution-state structure of the complex, the complex was analyzed by ESI mass spectrometry. Positive-mode ESI-MS reveals a single ion at m/z = 491. This may correspond to either the monomeric $Cu(DHMPE)_2^+$ ion (structure A in Figure 1) or the phosphine-bridged dimer, but each of these would display a different isotope pattern because of their different charge and molecular formula (Figure 5). Analysis of the isotope pattern corresponds to that of the monomer, $Cu(DHMPE)_2^+$, suggesting that the complex is monomeric in solution.

Figure 5. ESI mass spectrum of $Cu(DHMPE)_2Cl$.

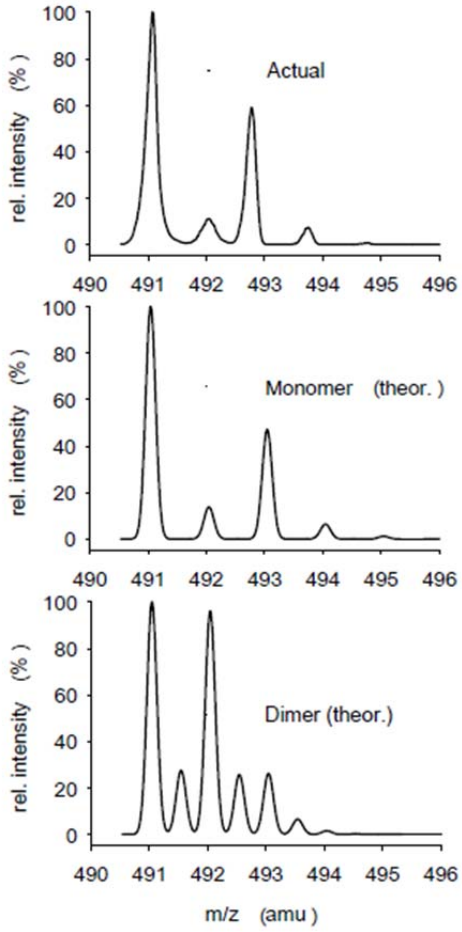

Attempted synthesis of **13** in THF does not proceed when CuCl and DHMPE are the only reactants. However, addition of a halide abstractor such as $NaPF_6$ or NaOTf causes complete conversion to $Cu(DHMPE)_2^+$ within a few minutes (Scheme 6). This presumably occurs via initial chloride ion abstraction, generating "bare" Cu^+ ions in solution, which are then coordinated by the phosphine. The reaction is driven to completion by precipitation of NaCl from solution. In this manner, $Cu(DHMPE)_2^+PF_6$ can be synthesized from DHMPE, CuCl, and a halide abstractor, without the need for a more expensive copper(I) source.

Scheme 6. Synthesis of $Cu(DHMPE)_2PF_6$.

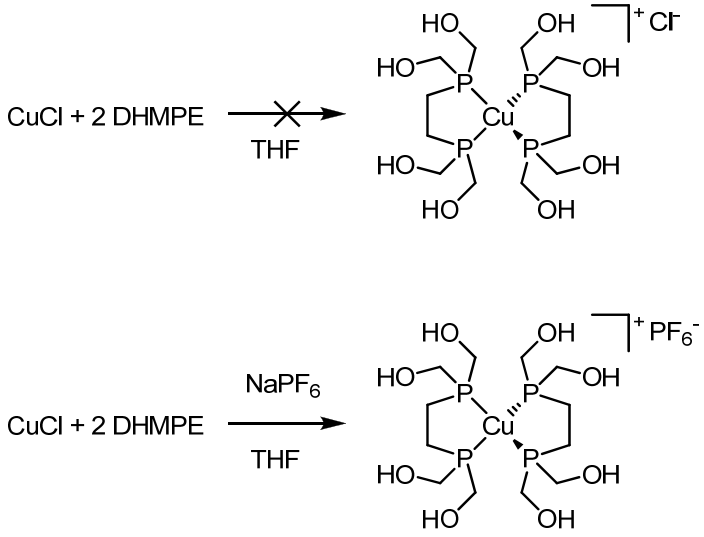

Copper(I) phosphine complexes have been sought after for biomedical purposes as potential anti-cancer drugs[18-22] and as PET imaging reagents.[23,24] Cu(I) complexes containing water-soluble phosphine ligands are especially attractive for these purposes. Indeed, $[Cu(DHMPE)_2]^+PF_6$ has been synthesized previously for these purposes, and

showed antitumor activity comparable to cisplatin.[21] However, the initial synthesis used the expensive starting material $[Cu(MeCN)_4]PF_6$, as opposed to our method, which uses CuCl and $NaPF_6$ to form this complex in one pot. In addition, the inherent toxicity of the PF_6^- anion [25] suggest that a complex with a more biocompatible anion, such as $[Cu(DHMPE)_2]Cl$ (**12**), might be more useful as a drug candidate.

5.4. Conclusion

Copper(I) complexes of secondary phosphines are effectively alkylated by 1,3-dibromopropane to form complexes whose molecular weight and spectra correspond to macrocyclic phosphine complexes. The resulting ligands can be liberated from the metals using NaSH and air, which precipitates the copper as Cu_2S and oxidizes the ligands to phosphine sulfides. MALDI-MS of one of these demetallated ligands suggests that it is not a tetraphosphine macrocycle, but instead is a small-ring bidentate phosphine. Molecular weight determinations of the other ligands is ongoing.

The metal template can also be acylated by reaction with dimethylmalonyl chloride in the presence of triethylamine. The molecular weight of this product corresponds to a macrocyclic complex; however, the macrocyclic structure has not yet been confirmed. Attempts at demetallating this complex have so far been unsuccessful, due to hydrolysis of the acylphosphine linkages upon demetallation. If this reaction does indeed produce phosphine macrocycles, it would represent a much faster method of synthesizing macrocyclic phosphine complexes. Efforts at obtaining definitive evidence of macrocycle formation, including crystal structures of the complexes and their demetallated ligands, are ongoing.

5.5. Bridge

Chapter V has explored the template synthesis of macrocyclic phosphine ligands around a d^{10} copper(I) template, . The Cu(I) template complexes have been the most successful so far, readily undergoing alkylation or acylation to form complexes whose molecular weights match those of phosphine macrocycles. In addition, these ligands can be removed from the metals using NaSH and air, as opposed to macrocycles formed around the more common d^8 (Ni(II), Pd(II), or Pt(II)) templates.

Chapter VI will summarize the research presented in this dissertation, and will also outline a new synthetic scheme for the synthesis of phosphine macrocycles, which will avoid the formation of small-ring by-products.

CHAPTER VI

SUMMARY AND FUTURE DIRECTIONS

6.1. Introduction

Macrocyclic phosphines have the potential to be a very useful class of ligands. Unfortunately, their development has been hampered by the lack of a general, high-yield synthetic method for their preparation. Template syntheses, while high yielding, typically result in complexes that cannot be demetallated, and only a few transition metals can act as templates for the synthesis of phosphine macrocycles.

This previous chapters have described our attempts to synthesize water-soluble phosphine macrocycles and their iron(II) complexes for use in the removal of dinitrogen from natural gas. Chapter I summarized previous phosphine macrocycle syntheses, and highlighted the challenges and successes in making these compounds. Chapter II discussed the synthesis of the water-soluble bidentate secondary phosphines for use as macrocycle precursors, and their coordination chemistry with iron(II). Unfortunately, these iron(II) phosphine complexes do not undergo alkylation, due to a lack of nucleophilicity of the coordinated ligands.

Indeed, the complexes are not even as nucleophilic as Proton Sponge (a supposedly "non-nucleophilic" base) when treated with strong electrophiles such as bromomaleic anhydride. Instead, of reacting with the iron template complexes, bromomaleic anhydride reacts quickly

with Proton Sponge to form the colorimetric base MAPS. The chemistry of this compound was explored in Chapter III.

In Chapter IV, we attempted to use a different kind of reaction – the phosphorus Mannich reaction – to form a macrocycle around an iron template. However, the coordinated hydroxymethylphosphine ligand (DHMPE) did not undergo this reaction, nor did other DHMPE complexes. This suggests that the phosphine lone pair is required for this reaction to occur, and that the currently-accepted mechanism for this reaction is incorrect.

In Chapter V, we showed that copper(I) complexes of these phosphines are readily alkylated by difunctional alkyl halides or acyl chlorides to give complexes whose molecular weights correspond to the macrocyclic complexes. However, in at least one case,analysis of the demetallated ligand shows that it is not a macrocycle, but instead is the small-ring product. The factors controlling formation of the macrocyclic phosphine ligand over the small-ring product are currently unknown.

Despite the lack of success in synthesizing a macrocyclic phosphine ligand so far, several lessons have been learned from the results discussed:

1. Bidentate secondary phosphines form *cis*-octahedral complexes with $FeCl_2$. These can be converted to *trans*-octahedral complexes by substitution of the chloro ligands with the less π-donating ligand acetonitrile.
2. Iron(II) complexes of secondary bidentate phosphines are not reactive towards alkylation, presumably because d^6 iron(II) is not electron-rich enough to increase the nucleophilicity of the deprotonated phosphido ligand.
3. Copper(I) complexes of secondary bidentate phosphines readily undergo alkylation with difunctional alkyl halide or acyl choride linkers.

4. The presence of the flexible, ambiphilic methoxypropyl functional groups on phosphine complexes often results in viscous liquids or amorphous solids, instead of crystalline solids. This not only complicates the handling of these complexes, but also complicates their characterization, since x-ray crystal structures cannot be obtained.

6.2. A Proposed General Synthesis of Phosphine Macrocycles

In light of these discoveries, we propose an alternative synthesis of phosphine macrocycles which will avoid the formation of small-ring side-products (Scheme 1). Instead of templating two equivalents of a bidentate phosphine ligand around Cu(I), a single tetradentate ligand will be synthesized, then coordinated to Cu(I), forming the template complex. Reaction of this ligand with a difunctional carbon electrophile will link the two reactive phosphine groups, forming the macrocyclic ring. This complex can then be demetallated and reacted with $FeCl_2$, and its coordination chemistry studied.

Scheme 1. Proposed synthesis and demetallation of a phosphine macrocycle.

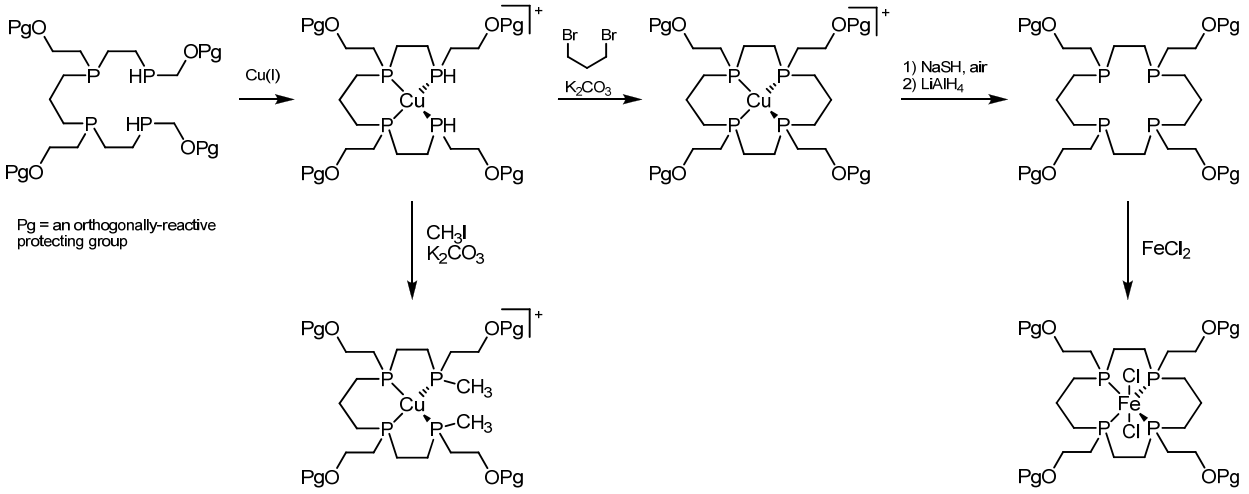

The synthetic method outlined in Scheme 1 also has the advantage that the tetradentate secondary phosphine complex can be alkylated with a small monofunctional alkylating agent (such as methyl iodide) to prepare an analogous open-chain tetradentate ligand. Comparison of the binding constants of this ligand and the macrocyclic ligand will provide the first ever quantification of the macrocyclic effect for a macrocyclic phosphine ligand.

Since X-ray structure determination is a key characterization method for conclusively determining the macrocyclic structure, functional groups which facilitate the formation of crystalline products are necessary. In order to achieve this, we envision incorporating the ligand with bulky alcohol protecting groups such as benzyl (-CH_2Ph) or trityl (-$C(Ph)_3$). After the alkylation reaction to form the macrocycle, single crystals of the complex can then be grown and analyzed by XRD to confirm the macrocyclic structure. Since the ultimate goal is a water-soluble macrocyclic phosphine complex, water solubility will be incorporated at the end of the synthesis, by deprotection of the alcohol groups. If these complexes are insufficiently soluble in water, the solubility can be increased by attaching other functional groups such as sulfonates, carboxylates, or polyether chains to the alcohols. The synthesis outlined in Scheme 1 should allow the preparation of a water-soluble macrocyclic phosphine complex for the separation of N_2 from natural gas (Scheme 2).

Scheme 2. Proposed synthesis of a water-soluble macrocyclic iron-phosphine complex for separation of N_2 from natural gas.

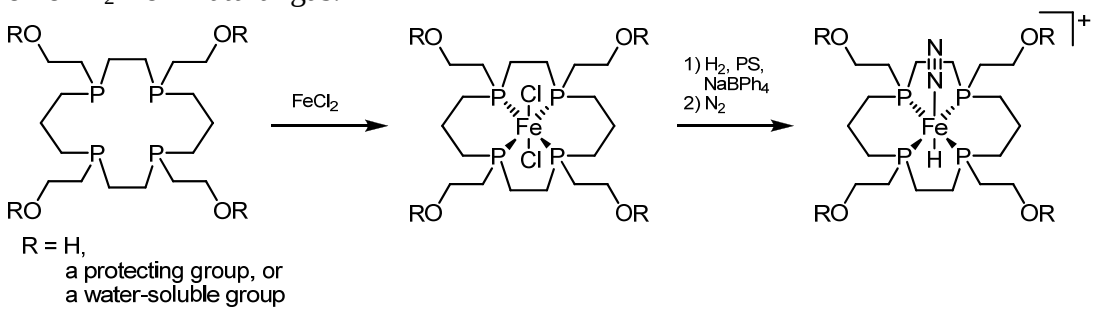

In addition, this method may form the basis for a variety of macrocyclic phosphine ligands and their complexes. This synthesis allows for variations in the size of the ring and the coordinated metal, and also allows the incorporation of additional functionality by tethering other groups at the ends of the arms. These macrocyclic phosphine ligands may eventually find uses in applications requiring robust complexes, such as long-lived homogeneous catalysts and radiopharmaceuticals.

APPENDIX A

SUPPORTING INFORMATION FOR CHAPTER II

A.1 Spectra

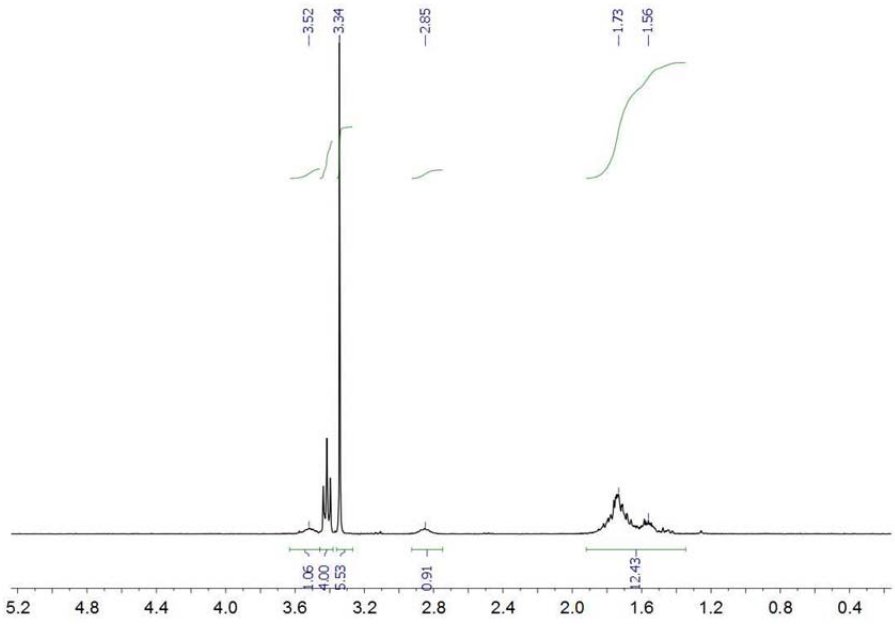

Figure A.1.1. ^{1}H NMR Spectrum of MeOPrPE in $CDCl_3$.

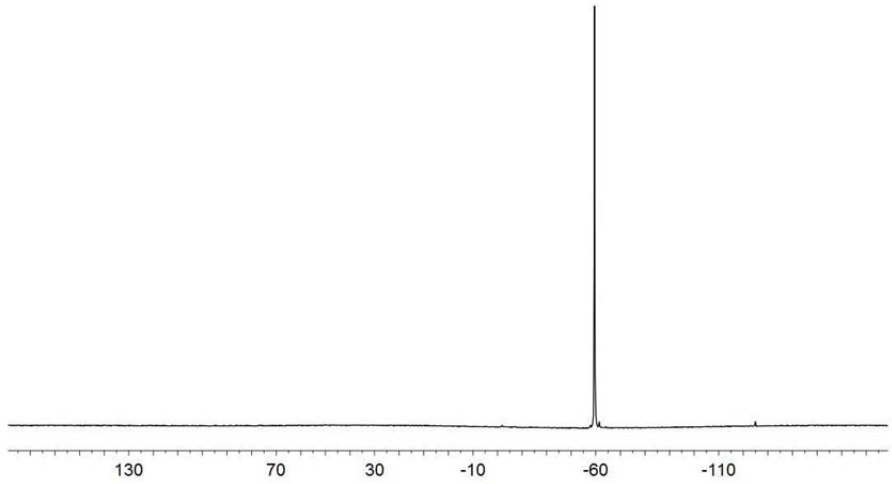

Figure A.1.2. ^{31}P NMR Spectrum of MeOPrPE in $CDCl_3$.

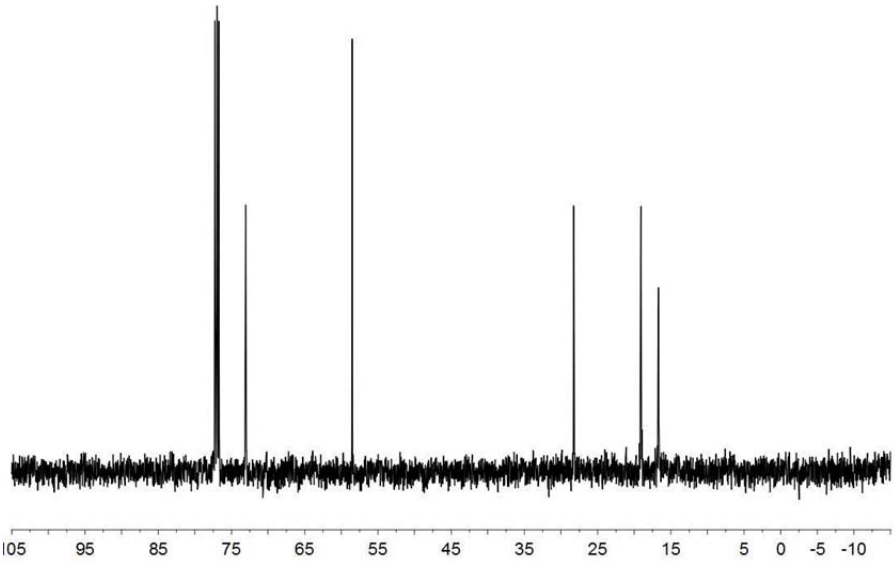

Figure A.1.3. ^{13}C NMR Spectrum of MeOPrPE in $CDCl_3$.

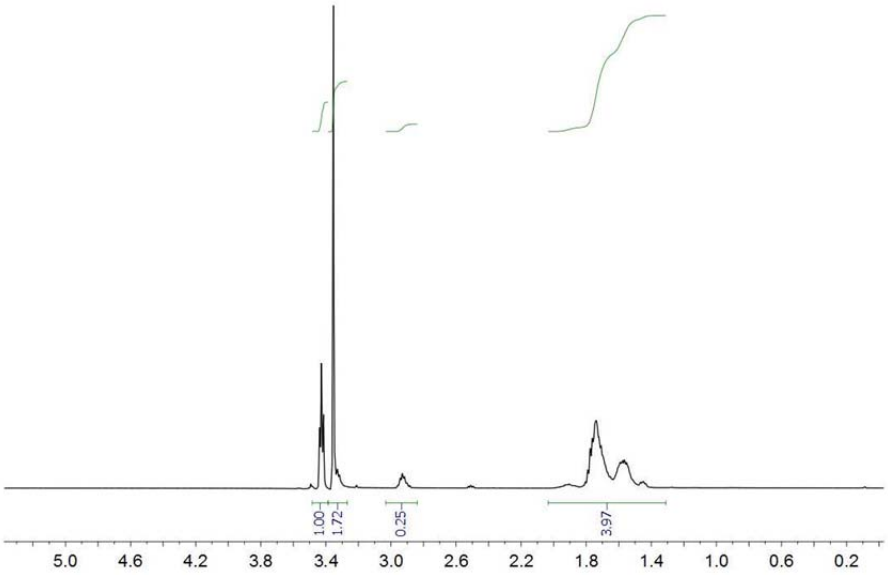

Figure A.1.4. ^{1}H NMR Spectrum of MeOPrPP in $CDCl_3$.

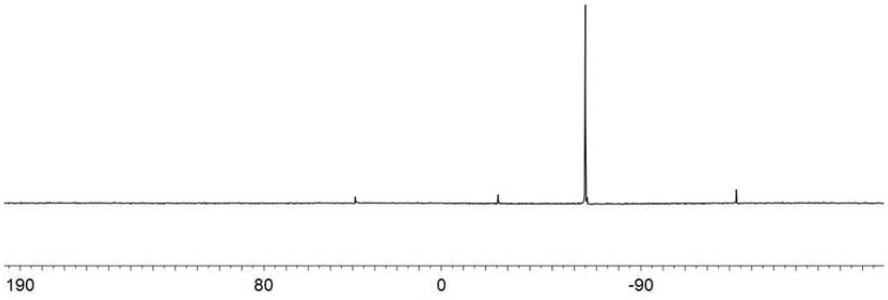

Figure A.1.5. ^{31}P NMR Spectrum of MeOPrPP in $CDCl_3$.

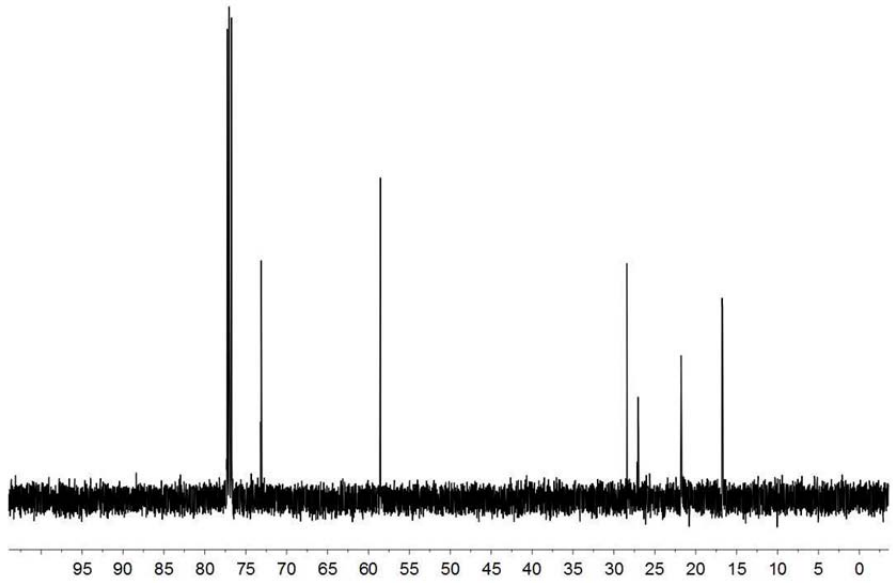

Figure A.1.6. ^{13}C NMR Spectrum of MeOPrPP in $CDCl_3$.

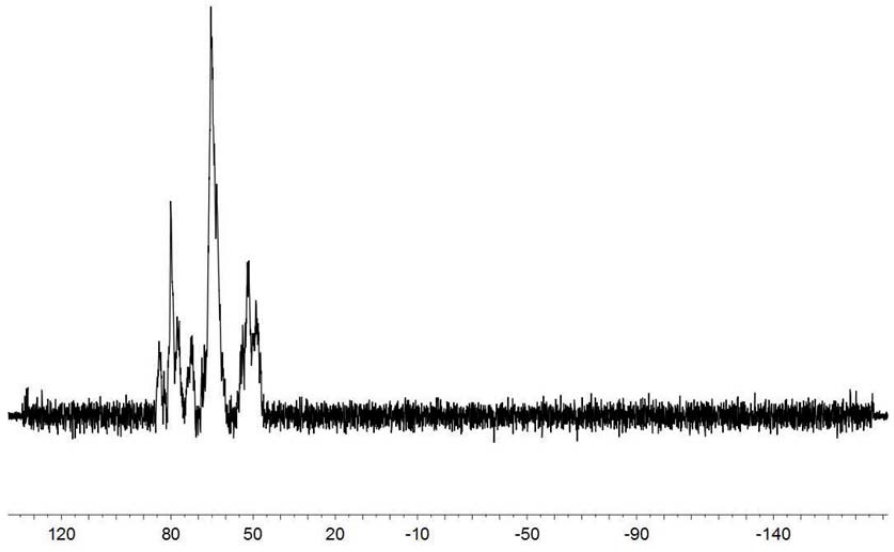

Figure A.1.7. ^{31}P NMR Spectrum of *cis*-$FeCl_2(MeOPrPE)_2$ in $CDCl_3$.

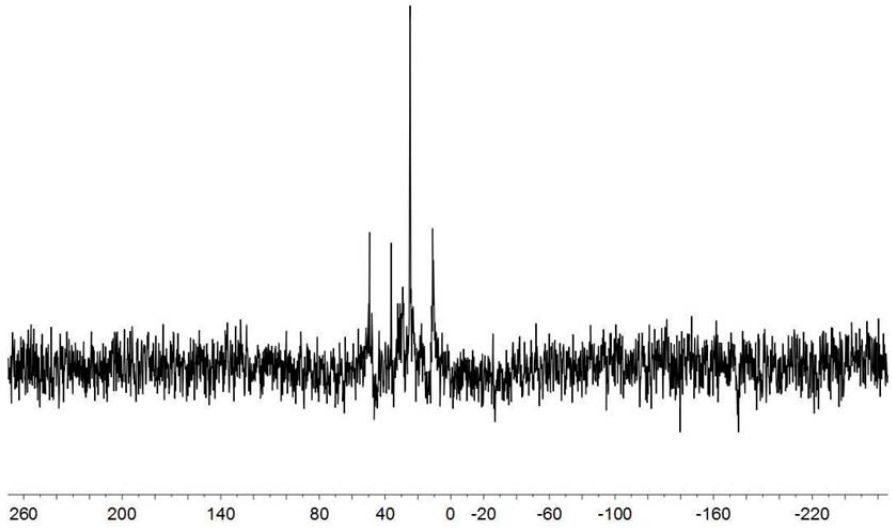

Figure A.1.8. ^{31}P NMR Spectrum of *cis*-Fe(MeOPrPP)$_2$Cl$_2$ in CDCl$_3$.

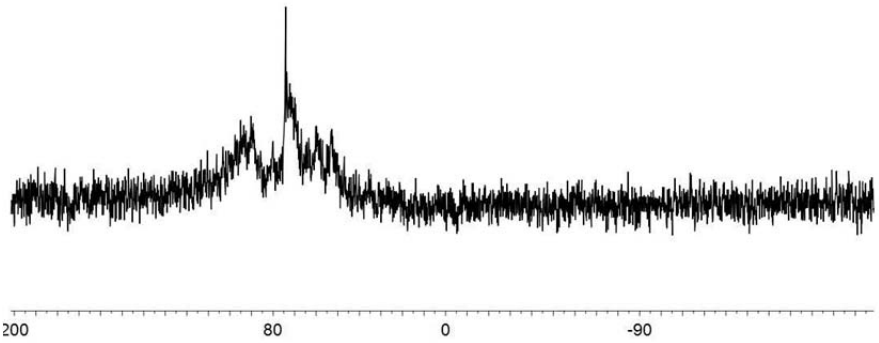

Figure A.1.9. ^{31}P NMR Spectrum of *cis*-Fe(MPPE)$_2$Cl$_2$ in CDCl$_3$.

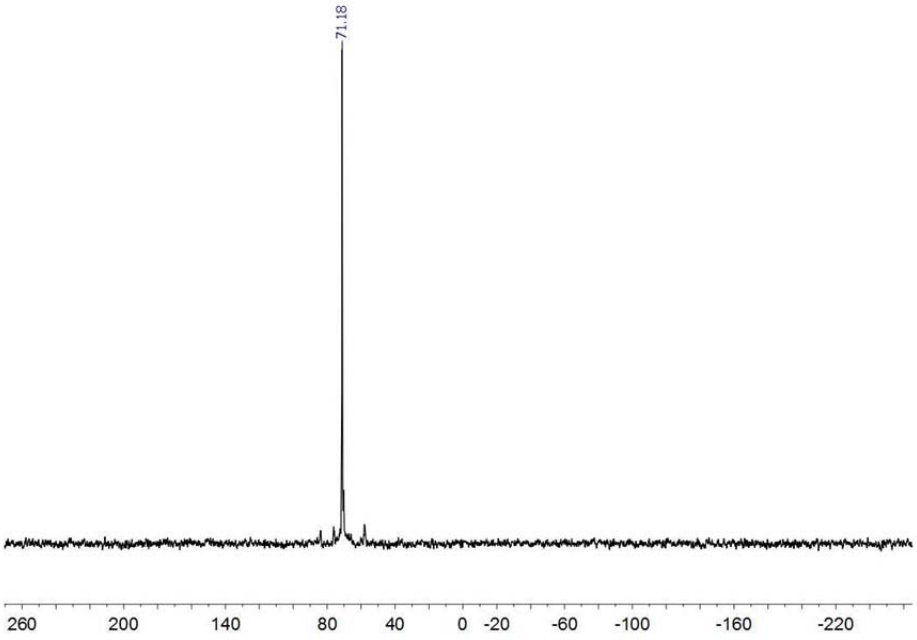

Figure A.1.10. ^{31}P NMR Spectrum of *trans*-Fe(MPPE)$_2$Cl$_2$ in CDCl$_3$.

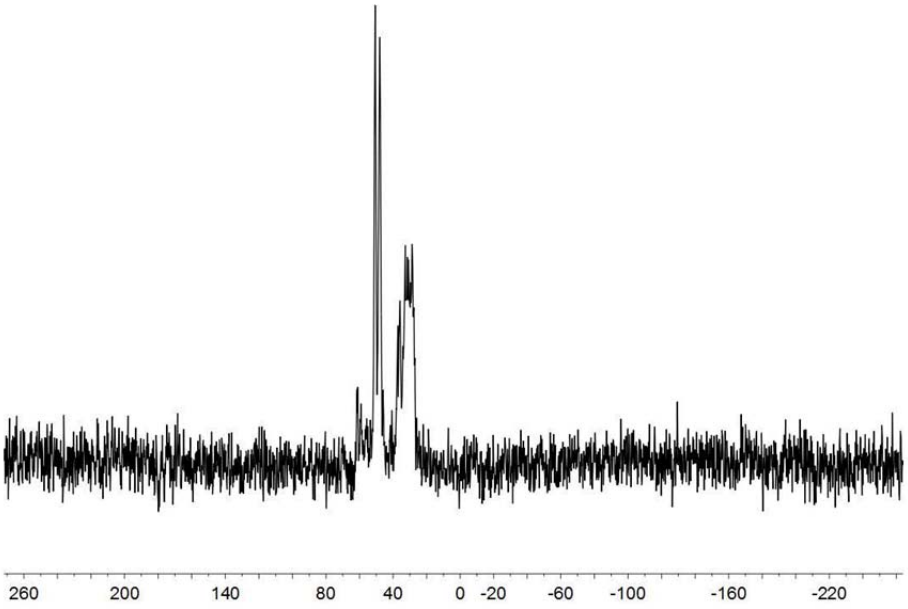

Figure A.1.11. ^{31}P NMR Spectrum of *cis*-Fe(MPPP)$_2$Cl$_2$ in CDCl$_3$.

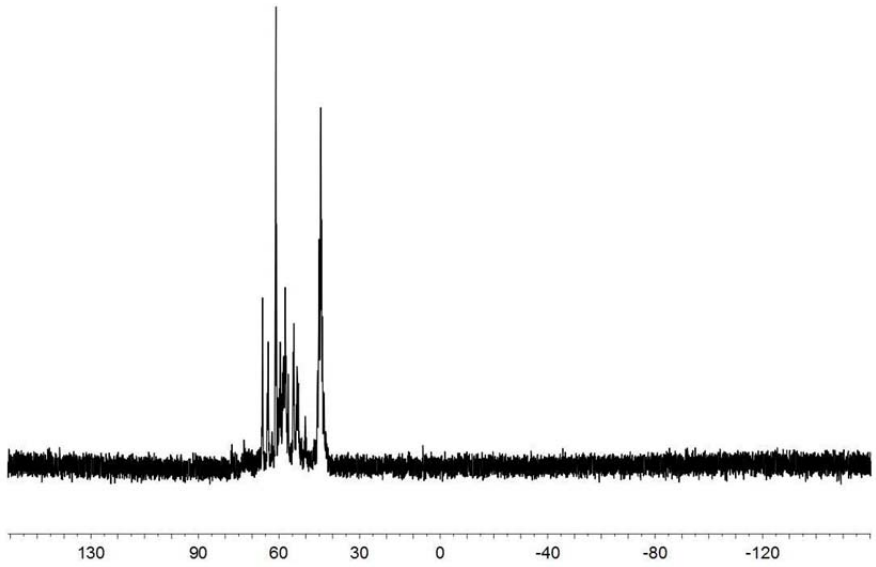

Figure A.1.12. $^{31}P\{^{1}H\}$ NMR spectrum of *trans*-$[Fe(MeOPrPE)_2(MeCN)_2](OTf)_2$ in d3-MeCN.

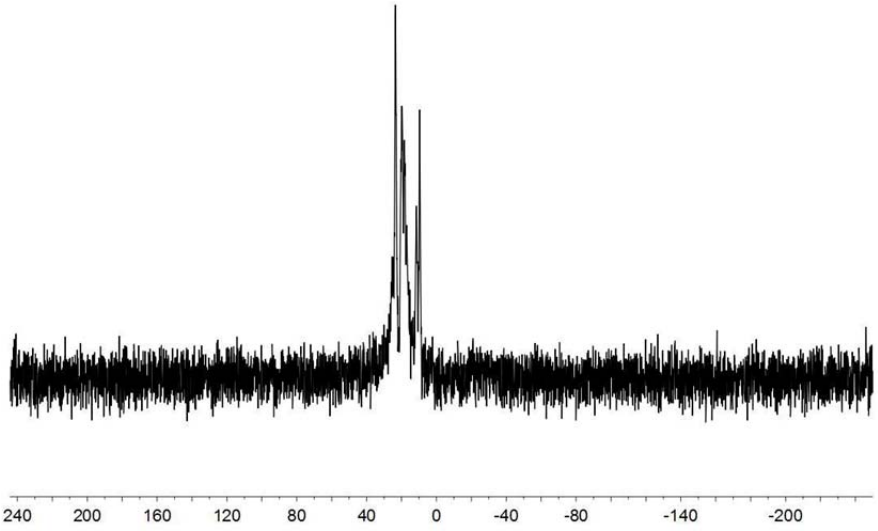

Figure A.1.13. $^{31}P\{^{1}H\}$ NMR spectrum of *trans*-$[Fe(MeOPrPP)_2(MeCN)_2](OTf)_2$ in d3-MeCN.

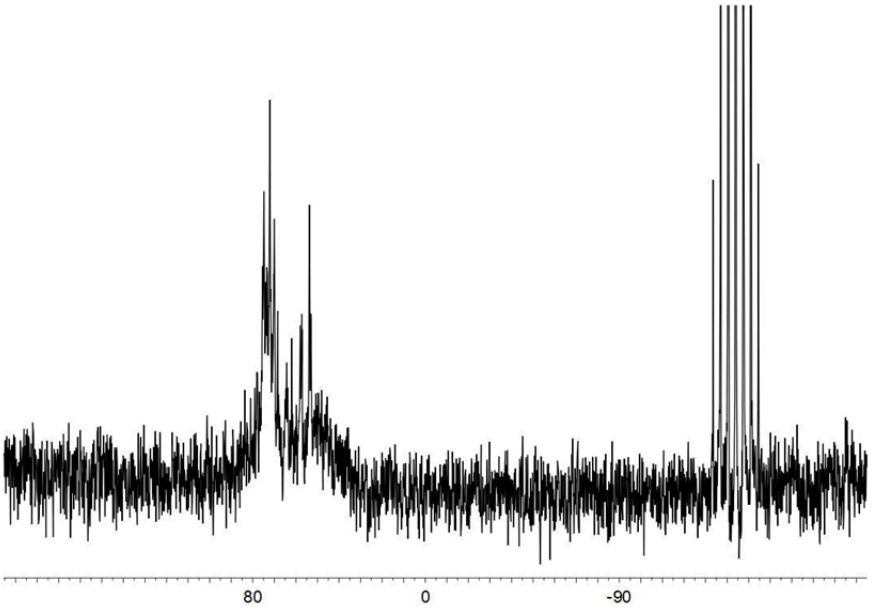

Figure A.1.14. $^{31}P\{^{1}H\}$ NMR spectrum of *trans*-$[Fe(MPPE)_2(MeCN)_2](PF_6)_2$ in d3-MeCN.

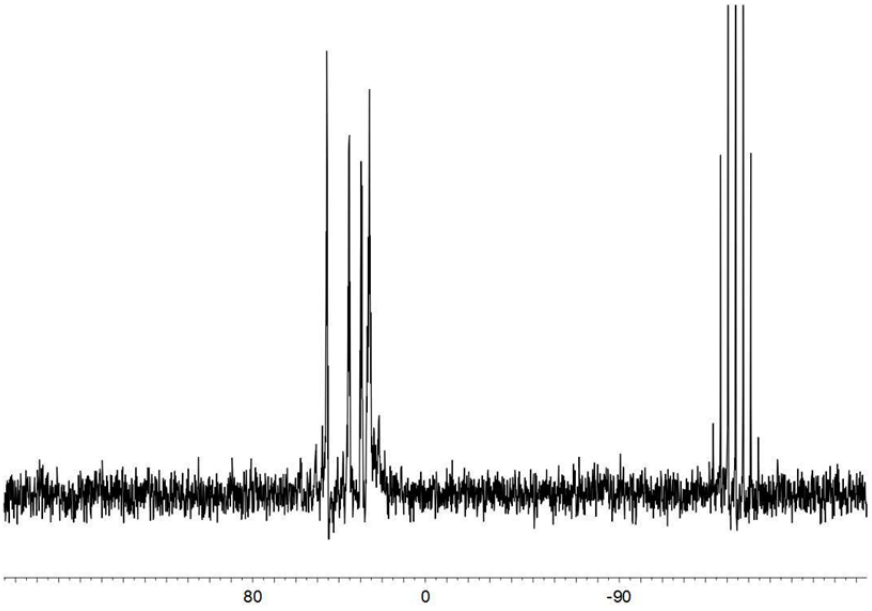

Figure A.1.15. $^{31}P\{^{1}H\}$ NMR spectrum of *trans*-$[Fe(MPPP)_2(MeCN)_2](PF_6)_2$ in d3-MeCN.

A.2 Crystal data for *cis*-Fe(MPPP)$_2$Cl$_2$

Table A.2.1. Crystal data and structure refinement for *cis*-Fe(MPPP)$_2$Cl$_2$.

Identification code	char1	
Empirical formula	C30 H36 Cl2 Fe P4	
Formula weight	647.22	
Temperature	173(2) K	
Wavelength	0.71073 Å	
Crystal system	Monoclinic	
Space group	P2(1)	
Unit cell dimensions	a = 9.194(2) Å	a= 90°.
	b = 16.406(4) Å	b= 111.439(4)°.
	c = 10.500(3) Å	g = 90°.
Volume	1474.3(7) Å^3	
Z	2	
Density (calculated)	1.458 Mg/m^3	
Absorption coefficient	0.930 mm^{-1}	
F(000)	672	
Crystal size	0.20 x 0.10 x 0.04 mm^3	
Theta range for data collection	2.08 to 25.98°.	
Index ranges	-11<=h<=11, -20<=k<=20, -12<=l<=12	
Reflections collected	12433	
Independent reflections	5700 [R(int) = 0.0412]	
Completeness to theta = 25.98°	99.7 %	
Absorption correction	Semi-empirical from equivalents	
Max. and min. transmission	1.000 and 0.770	
Refinement method	Full-matrix least-squares on F^2	
Data / restraints / parameters	5700 / 1 / 350	
Goodness-of-fit on F^2	1.038	
Final R indices [I>2sigma(I)]	R1 = 0.0460, wR2 = 0.0918	
R indices (all data)	R1 = 0.0578, wR2 = 0.0987	
Absolute structure parameter	0.08(2)	
Largest diff. peak and hole	0.752 and -0.388 e.Å^{-3}	

Table A.2.2. Atomic coordinates (x 10^4) and equivalent isotropic displacement parameters ($Å^2$x 10^3) for *cis*-Fe(MPPP)$_2$Cl$_2$. U(eq) is defined as one third of the trace of the orthogonalized U^{ij} tensor.

	x	y	z	U(eq)
Fe(1)	9512(1)	526(1)	4350(1)	17(1)
Cl(1)	10004(1)	1914(1)	5023(1)	27(1)
Cl(2)	6783(1)	775(1)	3446(1)	25(1)
P(1)	8968(1)	-765(1)	3824(1)	19(1)
P(2)	9022(1)	376(1)	6287(1)	22(1)
P(3)	9794(1)	866(1)	2382(1)	20(1)
P(4)	12051(1)	368(1)	5285(1)	20(1)
C(1)	7412(5)	-1249(3)	4266(5)	24(1)
C(2)	7714(6)	-1229(3)	5792(5)	29(1)
C(3)	7552(6)	-372(3)	6326(5)	27(1)
C(4)	11413(5)	1558(3)	2513(5)	24(1)
C(5)	13023(5)	1239(3)	3366(5)	27(1)
C(6)	13317(5)	1117(3)	4887(5)	24(1)
C(7)	8454(5)	-1108(3)	2059(5)	22(1)
C(8)	9280(6)	-1754(3)	1752(5)	31(1)
C(9)	8887(7)	-2007(3)	422(6)	38(1)
C(10)	7656(7)	-1665(3)	-607(6)	40(2)
C(11)	6804(6)	-1036(3)	-329(5)	36(1)
C(12)	7211(6)	-757(3)	1008(5)	29(1)
C(13)	10600(5)	257(3)	7951(5)	24(1)
C(14)	10933(6)	-476(3)	8660(5)	37(1)
C(15)	12200(7)	-546(4)	9892(6)	45(2)
C(16)	13159(7)	113(4)	10421(6)	45(2)
C(17)	12845(6)	845(4)	9734(5)	46(2)
C(18)	11579(6)	919(4)	8517(5)	37(1)
C(19)	8205(5)	1353(3)	996(5)	24(1)
C(20)	7475(6)	2041(3)	1278(5)	32(1)
C(21)	6259(6)	2413(3)	262(6)	45(2)
C(22)	5750(7)	2114(4)	-1054(6)	50(2)
C(23)	6497(7)	1453(4)	-1356(6)	46(2)
C(24)	7715(6)	1075(3)	-329(5)	34(1)

C(25)	12884(5)	-621(3)	5139(5)	21(1)
C(26)	13334(5)	-1161(3)	6234(5)	31(1)
C(27)	13767(6)	-1961(3)	6086(6)	36(1)
C(28)	13781(6)	-2214(3)	4846(6)	35(1)
C(29)	13364(6)	-1688(3)	3747(6)	34(1)
C(30)	12907(5)	-892(3)	3877(5)	29(1)

Table A.2.3. Bond lengths [Å] and angles [°] for *cis*-Fe(MPPP)$_2$Cl$_2$.

Fe(1)-P(4)	2.1918(14)
Fe(1)-P(1)	2.2009(13)
Fe(1)-P(3)	2.2455(14)
Fe(1)-P(2)	2.2517(14)
Fe(1)-Cl(2)	2.3710(13)
Fe(1)-Cl(1)	2.3780(13)
P(1)-C(7)	1.826(5)
P(1)-C(1)	1.839(4)
P(1)-H(1)	1.35(5)
P(2)-C(13)	1.829(5)
P(2)-C(3)	1.836(5)
P(2)-H(2)	1.28(4)
P(3)-C(19)	1.827(5)
P(3)-C(4)	1.837(5)
P(3)-H(3)	1.26(6)
P(4)-C(25)	1.824(4)
P(4)-C(6)	1.843(4)
P(4)-H(4)	1.38(4)
C(1)-C(2)	1.523(6)
C(1)-H(1B)	0.9900
C(1)-H(1A)	0.9900
C(2)-C(3)	1.540(6)
C(2)-H(2B)	0.9900
C(2)-H(2A)	0.9900
C(3)-H(3B)	0.9900
C(3)-H(3A)	0.9900
C(4)-C(5)	1.516(6)
C(4)-H(4B)	0.9900
C(4)-H(4A)	0.9900
C(5)-C(6)	1.532(6)
C(5)-H(5B)	0.9900
C(5)-H(5A)	0.9900
C(6)-H(6B)	0.9900
C(6)-H(6A)	0.9900

C(7)-C(12)	1.390(6)
C(7)-C(8)	1.408(6)
C(8)-C(9)	1.374(7)
C(8)-H(8)	0.9500
C(9)-C(10)	1.367(8)
C(9)-H(9)	0.9500
C(10)-C(11)	1.389(7)
C(10)-H(10)	0.9500
C(11)-C(12)	1.391(7)
C(11)-H(11)	0.9500
C(12)-H(12)	0.9500
C(13)-C(14)	1.389(7)
C(13)-C(18)	1.397(7)
C(14)-C(15)	1.394(7)
C(14)-H(14)	0.9500
C(15)-C(16)	1.377(8)
C(15)-H(15)	0.9500
C(16)-C(17)	1.377(8)
C(16)-H(16)	0.9500
C(17)-C(18)	1.384(7)
C(17)-H(17)	0.9500
C(18)-H(18)	0.9500
C(19)-C(24)	1.374(7)
C(19)-C(20)	1.400(7)
C(20)-C(21)	1.374(7)
C(20)-H(20)	0.9500
C(21)-C(22)	1.377(8)
C(21)-H(21)	0.9500
C(22)-C(23)	1.380(9)
C(22)-H(22)	0.9500
C(23)-C(24)	1.385(7)
C(23)-H(23)	0.9500
C(24)-H(24)	0.9500
C(25)-C(26)	1.389(6)
C(25)-C(30)	1.405(6)
C(26)-C(27)	1.398(7)

C(26)-H(26)	0.9500
C(27)-C(28)	1.370(8)
C(27)-H(27)	0.9500
C(28)-C(29)	1.379(7)
C(28)-H(28)	0.9500
C(29)-C(30)	1.394(6)
C(29)-H(29)	0.9500
C(30)-H(30)	0.9500

P(4)-Fe(1)-P(1)	96.04(5)
P(4)-Fe(1)-P(3)	88.81(5)
P(1)-Fe(1)-P(3)	95.73(5)
P(4)-Fe(1)-P(2)	96.57(5)
P(1)-Fe(1)-P(2)	91.09(5)
P(3)-Fe(1)-P(2)	170.83(5)
P(4)-Fe(1)-Cl(2)	175.97(5)
P(1)-Fe(1)-Cl(2)	87.44(5)
P(3)-Fe(1)-Cl(2)	92.87(5)
P(2)-Fe(1)-Cl(2)	81.29(5)
P(4)-Fe(1)-Cl(1)	85.68(5)
P(1)-Fe(1)-Cl(1)	176.05(5)
P(3)-Fe(1)-Cl(1)	87.86(5)
P(2)-Fe(1)-Cl(1)	85.16(5)
Cl(2)-Fe(1)-Cl(1)	90.72(4)
C(7)-P(1)-C(1)	100.8(2)
C(7)-P(1)-Fe(1)	120.14(14)
C(1)-P(1)-Fe(1)	118.58(16)
C(7)-P(1)-H(1)	104.2(19)
C(1)-P(1)-H(1)	101.9(19)
Fe(1)-P(1)-H(1)	109(2)
C(13)-P(2)-C(3)	104.0(2)
C(13)-P(2)-Fe(1)	121.58(15)
C(3)-P(2)-Fe(1)	119.02(16)
C(13)-P(2)-H(2)	96.8(18)
C(3)-P(2)-H(2)	102.8(18)
Fe(1)-P(2)-H(2)	109.0(18)

C(19)-P(3)-C(4)	100.3(2)
C(19)-P(3)-Fe(1)	120.92(16)
C(4)-P(3)-Fe(1)	116.57(16)
C(19)-P(3)-H(3)	94(2)
C(4)-P(3)-H(3)	92(2)
Fe(1)-P(3)-H(3)	127(3)
C(25)-P(4)-C(6)	104.7(2)
C(25)-P(4)-Fe(1)	118.64(15)
C(6)-P(4)-Fe(1)	118.49(15)
C(25)-P(4)-H(4)	97.1(18)
C(6)-P(4)-H(4)	102.4(17)
Fe(1)-P(4)-H(4)	112.3(16)
C(2)-C(1)-P(1)	113.4(3)
C(2)-C(1)-H(1B)	108.9
P(1)-C(1)-H(1B)	108.9
C(2)-C(1)-H(1A)	108.9
P(1)-C(1)-H(1A)	108.9
H(1B)-C(1)-H(1A)	107.7
C(1)-C(2)-C(3)	113.5(4)
C(1)-C(2)-H(2B)	108.9
C(3)-C(2)-H(2B)	108.9
C(1)-C(2)-H(2A)	108.9
C(3)-C(2)-H(2A)	108.9
H(2B)-C(2)-H(2A)	107.7
C(2)-C(3)-P(2)	115.6(3)
C(2)-C(3)-H(3B)	108.4
P(2)-C(3)-H(3B)	108.4
C(2)-C(3)-H(3A)	108.4
P(2)-C(3)-H(3A)	108.4
H(3B)-C(3)-H(3A)	107.4
C(5)-C(4)-P(3)	114.8(3)
C(5)-C(4)-H(4B)	108.6
P(3)-C(4)-H(4B)	108.6
C(5)-C(4)-H(4A)	108.6
P(3)-C(4)-H(4A)	108.6
H(4B)-C(4)-H(4A)	107.5

C(4)-C(5)-C(6)	115.1(4)
C(4)-C(5)-H(5B)	108.5
C(6)-C(5)-H(5B)	108.5
C(4)-C(5)-H(5A)	108.5
C(6)-C(5)-H(5A)	108.5
H(5B)-C(5)-H(5A)	107.5
C(5)-C(6)-P(4)	116.0(3)
C(5)-C(6)-H(6B)	108.3
P(4)-C(6)-H(6B)	108.3
C(5)-C(6)-H(6A)	108.3
P(4)-C(6)-H(6A)	108.3
H(6B)-C(6)-H(6A)	107.4
C(12)-C(7)-C(8)	119.1(4)
C(12)-C(7)-P(1)	120.7(3)
C(8)-C(7)-P(1)	120.2(4)
C(9)-C(8)-C(7)	119.8(5)
C(9)-C(8)-H(8)	120.1
C(7)-C(8)-H(8)	120.1
C(10)-C(9)-C(8)	120.9(5)
C(10)-C(9)-H(9)	119.6
C(8)-C(9)-H(9)	119.6
C(9)-C(10)-C(11)	120.5(5)
C(9)-C(10)-H(10)	119.8
C(11)-C(10)-H(10)	119.8
C(10)-C(11)-C(12)	119.4(5)
C(10)-C(11)-H(11)	120.3
C(12)-C(11)-H(11)	120.3
C(11)-C(12)-C(7)	120.3(5)
C(11)-C(12)-H(12)	119.9
C(7)-C(12)-H(12)	119.9
C(14)-C(13)-C(18)	117.7(5)
C(14)-C(13)-P(2)	123.1(4)
C(18)-C(13)-P(2)	119.1(4)
C(13)-C(14)-C(15)	120.9(5)
C(13)-C(14)-H(14)	119.5
C(15)-C(14)-H(14)	119.5

C(16)-C(15)-C(14)	120.3(6)
C(16)-C(15)-H(15)	119.9
C(14)-C(15)-H(15)	119.9
C(17)-C(16)-C(15)	119.6(5)
C(17)-C(16)-H(16)	120.2
C(15)-C(16)-H(16)	120.2
C(16)-C(17)-C(18)	120.3(5)
C(16)-C(17)-H(17)	119.8
C(18)-C(17)-H(17)	119.8
C(17)-C(18)-C(13)	121.2(5)
C(17)-C(18)-H(18)	119.4
C(13)-C(18)-H(18)	119.4
C(24)-C(19)-C(20)	118.5(5)
C(24)-C(19)-P(3)	122.2(4)
C(20)-C(19)-P(3)	119.3(4)
C(21)-C(20)-C(19)	120.7(5)
C(21)-C(20)-H(20)	119.7
C(19)-C(20)-H(20)	119.7
C(20)-C(21)-C(22)	120.2(5)
C(20)-C(21)-H(21)	119.9
C(22)-C(21)-H(21)	119.9
C(23)-C(22)-C(21)	119.7(5)
C(23)-C(22)-H(22)	120.2
C(21)-C(22)-H(22)	120.2
C(22)-C(23)-C(24)	120.1(6)
C(22)-C(23)-H(23)	119.9
C(24)-C(23)-H(23)	119.9
C(19)-C(24)-C(23)	120.8(5)
C(19)-C(24)-H(24)	119.6
C(23)-C(24)-H(24)	119.6
C(26)-C(25)-C(30)	118.4(4)
C(26)-C(25)-P(4)	120.3(3)
C(30)-C(25)-P(4)	120.8(3)
C(25)-C(26)-C(27)	121.2(5)
C(25)-C(26)-H(26)	119.4
C(27)-C(26)-H(26)	119.4

C(28)-C(27)-C(26)	119.5(5)
C(28)-C(27)-H(27)	120.3
C(26)-C(27)-H(27)	120.3
C(27)-C(28)-C(29)	120.6(5)
C(27)-C(28)-H(28)	119.7
C(29)-C(28)-H(28)	119.7
C(28)-C(29)-C(30)	120.4(5)
C(28)-C(29)-H(29)	119.8
C(30)-C(29)-H(29)	119.8
C(29)-C(30)-C(25)	119.9(5)
C(29)-C(30)-H(30)	120.1
C(25)-C(30)-H(30)	120.1

Symmetry transformations used to generate equivalent atoms:

Table A.2.4. Anisotropic displacement parameters ($Å^2 x\ 10^3$) for *cis*-Fe(MPPP)$_2$Cl$_2$. The anisotropic displacement factor exponent takes the form: $-2p^2[\ h^2\ a^{*2}U^{11} + ...\ + 2\ h\ k\ a^*\ b^*\ U^{12}\ ]$

	U^{11}	U^{22}	U^{33}	U^{23}	U^{13}	U^{12}
Fe(1)	20(1)	10(1)	22(1)	0(1)	9(1)	1(1)
Cl(1)	33(1)	12(1)	38(1)	-4(1)	17(1)	-1(1)
Cl(2)	21(1)	22(1)	31(1)	2(1)	9(1)	3(1)
P(1)	23(1)	13(1)	23(1)	-2(1)	9(1)	-2(1)
P(2)	25(1)	18(1)	25(1)	-2(1)	12(1)	1(1)
P(3)	22(1)	15(1)	24(1)	1(1)	9(1)	0(1)
P(4)	22(1)	15(1)	22(1)	-2(1)	8(1)	-1(1)
C(1)	23(3)	17(2)	31(3)	-4(2)	9(2)	-6(2)
C(2)	31(3)	24(3)	32(3)	-1(2)	13(2)	-8(2)
C(3)	29(3)	24(3)	32(3)	-2(2)	16(2)	-2(2)
C(4)	28(3)	19(2)	25(3)	5(2)	11(2)	-4(2)
C(5)	26(3)	25(3)	33(3)	0(2)	14(2)	-8(2)
C(6)	21(3)	15(2)	35(3)	-3(2)	10(2)	-1(2)
C(7)	25(3)	18(2)	23(3)	-5(2)	10(2)	-7(2)
C(8)	40(3)	18(2)	35(3)	-6(2)	12(3)	1(2)
C(9)	54(4)	28(3)	35(3)	-8(2)	19(3)	-3(2)
C(10)	69(4)	30(3)	27(3)	-11(2)	24(3)	-16(3)
C(11)	38(3)	36(3)	28(3)	1(2)	4(2)	-12(2)
C(12)	32(3)	22(2)	29(3)	-1(2)	8(2)	-4(2)
C(13)	28(3)	27(3)	23(3)	-8(2)	15(2)	-4(2)
C(14)	43(3)	27(3)	35(3)	1(2)	7(3)	4(2)
C(15)	52(4)	44(4)	33(3)	2(3)	9(3)	19(3)
C(16)	27(3)	71(5)	35(3)	-7(3)	9(3)	8(3)
C(17)	36(3)	69(4)	35(3)	-25(3)	16(3)	-21(3)
C(18)	45(3)	44(3)	28(3)	-8(3)	18(3)	-11(3)
C(19)	24(3)	23(2)	24(3)	5(2)	8(2)	-6(2)
C(20)	30(3)	32(3)	36(3)	6(2)	13(2)	4(2)
C(21)	39(3)	39(3)	60(4)	23(3)	22(3)	15(3)
C(22)	34(3)	64(4)	47(4)	35(3)	11(3)	8(3)
C(23)	40(4)	67(4)	25(3)	12(3)	2(3)	-6(3)
C(24)	31(3)	39(3)	30(3)	4(2)	9(2)	-2(2)

C(25)	17(2)	18(2)	29(3)	-2(2)	8(2)	1(2)
C(26)	27(3)	31(3)	36(3)	5(2)	13(2)	4(2)
C(27)	35(3)	23(3)	52(4)	15(2)	19(3)	6(2)
C(28)	31(3)	19(2)	58(4)	3(2)	18(3)	1(2)
C(29)	40(3)	25(3)	44(3)	-8(2)	23(3)	5(2)
C(30)	34(3)	17(2)	37(3)	2(2)	15(2)	4(2)

Table A.2.5. Hydrogen coordinates (x 10^4) and isotropic displacement parameters ($Å^2$x 10^3) for *cis*-Fe(MPPP)$_2$Cl$_2$.

	x	y	z	U(eq)
H(1B)	6411	-969	3767	29
H(1A)	7301	-1824	3956	29
H(2B)	8782	-1434	6301	34
H(2A)	6969	-1600	5981	34
H(3B)	7605	-423	7281	32
H(3A)	6504	-157	5774	32
H(4B)	11385	1675	1580	28
H(4A)	11245	2080	2913	28
H(5B)	13813	1624	3286	33
H(5A)	13180	711	2979	33
H(6B)	13189	1649	5278	29
H(6A)	14417	946	5355	29
H(8)	10106	-2015	2464	38
H(9)	9479	-2425	213	46
H(10)	7381	-1859	-1517	48
H(11)	5950	-799	-1046	43
H(12)	6638	-325	1203	34
H(14)	10287	-937	8300	45
H(15)	12403	-1051	10370	54
H(16)	14032	62	11254	54
H(17)	13500	1302	10098	55
H(18)	11371	1430	8058	45
H(20)	7823	2253	2182	39
H(21)	5768	2877	467	53
H(22)	4890	2361	-1751	59
H(23)	6176	1258	-2269	56
H(24)	8218	618	-543	41
H(26)	13347	-982	7099	37
H(27)	14049	-2327	6838	43
H(28)	14081	-2757	4744	42

H(29)	13388	-1869	2896	41
H(30)	12612	-534	3114	35
H(1)	10220(50)	-1220(30)	4540(40)	32(13)
H(2)	8480(50)	1050(30)	6550(40)	23(12)
H(3)	10140(60)	390(40)	1590(50)	63(17)
H(4)	12590(50)	390(30)	6700(40)	24(11)

A.3 Crystal data for *trans*-[Fe(MPPP)$_2$(MeCN)$_2$](PF$_6$)$_2$

Table A.3.1. Crystal data and structure refinement for *trans*-[Fe(MPPP)$_2$(MeCN)$_2$](PF$_6$)$_2$.

Identification code	char7	
Empirical formula	C36 H45 F12 Fe N3 P6	
Formula weight	989.42	
Temperature	173(2) K	
Wavelength	0.71073 Å	
Crystal system	Triclinic	
Space group	P-1	
Unit cell dimensions	a = 9.7075(8) Å	□= 96.9270(10)°.
	b = 10.7282(8) Å	□= 94.8200(10)°.
	c = 11.8667(9) Å	□ = 115.6710(10)°.
Volume	1092.83(15) Å^3	
Z	1	
Density (calculated)	1.503 Mg/m^3	
Absorption coefficient	0.647 mm^{-1}	
F(000)	506	
Crystal size	0.37 x 0.16 x 0.04 mm^3	
Theta range for data collection	1.75 to 27.00°.	
Index ranges	-12<=h<=12, -13<=k<=13, -15<=l<=15	
Reflections collected	12344	
Independent reflections	4732 [R(int) = 0.0161]	
Completeness to theta = 27.00°	99.2 %	
Absorption correction	Semi-empirical from equivalents	
Max. and min. transmission	0.9746 and 0.7958	
Refinement method	Full-matrix least-squares on F^2	
Data / restraints / parameters	4732 / 0 / 358	
Goodness-of-fit on F^2	1.064	
Final R indices [I>2sigma(I)]	R1 = 0.0362, wR2 = 0.0969	
R indices (all data)	R1 = 0.0400, wR2 = 0.1004	
Largest diff. peak and hole	0.413 and -0.462 e.Å^{-3}	

Table A.3.2. Atomic coordinates (x 10^4) and equivalent isotropic displacement parameters ($Å^2$x 10^3) for *trans*-$[Fe(MPPP)_2(MeCN)_2](PF_6)_2$. U(eq) is defined as one third of the trace of the orthogonalized U^{ij} tensor.

	x	y	z	U(eq)
Fe(1)	0	0	5000	20(1)
P(1)	-2361(1)	-193(1)	5285(1)	24(1)
P(2)	-409(1)	567(1)	3264(1)	24(1)
N(1)	-894(2)	-1954(2)	4351(1)	24(1)
C(1)	-1431(2)	-3109(2)	3951(2)	30(1)
C(2)	-2117(4)	-4593(3)	3422(3)	47(1)
C(3)	-2820(3)	1188(2)	4863(2)	33(1)
C(4)	-2890(3)	1247(3)	3582(2)	38(1)
C(5)	-1328(2)	1732(2)	3167(2)	33(1)
C(6)	-3010(2)	-364(2)	6679(2)	28(1)
C(7)	-3680(2)	-1692(2)	6991(2)	32(1)
C(8)	-4144(3)	-1832(3)	8061(2)	40(1)
C(9)	-3951(3)	-663(3)	8818(2)	47(1)
C(10)	-3313(3)	643(3)	8512(2)	47(1)
C(11)	-2826(3)	805(3)	7449(2)	38(1)
C(12)	-1368(2)	-863(2)	2051(2)	29(1)
C(13)	-2882(3)	-1897(2)	2007(2)	40(1)
C(14)	-3557(3)	-3002(3)	1083(2)	48(1)
C(15)	-2730(3)	-3095(3)	215(2)	47(1)
C(16)	-1239(3)	-2080(3)	249(2)	43(1)
C(17)	-557(3)	-964(2)	1159(2)	35(1)
P(3)	-7125(1)	-4725(1)	3205(1)	42(1)
F(1)	-6833(3)	-3659(3)	2341(3)	117(1)
F(2)	-8264(3)	-5964(2)	2206(2)	80(1)
F(3)	-7464(2)	-5868(2)	4013(2)	66(1)
F(4)	-6015(2)	-3505(2)	4192(2)	104(1)
F(5)	-5718(2)	-4987(2)	2829(2)	72(1)
F(6)	-8547(2)	-4480(2)	3554(2)	75(1)
N(1S)	-7698(9)	-3512(8)	9159(6)	94(2)
C(1S)	-8739(9)	-4213(7)	9532(6)	67(2)

C(2S)	-10000	-5000	10000	89(2)

Table A.3.3. Bond lengths [Å] and angles [°] for *trans*-[Fe(MPPP)$_2$(MeCN)$_2$](PF$_6$)$_2$.

Fe(1)-N(1)	1.9134(16)
Fe(1)-N(1)#1	1.9134(16)
Fe(1)-P(2)	2.2686(5)
Fe(1)-P(2)#1	2.2686(5)
Fe(1)-P(1)#1	2.2687(5)
Fe(1)-P(1)	2.2687(5)
P(1)-C(6)	1.821(2)
P(1)-C(3)	1.832(2)
P(1)-H(1)	1.29(2)
P(2)-C(12)	1.816(2)
P(2)-C(5)	1.831(2)
P(2)-H(2)	1.28(2)
N(1)-C(1)	1.136(3)
C(1)-C(2)	1.463(3)
C(2)-H(2A)	0.89(4)
C(2)-H(2B)	0.88(4)
C(2)-H(2C)	0.95(5)
C(3)-C(4)	1.525(3)
C(3)-H(3A)	0.95(3)
C(3)-H(3B)	0.88(2)
C(4)-C(5)	1.522(3)
C(4)-H(4A)	0.95(3)
C(4)-H(4B)	0.96(3)
C(5)-H(5A)	0.92(3)
C(5)-H(5B)	0.98(3)
C(6)-C(11)	1.394(3)
C(6)-C(7)	1.398(3)
C(7)-C(8)	1.386(3)
C(7)-H(7)	0.95(3)
C(8)-C(9)	1.383(4)
C(8)-H(8)	0.92(3)
C(9)-C(10)	1.374(4)
C(9)-H(9)	0.90(3)
C(10)-C(11)	1.388(3)

C(10)-H(10)	0.91(3)
C(11)-H(11)	0.87(3)
C(12)-C(17)	1.392(3)
C(12)-C(13)	1.398(3)
C(13)-C(14)	1.390(3)
C(13)-H(13)	0.92(2)
C(14)-C(15)	1.377(4)
C(14)-H(14)	0.98(3)
C(15)-C(16)	1.377(4)
C(15)-H(15)	0.94(3)
C(16)-C(17)	1.385(3)
C(16)-H(16)	0.89(3)
C(17)-H(17)	0.96(2)
P(3)-F(4)	1.5622(19)
P(3)-F(1)	1.578(2)
P(3)-F(3)	1.5870(18)
P(3)-F(2)	1.5883(19)
P(3)-F(6)	1.5907(17)
P(3)-F(5)	1.5963(17)
N(1S)-C(1S)	1.131(9)
C(1S)-C(2S)	1.361(9)
C(2S)-C(1S)#2	1.361(9)

N(1)-Fe(1)-N(1)#1	180.00(9)
N(1)-Fe(1)-P(2)	91.55(5)
N(1)#1-Fe(1)-P(2)	88.45(5)
N(1)-Fe(1)-P(2)#1	88.45(5)
N(1)#1-Fe(1)-P(2)#1	91.55(5)
P(2)-Fe(1)-P(2)#1	180.0
N(1)-Fe(1)-P(1)#1	89.30(5)
N(1)#1-Fe(1)-P(1)#1	90.70(5)
P(2)-Fe(1)-P(1)#1	92.172(17)
P(2)#1-Fe(1)-P(1)#1	87.828(17)
N(1)-Fe(1)-P(1)	90.70(5)
N(1)#1-Fe(1)-P(1)	89.30(5)
P(2)-Fe(1)-P(1)	87.828(17)

P(2)#1-Fe(1)-P(1)	92.172(17)
P(1)#1-Fe(1)-P(1)	180.0
C(6)-P(1)-C(3)	102.52(10)
C(6)-P(1)-Fe(1)	121.99(6)
C(3)-P(1)-Fe(1)	115.94(7)
C(6)-P(1)-H(1)	99.6(10)
C(3)-P(1)-H(1)	103.6(11)
Fe(1)-P(1)-H(1)	110.6(11)
C(12)-P(2)-C(5)	106.27(10)
C(12)-P(2)-Fe(1)	117.43(7)
C(5)-P(2)-Fe(1)	118.21(8)
C(12)-P(2)-H(2)	100.9(11)
C(5)-P(2)-H(2)	96.3(11)
Fe(1)-P(2)-H(2)	114.5(11)
C(1)-N(1)-Fe(1)	178.97(17)
N(1)-C(1)-C(2)	179.3(3)
C(1)-C(2)-H(2A)	109(3)
C(1)-C(2)-H(2B)	113(3)
H(2A)-C(2)-H(2B)	118(4)
C(1)-C(2)-H(2C)	107(3)
H(2A)-C(2)-H(2C)	101(4)
H(2B)-C(2)-H(2C)	108(4)
C(4)-C(3)-P(1)	114.49(16)
C(4)-C(3)-H(3A)	110.1(15)
P(1)-C(3)-H(3A)	106.0(15)
C(4)-C(3)-H(3B)	109.5(15)
P(1)-C(3)-H(3B)	106.0(15)
H(3A)-C(3)-H(3B)	111(2)
C(5)-C(4)-C(3)	113.93(18)
C(5)-C(4)-H(4A)	110.1(15)
C(3)-C(4)-H(4A)	109.2(15)
C(5)-C(4)-H(4B)	108.3(16)
C(3)-C(4)-H(4B)	106.6(16)
H(4A)-C(4)-H(4B)	108(2)
C(4)-C(5)-P(2)	115.63(16)
C(4)-C(5)-H(5A)	109.5(15)

P(2)-C(5)-H(5A)	108.8(16)
C(4)-C(5)-H(5B)	109.4(15)
P(2)-C(5)-H(5B)	104.8(15)
H(5A)-C(5)-H(5B)	108(2)
C(11)-C(6)-C(7)	119.4(2)
C(11)-C(6)-P(1)	121.31(17)
C(7)-C(6)-P(1)	119.30(15)
C(8)-C(7)-C(6)	119.9(2)
C(8)-C(7)-H(7)	120.1(15)
C(6)-C(7)-H(7)	120.0(15)
C(9)-C(8)-C(7)	120.2(2)
C(9)-C(8)-H(8)	122.9(17)
C(7)-C(8)-H(8)	116.7(17)
C(10)-C(9)-C(8)	120.3(2)
C(10)-C(9)-H(9)	123(2)
C(8)-C(9)-H(9)	116(2)
C(9)-C(10)-C(11)	120.3(2)
C(9)-C(10)-H(10)	122.2(18)
C(11)-C(10)-H(10)	117.5(19)
C(10)-C(11)-C(6)	119.9(2)
C(10)-C(11)-H(11)	118.5(17)
C(6)-C(11)-H(11)	121.5(17)
C(17)-C(12)-C(13)	118.96(19)
C(17)-C(12)-P(2)	119.25(15)
C(13)-C(12)-P(2)	121.75(16)
C(14)-C(13)-C(12)	120.0(2)
C(14)-C(13)-H(13)	119.2(15)
C(12)-C(13)-H(13)	120.7(15)
C(15)-C(14)-C(13)	120.2(2)
C(15)-C(14)-H(14)	124.1(16)
C(13)-C(14)-H(14)	115.7(16)
C(14)-C(15)-C(16)	120.2(2)
C(14)-C(15)-H(15)	121.2(19)
C(16)-C(15)-H(15)	118.6(19)
C(15)-C(16)-C(17)	120.2(2)
C(15)-C(16)-H(16)	119.7(18)

C(17)-C(16)-H(16)	120.0(18)
C(16)-C(17)-C(12)	120.4(2)
C(16)-C(17)-H(17)	120.4(14)
C(12)-C(17)-H(17)	119.2(14)
F(4)-P(3)-F(1)	90.64(17)
F(4)-P(3)-F(3)	92.54(13)
F(1)-P(3)-F(3)	176.74(15)
F(4)-P(3)-F(2)	179.58(12)
F(1)-P(3)-F(2)	89.42(15)
F(3)-P(3)-F(2)	87.40(11)
F(4)-P(3)-F(6)	90.10(11)
F(1)-P(3)-F(6)	90.37(12)
F(3)-P(3)-F(6)	90.34(11)
F(2)-P(3)-F(6)	89.49(11)
F(4)-P(3)-F(5)	91.02(12)
F(1)-P(3)-F(5)	89.15(11)
F(3)-P(3)-F(5)	90.09(10)
F(2)-P(3)-F(5)	89.39(11)
F(6)-P(3)-F(5)	178.78(12)
N(1S)-C(1S)-C(2S)	177.2(7)
C(1S)-C(2S)-C(1S)#2	180.000(2)

Symmetry transformations used to generate equivalent atoms:

#1 -x,-y,-z+1 #2 -x-2,-y-1,-z+2

Table A.3.4. Anisotropic displacement parameters ($Å^2$x 10^3)for *trans*-$[Fe(MPPP)_2(MeCN)_2](PF_6)_2$. The anisotropic displacement factor exponent takes the form: $-2\pi^2[h^2a^{*2}U^{11} + ... + 2 h k a^* b^* U^{12}]$

	U^{11}	U^{22}	U^{33}	U^{23}	U^{13}	U^{12}
Fe(1)	15(1)	18(1)	24(1)	0(1)	0(1)	7(1)
P(1)	17(1)	24(1)	30(1)	1(1)	2(1)	9(1)
P(2)	18(1)	24(1)	28(1)	3(1)	0(1)	7(1)
N(1)	20(1)	24(1)	26(1)	0(1)	1(1)	9(1)
C(1)	28(1)	27(1)	32(1)	1(1)	3(1)	11(1)
C(2)	49(2)	26(1)	54(2)	-10(1)	2(1)	10(1)
C(3)	24(1)	33(1)	47(1)	7(1)	6(1)	17(1)
C(4)	26(1)	44(1)	49(1)	14(1)	3(1)	20(1)
C(5)	28(1)	35(1)	41(1)	13(1)	4(1)	17(1)
C(6)	20(1)	33(1)	32(1)	1(1)	5(1)	14(1)
C(7)	23(1)	36(1)	38(1)	5(1)	5(1)	16(1)
C(8)	30(1)	52(1)	43(1)	16(1)	9(1)	20(1)
C(9)	41(1)	74(2)	33(1)	9(1)	11(1)	31(1)
C(10)	44(1)	57(2)	41(1)	-8(1)	7(1)	28(1)
C(11)	35(1)	38(1)	41(1)	-1(1)	5(1)	20(1)
C(12)	27(1)	29(1)	25(1)	4(1)	-2(1)	9(1)
C(13)	33(1)	41(1)	29(1)	3(1)	2(1)	3(1)
C(14)	44(1)	39(1)	35(1)	2(1)	-4(1)	-2(1)
C(15)	61(2)	35(1)	30(1)	-2(1)	-5(1)	12(1)
C(16)	53(1)	45(1)	30(1)	2(1)	7(1)	22(1)
C(17)	34(1)	36(1)	32(1)	6(1)	4(1)	14(1)
P(3)	39(1)	31(1)	57(1)	6(1)	14(1)	16(1)
F(1)	122(2)	107(2)	190(3)	106(2)	82(2)	83(2)
F(2)	93(2)	80(1)	55(1)	-12(1)	2(1)	36(1)
F(3)	78(1)	63(1)	61(1)	22(1)	26(1)	29(1)
F(4)	53(1)	61(1)	157(2)	-49(1)	-20(1)	12(1)
F(5)	67(1)	65(1)	112(2)	37(1)	47(1)	44(1)
F(6)	44(1)	59(1)	118(2)	-15(1)	18(1)	25(1)
N(1S)	101(5)	78(4)	77(4)	-7(3)	26(4)	17(4)
C(1S)	80(5)	53(4)	60(4)	-8(3)	-4(3)	30(3)
C(2S)	75(4)	90(4)	115(5)	45(4)	17(3)	41(3)

Table A.3.5. Hydrogen coordinates (x 10^4) and isotropic displacement parameters ($Å^2$x 10^3) for *trans*-$[Fe(MPPP)_2(MeCN)_2](PF_6)_2$.

	x	y	z	U(eq)
H(1)	-3440(30)	-1330(20)	4675(19)	34(6)
H(2)	820(30)	1340(30)	2890(20)	38(6)
H(2A)	-3010(50)	-5040(40)	3670(30)	91(13)
H(2B)	-1450(50)	-4940(40)	3460(30)	93(13)
H(2C)	-2470(60)	-4650(50)	2630(50)	130(17)
H(3A)	-3800(30)	1010(30)	5090(20)	39(7)
H(3B)	-2090(30)	1990(30)	5260(20)	29(6)
H(4A)	-3600(30)	350(30)	3160(20)	35(6)
H(4B)	-3280(30)	1900(30)	3450(20)	45(7)
H(5A)	-1430(30)	1860(30)	2420(20)	36(6)
H(5B)	-590(30)	2630(30)	3640(20)	40(7)
H(7)	-3830(30)	-2500(30)	6470(20)	39(7)
H(8)	-4500(30)	-2710(30)	8250(20)	47(7)
H(9)	-4290(40)	-820(30)	9500(30)	64(9)
H(10)	-3200(30)	1420(30)	8980(20)	51(8)
H(11)	-2440(30)	1640(30)	7270(20)	36(6)
H(13)	-3430(30)	-1870(20)	2590(20)	32(6)
H(14)	-4630(30)	-3680(30)	1100(20)	50(8)
H(15)	-3170(40)	-3840(30)	-410(30)	60(9)
H(16)	-740(30)	-2110(30)	-340(20)	49(8)
H(17)	480(30)	-250(30)	1180(20)	36(6)

Table A.3.6. Torsion angles [°] for *trans*-[Fe(MPPP)$_2$(MeCN)$_2$](PF$_6$)$_2$.

N(1)-Fe(1)-P(1)-C(6)	99.33(9)
N(1)#1-Fe(1)-P(1)-C(6)	-80.67(9)
P(2)-Fe(1)-P(1)-C(6)	-169.15(8)
P(2)#1-Fe(1)-P(1)-C(6)	10.85(8)
P(1)#1-Fe(1)-P(1)-C(6)	-6(100)
N(1)-Fe(1)-P(1)-C(3)	-134.66(10)
N(1)#1-Fe(1)-P(1)-C(3)	45.34(10)
P(2)-Fe(1)-P(1)-C(3)	-43.14(9)
P(2)#1-Fe(1)-P(1)-C(3)	136.86(9)
P(1)#1-Fe(1)-P(1)-C(3)	120(100)
N(1)-Fe(1)-P(2)-C(12)	1.59(9)
N(1)#1-Fe(1)-P(2)-C(12)	-178.41(9)
P(2)#1-Fe(1)-P(2)-C(12)	-148(100)
P(1)#1-Fe(1)-P(2)-C(12)	90.95(8)
P(1)-Fe(1)-P(2)-C(12)	-89.05(8)
N(1)-Fe(1)-P(2)-C(5)	131.13(9)
N(1)#1-Fe(1)-P(2)-C(5)	-48.87(9)
P(2)#1-Fe(1)-P(2)-C(5)	-18(100)
P(1)#1-Fe(1)-P(2)-C(5)	-139.51(8)
P(1)-Fe(1)-P(2)-C(5)	40.49(8)
N(1)#1-Fe(1)-N(1)-C(1)	140(100)
P(2)-Fe(1)-N(1)-C(1)	-6(9)
P(2)#1-Fe(1)-N(1)-C(1)	174(100)
P(1)#1-Fe(1)-N(1)-C(1)	-98(9)
P(1)-Fe(1)-N(1)-C(1)	82(9)
Fe(1)-N(1)-C(1)-C(2)	37(28)
C(6)-P(1)-C(3)-C(4)	-161.33(16)
Fe(1)-P(1)-C(3)-C(4)	63.32(17)
P(1)-C(3)-C(4)-C(5)	-68.9(2)
C(3)-C(4)-C(5)-P(2)	64.7(2)
C(12)-P(2)-C(5)-C(4)	78.59(19)
Fe(1)-P(2)-C(5)-C(4)	-55.9(2)
C(3)-P(1)-C(6)-C(11)	-37.50(19)
Fe(1)-P(1)-C(6)-C(11)	94.34(17)

C(3)-P(1)-C(6)-C(7)	143.73(16)
Fe(1)-P(1)-C(6)-C(7)	-84.43(16)
C(11)-C(6)-C(7)-C(8)	-0.4(3)
P(1)-C(6)-C(7)-C(8)	178.39(16)
C(6)-C(7)-C(8)-C(9)	0.2(3)
C(7)-C(8)-C(9)-C(10)	0.6(4)
C(8)-C(9)-C(10)-C(11)	-1.4(4)
C(9)-C(10)-C(11)-C(6)	1.2(4)
C(7)-C(6)-C(11)-C(10)	-0.3(3)
P(1)-C(6)-C(11)-C(10)	-179.08(18)
C(5)-P(2)-C(12)-C(17)	110.51(18)
Fe(1)-P(2)-C(12)-C(17)	-114.56(16)
C(5)-P(2)-C(12)-C(13)	-71.9(2)
Fe(1)-P(2)-C(12)-C(13)	63.0(2)
C(17)-C(12)-C(13)-C(14)	-0.1(4)
P(2)-C(12)-C(13)-C(14)	-177.7(2)
C(12)-C(13)-C(14)-C(15)	1.0(4)
C(13)-C(14)-C(15)-C(16)	-1.1(4)
C(14)-C(15)-C(16)-C(17)	0.4(4)
C(15)-C(16)-C(17)-C(12)	0.5(4)
C(13)-C(12)-C(17)-C(16)	-0.6(3)
P(2)-C(12)-C(17)-C(16)	177.07(18)
N(1S)-C(1S)-C(2S)-C(1S)#2	30(100)

Symmetry transformations used to generate equivalent atoms:

#1 -x,-y,-z+1 #2 -x-2,-y-1,-z+2

APPENDIX B

SUPPORTING INFORMATION FOR CHAPTER III

B.1 Spectra

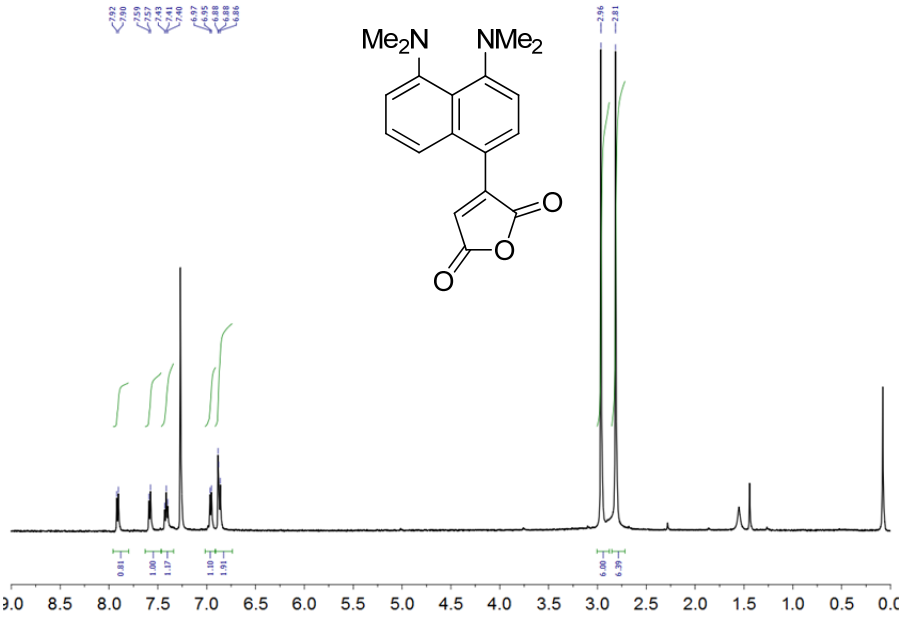

B.1.1 ^{1}H NMR Spectrum of MAPS ($CDCl_3$, 500 MHz)

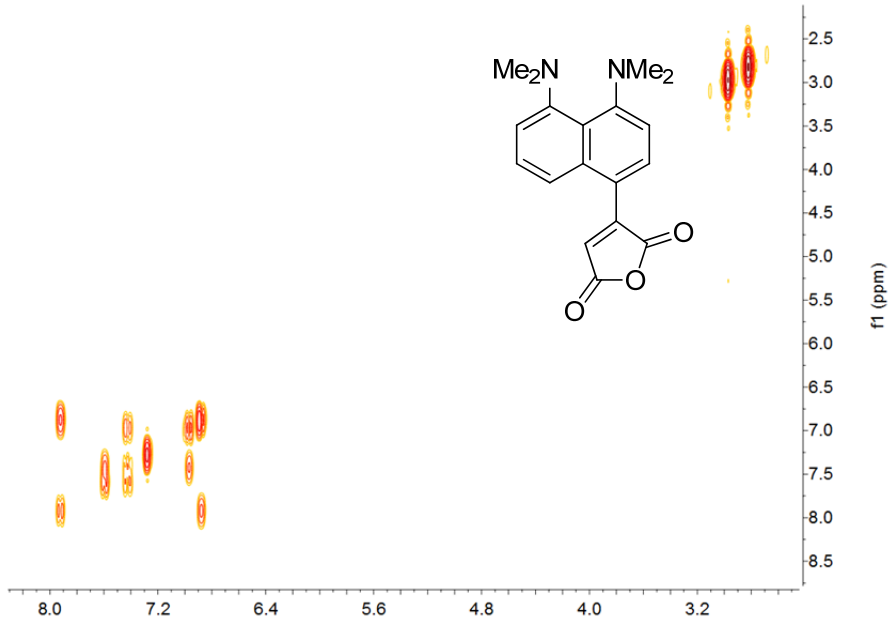

B.1.2 ^{1}H-^{1}H COSY NMR Spectrum of MAPS ($CDCl_3$, 500 MHz)

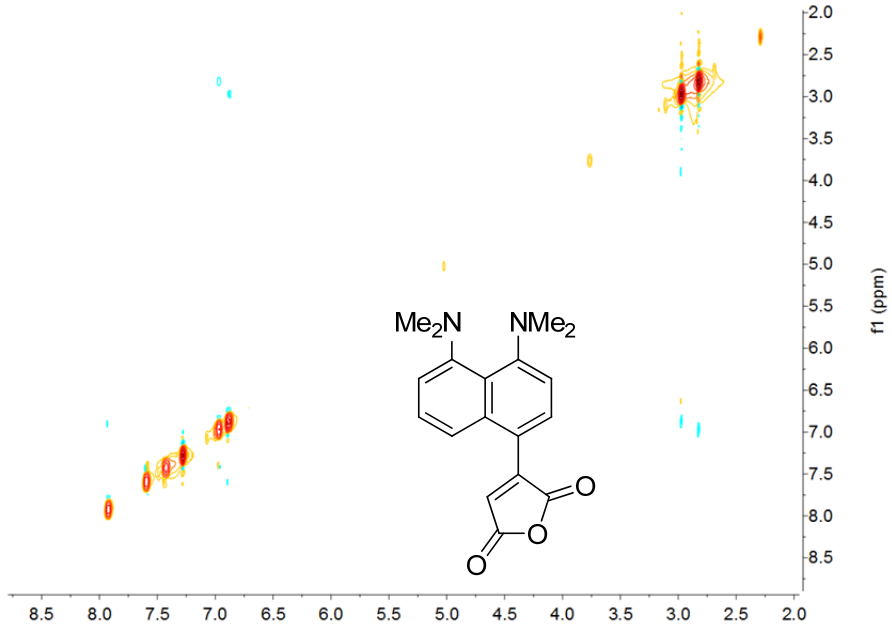

B.1.3 ^{1}H NOESY NMR Spectrum of MAPS ($CDCl_3$, 500 MHz)

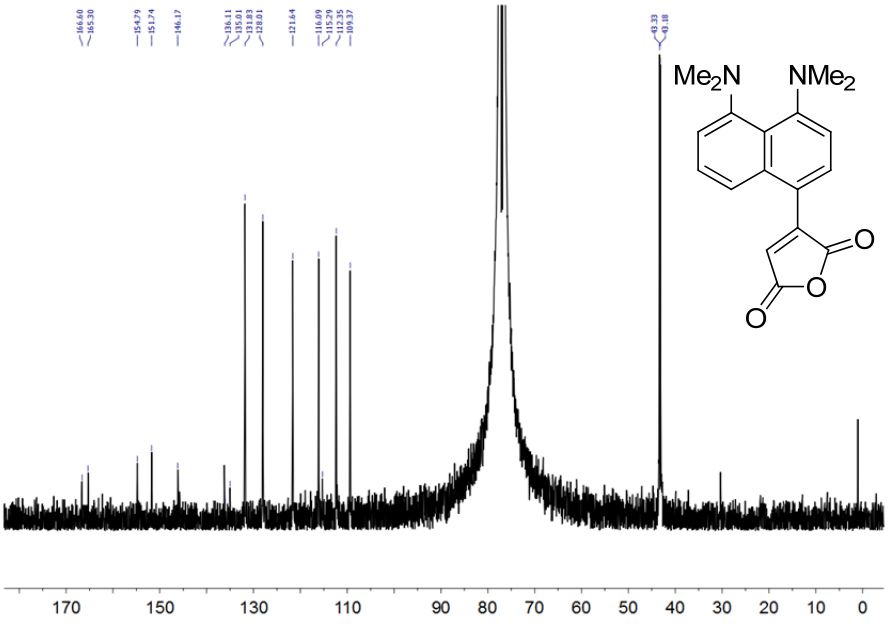

B.1.4 ^{13}C NMR Spectrum of MAPS ($CDCl_3$, 500 MHz)

B.2 pK_a titration of MAPS

B.2.1. UV-Vis titration spectra.

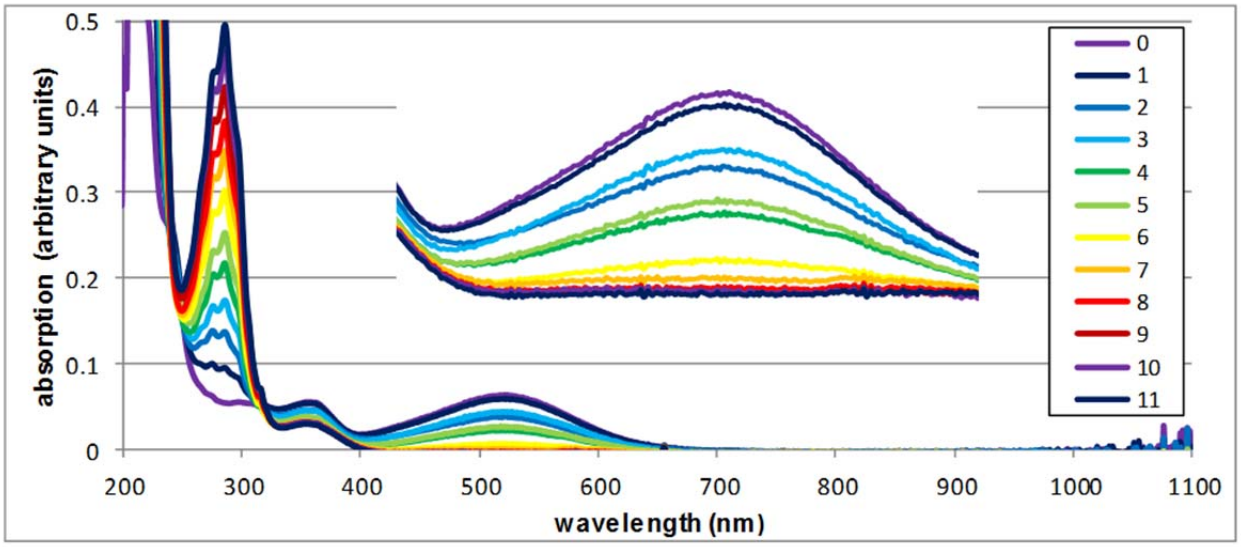

B.2.2. UV-Vis titration curve for MAPS.

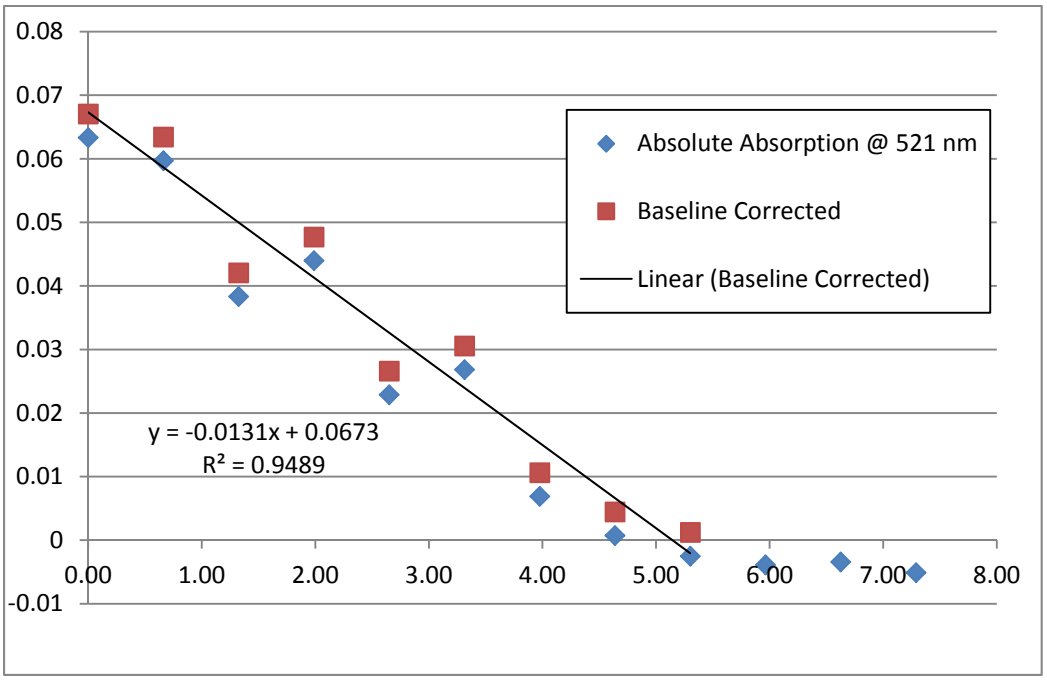

B.3 Crystal data for MAPS

Table B.3.1. Crystal data and structure refinement for MAPS.

Identification code	char8	
Empirical formula	C18 H18 N2 O3	
Formula weight	310.34	
Temperature	173(2) K	
Wavelength	0.71073 Å	
Crystal system	Monoclinic	
Space group	P2(1)	
Unit cell dimensions	a = 7.0429(6) Å	□= 90°.
	b = 17.4903(16) Å	□= 96.697(2)°.
	c = 12.7831(11) Å	□ = 90°.
Volume	1563.9(2) $Å^3$	
Z	4	
Density (calculated)	1.318 Mg/m^3	
Absorption coefficient	0.091 mm^{-1}	
F(000)	656	
Crystal size	0.28 x 0.10 x 0.02 mm^3	
Theta range for data collection	1.60 to 27.00°.	
Index ranges	-8<=h<=8, -22<=k<=22, -16<=l<=16	
Reflections collected	17571	
Independent reflections	6786 [R(int) = 0.0362]	
Completeness to theta = 27.00°	100.0 %	
Absorption correction	Semi-empirical from equivalents	
Max. and min. transmission	0.9982 and 0.9750	
Refinement method	Full-matrix least-squares on F^2	
Data / restraints / parameters	6786 / 1 / 559	
Goodness-of-fit on F^2	1.059	
Final R indices [I>2sigma(I)]	R1 = 0.0446, wR2 = 0.0747	
R indices (all data)	R1 = 0.0608, wR2 = 0.0811	
Absolute structure parameter	-0.5(9)	
Largest diff. peak and hole	0.156 and -0.145 $e.Å^{-3}$	

Table B. 3.2. Atomic coordinates (x 10^4) and equivalent isotropic displacement parameters ($Å^2$x 10^3) for MAPS. U(eq) is defined as one third of the trace of the orthogonalized U^{ij} tensor.

	x	y	z	U(eq)
O(1)	9127(3)	162(1)	1366(2)	59(1)
O(2)	8515(3)	280(1)	3037(2)	55(1)
O(3)	9753(3)	448(1)	-286(2)	81(1)
N(1)	11152(2)	4597(1)	3993(1)	31(1)
N(2)	9849(3)	3528(1)	5404(1)	32(1)
C(1)	10220(3)	4099(1)	3240(2)	27(1)
C(2)	9593(3)	4344(1)	2235(2)	31(1)
C(3)	8818(3)	3827(1)	1470(2)	34(1)
C(4)	8840(3)	3059(1)	1663(2)	30(1)
C(5)	9479(3)	2777(1)	2678(2)	26(1)
C(6)	9913(3)	3310(1)	3512(2)	24(1)
C(7)	10027(3)	3037(1)	4587(2)	26(1)
C(8)	10277(3)	2256(1)	4768(2)	30(1)
C(9)	10119(3)	1744(1)	3934(2)	30(1)
C(10)	9677(3)	1968(1)	2900(2)	28(1)
C(11)	11014(4)	5409(1)	3785(2)	44(1)
C(12)	13020(4)	4377(2)	4510(2)	43(1)
C(13)	8388(3)	4124(1)	5317(2)	37(1)
C(14)	10366(5)	3269(2)	6480(2)	44(1)
C(15)	9557(3)	1391(1)	2069(2)	33(1)
C(16)	9026(3)	572(1)	2279(2)	44(1)
C(17)	9622(4)	667(2)	597(2)	55(1)
C(18)	9901(3)	1420(2)	1063(2)	42(1)
O(1')	5322(2)	6309(1)	5163(1)	52(1)
O(2')	6290(3)	5479(1)	6447(1)	55(1)
O(3')	4378(3)	7393(1)	4297(1)	72(1)
N(1')	4566(3)	7980(1)	11355(1)	38(1)
N(2')	5766(3)	6435(1)	11323(1)	38(1)
C(1')	5315(3)	8004(1)	10395(2)	33(1)
C(2')	5919(3)	8679(1)	9985(2)	39(1)
C(3')	6460(3)	8713(1)	8974(2)	40(1)

C(4')	6242(3)	8102(1)	8321(2)	33(1)
C(5')	5704(3)	7381(1)	8700(2)	29(1)
C(6')	5493(3)	7306(1)	9798(2)	28(1)
C(7')	5517(3)	6545(1)	10246(2)	31(1)
C(8')	5297(3)	5924(1)	9567(2)	34(1)
C(9')	5227(3)	6014(1)	8487(2)	34(1)
C(10')	5441(3)	6720(1)	8021(2)	30(1)
C(11')	4661(5)	8674(2)	11995(2)	54(1)
C(12')	2758(4)	7582(2)	11399(2)	48(1)
C(13')	7379(4)	6795(2)	11946(2)	50(1)
C(14')	5271(4)	5697(2)	11742(2)	47(1)
C(15')	5296(3)	6773(1)	6882(2)	34(1)
C(16')	5701(3)	6100(2)	6212(2)	42(1)
C(17')	4747(3)	7081(2)	5121(2)	51(1)
C(18')	4745(3)	7336(2)	6201(2)	42(1)

Table B.3.3. Bond lengths [Å] and angles [°] for char8.

O(1)-C(16)	1.378(3)	C(13)-H(13B)	1.01(2)
O(1)-C(17)	1.397(3)	C(13)-H(13C)	0.98(2)
O(2)-C(16)	1.188(3)	C(14)-H(14A)	0.93(2)
O(3)-C(17)	1.206(3)	C(14)-H(14B)	1.06(3)
N(1)-C(1)	1.402(2)	C(14)-H(14C)	1.01(3)
N(1)-C(11)	1.446(3)	C(15)-C(18)	1.337(3)
N(1)-C(12)	1.454(3)	C(15)-C(16)	1.513(3)
N(2)-C(7)	1.369(2)	C(17)-C(18)	1.449(3)
N(2)-C(14)	1.454(3)	C(18)-H(18)	0.96(2)
N(2)-C(13)	1.461(3)	O(1')-C(16')	1.387(3)
C(1)-C(2)	1.376(3)	O(1')-C(17')	1.409(3)
C(1)-C(6)	1.446(3)	O(2')-C(16')	1.188(3)
C(2)-C(3)	1.396(3)	O(3')-C(17')	1.188(3)
C(2)-H(2)	0.95(2)	N(1')-C(1')	1.392(3)
C(3)-C(4)	1.366(3)	N(1')-C(12')	1.457(3)
C(3)-H(3)	0.954(19)	N(1')-C(11')	1.461(3)
C(4)-C(5)	1.412(3)	N(2')-C(7')	1.380(3)
C(4)-H(4)	0.97(2)	N(2')-C(13')	1.452(3)
C(5)-C(6)	1.423(3)	N(2')-C(14')	1.456(3)
C(5)-C(10)	1.446(3)	C(1')-C(2')	1.380(3)
C(6)-C(7)	1.449(3)	C(1')-C(6')	1.453(3)
C(7)-C(8)	1.393(3)	C(2')-C(3')	1.391(3)
C(8)-C(9)	1.386(3)	C(2')-H(2')	0.95(2)
C(8)-H(8)	0.985(19)	C(3')-C(4')	1.354(3)
C(9)-C(10)	1.379(3)	C(3')-H(3')	0.99(2)
C(9)-H(9)	0.918(19)	C(4')-C(5')	1.418(3)
C(10)-C(15)	1.460(3)	C(4')-H(4')	0.983(19)
C(11)-H(11A)	1.02(3)	C(5')-C(6')	1.434(3)
C(11)-H(11B)	0.96(3)	C(5')-C(10')	1.444(3)
C(11)-H(11C)	1.02(2)	C(6')-C(7')	1.449(3)
C(12)-H(12A)	0.99(2)	C(7')-C(8')	1.388(3)
C(12)-H(12B)	1.00(3)	C(8')-C(9')	1.384(3)
C(12)-H(12C)	1.00(2)	C(8')-H(8')	0.97(2)
C(13)-H(13A)	1.09(3)	C(9')-C(10')	1.387(3)

C(9')-H(9')	0.91(2)	C(5)-C(4)-H(4)	119.7(12)
C(10')-C(15')	1.451(3)	C(4)-C(5)-C(6)	118.43(18)
C(11')-H(11D)	1.08(3)	C(4)-C(5)-C(10)	122.36(18)
C(11')-H(11E)	1.00(3)	C(6)-C(5)-C(10)	119.20(18)
C(11')-H(11F)	0.99(2)	C(5)-C(6)-C(1)	118.10(17)
C(12')-H(12D)	1.02(3)	C(5)-C(6)-C(7)	118.49(17)
C(12')-H(12E)	1.05(2)	C(1)-C(6)-C(7)	123.40(17)
C(12')-H(12F)	0.97(3)	N(2)-C(7)-C(8)	120.66(18)
C(13')-H(13D)	1.04(3)	N(2)-C(7)-C(6)	121.10(17)
C(13')-H(13E)	0.95(3)	C(8)-C(7)-C(6)	118.22(18)
C(13')-H(13F)	0.99(3)	C(9)-C(8)-C(7)	120.6(2)
C(14')-H(14D)	1.00(3)	C(9)-C(8)-H(8)	120.1(10)
C(14')-H(14E)	1.01(2)	C(7)-C(8)-H(8)	118.5(10)
C(14')-H(14F)	1.03(3)	C(10)-C(9)-C(8)	122.9(2)
C(15')-C(18')	1.342(3)	C(10)-C(9)-H(9)	120.9(12)
C(15')-C(16')	1.502(3)	C(8)-C(9)-H(9)	116.1(11)
C(17')-C(18')	1.451(3)	C(9)-C(10)-C(5)	118.08(18)
C(18')-H(18')	0.94(2)	C(9)-C(10)-C(15)	119.28(18)
C(16)-O(1)-C(17)	107.95(19)	C(5)-C(10)-C(15)	122.50(18)
C(1)-N(1)-C(11)	117.85(18)	N(1)-C(11)-H(11A)	110.4(15)
C(1)-N(1)-C(12)	118.31(18)	N(1)-C(11)-H(11B)	109.4(15)
C(11)-N(1)-C(12)	112.41(19)	H(11A)-C(11)-H(11B)	106(2)
C(7)-N(2)-C(14)	119.44(18)	N(1)-C(11)-H(11C)	113.3(14)
C(7)-N(2)-C(13)	121.08(17)	H(11A)-C(11)-H(11C)	107.5(19)
C(14)-N(2)-C(13)	113.03(19)	H(11B)-C(11)-H(11C)	109(2)
C(2)-C(1)-N(1)	121.43(18)	N(1)-C(12)-H(12A)	111.0(14)
C(2)-C(1)-C(6)	118.71(19)	N(1)-C(12)-H(12B)	108.7(17)
N(1)-C(1)-C(6)	119.85(17)	H(12A)-C(12)-H(12B)	111(2)
C(1)-C(2)-C(3)	120.7(2)	N(1)-C(12)-H(12C)	112.1(13)
C(1)-C(2)-H(2)	117.0(12)	H(12A)-C(12)-H(12C)	103(2)
C(3)-C(2)-H(2)	121.9(12)	H(12B)-C(12)-H(12C)	111(2)
C(4)-C(3)-C(2)	121.0(2)	N(2)-C(13)-H(13A)	110.6(13)
C(4)-C(3)-H(3)	121.0(11)	N(2)-C(13)-H(13B)	108.9(12)
C(2)-C(3)-H(3)	118.0(11)	H(13A)-C(13)-H(13B)	110.5(16)
C(3)-C(4)-C(5)	120.4(2)	N(2)-C(13)-H(13C)	113.6(12)
C(3)-C(4)-H(4)	119.8(12)	H(13A)-C(13)-H(13C)	104.4(18)

H(13B)-C(13)-H(13C)	108.8(18)	C(3')-C(4')-H(4')	122.5(12)
N(2)-C(14)-H(14A)	106.5(12)	C(5')-C(4')-H(4')	116.6(12)
N(2)-C(14)-H(14B)	110.3(13)	C(4')-C(5')-C(6')	118.51(19)
H(14A)-C(14)-H(14B)	111.1(19)	C(4')-C(5')-C(10')	121.79(19)
N(2)-C(14)-H(14C)	110.3(13)	C(6')-C(5')-C(10')	119.65(18)
H(14A)-C(14)-H(14C)	113.2(19)	C(5')-C(6')-C(7')	118.23(17)
H(14B)-C(14)-H(14C)	105.5(19)	C(5')-C(6')-C(1')	117.62(18)
C(18)-C(15)-C(10)	132.2(2)	C(7')-C(6')-C(1')	124.13(18)
C(18)-C(15)-C(16)	106.4(2)	N(2')-C(7')-C(8')	120.50(19)
C(10)-C(15)-C(16)	121.32(19)	N(2')-C(7')-C(6')	121.09(17)
O(2)-C(16)-O(1)	121.2(2)	C(8')-C(7')-C(6')	118.41(19)
O(2)-C(16)-C(15)	131.0(2)	C(9')-C(8')-C(7')	121.6(2)
O(1)-C(16)-C(15)	107.7(2)	C(9')-C(8')-H(8')	122.3(12)
O(3)-C(17)-O(1)	120.7(3)	C(7')-C(8')-H(8')	116.1(12)
O(3)-C(17)-C(18)	130.8(3)	C(8')-C(9')-C(10')	122.4(2)
O(1)-C(17)-C(18)	108.6(2)	C(8')-C(9')-H(9')	118.3(14)
C(15)-C(18)-C(17)	109.3(2)	C(10')-C(9')-H(9')	119.3(14)
C(15)-C(18)-H(18)	128.8(12)	C(9')-C(10')-C(5')	117.84(19)
C(17)-C(18)-H(18)	121.9(12)	C(9')-C(10')-C(15')	119.31(19)
C(16')-O(1')-C(17')	108.20(19)	C(5')-C(10')-C(15')	122.77(19)
C(1')-N(1')-C(12')	118.09(19)	N(1')-C(11')-H(11D)	105.1(13)
C(1')-N(1')-C(11')	118.1(2)	N(1')-C(11')-H(11E)	109.6(15)
C(12')-N(1')-C(11')	111.0(2)	H(11D)-C(11')-H(11E)	113(2)
C(7')-N(2')-C(13')	119.1(2)	N(1')-C(11')-H(11F)	110.5(14)
C(7')-N(2')-C(14')	118.84(18)	H(11D)-C(11')-H(11F)	110.5(19)
C(13')-N(2')-C(14')	112.77(19)	H(11E)-C(11')-H(11F)	108(2)
C(2')-C(1')-N(1')	121.7(2)	N(1')-C(12')-H(12D)	112.5(15)
C(2')-C(1')-C(6')	118.03(19)	N(1')-C(12')-H(12E)	109.9(13)
N(1')-C(1')-C(6')	120.23(19)	H(12D)-C(12')-H(12E)	107.3(18)
C(1')-C(2')-C(3')	121.3(2)	N(1')-C(12')-H(12F)	111.8(14)
C(1')-C(2')-H(2')	118.6(13)	H(12D)-C(12')-H(12F)	109(2)
C(3')-C(2')-H(2')	120.1(13)	H(12E)-C(12')-H(12F)	107(2)
C(4')-C(3')-C(2')	121.0(2)	N(2')-C(13')-H(13D)	112.9(13)
C(4')-C(3')-H(3')	118.1(13)	N(2')-C(13')-H(13E)	109.3(18)
C(2')-C(3')-H(3')	120.6(13)	H(13D)-C(13')-H(13E)	107(2)
C(3')-C(4')-C(5')	120.5(2)	N(2')-C(13')-H(13F)	110.2(15)

H(13D)-C(13')-H(13F)	107(2)	C(10')-C(15')-C(16')	121.7(2)
H(13E)-C(13')-H(13F)	110(2)	O(2')-C(16')-O(1')	120.6(2)
N(2')-C(14')-H(14D)	113.7(14)	O(2')-C(16')-C(15')	131.0(2)
N(2')-C(14')-H(14E)	107.1(15)	O(1')-C(16')-C(15')	108.4(2)
H(14D)-C(14')-H(14E)	109.0(19)	O(3')-C(17')-O(1')	120.3(2)
N(2')-C(14')-H(14F)	107.3(14)	O(3')-C(17')-C(18')	132.8(3)
H(14D)-C(14')-H(14F)	103.5(19)	O(1')-C(17')-C(18')	106.9(2)
H(14E)-C(14')-H(14F)	116(2)	C(15')-C(18')-C(17')	111.0(3)
C(18')-C(15')-C(10')	132.8(2)	C(15')-C(18')-H(18')	129.9(14)
C(18')-C(15')-C(16')	105.4(2)	C(17')-C(18')-H(18')	119.1(14)

Symmetry transformations used to generate equivalent atoms:

Table B.3.4. Anisotropic displacement parameters ($Å^2 x\ 10^3$)for char8. The anisotropic displacement factor exponent takes the form: $-2\pi^2[\ h^2a^{*2}U^{11} + ... + 2\ h\ k\ a^*\ b^*\ U^{12}\ ]$

	U^{11}	U^{22}	U^{33}	U^{23}	U^{13}	U^{12}
O(1)	58(1)	38(1)	76(1)	-25(1)	-10(1)	3(1)
O(2)	57(1)	33(1)	68(1)	6(1)	-14(1)	-6(1)
O(3)	76(1)	91(2)	76(1)	-55(1)	8(1)	1(1)
N(1)	32(1)	22(1)	36(1)	0(1)	-2(1)	-1(1)
N(2)	42(1)	29(1)	24(1)	-1(1)	2(1)	5(1)
C(1)	22(1)	27(1)	31(1)	0(1)	5(1)	0(1)
C(2)	30(1)	28(1)	35(1)	7(1)	6(1)	1(1)
C(3)	34(1)	43(1)	25(1)	7(1)	1(1)	2(1)
C(4)	26(1)	38(1)	27(1)	-5(1)	1(1)	-4(1)
C(5)	19(1)	31(1)	28(1)	-2(1)	6(1)	-2(1)
C(6)	17(1)	28(1)	27(1)	-1(1)	2(1)	1(1)
C(7)	23(1)	28(1)	27(1)	1(1)	1(1)	0(1)
C(8)	30(1)	31(1)	28(1)	6(1)	2(1)	3(1)
C(9)	29(1)	21(1)	39(1)	1(1)	3(1)	1(1)
C(10)	21(1)	29(1)	36(1)	-5(1)	4(1)	1(1)
C(11)	56(2)	28(1)	48(2)	-5(1)	3(1)	-4(1)
C(12)	33(1)	38(2)	54(2)	-5(1)	-7(1)	-1(1)
C(13)	36(1)	37(1)	38(1)	-3(1)	7(1)	5(1)
C(14)	61(2)	41(2)	29(1)	0(1)	2(1)	2(1)
C(15)	21(1)	33(1)	45(1)	-8(1)	-1(1)	1(1)
C(16)	33(1)	33(1)	61(2)	-12(1)	-10(1)	3(1)
C(17)	41(2)	64(2)	60(2)	-34(2)	-2(1)	7(1)
C(18)	29(1)	50(2)	44(1)	-18(1)	3(1)	-3(1)
O(1')	47(1)	70(1)	38(1)	-16(1)	7(1)	-15(1)
O(2')	60(1)	45(1)	61(1)	-17(1)	18(1)	-2(1)
O(3')	62(1)	113(2)	39(1)	13(1)	5(1)	7(1)
N(1')	47(1)	32(1)	35(1)	-6(1)	5(1)	4(1)
N(2')	46(1)	28(1)	38(1)	4(1)	-6(1)	-2(1)
C(1')	29(1)	30(1)	39(1)	0(1)	-1(1)	2(1)
C(2')	40(1)	23(1)	53(2)	-5(1)	6(1)	4(1)
C(3')	32(1)	27(1)	64(2)	6(1)	14(1)	2(1)

C(4')	28(1)	31(1)	41(1)	2(1)	10(1)	4(1)
C(5')	18(1)	28(1)	40(1)	-1(1)	5(1)	5(1)
C(6')	22(1)	26(1)	35(1)	0(1)	-1(1)	1(1)
C(7')	27(1)	28(1)	37(1)	-1(1)	-2(1)	-1(1)
C(8')	35(1)	24(1)	43(1)	2(1)	-2(1)	1(1)
C(9')	27(1)	31(1)	44(1)	-10(1)	2(1)	-1(1)
C(10')	20(1)	32(1)	38(1)	-1(1)	4(1)	4(1)
C(11')	75(2)	42(2)	45(2)	-12(1)	6(2)	8(2)
C(12')	50(2)	51(2)	44(2)	-3(1)	14(1)	4(1)
C(13')	55(2)	41(2)	48(2)	2(1)	-17(1)	-5(1)
C(14')	61(2)	37(2)	42(2)	7(1)	-2(1)	-5(1)
C(15')	21(1)	41(1)	40(1)	-6(1)	5(1)	0(1)
C(16')	32(1)	51(2)	45(2)	-10(1)	9(1)	-7(1)
C(17')	35(1)	73(2)	44(2)	-2(1)	7(1)	-3(1)
C(18')	32(1)	55(2)	40(1)	-1(1)	8(1)	9(1)

Table B.3.5. Hydrogen coordinates (x 10^4) and isotropic displacement parameters ($Å^2$x 10^3) for MAPS.

	x	y	z	U(eq)
H(2)	9840(30)	4864(11)	2070(15)	28(5)
H(2')	5930(30)	9131(13)	10404(17)	41(6)
H(3)	8340(30)	4024(10)	795(16)	25(5)
H(3')	6900(30)	9201(14)	8689(17)	52(7)
H(4)	8410(30)	2706(12)	1103(15)	31(5)
H(4')	6570(30)	8117(11)	7596(16)	33(6)
H(8)	10340(20)	2067(10)	5496(15)	21(5)
H(8')	5240(30)	5425(13)	9895(16)	37(6)
H(9)	10260(30)	1237(11)	4109(14)	18(5)
H(9')	5080(30)	5591(14)	8077(17)	41(6)
H(11A)	9620(40)	5568(15)	3616(18)	62(8)
H(11B)	11510(30)	5686(15)	4409(19)	55(7)
H(11C)	11720(30)	5576(14)	3172(19)	59(8)
H(11D)	4250(40)	8497(14)	12750(20)	62(8)
H(11E)	5980(40)	8892(15)	12047(19)	61(8)
H(11F)	3770(30)	9063(14)	11668(17)	46(7)
H(12A)	14040(40)	4527(14)	4084(18)	49(7)
H(12B)	13220(40)	4624(17)	5220(20)	81(9)
H(12C)	13170(30)	3806(14)	4567(16)	38(6)
H(12D)	1610(40)	7933(15)	11237(19)	64(8)
H(12E)	2700(30)	7358(14)	12158(19)	55(7)
H(12F)	2620(30)	7154(14)	10918(19)	50(7)
H(13A)	9000(40)	4670(15)	5602(18)	58(7)
H(13B)	7330(30)	3967(11)	5736(15)	30(6)
H(13C)	7840(30)	4229(12)	4588(18)	40(6)
H(13D)	7780(30)	7311(16)	11627(18)	59(7)
H(13E)	7050(40)	6903(16)	12630(20)	78(10)
H(13F)	8510(40)	6452(15)	11997(19)	64(8)
H(14A)	11580(30)	3056(12)	6504(15)	32(6)
H(14B)	10350(30)	3734(15)	7012(18)	54(7)

H(14C)	9380(30)	2897(15)	6689(18)	53(7)
H(14D)	3990(40)	5501(14)	11435(17)	51(7)
H(14E)	5270(30)	5761(15)	12528(19)	55(7)
H(14F)	6210(40)	5301(15)	11503(17)	54(7)
H(18)	10270(30)	1851(13)	667(16)	32(6)
H(18')	4360(30)	7838(13)	6329(17)	40(7)

Table B.3.6. Torsion angles [°] for MAPS.

C(11)-N(1)-C(1)-C(2)	15.5(3)
C(12)-N(1)-C(1)-C(2)	-125.3(2)
C(11)-N(1)-C(1)-C(6)	-164.96(19)
C(12)-N(1)-C(1)-C(6)	54.3(3)
N(1)-C(1)-C(2)-C(3)	174.42(19)
C(6)-C(1)-C(2)-C(3)	-5.2(3)
C(1)-C(2)-C(3)-C(4)	-6.8(3)
C(2)-C(3)-C(4)-C(5)	6.3(3)
C(3)-C(4)-C(5)-C(6)	6.2(3)
C(3)-C(4)-C(5)-C(10)	-174.8(2)
C(4)-C(5)-C(6)-C(1)	-17.7(3)
C(10)-C(5)-C(6)-C(1)	163.26(17)
C(4)-C(5)-C(6)-C(7)	162.39(17)
C(10)-C(5)-C(6)-C(7)	-16.7(3)
C(2)-C(1)-C(6)-C(5)	17.3(3)
N(1)-C(1)-C(6)-C(5)	-162.33(17)
C(2)-C(1)-C(6)-C(7)	-162.83(18)
N(1)-C(1)-C(6)-C(7)	17.6(3)
C(14)-N(2)-C(7)-C(8)	14.5(3)
C(13)-N(2)-C(7)-C(8)	-135.4(2)
C(14)-N(2)-C(7)-C(6)	-167.1(2)
C(13)-N(2)-C(7)-C(6)	43.1(3)
C(5)-C(6)-C(7)-N(2)	-159.68(17)
C(1)-C(6)-C(7)-N(2)	20.4(3)
C(5)-C(6)-C(7)-C(8)	18.8(3)
C(1)-C(6)-C(7)-C(8)	-161.12(18)
N(2)-C(7)-C(8)-C(9)	168.53(18)
C(6)-C(7)-C(8)-C(9)	-10.0(3)
C(7)-C(8)-C(9)-C(10)	-1.3(3)
C(8)-C(9)-C(10)-C(5)	3.6(3)
C(8)-C(9)-C(10)-C(15)	179.43(19)
C(4)-C(5)-C(10)-C(9)	-173.38(18)
C(6)-C(5)-C(10)-C(9)	5.6(3)
C(4)-C(5)-C(10)-C(15)	10.9(3)

C(6)-C(5)-C(10)-C(15)	-170.05(17)
C(9)-C(10)-C(15)-C(18)	-149.8(2)
C(5)-C(10)-C(15)-C(18)	25.8(3)
C(9)-C(10)-C(15)-C(16)	27.7(3)
C(5)-C(10)-C(15)-C(16)	-156.70(19)
C(17)-O(1)-C(16)-O(2)	175.4(2)
C(17)-O(1)-C(16)-C(15)	-1.8(2)
C(18)-C(15)-C(16)-O(2)	-175.8(2)
C(10)-C(15)-C(16)-O(2)	6.2(4)
C(18)-C(15)-C(16)-O(1)	1.0(2)
C(10)-C(15)-C(16)-O(1)	-177.03(17)
C(16)-O(1)-C(17)-O(3)	-178.1(2)
C(16)-O(1)-C(17)-C(18)	1.9(3)
C(10)-C(15)-C(18)-C(17)	177.9(2)
C(16)-C(15)-C(18)-C(17)	0.2(2)
O(3)-C(17)-C(18)-C(15)	178.7(3)
O(1)-C(17)-C(18)-C(15)	-1.3(3)
C(12')-N(1')-C(1')-C(2')	130.2(2)
C(11')-N(1')-C(1')-C(2')	-8.0(3)
C(12')-N(1')-C(1')-C(6')	-50.2(3)
C(11')-N(1')-C(1')-C(6')	171.6(2)
N(1')-C(1')-C(2')-C(3')	-172.6(2)
C(6')-C(1')-C(2')-C(3')	7.8(3)
C(1')-C(2')-C(3')-C(4')	6.4(4)
C(2')-C(3')-C(4')-C(5')	-8.8(3)
C(3')-C(4')-C(5')-C(6')	-3.1(3)
C(3')-C(4')-C(5')-C(10')	179.4(2)
C(4')-C(5')-C(6')-C(7')	-161.74(18)
C(10')-C(5')-C(6')-C(7')	15.9(3)
C(4')-C(5')-C(6')-C(1')	16.8(3)
C(10')-C(5')-C(6')-C(1')	-165.63(18)
C(2')-C(1')-C(6')-C(5')	-19.1(3)
N(1')-C(1')-C(6')-C(5')	161.33(18)
C(2')-C(1')-C(6')-C(7')	159.3(2)
N(1')-C(1')-C(6')-C(7')	-20.3(3)
C(13')-N(2')-C(7')-C(8')	127.5(2)

C(14')-N(2')-C(7')-C(8')	-16.9(3)
C(13')-N(2')-C(7')-C(6')	-52.1(3)
C(14')-N(2')-C(7')-C(6')	163.5(2)
C(5')-C(6')-C(7')-N(2')	164.87(18)
C(1')-C(6')-C(7')-N(2')	-13.5(3)
C(5')-C(6')-C(7')-C(8')	-14.7(3)
C(1')-C(6')-C(7')-C(8')	166.9(2)
N(2')-C(7')-C(8')-C(9')	-173.8(2)
C(6')-C(7')-C(8')-C(9')	5.8(3)
C(7')-C(8')-C(9')-C(10')	2.5(3)
C(8')-C(9')-C(10')-C(5')	-1.4(3)
C(8')-C(9')-C(10')-C(15')	-178.2(2)
C(4')-C(5')-C(10')-C(9')	169.61(19)
C(6')-C(5')-C(10')-C(9')	-7.9(3)
C(4')-C(5')-C(10')-C(15')	-13.7(3)
C(6')-C(5')-C(10')-C(15')	168.80(18)
C(9')-C(10')-C(15')-C(18')	151.5(2)
C(5')-C(10')-C(15')-C(18')	-25.2(4)
C(9')-C(10')-C(15')-C(16')	-24.9(3)
C(5')-C(10')-C(15')-C(16')	158.46(19)
C(17')-O(1')-C(16')-O(2')	-176.9(2)
C(17')-O(1')-C(16')-C(15')	1.5(2)
C(18')-C(15')-C(16')-O(2')	177.0(3)
C(10')-C(15')-C(16')-O(2')	-5.8(4)
C(18')-C(15')-C(16')-O(1')	-1.1(2)
C(10')-C(15')-C(16')-O(1')	176.08(18)
C(16')-O(1')-C(17')-O(3')	178.6(2)
C(16')-O(1')-C(17')-C(18')	-1.3(2)
C(10')-C(15')-C(18')-C(17')	-176.5(2)
C(16')-C(15')-C(18')-C(17')	0.3(3)
O(3')-C(17')-C(18')-C(15')	-179.3(3)
O(1')-C(17')-C(18')-C(15')	0.6(3)

APPENDIX C

SUPPORTING INFORMATION FOR CHAPTER IV

C.1 Spectra

C.1.1. ^{1}H NMR Spectrum of *trans*-Fe(DHMPE)$_2$Cl$_2$ (d6-DMSO)

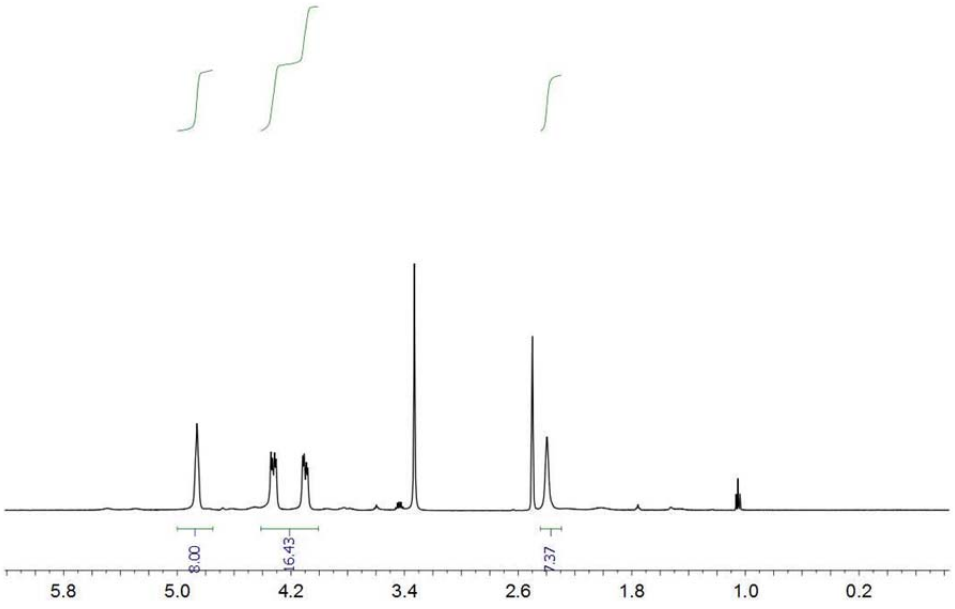

C.1.2. $^{31}P\{^{1}H\}$ NMR Spectrum of *trans*-$Fe(DHMPE)_2Cl_2$ (d6-DMSO)

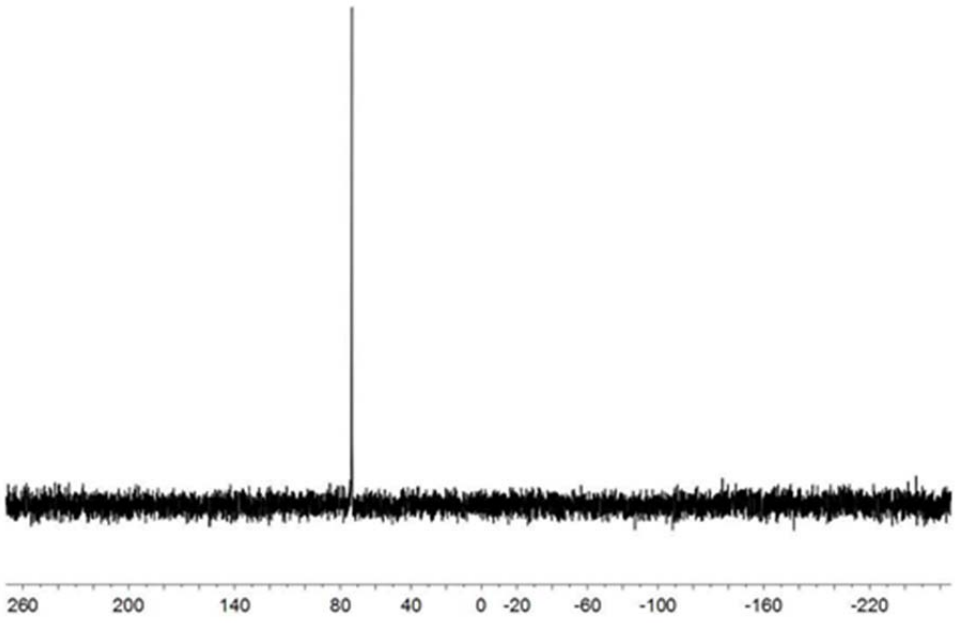

C.1.3. ^{13}C NMR Spectrum of *trans*- $Fe(DHMPE)_2Cl_2$ (d6-DMSO)

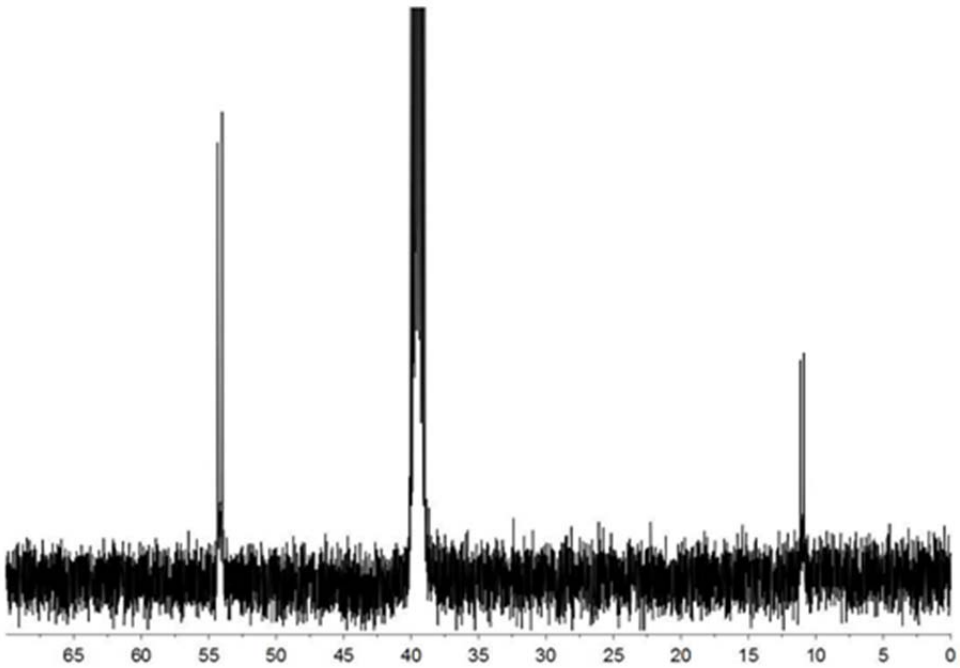

C.1.4. ^{1}H NMR Spectrum of DHMPE·$2BH_3$ (d6-DMSO)

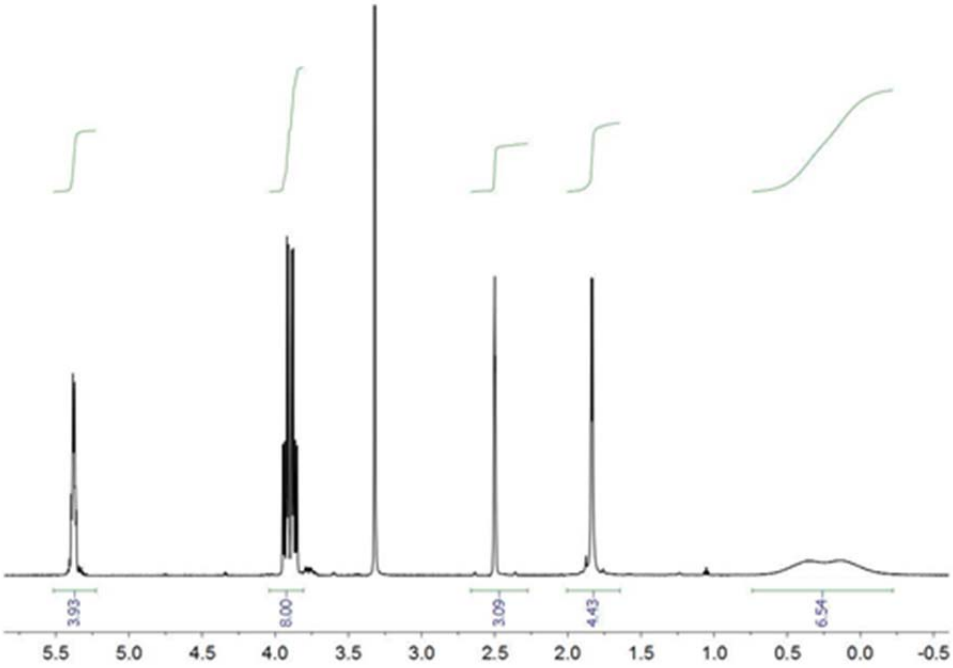

C.1.5. $^{31}P\{^{1}H\}$ NMR Spectrum of DHMPE·$2BH_3$ (d6-DMSO)

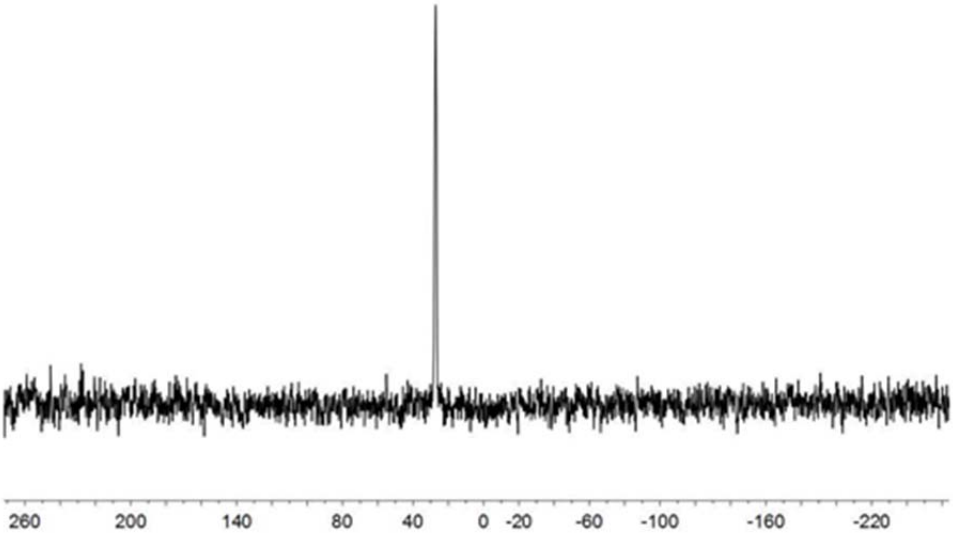

C.1.6. ^{13}C NMR Spectrum of DHMPE·$2BH_3$(d6-DMSO)

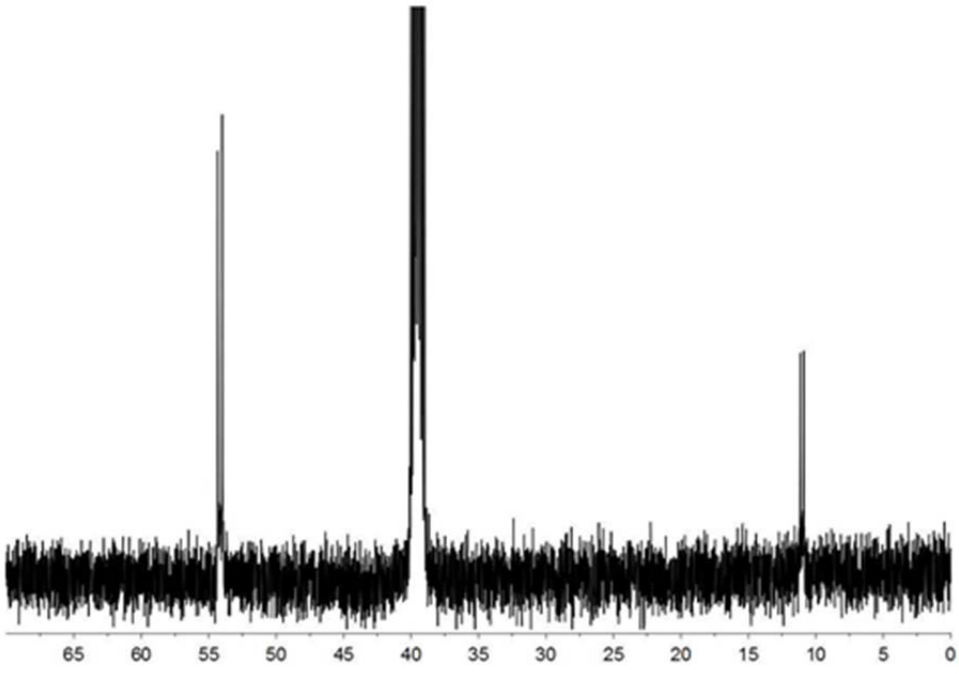

C.1.7. ^{11}B NMR Spectrum of DHMPE·$2BH_3$(d6-DMSO)

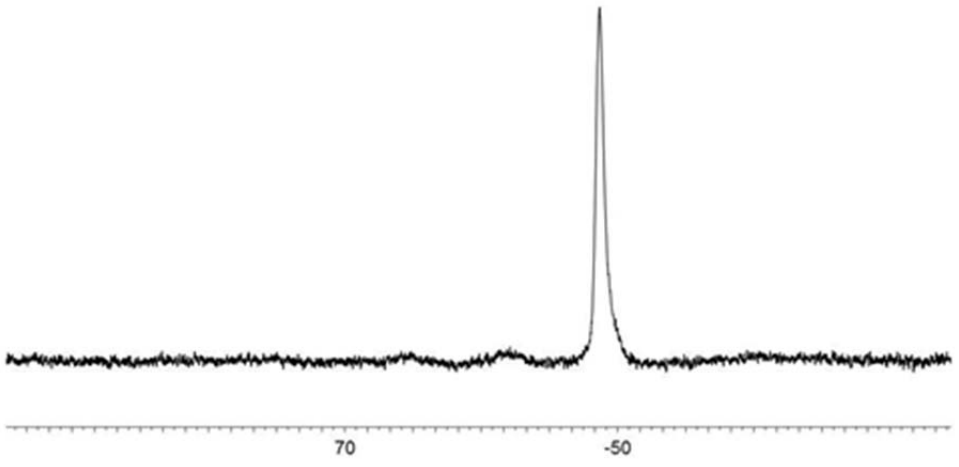

C.1.7. ^{1}H NMR Spectra of $Ph_2PCH_2OH + Et_2NH$ (d6-ethanol)

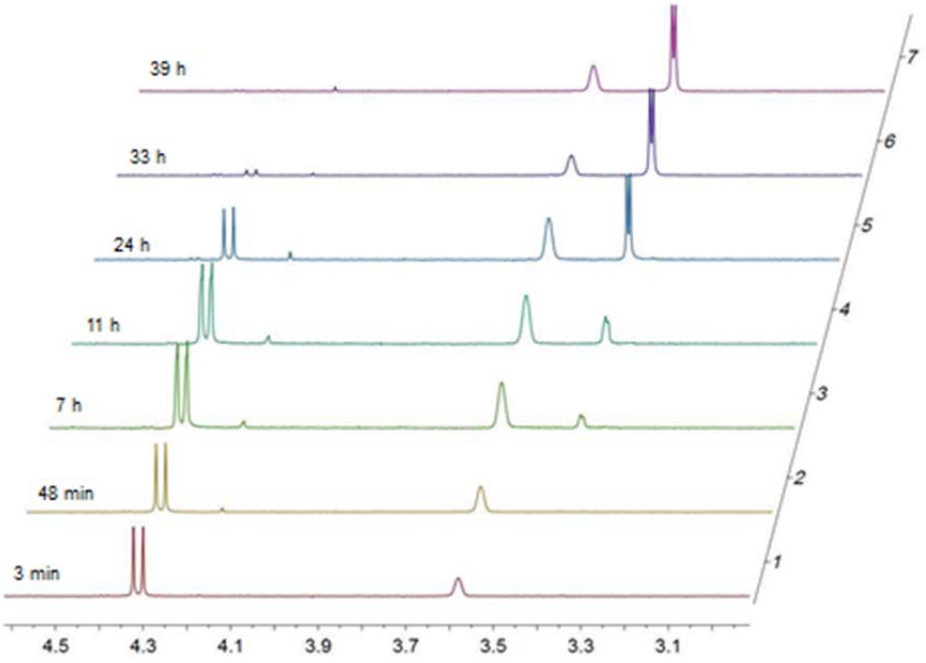

C.1.8. $^{31}P\{^{1}H\}$ NMR Spectra of $Ph_2PCH_2OH + Et_2NH$ (d6-ethanol)

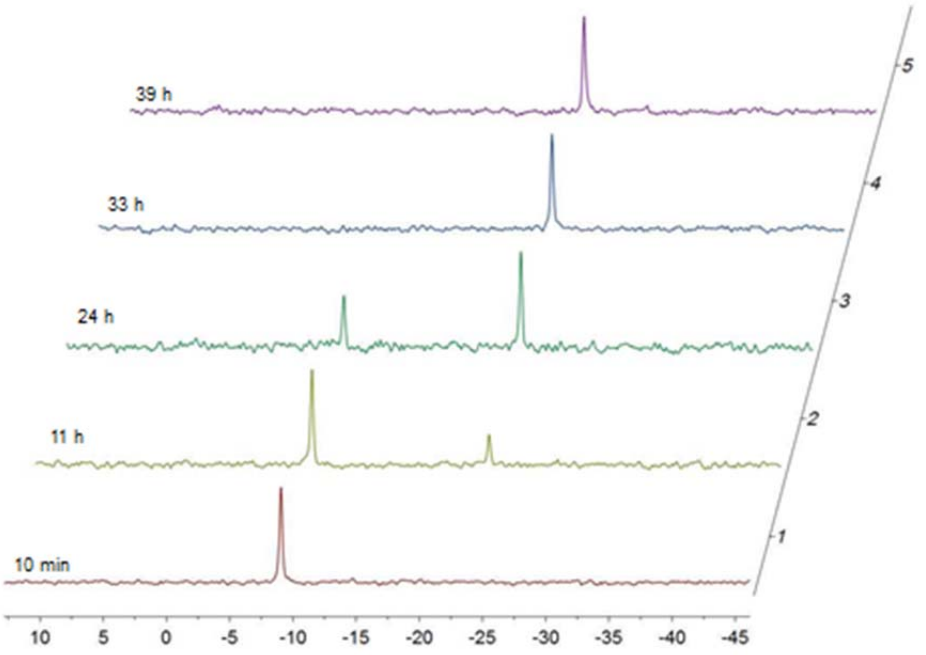

C.1.9. ^{1}H NMR Spectra of $Ph_2PCH_2OH{\cdot}BH_3$ + Et_2NH (d6-ethanol)

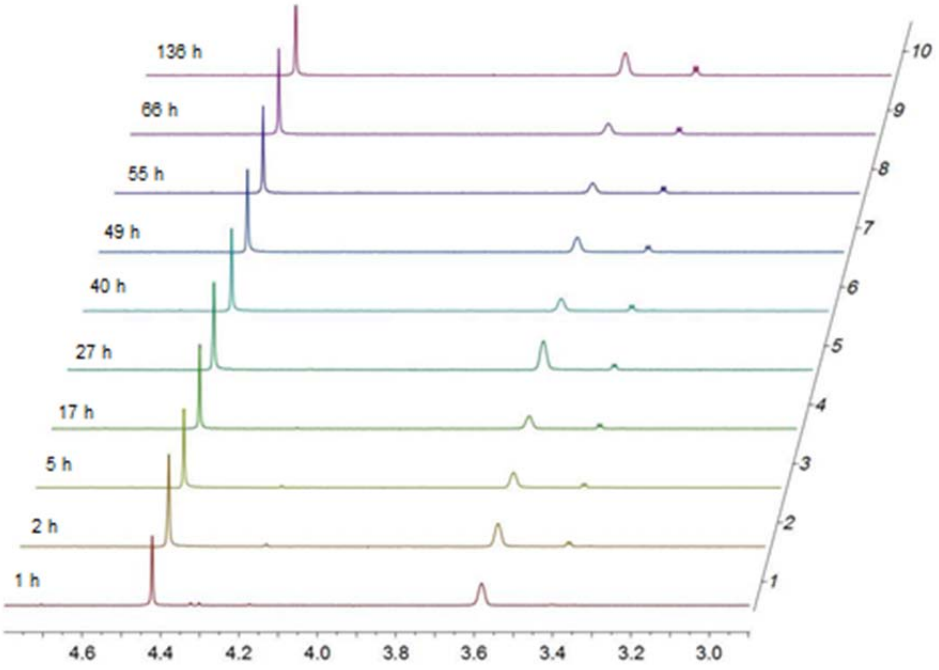

C.1.10. $^{31}P\{^{1}H\}$ NMR Spectra of $Ph_2PCH_2OH{\cdot}BH_3$ + Et_2NH (d6-ethanol)

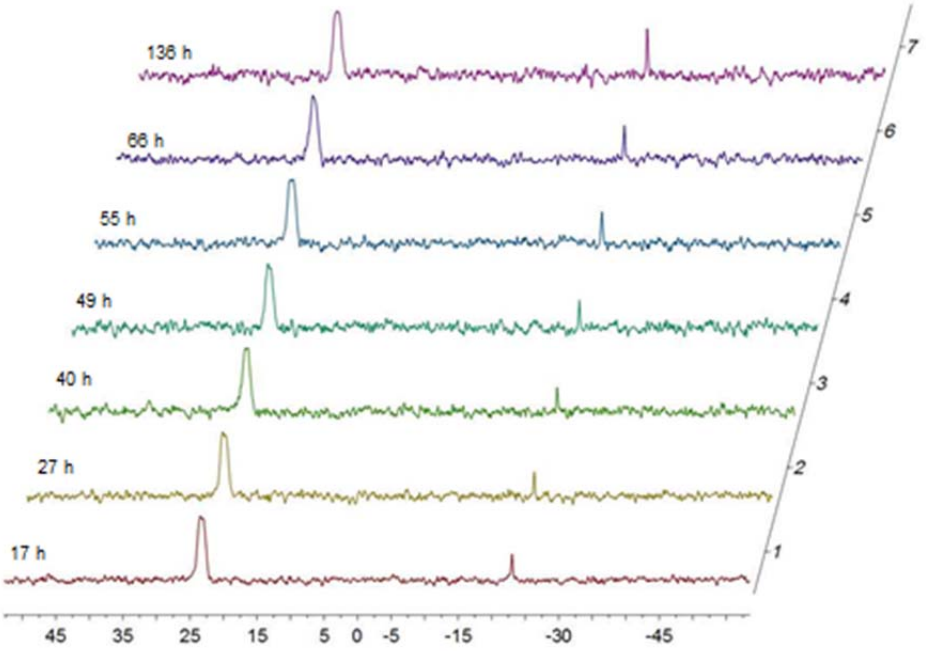

C.1.11. ^{1}H NMR Spectra of DHMPE + Et_2NH (d4-methanol)

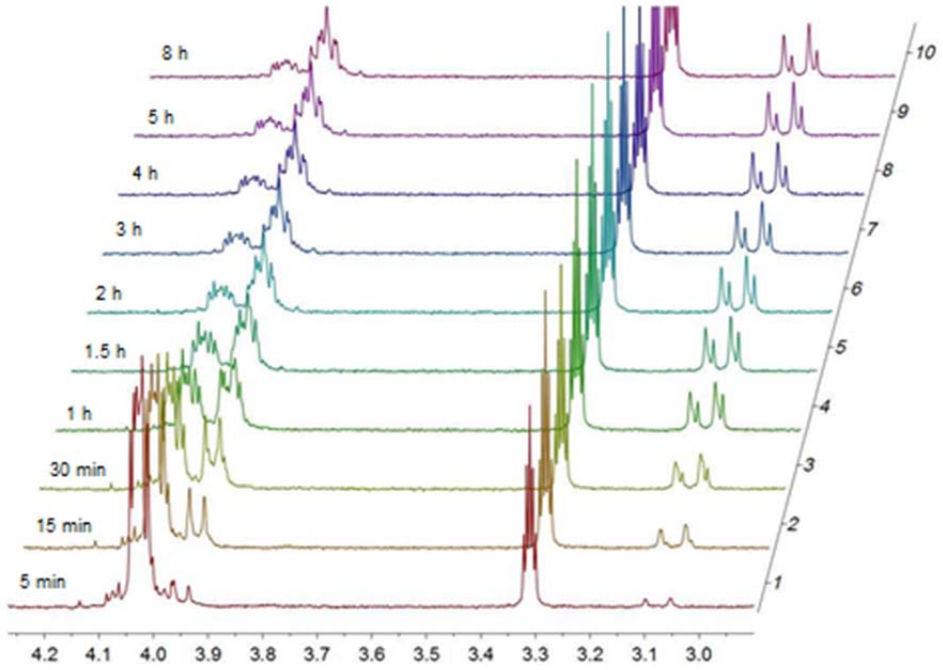

C.1.12. $^{31}P\{^{1}H\}$ NMR Spectra of DHMPE + Et_2NH (d4-methanol)

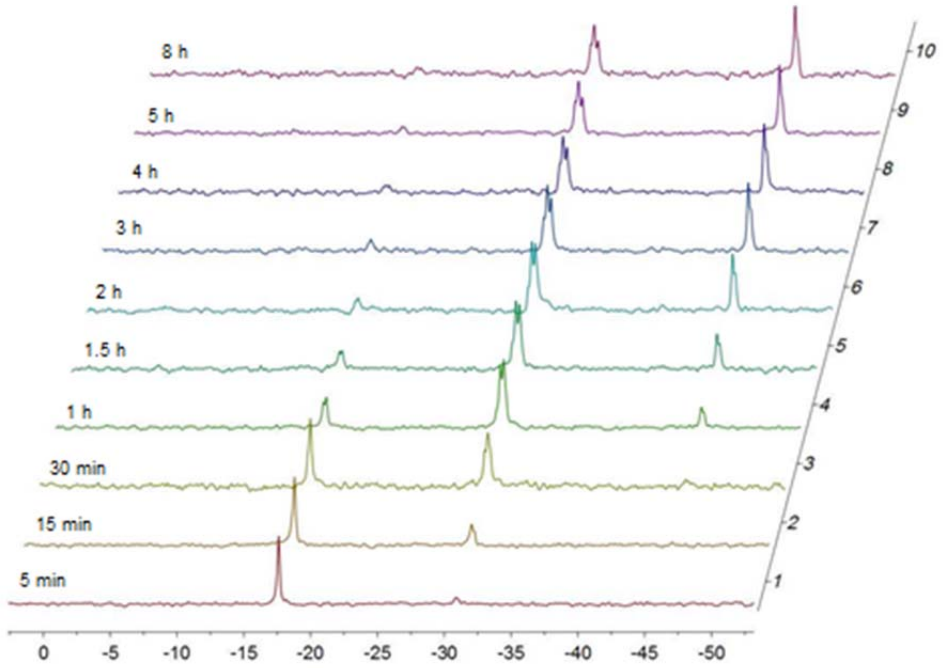

C.1.13. ^{1}H NMR Spectra of DHMPE·$2BH_3$ + Et_2NH (d4-methanol)

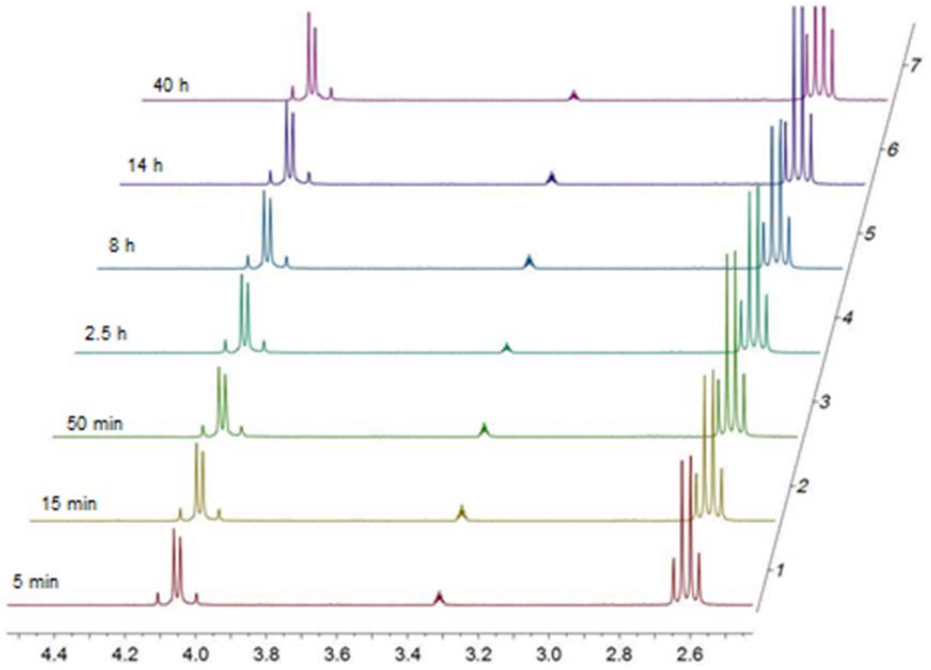

C.1.14. $^{31}P\{^{1}H\}$ NMR Spectra of DHMPE·$2BH_3$ + Et_2NH (d4-methanol)

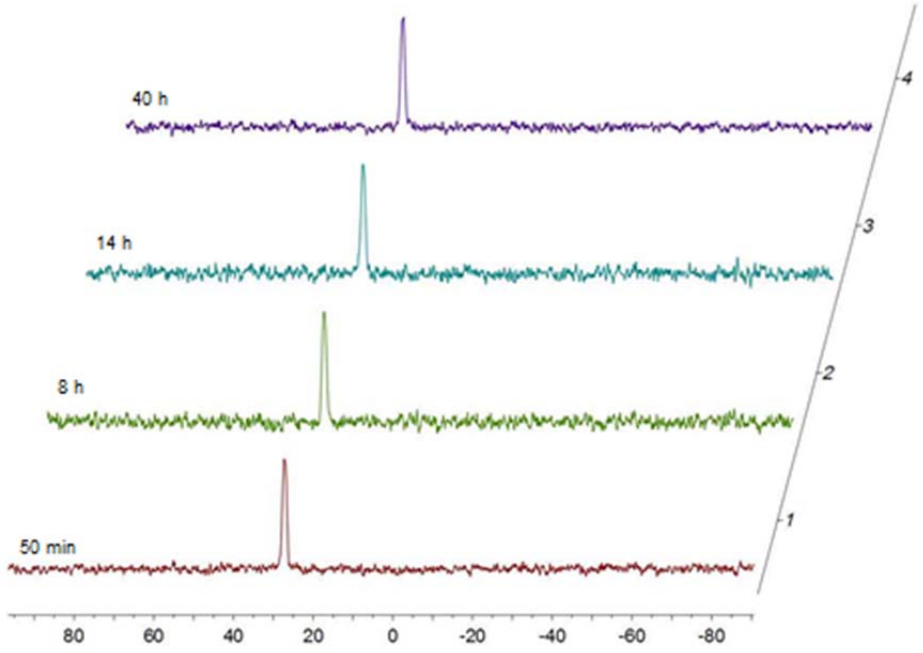

C.1.15. ESI-mass spectrum of $Fe(DHMPE)_2Cl_2$ + $BuNH_2$.

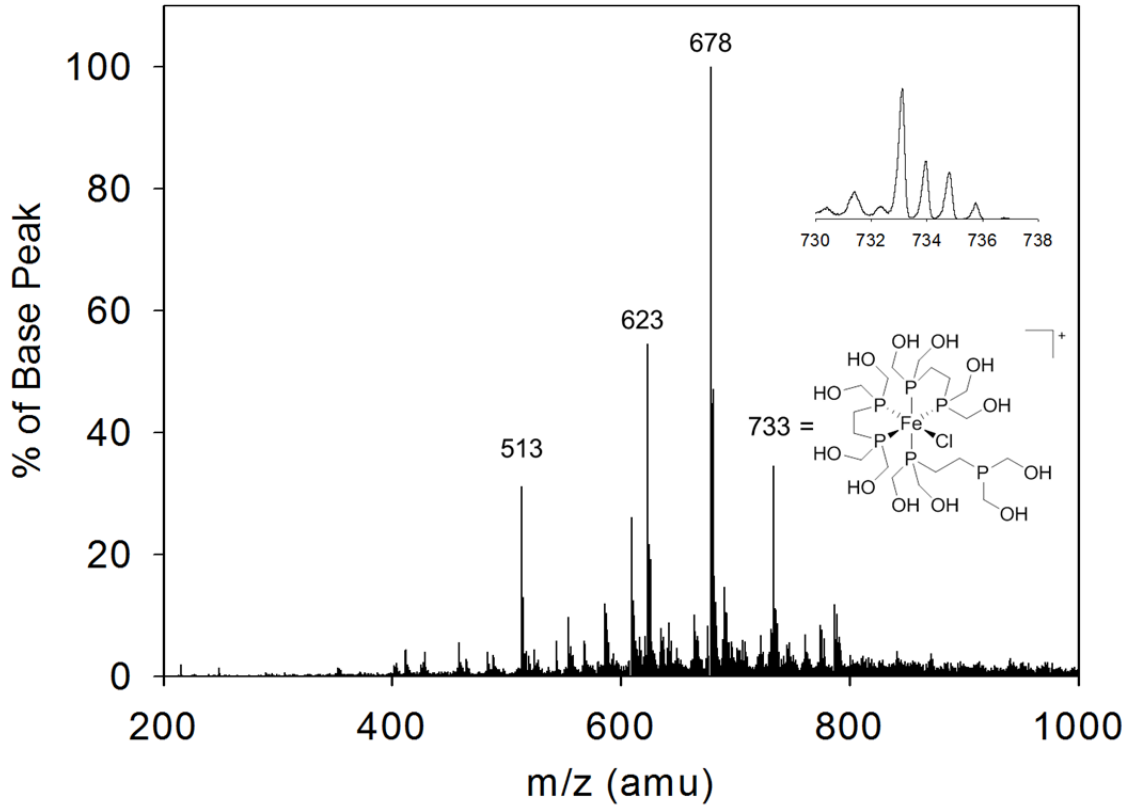

C.1.16. ESI-mass spectrum of $[Fe(DHMPE)_3]^{2+}$.

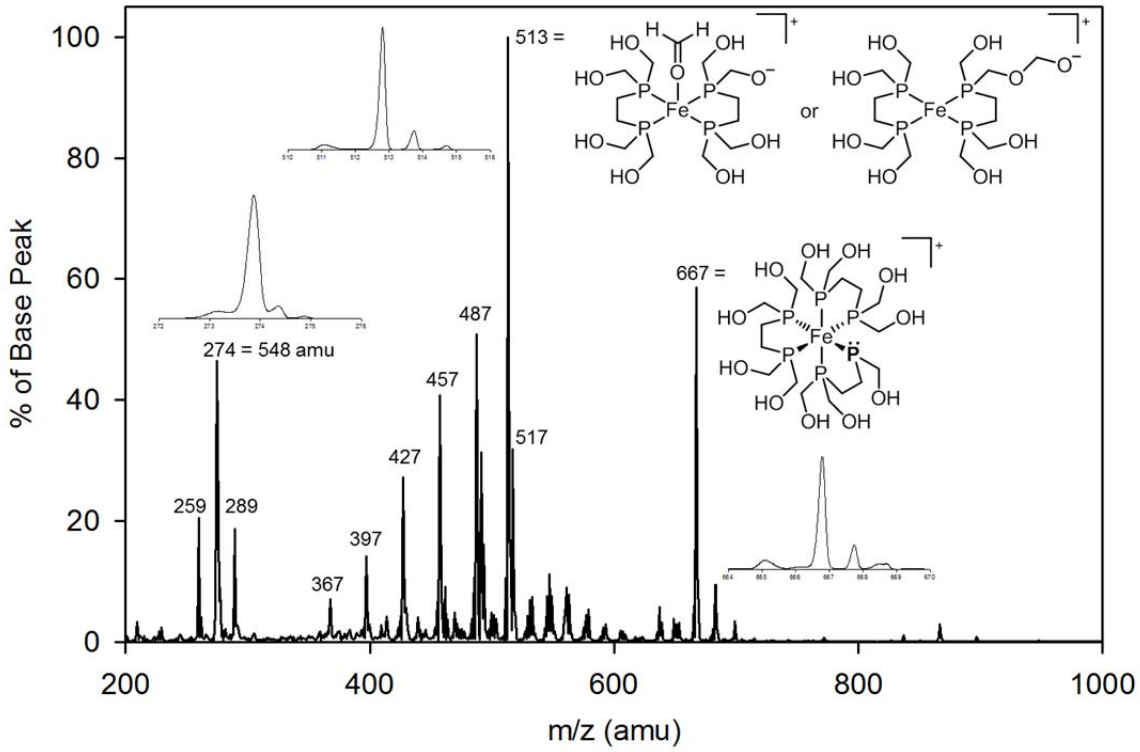

C.1.17. ESI-MS zoom scan of $[Fe(DHMPE)_3]^{2+}$

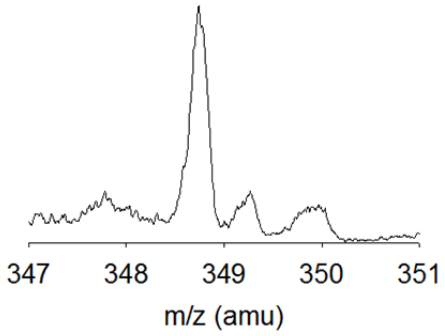

C.2. Crystal Data

C.2.1. Crystallographic Data for *trans*-Fe(DHMPE)$_2$Cl$_2$

Table C.2.1.1. Crystal data and structure refinement for *trans*-Fe(DHMPE)$_2$Cl$_2$.

Identification code	char2	
Empirical formula	C24 H64 Cl4 Fe2 O16 P8	
Formula weight	1110.01	
Temperature	173(2) K	
Wavelength	0.71073 Å	
Crystal system	Monoclinic	
Space group	P2(1)/n	
Unit cell dimensions	a = 7.7855(4) Å	□= 90°.
	b = 13.0809(7) Å	□= 92.3930(10)°.
	c = 10.4136(6) Å	□ = 90°.
Volume	1059.61(10) Å^3	
Z	1	
Density (calculated)	1.740 Mg/m^3	
Absorption coefficient	1.303 mm^{-1}	
F(000)	576	
Crystal size	0.09 x 0.07 x 0.04 mm^3	
Theta range for data collection	2.50 to 27.50°.	
Index ranges	-10<=h<=9, -16<=k<=16, -13<=l<=13	
Reflections collected	11961	
Independent reflections	2428 [R(int) = 0.0494]	
Completeness to theta = 27.50°	99.6 %	
Absorption correction	Semi-empirical from equivalents	
Max. and min. transmission	0.9497 and 0.8917	
Refinement method	Full-matrix least-squares on F^2	
Data / restraints / parameters	2428 / 0 / 188	
Goodness-of-fit on F^2	1.073	
Final R indices [I>2sigma(I)]	R1 = 0.0355, wR2 = 0.0729	
R indices (all data)	R1 = 0.0500, wR2 = 0.0800	
Largest diff. peak and hole	0.477 and -0.290 e.Å^{-3}	

Table C.2.1.2. Atomic coordinates (x 10^4) and equivalent isotropic displacement parameters ($Å^2$x 10^3) for *trans*-Fe(DHMPE)$_2$Cl$_2$. U(eq) is defined as one third of the trace of the orthogonalized U^{ij} tensor.

	x	y	z	U(eq)
Fe(1)	0	5000	5000	11(1)
Cl(1)	2868(1)	5396(1)	5646(1)	17(1)
P(1)	535(1)	3321(1)	5249(1)	13(1)
P(2)	-551(1)	4954(1)	7085(1)	13(1)
O(1)	-591(3)	1350(2)	4920(2)	21(1)
O(2)	3965(3)	3171(2)	5826(2)	28(1)
O(3)	-1119(3)	6758(2)	8186(2)	24(1)
O(4)	-2957(3)	4716(2)	8901(2)	22(1)
C(1)	327(4)	2929(2)	6944(3)	18(1)
C(2)	567(4)	3855(2)	7823(3)	17(1)
C(3)	-865(4)	2355(2)	4437(3)	17(1)
C(4)	2695(3)	2844(2)	4890(3)	19(1)
C(5)	127(4)	5960(2)	8227(3)	17(1)
C(6)	-2789(4)	4759(2)	7542(3)	18(1)

Table C.2.1.3. Bond lengths [Å] and angles [°] for *trans*-Fe(DHMPE)$_2$Cl$_2$.

Fe(1)-P(2)#1	2.2311(6)
Fe(1)-P(2)	2.2311(6)
Fe(1)-P(1)#1	2.2486(6)
Fe(1)-P(1)	2.2486(6)
Fe(1)-Cl(1)	2.3624(6)
Fe(1)-Cl(1)#1	2.3624(6)
P(1)-C(4)	1.847(3)
P(1)-C(3)	1.850(3)
P(1)-C(1)	1.852(3)
P(2)-C(2)	1.833(3)
P(2)-C(5)	1.836(3)
P(2)-C(6)	1.843(3)
O(1)-C(3)	1.420(3)
O(1)-H(1O)	0.62(3)
O(2)-C(4)	1.425(3)
O(2)-H(2O)	0.68(3)
O(3)-C(5)	1.425(3)
O(3)-H(3O)	0.75(4)
O(4)-C(6)	1.428(3)
O(4)-H(4O)	0.62(3)
C(1)-C(2)	1.525(4)
C(1)-H(1A)	0.96(3)
C(1)-H(1B)	0.91(3)
C(2)-H(2A)	0.99(3)
C(2)-H(2B)	0.96(3)
C(3)-H(3A)	0.94(3)
C(3)-H(3B)	0.93(3)
C(4)-H(4A)	0.94(3)
C(4)-H(4B)	0.95(3)
C(5)-H(5A)	0.95(3)
C(5)-H(5B)	1.00(3)
C(6)-H(6A)	0.89(3)
C(6)-H(6B)	0.94(3)

P(2)#1-Fe(1)-P(2)	180.0
P(2)#1-Fe(1)-P(1)#1	84.48(2)
P(2)-Fe(1)-P(1)#1	95.52(2)
P(2)#1-Fe(1)-P(1)	95.52(2)
P(2)-Fe(1)-P(1)	84.48(2)
P(1)#1-Fe(1)-P(1)	180.00(3)
P(2)#1-Fe(1)-Cl(1)	93.07(2)
P(2)-Fe(1)-Cl(1)	86.93(2)
P(1)#1-Fe(1)-Cl(1)	89.27(2)
P(1)-Fe(1)-Cl(1)	90.73(2)
P(2)#1-Fe(1)-Cl(1)#1	86.93(2)
P(2)-Fe(1)-Cl(1)#1	93.07(2)
P(1)#1-Fe(1)-Cl(1)#1	90.73(2)
P(1)-Fe(1)-Cl(1)#1	89.27(2)
Cl(1)-Fe(1)-Cl(1)#1	180.0
C(4)-P(1)-C(3)	101.58(13)
C(4)-P(1)-C(1)	102.46(13)
C(3)-P(1)-C(1)	99.99(13)
C(4)-P(1)-Fe(1)	118.22(10)
C(3)-P(1)-Fe(1)	120.77(9)
C(1)-P(1)-Fe(1)	110.93(9)
C(2)-P(2)-C(5)	99.86(12)
C(2)-P(2)-C(6)	102.70(13)
C(5)-P(2)-C(6)	100.43(13)
C(2)-P(2)-Fe(1)	108.79(9)
C(5)-P(2)-Fe(1)	123.34(10)
C(6)-P(2)-Fe(1)	118.53(9)
C(3)-O(1)-H(1O)	107(3)
C(4)-O(2)-H(2O)	109(3)
C(5)-O(3)-H(3O)	104(3)
C(6)-O(4)-H(4O)	109(3)
C(2)-C(1)-P(1)	109.81(18)
C(2)-C(1)-H(1A)	111.4(15)
P(1)-C(1)-H(1A)	109.2(15)
C(2)-C(1)-H(1B)	111.5(17)
P(1)-C(1)-H(1B)	102.1(16)

H(1A)-C(1)-H(1B)	113(2)
C(1)-C(2)-P(2)	109.09(19)
C(1)-C(2)-H(2A)	111.3(16)
P(2)-C(2)-H(2A)	105.6(16)
C(1)-C(2)-H(2B)	111.4(16)
P(2)-C(2)-H(2B)	110.3(16)
H(2A)-C(2)-H(2B)	109(2)
O(1)-C(3)-P(1)	113.16(19)
O(1)-C(3)-H(3A)	105.3(19)
P(1)-C(3)-H(3A)	106.9(19)
O(1)-C(3)-H(3B)	109.5(16)
P(1)-C(3)-H(3B)	109.2(17)
H(3A)-C(3)-H(3B)	113(2)
O(2)-C(4)-P(1)	111.80(19)
O(2)-C(4)-H(4A)	110.1(15)
P(1)-C(4)-H(4A)	110.4(15)
O(2)-C(4)-H(4B)	106.4(15)
P(1)-C(4)-H(4B)	110.3(15)
H(4A)-C(4)-H(4B)	108(2)
O(3)-C(5)-P(2)	109.21(18)
O(3)-C(5)-H(5A)	111.1(17)
P(2)-C(5)-H(5A)	105.8(17)
O(3)-C(5)-H(5B)	111.1(17)
P(2)-C(5)-H(5B)	110.1(16)
H(5A)-C(5)-H(5B)	109(2)
O(4)-C(6)-P(2)	112.87(19)
O(4)-C(6)-H(6A)	112.1(18)
P(2)-C(6)-H(6A)	108.4(18)
O(4)-C(6)-H(6B)	107.6(18)
P(2)-C(6)-H(6B)	106.3(18)
H(6A)-C(6)-H(6B)	109(2)

Symmetry transformations used to generate equivalent atoms:

#1 -x,-y+1,-z+1

Table C.2.1.4. Anisotropic displacement parameters ($Å^2 x\ 10^3$)for *trans*-$Fe(DHMPE)_2Cl_2$. The anisotropic displacement factor exponent takes the form: $-2\pi^2[h^2a^{*2}U^{11} + ... + 2\ h\ k\ a^*\ b^*\ U^{12}]$

	U^{11}	U^{22}	U^{33}	U^{23}	U^{13}	U^{12}
Fe(1)	11(1)	10(1)	11(1)	0(1)	1(1)	0(1)
Cl(1)	13(1)	16(1)	22(1)	-1(1)	0(1)	-1(1)
P(1)	14(1)	11(1)	13(1)	0(1)	1(1)	1(1)
P(2)	15(1)	12(1)	12(1)	0(1)	2(1)	0(1)
O(1)	22(1)	12(1)	31(1)	-1(1)	12(1)	3(1)
O(2)	21(1)	16(1)	47(1)	5(1)	-10(1)	1(1)
O(3)	22(1)	17(1)	34(1)	-10(1)	0(1)	1(1)
O(4)	30(1)	15(1)	21(1)	-2(1)	13(1)	-1(1)
C(1)	21(2)	16(1)	17(1)	3(1)	3(1)	1(1)
C(2)	22(2)	16(1)	13(1)	2(1)	3(1)	2(1)
C(3)	21(2)	12(1)	20(2)	-1(1)	0(1)	-2(1)
C(4)	20(1)	17(1)	21(2)	4(1)	4(1)	5(1)
C(5)	23(2)	15(1)	14(1)	-2(1)	1(1)	-1(1)
C(6)	21(2)	14(1)	19(1)	2(1)	5(1)	0(1)

Table C.2.1.5. Hydrogen coordinates (x 10^4) and isotropic displacement parameters ($Å^2$x 10^3) for *trans*-Fe(DHMPE)$_2$Cl$_2$.

	x	y	z	U(eq)
H(1O)	50(30)	1180(20)	4660(30)	5(9)
H(2O)	4050(40)	3690(20)	5780(30)	16(9)
H(3O)	-650(50)	7200(30)	8480(40)	49(12)
H(4O)	-3020(40)	5160(20)	9110(30)	20(11)
H(1A)	1160(30)	2407(19)	7150(20)	13(7)
H(1B)	-780(40)	2690(20)	6940(20)	16(7)
H(2A)	1790(40)	4060(20)	7910(30)	25(8)
H(2B)	140(30)	3720(20)	8660(30)	14(7)
H(3A)	-2010(40)	2520(20)	4630(30)	37(9)
H(3B)	-680(30)	2360(20)	3560(30)	18(7)
H(4A)	3000(30)	3056(19)	4070(20)	10(7)
H(4B)	2710(30)	2120(20)	4900(20)	9(6)
H(5A)	190(30)	5640(20)	9040(30)	21(8)
H(5B)	1280(40)	6220(20)	8020(30)	25(8)
H(6A)	-3440(40)	5250(20)	7180(30)	18(8)
H(6B)	-3130(40)	4120(20)	7200(30)	25(8)

Table C.2.1.6. Hydrogen bonds for *trans*-Fe(DHMPE)$_2$Cl$_2$ [Å and °].

D-H...A	d(D-H)	d(H...A)	d(D...A)	<(DHA)
O(3)-H(3O)...O(2)#2	0.75(4)	1.94(4)	2.672(3)	167(4)
O(2)-H(2O)...Cl(1)	0.68(3)	2.42(3)	3.036(2)	152(3)
O(1)-H(1O)...O(4)#3	0.62(3)	2.12(3)	2.731(3)	168(4)
O(4)-H(4O)...O(1)#4	0.62(3)	2.17(3)	2.733(3)	152(4)

Symmetry transformations used to generate equivalent atoms:

#1 -x,-y+1,-z+1 #2 -x+1/2,y+1/2,-z+3/2 #3 x+1/2,-y+1/2,z-1/2

#4 -x-1/2,y+1/2,-z+3/2

C.2.2. Crystallographic Data for DHMPE·2BH$_3$

Table C.2.2.1. Crystal data and structure refinement for DHMPE·2BH$_3$.

Identification code	char5	
Empirical formula	C6 H22 B2 O4 P2	
Formula weight	241.80	
Temperature	173(2) K	
Wavelength	0.71073 Å	
Crystal system	Monoclinic	
Space group	C2/c	
Unit cell dimensions	a = 18.092(3) Å	□= 90°.
	b = 6.2042(11) Å	□= 100.688(3)°.
	c = 11.757(2) Å	□ = 90°.
Volume	1296.8(4) Å^3	
Z	4	
Density (calculated)	1.238 Mg/m^3	
Absorption coefficient	0.323 mm^{-1}	
F(000)	520	
Crystal size	0.27 x 0.12 x 0.02 mm^3	
Theta range for data collection	2.29 to 27.00°.	
Index ranges	-22<=h<=22, -7<=k<=7, -14<=l<=15	
Reflections collected	6768	
Independent reflections	1408 [R(int) = 0.0549]	
Completeness to theta = 27.00°	100.0 %	
Absorption correction	Semi-empirical from equivalents	
Max. and min. transmission	0.9936 and 0.9179	
Refinement method	Full-matrix least-squares on F^2	
Data / restraints / parameters	1408 / 0 / 108	
Goodness-of-fit on F^2	1.058	
Final R indices [I>2sigma(I)]	R1 = 0.0484, wR2 = 0.1126	
R indices (all data)	R1 = 0.0631, wR2 = 0.1224	
Largest diff. peak and hole	1.153 and -0.301 e.Å^{-3}	

Table C.2.2.2. Atomic coordinates (x 10^4) and equivalent isotropic displacement parameters ($Å^2$x 10^3) for DHMPE·$2BH_3$. U(eq) is defined as one third of the trace of the orthogonalized U^{ij} tensor.

	x	y	z	U(eq)
P(1)	3940(1)	1883(1)	9624(1)	19(1)
O(1)	2934(1)	4239(3)	8184(2)	27(1)
O(2)	3128(1)	-1573(3)	8688(2)	32(1)
B(1)	4048(2)	3741(5)	10936(3)	29(1)
C(1)	3635(2)	3193(4)	8220(2)	26(1)
C(2)	3235(2)	-201(4)	9666(2)	24(1)
C(3)	4789(1)	479(4)	9432(2)	23(1)

Table C.2.2.3. Bond lengths [Å] and angles [°] for DHMPE·2BH_3.

P(1)-C(3)	1.815(2)
P(1)-C(2)	1.824(3)
P(1)-C(1)	1.831(3)
P(1)-B(1)	1.906(3)
O(1)-C(1)	1.418(3)
O(1)-H(1O)	0.78(2)
O(2)-C(2)	1.415(3)
O(2)-H(2O)	0.71(3)
B(1)-H(1B)	1.13(4)
B(1)-H(2B)	1.16(3)
B(1)-H(3B)	1.06(3)
C(1)-H(1A)	0.92(3)
C(1)-H(1C)	0.98(3)
C(2)-H(2A)	0.95(3)
C(2)-H(2C)	0.94(3)
C(3)-C(3)#1	1.530(4)
C(3)-H(3A)	0.96(3)
C(3)-H(3C)	0.90(2)
C(3)-P(1)-C(2)	105.97(12)
C(3)-P(1)-C(1)	102.84(11)
C(2)-P(1)-C(1)	104.10(12)
C(3)-P(1)-B(1)	115.37(13)
C(2)-P(1)-B(1)	111.95(13)
C(1)-P(1)-B(1)	115.44(13)
C(1)-O(1)-H(1O)	109.6(16)
C(2)-O(2)-H(2O)	112(3)
P(1)-B(1)-H(1B)	102.5(19)
P(1)-B(1)-H(2B)	106.0(15)
H(1B)-B(1)-H(2B)	116(2)
P(1)-B(1)-H(3B)	106.9(17)
H(1B)-B(1)-H(3B)	115(3)
H(2B)-B(1)-H(3B)	109(2)
O(1)-C(1)-P(1)	110.43(17)

O(1)-C(1)-H(1A)	110.1(17)
P(1)-C(1)-H(1A)	108.2(17)
O(1)-C(1)-H(1C)	108.6(17)
P(1)-C(1)-H(1C)	104.7(16)
H(1A)-C(1)-H(1C)	115(2)
O(2)-C(2)-P(1)	113.28(18)
O(2)-C(2)-H(2A)	106.6(16)
P(1)-C(2)-H(2A)	108.6(16)
O(2)-C(2)-H(2C)	111.3(18)
P(1)-C(2)-H(2C)	109.2(18)
H(2A)-C(2)-H(2C)	108(2)
C(3)#1-C(3)-P(1)	112.0(2)
C(3)#1-C(3)-H(3A)	109.2(17)
P(1)-C(3)-H(3A)	105.7(17)
C(3)#1-C(3)-H(3C)	109.0(15)
P(1)-C(3)-H(3C)	109.5(15)
H(3A)-C(3)-H(3C)	111(2)

Symmetry transformations used to generate equivalent atoms:

#1 -x+1,-y,-z+2

Table C.2.2.4. Anisotropic displacement parameters ($Å^2$x 10^3)for DHMPE·$2BH_3$. The anisotropic displacement factor exponent takes the form: -2□^{2}[$h^2a^{*2}U^{11}$ + ... + 2 h k a* b* U^{12}]

	U^{11}	U^{22}	U^{33}	U^{23}	U^{13}	U^{12}
P(1)	20(1)	17(1)	18(1)	0(1)	0(1)	2(1)
O(1)	29(1)	17(1)	31(1)	-1(1)	-7(1)	3(1)
O(2)	36(1)	21(1)	33(1)	-3(1)	-13(1)	1(1)
B(1)	32(2)	26(1)	27(2)	-6(1)	1(1)	2(1)
C(1)	30(1)	24(1)	23(1)	2(1)	0(1)	2(1)
C(2)	24(1)	20(1)	27(1)	1(1)	1(1)	0(1)
C(3)	23(1)	24(1)	20(1)	0(1)	2(1)	4(1)

Table 11. Hydrogen coordinates (x 10^4) and isotropic displacement parameters ($Å^2$x 10^3) for DHMPE·$2BH_3$.

	x	y	z	U(eq)
H(1O)	3002(12)	5430(40)	8371(18)	9(6)
H(2O)	2836(19)	-1200(50)	8240(30)	47(11)
H(1B)	4090(20)	2570(60)	11680(30)	69(10)
H(2B)	3520(17)	4840(50)	10790(30)	55(9)
H(3B)	4537(18)	4690(50)	10930(30)	54(9)
H(1A)	3994(15)	4180(50)	8120(20)	36(8)
H(1C)	3565(16)	2010(50)	7660(20)	41(8)
H(2A)	3398(15)	-1080(40)	10320(20)	30(7)
H(2C)	2783(17)	450(50)	9760(20)	38(8)
H(3A)	5100(16)	1550(40)	9160(20)	38(8)
H(3C)	4669(13)	-580(40)	8920(20)	15(6)

Table C.2.2.5. Torsion angles [°] for DHMPE·2BH_3.

C(3)-P(1)-C(1)-O(1)	175.25(18)
C(2)-P(1)-C(1)-O(1)	64.9(2)
B(1)-P(1)-C(1)-O(1)	-58.2(2)
C(3)-P(1)-C(2)-O(2)	-54.9(2)
C(1)-P(1)-C(2)-O(2)	53.1(2)
B(1)-P(1)-C(2)-O(2)	178.49(18)
C(2)-P(1)-C(3)-C(3)#1	-79.4(3)
C(1)-P(1)-C(3)-C(3)#1	171.6(3)
B(1)-P(1)-C(3)-C(3)#1	45.0(3)

Symmetry transformations used to generate equivalent atoms:

#1 -x+1,-y,-z+2

Table C.2.2.6. Hydrogen bonds for DHMPE·2BH_3 [Å and °].

D-H...A	d(D-H)	d(H...A)	d(D...A)	<(DHA)
O(1)-H(1O)...O(2)#2	0.78(2)	1.90(3)	2.674(3)	175(2)
O(2)-H(2O)...O(1)#3	0.71(3)	1.99(3)	2.687(3)	167(4)

Symmetry transformations used to generate equivalent atoms:

#1 -x+1,-y,-z+2 #2 x,y+1,z #3 -x+1/2,y-1/2,-z+3/2

APPENDIX D

SUPPORTING INFORMATION FOR CHAPTER V

D.1 Spectra

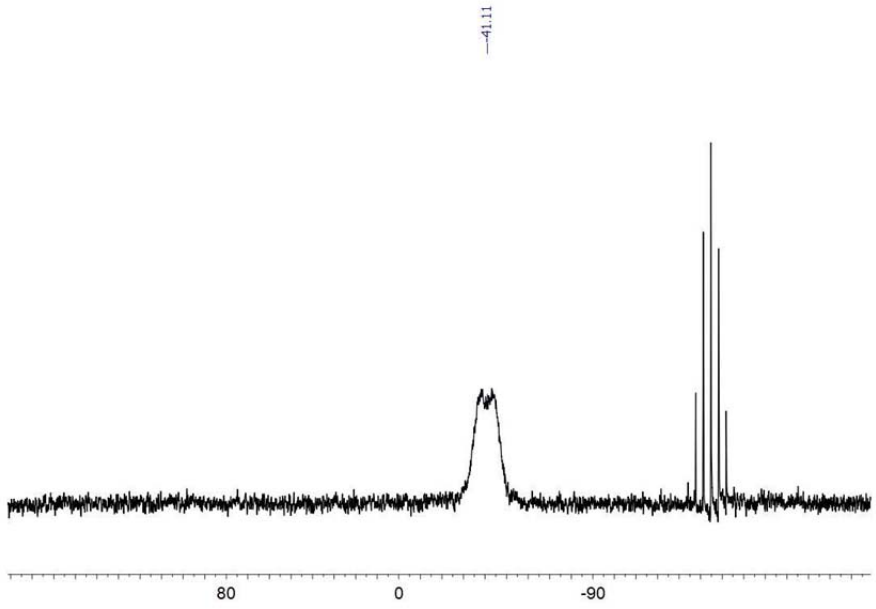

Figure D.1.1. ^{31}P {^{1}H} spectrum of $[Cu(MeOPrPE)_2]PF_6$ (**1**) in $CDCl_3$.

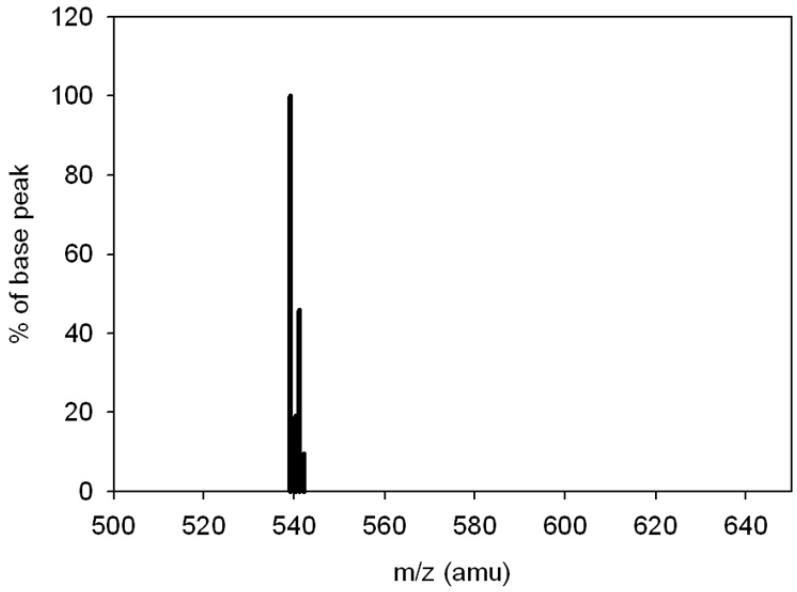

Figure D.1.2. ESI mass spectrum of $[Cu(MeOPrPE)_2]PF_6$ (**1**) in THF.

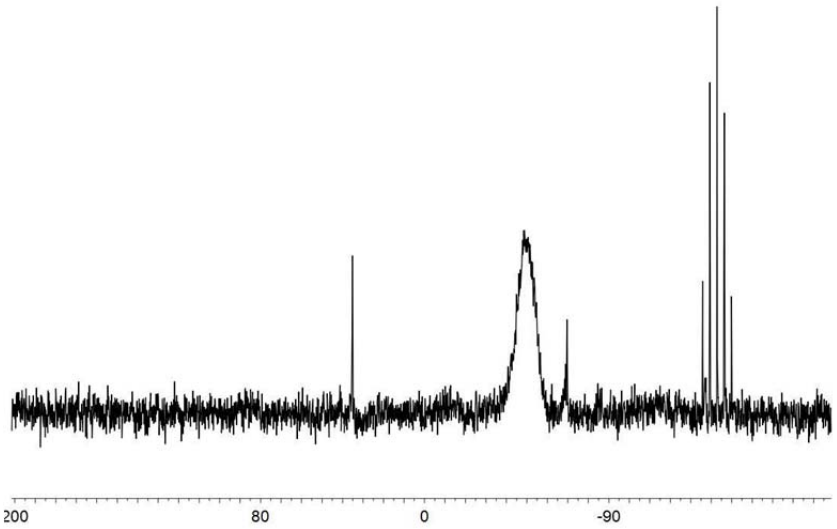

Figure D.1.3. ^{31}P $\{^{1}H\}$ spectrum of $[Cu(MeOPrPP)_2]PF_6$ (**2**) in $CDCl_3$. Impurities at -70 ppm and +35 ppm are free MeOPrPP and oxidized MeOPrPP.

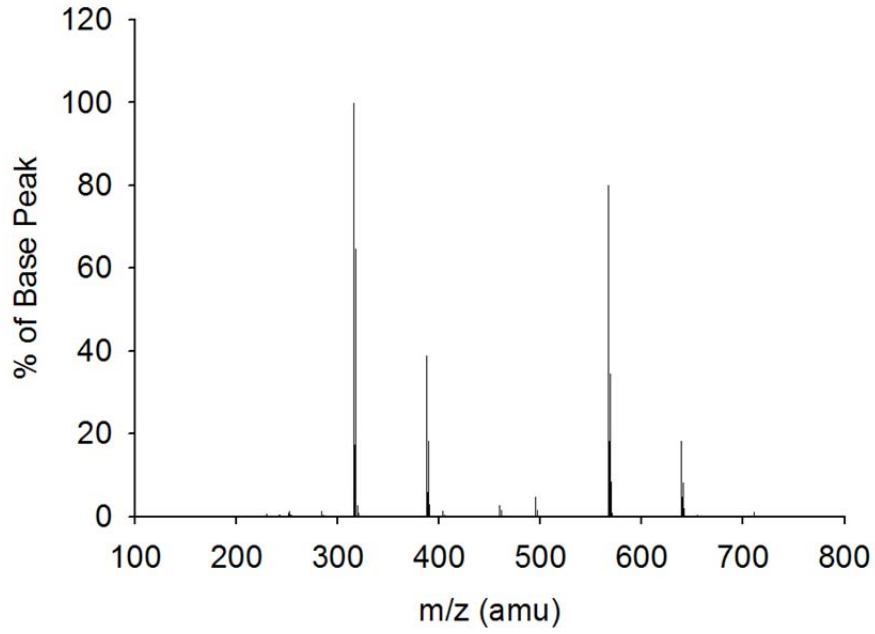

Figure D.1.4. ESI mass spectrum of $[Cu(MeOPrPP)_2]PF_6$ (**2**) in THF.

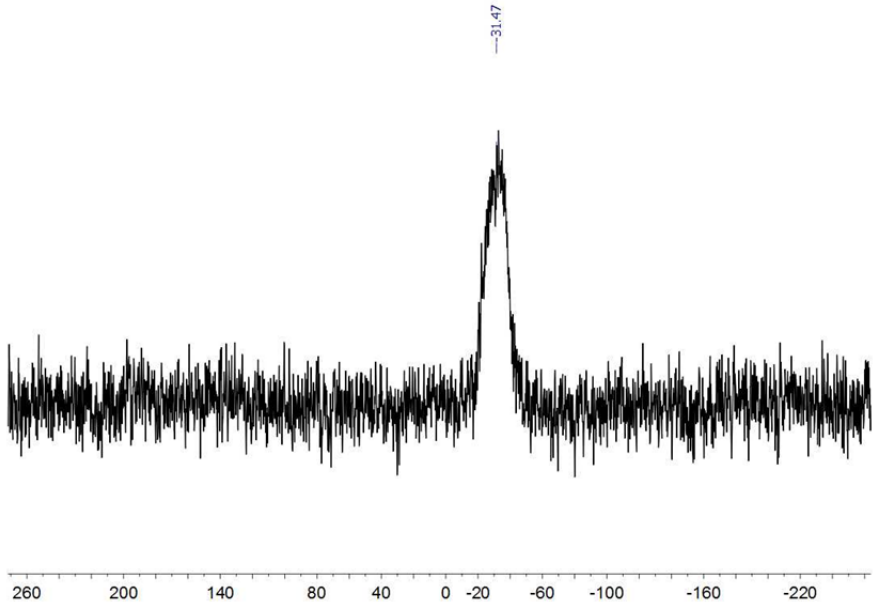

Figure D.1.5. ^{31}P $\{^{1}H\}$ spectrum of $[Cu(MPPE)_2]BPh_4$ (**3**) in THF.

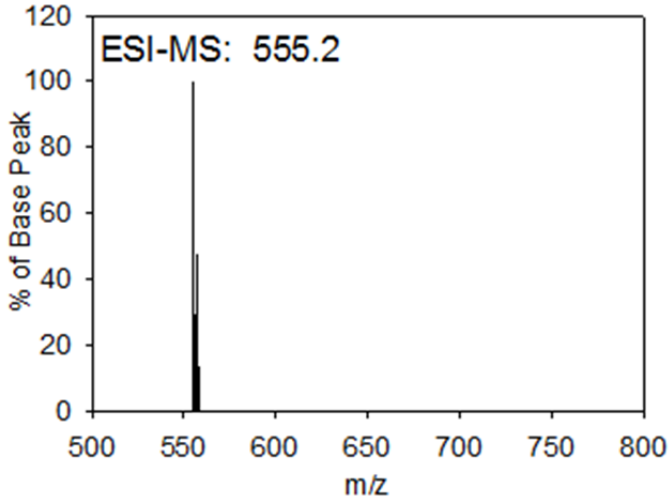

Figure D.1.6. ESI mass spectrum of $[Cu(MPPE)_2]BPh_4$ (**3**) in THF.

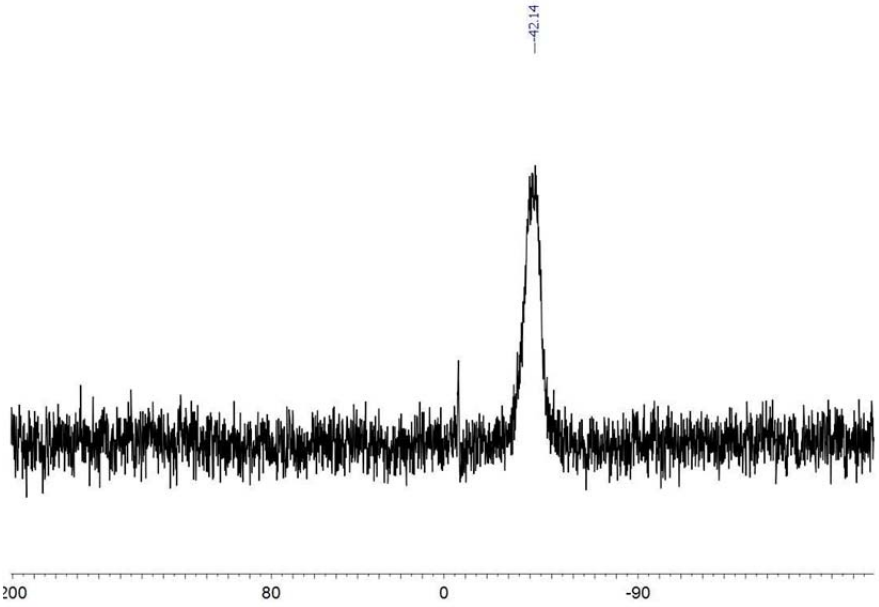

Figure D.1.7. ^{31}P $\{^{1}H\}$ spectrum of $[Cu(MPPP)_2]BPh_4$ (**4**) in $CDCl_3$.

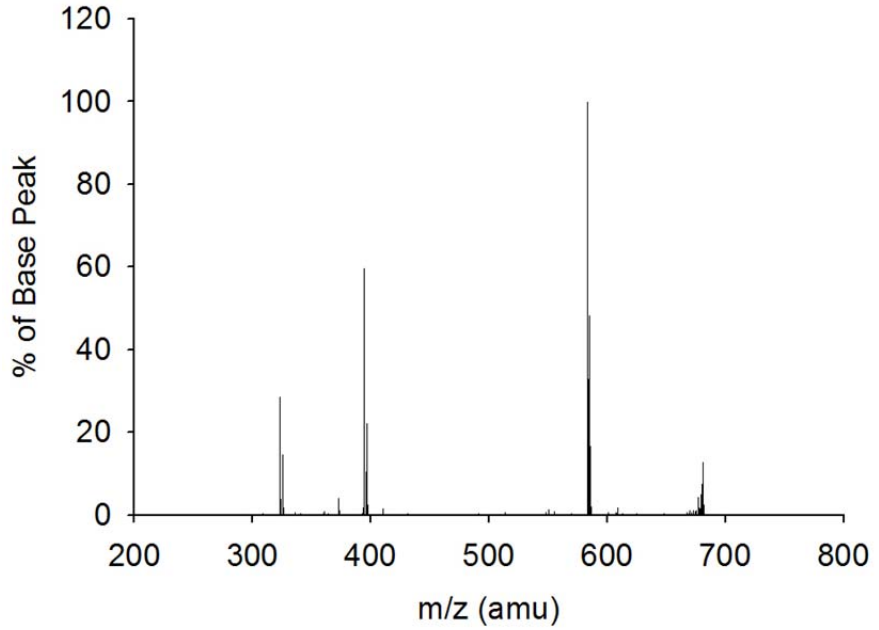

Figure D.1.8. ESI mass spectrum of $[Cu(MPPP)_2]BPh_4$ (**4**) in THF.

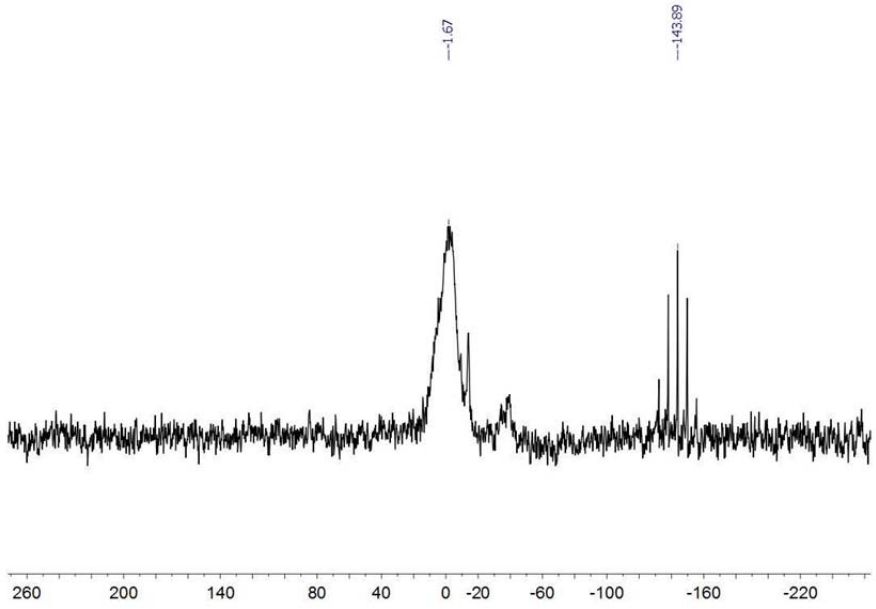

Figure D.1.9. ^{31}P $\{^{1}H\}$ spectrum of compound **5** in THF.

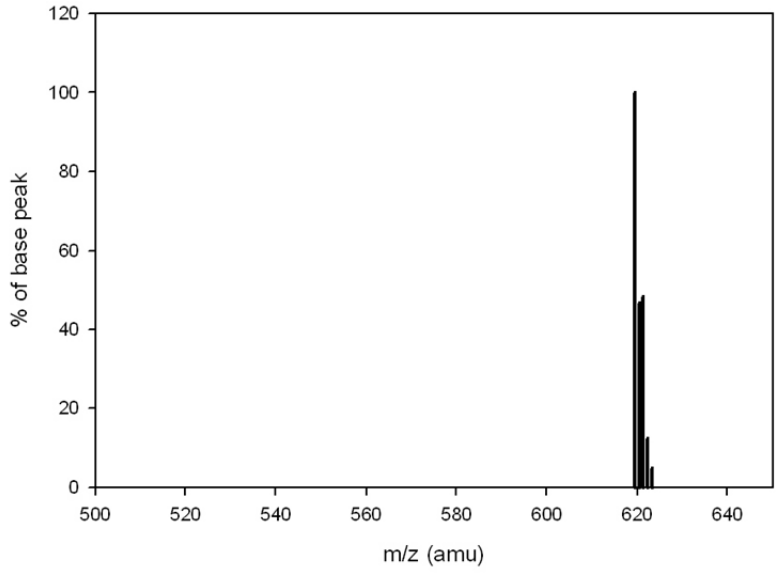

Figure D.1.10. ESI mass spectrum of compound **5** in THF.

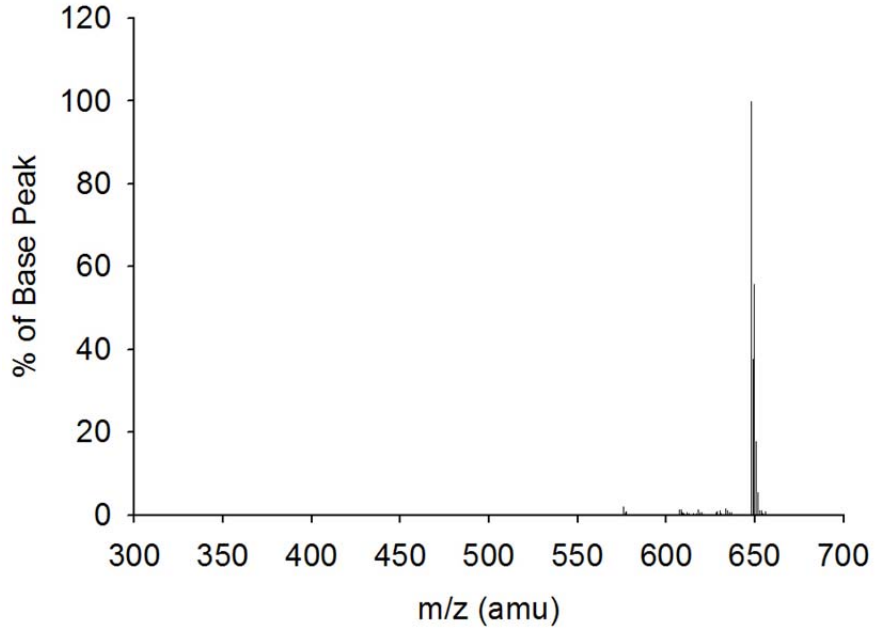

Figure D.1.11. ESI mass spectrum of compound **6** in THF.

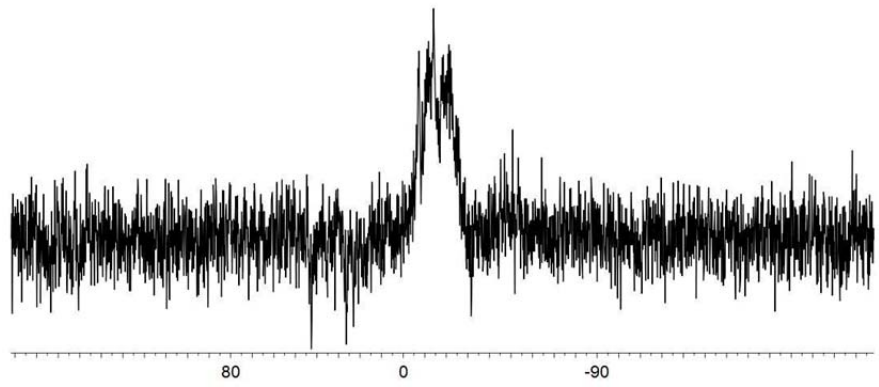

Figure D.1.14. $^{31}P\ \{^{1}H\}$ spectrum of compound **7** in THF.

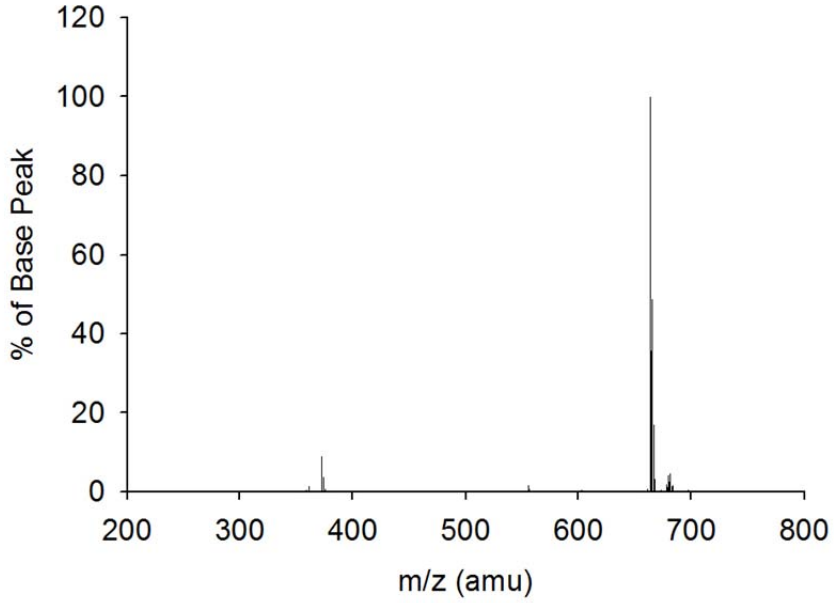

Figure D.1.15. ESI mass spectrum of compound **7** in THF.

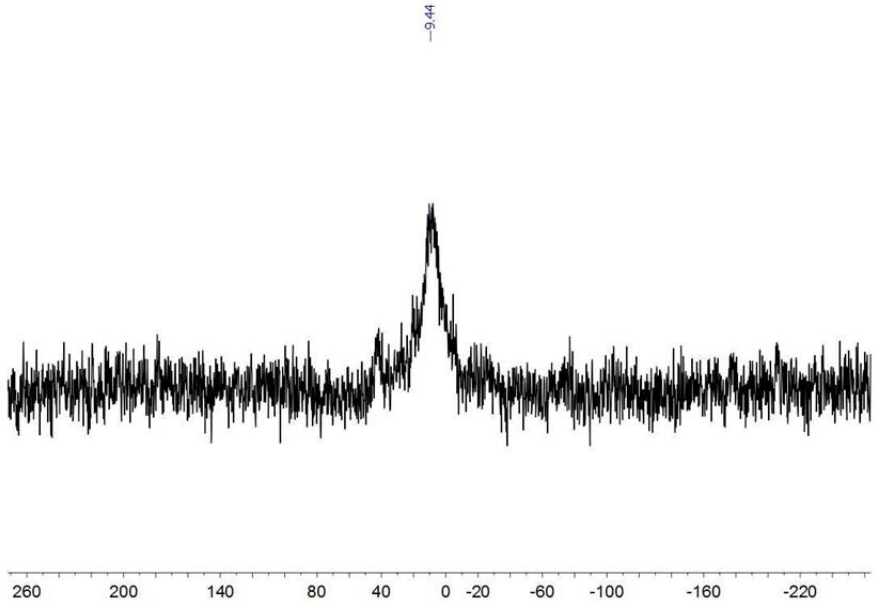

Figure D.1.16. $^{31}P\ \{^{1}H\}$ spectrum of compound **8** in THF.

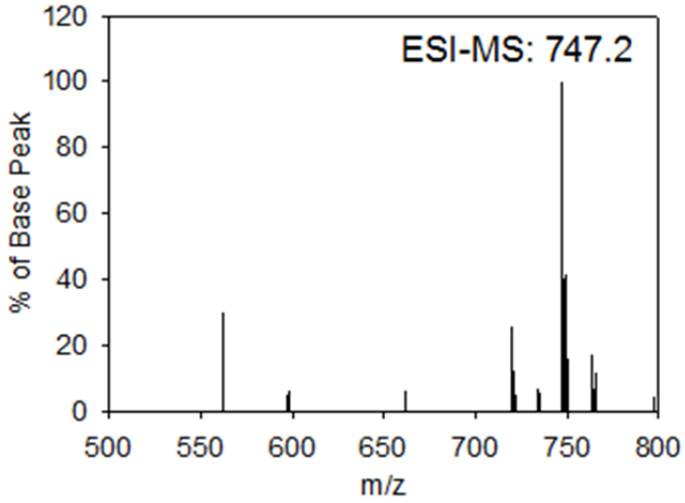

Figure D.1.17. ESI mass spectrum of compound **8** in THF.

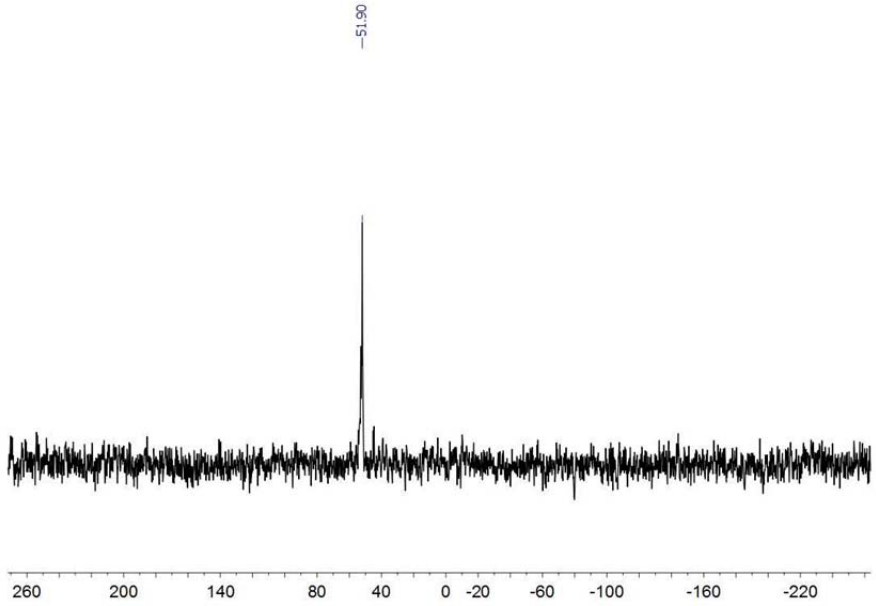

Figure D.1.18. ^{31}P $\{^{1}H\}$ spectrum of compound **9** in$CDCl_3$.

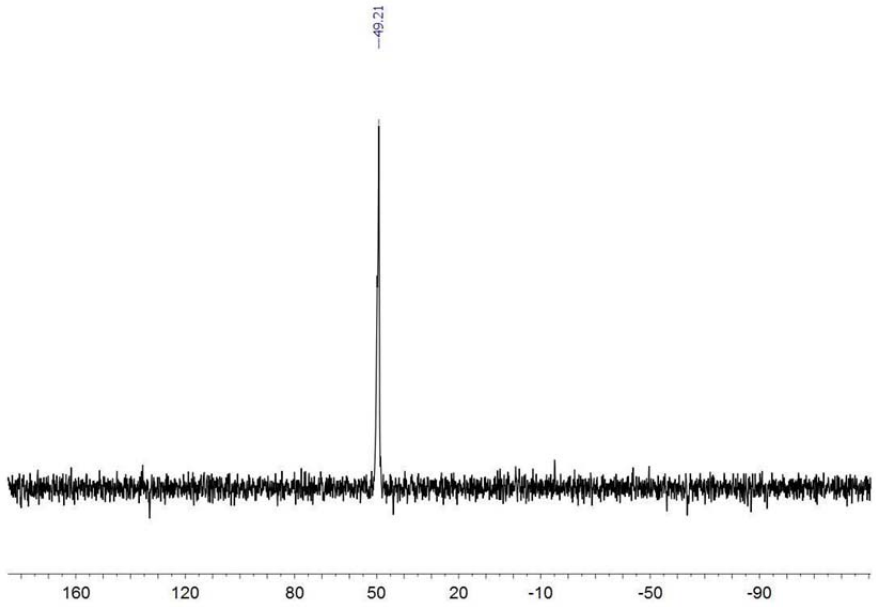

Figure D.1.19. ^{31}P $\{^{1}H\}$ spectrum of compound **10** in$CDCl_3$.

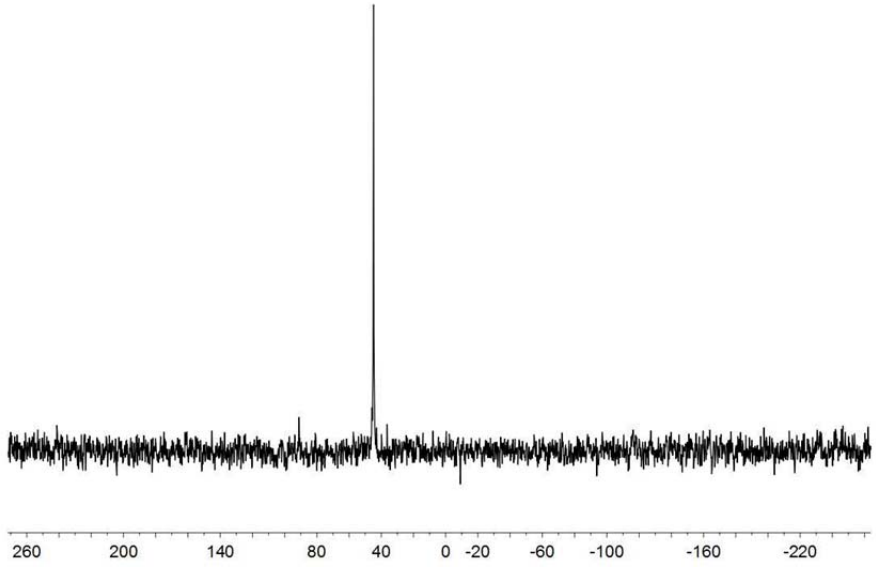

Figure D.1.20. ^{31}P $\{^{1}H\}$ spectrum of compound **11** in$CDCl_3$.

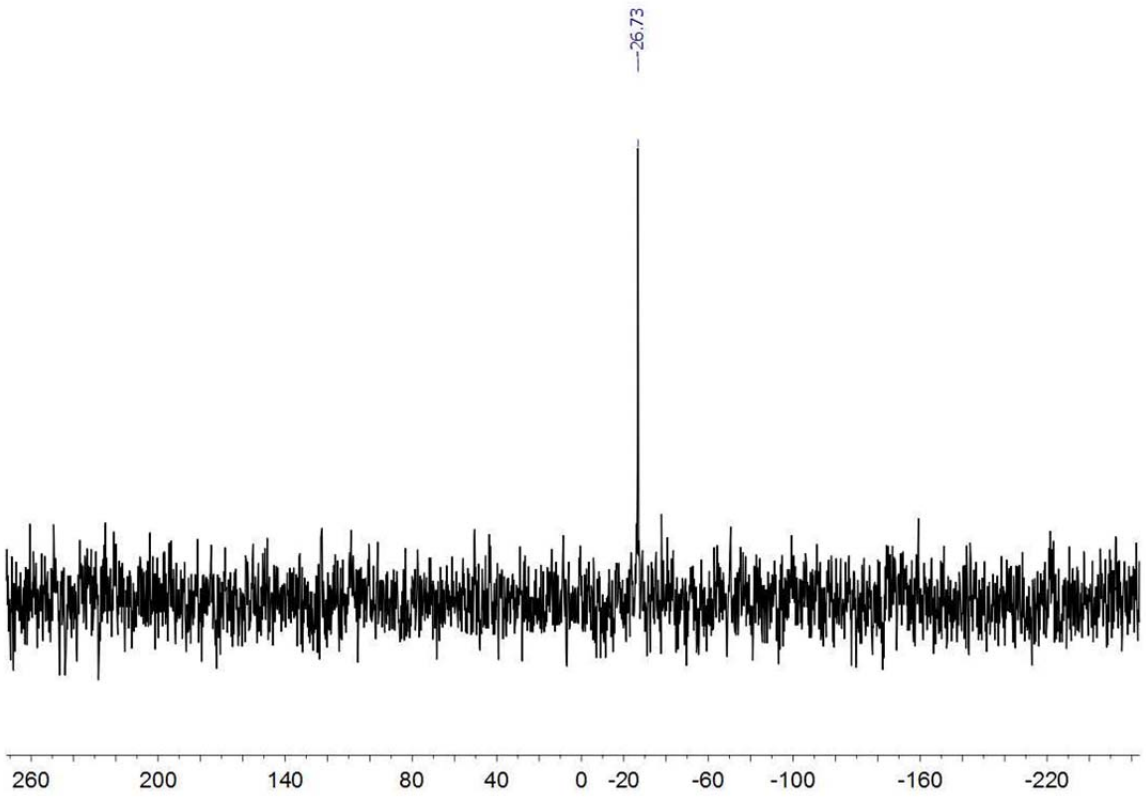

Figure D.1.21. ^{31}P $\{^{1}H\}$ spectrum of compound **12** in$CDCl_3$.

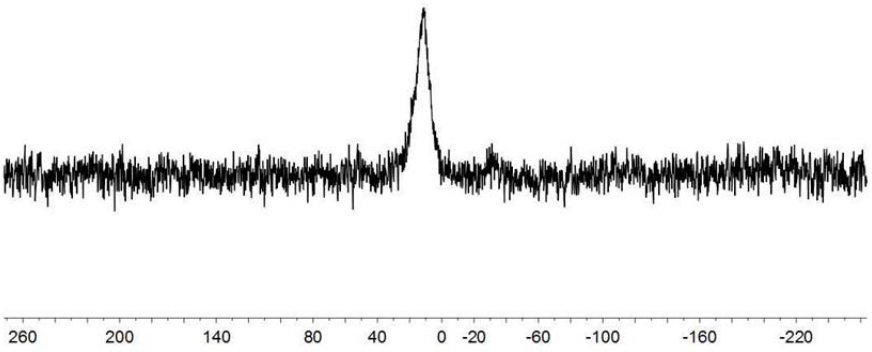

Figure D.1.22. ^{31}P NMR spectrum of $Cu(DHMPE)_2Cl$ in D_2O.

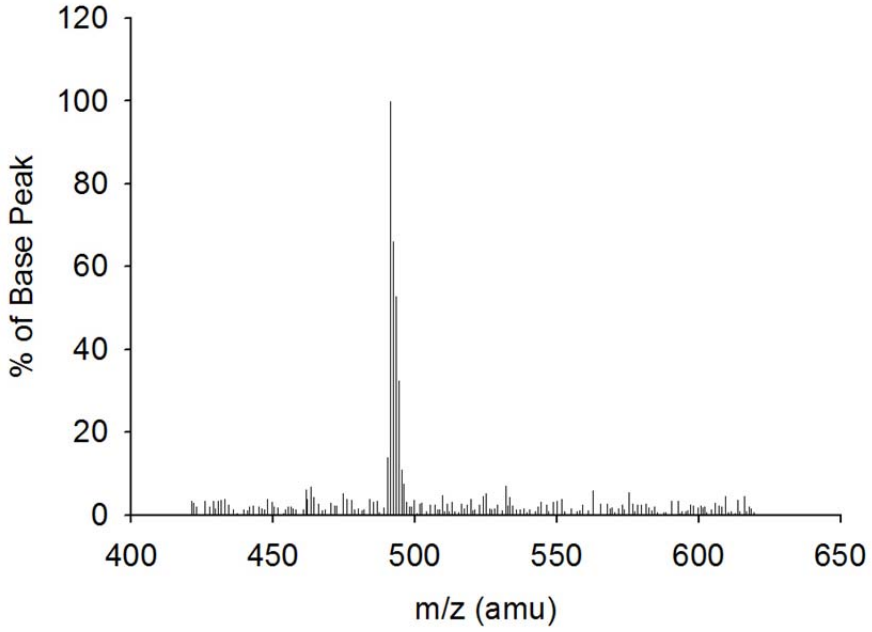

Figure D.1.23. ESI mass spectrum of $Cu(DHMPE)_2Cl$ in MeOH.

D.2 Crystal Data

Table D.2.1. Crystal data and structure refinement for $[Cu_2(DHMPE)_4]Cl_2$

Identification code	char10	
Empirical formula	C26 H72 Cl2 Cu2 O18 P8	
Formula weight	1118.58	
Temperature	173(2) K	
Wavelength	0.71073 Å	
Crystal system	Monoclinic	
Space group	C2/c	
Unit cell dimensions	a = 29.353(13) Å	α= 90°.
	b = 10.653(5) Å	β= 125.771(8)°.
	c = 18.737(9) Å	γ = 90°.
Volume	4754(4) $Å^3$	
Z	4	
Density (calculated)	1.563 Mg/m^3	
Absorption coefficient	1.340 mm^{-1}	
F(000)	2336	
Crystal size	0.16 x 0.14 x 0.03 mm^3	
Theta range for data collection	1.71 to 25.00°.	
Index ranges	-34<=h<=34, -12<=k<=12, -22<=l<=22	
Reflections collected	22316	
Independent reflections	4196 [R(int) = 0.0800]	
Completeness to theta = 25.00°	100.0 %	
Absorption correction	Semi-empirical from equivalents	
Max. and min. transmission	0.9609 and 0.8142	
Refinement method	Full-matrix least-squares on F^2	
Data / restraints / parameters	4196 / 7 / 291	
Goodness-of-fit on F^2	1.025	
Final R indices [I>2sigma(I)]	R1 = 0.0427, wR2 = 0.0910	
R indices (all data)	R1 = 0.0630, wR2 = 0.1014	
Largest diff. peak and hole	0.757 and -0.488 e.$Å^{-3}$	

Table D.2.2. Atomic coordinates (x 10^4) and equivalent isotropic displacement parameters ($Å^2$x 10^3) for $[Cu_2(DHMPE)_4]Cl_2$. U(eq) is defined as one third of the trace of the orthogonalized U^{ij} tensor.

	x	y	z	U(eq)
Cu(1)	1190(1)	4934(1)	641(1)	17(1)
Cl(1)	2752(1)	4875(1)	-607(1)	36(1)
P(1)	1103(1)	6643(1)	-162(1)	18(1)
P(2)	2100(1)	4784(1)	1132(1)	19(1)
P(3)	697(1)	3203(1)	-87(1)	19(1)
P(4)	1060(1)	5353(1)	1692(1)	18(1)
O(1)	34(1)	7209(3)	-1438(2)	34(1)
O(2)	1063(1)	9215(3)	-239(2)	32(1)
O(3)	2593(1)	3375(3)	2575(2)	40(1)
O(4)	2842(1)	3640(3)	913(2)	29(1)
O(5)	568(2)	797(3)	306(2)	46(1)
O(7)	1781(1)	3605(3)	2899(2)	32(1)
O(8)	1382(1)	6923(3)	3044(2)	34(1)
C(1)	1747(2)	6648(4)	-111(3)	22(1)
C(2)	2255(2)	6256(4)	809(3)	22(1)
C(3)	539(2)	6895(4)	-1338(3)	28(1)
C(4)	1118(2)	8188(3)	289(3)	24(1)
C(5)	2667(2)	4558(4)	2302(3)	32(1)
C(6)	2274(2)	3576(4)	630(3)	25(1)
C(7)	-61(2)	3267(4)	-630(2)	20(1)
C(8)	-341(2)	4307(4)	-1321(2)	19(1)
C(9)	915(2)	1863(4)	663(3)	32(1)
C(10)	753(2)	2568(4)	-949(3)	32(1)
O(6)	717(2)	3578(5)	-1459(3)	75(2)
C(10A)	753(2)	2568(4)	-949(3)	32(1)
O(6A)	276(6)	1727(14)	-1597(10)	55(6)
C(11)	1240(2)	4135(4)	2517(2)	21(1)
C(12)	1470(2)	6684(4)	2387(3)	24(1)
O(1S)	-287(2)	9653(4)	-1525(3)	70(1)
C(1S)	-770(3)	9917(5)	-2359(4)	68(2)

Table D.2.3. Bond lengths [Å] and angles [°] for $[Cu_2(DHMPE)_4]Cl_2$.

Cu(1)-P(3)	2.2481(13)
Cu(1)-P(4)	2.2586(14)
Cu(1)-P(2)	2.2651(16)
Cu(1)-P(1)	2.2792(13)
P(1)-C(1)	1.837(4)
P(1)-C(4)	1.839(4)
P(1)-C(3)	1.845(4)
P(2)-C(2)	1.832(4)
P(2)-C(5)	1.834(4)
P(2)-C(6)	1.834(4)
P(3)-C(7)	1.827(4)
P(3)-C(9)	1.835(4)
P(3)-C(10)	1.845(4)
P(4)-C(12)	1.823(4)
P(4)-C(8)#1	1.832(4)
P(4)-C(11)	1.844(4)
O(1)-C(3)	1.420(5)
O(1)-H(1O)	0.95(2)
O(2)-C(4)	1.419(5)
O(2)-H(2O)	0.938(18)
O(3)-C(5)	1.423(5)
O(3)-H(3O)	0.957(19)
O(4)-C(6)	1.426(5)
O(4)-H(4O)	0.944(19)
O(5)-C(9)	1.407(5)
O(5)-H(5O)	0.97(2)
O(7)-C(11)	1.424(5)
O(7)-H(7O)	0.96(2)
O(8)-C(12)	1.423(4)
O(8)-H(8O)	0.95(2)
C(1)-C(2)	1.537(5)
C(1)-H(1B)	0.9900
C(1)-H(1C)	0.9900
C(2)-H(2B)	0.9900

C(2)-H(2C)	0.9900
C(3)-H(3B)	0.9900
C(3)-H(3C)	0.9900
C(4)-H(4B)	0.9900
C(4)-H(4C)	0.9900
C(5)-H(5B)	0.9900
C(5)-H(5C)	0.9900
C(6)-H(6A)	0.9900
C(6)-H(6B)	0.9900
C(7)-C(8)	1.527(5)
C(7)-H(7B)	0.9900
C(7)-H(7C)	0.9900
C(8)-P(4)#1	1.832(4)
C(8)-H(8B)	0.9900
C(8)-H(8C)	0.9900
C(9)-H(9A)	0.9900
C(9)-H(9B)	0.9900
C(10)-O(6)	1.401(6)
C(10)-H(10A)	0.9900
C(10)-H(10B)	0.9900
O(6)-H(6C)	0.8400
O(6A)-H(6AA)	0.8400
C(11)-H(11A)	0.9900
C(11)-H(11B)	0.9900
C(12)-H(12A)	0.9900
C(12)-H(12B)	0.9900
O(1S)-C(1S)	1.393(6)
C(1S)-H(1SA)	0.9800
C(1S)-H(1SB)	0.9800
C(1S)-H(1SC)	0.9800

P(3)-Cu(1)-P(4)	108.29(4)
P(3)-Cu(1)-P(2)	112.14(4)
P(4)-Cu(1)-P(2)	114.83(4)
P(3)-Cu(1)-P(1)	118.08(5)
P(4)-Cu(1)-P(1)	114.03(5)

P(2)-Cu(1)-P(1)	88.59(4)
C(1)-P(1)-C(4)	103.11(18)
C(1)-P(1)-C(3)	103.92(19)
C(4)-P(1)-C(3)	100.50(19)
C(1)-P(1)-Cu(1)	104.64(12)
C(4)-P(1)-Cu(1)	116.61(13)
C(3)-P(1)-Cu(1)	125.49(14)
C(2)-P(2)-C(5)	106.30(19)
C(2)-P(2)-C(6)	103.48(18)
C(5)-P(2)-C(6)	101.02(19)
C(2)-P(2)-Cu(1)	105.48(13)
C(5)-P(2)-Cu(1)	121.65(14)
C(6)-P(2)-Cu(1)	117.18(14)
C(7)-P(3)-C(9)	102.86(19)
C(7)-P(3)-C(10)	103.27(19)
C(9)-P(3)-C(10)	102.4(2)
C(7)-P(3)-Cu(1)	116.72(13)
C(9)-P(3)-Cu(1)	111.11(15)
C(10)-P(3)-Cu(1)	118.44(15)
C(12)-P(4)-C(8)#1	104.55(18)
C(12)-P(4)-C(11)	101.69(19)
C(8)#1-P(4)-C(11)	99.14(17)
C(12)-P(4)-Cu(1)	113.46(13)
C(8)#1-P(4)-Cu(1)	116.92(13)
C(11)-P(4)-Cu(1)	118.75(13)
C(3)-O(1)-H(1O)	112(4)
C(4)-O(2)-H(2O)	109(2)
C(5)-O(3)-H(3O)	102(3)
C(6)-O(4)-H(4O)	106(3)
C(9)-O(5)-H(5O)	105(5)
C(11)-O(7)-H(7O)	103(3)
C(12)-O(8)-H(8O)	106(4)
C(2)-C(1)-P(1)	110.6(3)
C(2)-C(1)-H(1B)	109.5
P(1)-C(1)-H(1B)	109.5
C(2)-C(1)-H(1C)	109.5

P(1)-C(1)-H(1C)	109.5
H(1B)-C(1)-H(1C)	108.1
C(1)-C(2)-P(2)	109.7(3)
C(1)-C(2)-H(2B)	109.7
P(2)-C(2)-H(2B)	109.7
C(1)-C(2)-H(2C)	109.7
P(2)-C(2)-H(2C)	109.7
H(2B)-C(2)-H(2C)	108.2
O(1)-C(3)-P(1)	109.3(3)
O(1)-C(3)-H(3B)	109.8
P(1)-C(3)-H(3B)	109.8
O(1)-C(3)-H(3C)	109.8
P(1)-C(3)-H(3C)	109.8
H(3B)-C(3)-H(3C)	108.3
O(2)-C(4)-P(1)	114.0(3)
O(2)-C(4)-H(4B)	108.7
P(1)-C(4)-H(4B)	108.7
O(2)-C(4)-H(4C)	108.7
P(1)-C(4)-H(4C)	108.7
H(4B)-C(4)-H(4C)	107.6
O(3)-C(5)-P(2)	108.9(3)
O(3)-C(5)-H(5B)	109.9
P(2)-C(5)-H(5B)	109.9
O(3)-C(5)-H(5C)	109.9
P(2)-C(5)-H(5C)	109.9
H(5B)-C(5)-H(5C)	108.3
O(4)-C(6)-P(2)	113.0(3)
O(4)-C(6)-H(6A)	109.0
P(2)-C(6)-H(6A)	109.0
O(4)-C(6)-H(6B)	109.0
P(2)-C(6)-H(6B)	109.0
H(6A)-C(6)-H(6B)	107.8
C(8)-C(7)-P(3)	112.0(2)
C(8)-C(7)-H(7B)	109.2
P(3)-C(7)-H(7B)	109.2
C(8)-C(7)-H(7C)	109.2

P(3)-C(7)-H(7C)	109.2
H(7B)-C(7)-H(7C)	107.9
C(7)-C(8)-P(4)#1	113.2(2)
C(7)-C(8)-H(8B)	108.9
P(4)#1-C(8)-H(8B)	108.9
C(7)-C(8)-H(8C)	108.9
P(4)#1-C(8)-H(8C)	108.9
H(8B)-C(8)-H(8C)	107.7
O(5)-C(9)-P(3)	115.6(3)
O(5)-C(9)-H(9A)	108.4
P(3)-C(9)-H(9A)	108.4
O(5)-C(9)-H(9B)	108.4
P(3)-C(9)-H(9B)	108.4
H(9A)-C(9)-H(9B)	107.4
O(6)-C(10)-P(3)	107.8(3)
O(6)-C(10)-H(10A)	110.1
P(3)-C(10)-H(10A)	110.1
O(6)-C(10)-H(10B)	110.1
P(3)-C(10)-H(10B)	110.1
H(10A)-C(10)-H(10B)	108.5
C(10)-O(6)-H(6C)	109.5
O(7)-C(11)-P(4)	112.8(3)
O(7)-C(11)-H(11A)	109.0
P(4)-C(11)-H(11A)	109.0
O(7)-C(11)-H(11B)	109.0
P(4)-C(11)-H(11B)	109.0
H(11A)-C(11)-H(11B)	107.8
O(8)-C(12)-P(4)	112.2(3)
O(8)-C(12)-H(12A)	109.2
P(4)-C(12)-H(12A)	109.2
O(8)-C(12)-H(12B)	109.2
P(4)-C(12)-H(12B)	109.2
H(12A)-C(12)-H(12B)	107.9
O(1S)-C(1S)-H(1SA)	109.5
O(1S)-C(1S)-H(1SB)	109.5
H(1SA)-C(1S)-H(1SB)	109.5

O(1S)-C(1S)-H(1SC)	109.5
H(1SA)-C(1S)-H(1SC)	109.5
H(1SB)-C(1S)-H(1SC)	109.5

Symmetry transformations used to generate equivalent atoms:

#1 -x,-y+1,-z

Table D.2.4. Anisotropic displacement parameters ($Å^2 x\ 10^3$)for $[Cu_2(DHMPE)_4]Cl_2$. The anisotropic displacement factor exponent takes the form: $-2\pi^2[\ h^2a^{*2}U^{11} + ... + 2\ h\ k\ a^*\ b^*\ U^{12}\ ]$

	U^{11}	U^{22}	U^{33}	U^{23}	U^{13}	U^{12}
Cu(1)	16(1)	19(1)	16(1)	1(1)	9(1)	1(1)
Cl(1)	34(1)	41(1)	30(1)	6(1)	18(1)	-6(1)
P(1)	18(1)	18(1)	16(1)	1(1)	10(1)	1(1)
P(2)	15(1)	26(1)	16(1)	0(1)	9(1)	2(1)
P(3)	20(1)	18(1)	19(1)	0(1)	12(1)	2(1)
P(4)	16(1)	22(1)	16(1)	-1(1)	10(1)	-1(1)
O(1)	20(2)	34(2)	35(2)	8(2)	9(1)	2(1)
O(2)	31(2)	18(2)	41(2)	6(1)	18(2)	0(1)
O(3)	36(2)	59(2)	29(2)	22(2)	22(2)	24(2)
O(4)	26(2)	38(2)	30(2)	14(1)	21(2)	15(1)
O(5)	63(2)	24(2)	65(2)	0(2)	45(2)	-3(2)
O(7)	30(2)	38(2)	29(2)	9(2)	18(2)	11(2)
O(8)	32(2)	48(2)	31(2)	-20(2)	24(2)	-15(2)
C(1)	22(2)	20(2)	28(2)	3(2)	17(2)	-1(2)
C(2)	16(2)	21(2)	27(2)	-4(2)	12(2)	-2(2)
C(3)	31(3)	27(2)	20(2)	0(2)	11(2)	-2(2)
C(4)	23(2)	21(2)	30(2)	-5(2)	17(2)	-2(2)
C(5)	20(2)	54(3)	19(2)	3(2)	10(2)	7(2)
C(6)	26(2)	29(2)	22(2)	0(2)	15(2)	2(2)
C(7)	19(2)	20(2)	22(2)	-4(2)	13(2)	-3(2)
C(8)	15(2)	25(2)	20(2)	-3(2)	11(2)	-1(2)
C(9)	41(3)	22(2)	36(3)	6(2)	25(2)	4(2)
C(10)	32(3)	42(3)	31(2)	-6(2)	24(2)	1(2)
O(6)	100(4)	100(4)	73(4)	58(3)	77(4)	71(3)
C(10A)	32(3)	42(3)	31(2)	-6(2)	24(2)	1(2)
O(6A)	61(11)	67(11)	56(10)	-50(9)	45(9)	-37(8)
C(11)	19(2)	29(2)	18(2)	0(2)	12(2)	0(2)
C(12)	20(2)	30(2)	25(2)	-3(2)	15(2)	-3(2)
O(1S)	52(3)	58(3)	79(3)	8(2)	26(2)	6(2)
C(1S)	72(4)	62(4)	61(4)	23(3)	33(4)	33(3)

Table D.2.5. Hydrogen coordinates (x 10^4) and isotropic displacement parameters ($Å^2$x 10^3) for $[Cu_2(DHMPE)_4]Cl_2$.

	x	y	z	U(eq)
H(1B)	1705	6060	-555	26
H(1C)	1811	7499	-249	26
H(2B)	2341	6922	1240	26
H(2C)	2588	6144	804	26
H(3B)	644	7582	-1570	34
H(3C)	482	6122	-1675	34
H(4B)	809	8227	360	29
H(4C)	1476	8275	880	29
H(5B)	3035	4583	2395	38
H(5C)	2658	5238	2653	38
H(6A)	2205	2738	778	30
H(6B)	2022	3670	-18	30
H(7B)	-230	2450	-916	23
H(7C)	-134	3412	-183	23
H(8B)	-346	4058	-1834	23
H(8C)	-113	5081	-1071	23
H(9A)	1299	1616	870	38
H(9B)	934	2141	1183	38
H(10A)	1116	2128	-677	38
H(10B)	446	1963	-1321	38
H(6C)	923	3439	-1625	113
H(10C)	773	3278	-1271	38
H(10D)	1109	2092	-663	38
H(6AA)	171	1910	-2108	83
H(11A)	1226	4506	2989	26
H(11B)	955	3458	2235	26
H(12A)	1874	6514	2675	28
H(12B)	1368	7440	2015	28
H(1SA)	-880	10793	-2381	102
H(1SB)	-1074	9361	-2484	102

H(1SC)	-695	9784	-2800	102
H(2O)	1422(10)	9480(40)	-50(20)	28(12)
H(3O)	2242(13)	3490(50)	2490(40)	80(20)
H(4O)	2840(20)	4080(40)	470(20)	68(17)
H(8O)	1687(18)	7430(50)	3470(30)	110(20)
H(5O)	630(40)	450(80)	-110(50)	190(40)
H(1O)	-20(20)	8090(20)	-1450(40)	90(20)
H(7O)	2028(19)	4170(40)	3370(30)	78(19)

Table D.2.6. Torsion angles [°] for $[Cu_2(DHMPE)_4]Cl_2$.

P(3)-Cu(1)-P(1)-C(1)	-103.09(14)
P(4)-Cu(1)-P(1)-C(1)	128.05(14)
P(2)-Cu(1)-P(1)-C(1)	11.38(14)
P(3)-Cu(1)-P(1)-C(4)	143.76(15)
P(4)-Cu(1)-P(1)-C(4)	14.91(16)
P(2)-Cu(1)-P(1)-C(4)	-101.77(15)
P(3)-Cu(1)-P(1)-C(3)	16.35(18)
P(4)-Cu(1)-P(1)-C(3)	-112.50(18)
P(2)-Cu(1)-P(1)-C(3)	130.82(17)
P(3)-Cu(1)-P(2)-C(2)	132.02(14)
P(4)-Cu(1)-P(2)-C(2)	-103.81(14)
P(1)-Cu(1)-P(2)-C(2)	12.13(13)
P(3)-Cu(1)-P(2)-C(5)	-107.13(18)
P(4)-Cu(1)-P(2)-C(5)	17.05(19)
P(1)-Cu(1)-P(2)-C(5)	132.98(18)
P(3)-Cu(1)-P(2)-C(6)	17.55(16)
P(4)-Cu(1)-P(2)-C(6)	141.72(15)
P(1)-Cu(1)-P(2)-C(6)	-102.34(16)
P(4)-Cu(1)-P(3)-C(7)	59.19(14)
P(2)-Cu(1)-P(3)-C(7)	-173.07(14)
P(1)-Cu(1)-P(3)-C(7)	-72.29(14)
P(4)-Cu(1)-P(3)-C(9)	-58.29(16)
P(2)-Cu(1)-P(3)-C(9)	69.44(16)
P(1)-Cu(1)-P(3)-C(9)	170.22(15)
P(4)-Cu(1)-P(3)-C(10)	-176.41(17)
P(2)-Cu(1)-P(3)-C(10)	-48.67(17)
P(1)-Cu(1)-P(3)-C(10)	52.10(17)
P(3)-Cu(1)-P(4)-C(12)	176.43(15)
P(2)-Cu(1)-P(4)-C(12)	50.25(16)
P(1)-Cu(1)-P(4)-C(12)	-49.92(16)
P(3)-Cu(1)-P(4)-C(8)#1	-61.72(15)
P(2)-Cu(1)-P(4)-C(8)#1	172.09(14)
P(1)-Cu(1)-P(4)-C(8)#1	71.92(15)
P(3)-Cu(1)-P(4)-C(11)	57.08(15)

P(2)-Cu(1)-P(4)-C(11)	-69.10(15)
P(1)-Cu(1)-P(4)-C(11)	-169.27(15)
C(4)-P(1)-C(1)-C(2)	83.8(3)
C(3)-P(1)-C(1)-C(2)	-171.7(3)
Cu(1)-P(1)-C(1)-C(2)	-38.7(3)
P(1)-C(1)-C(2)-P(2)	51.3(3)
C(5)-P(2)-C(2)-C(1)	-169.4(3)
C(6)-P(2)-C(2)-C(1)	84.7(3)
Cu(1)-P(2)-C(2)-C(1)	-39.0(3)
C(1)-P(1)-C(3)-O(1)	-166.2(3)
C(4)-P(1)-C(3)-O(1)	-59.7(3)
Cu(1)-P(1)-C(3)-O(1)	74.1(3)
C(1)-P(1)-C(4)-O(2)	65.9(3)
C(3)-P(1)-C(4)-O(2)	-41.3(3)
Cu(1)-P(1)-C(4)-O(2)	179.9(2)
C(2)-P(2)-C(5)-O(3)	-175.4(3)
C(6)-P(2)-C(5)-O(3)	-67.7(3)
Cu(1)-P(2)-C(5)-O(3)	64.1(3)
C(2)-P(2)-C(6)-O(4)	58.2(3)
C(5)-P(2)-C(6)-O(4)	-51.8(3)
Cu(1)-P(2)-C(6)-O(4)	173.7(2)
C(9)-P(3)-C(7)-C(8)	-178.0(3)
C(10)-P(3)-C(7)-C(8)	-71.7(3)
Cu(1)-P(3)-C(7)-C(8)	60.1(3)
P(3)-C(7)-C(8)-P(4)#1	-166.46(19)
C(7)-P(3)-C(9)-O(5)	43.4(4)
C(10)-P(3)-C(9)-O(5)	-63.6(4)
Cu(1)-P(3)-C(9)-O(5)	169.0(3)
C(7)-P(3)-C(10)-O(6)	86.2(4)
C(9)-P(3)-C(10)-O(6)	-167.2(3)
Cu(1)-P(3)-C(10)-O(6)	-44.6(4)
C(12)-P(4)-C(11)-O(7)	-76.8(3)
C(8)#1-P(4)-C(11)-O(7)	176.2(3)
Cu(1)-P(4)-C(11)-O(7)	48.5(3)
C(8)#1-P(4)-C(12)-O(8)	51.7(3)
C(11)-P(4)-C(12)-O(8)	-51.1(3)

Cu(1)-P(4)-C(12)-O(8)	-179.8(2)

Symmetry transformations used to generate equivalent atoms:

#1 -x,-y+1,-z

Table D.2.7. Hydrogen bonds for $[Cu_2(DHMPE)_4]Cl_2$ [Å and °].

D-H...A	d(D-H)	d(H...A)	d(D...A)	<(DHA)
O(6)-H(6C)...O(8)#2	0.84	1.82	2.662(5)	177.5
O(6A)-H(6AA)...O(6A)#3	0.84	1.98	2.77(3)	156.0
O(2)-H(2O)...Cl(1)#4	0.938(18)	2.09(2)	3.017(3)	169(3)
O(3)-H(3O)...O(7)	0.957(19)	1.90(3)	2.792(4)	153(5)
O(4)-H(4O)...Cl(1)	0.944(19)	2.07(2)	3.005(3)	172(5)
O(8)-H(8O)...O(4)#5	0.95(2)	1.74(2)	2.675(4)	167(6)
O(5)-H(5O)...O(2)#6	0.97(2)	1.94(6)	2.781(5)	143(7)
O(5)-H(5O)...O(1S)#6	0.97(2)	2.58(8)	3.081(6)	112(6)
O(1)-H(1O)...O(1S)	0.95(2)	1.81(2)	2.741(5)	165(5)
O(7)-H(7O)...Cl(1)#7	0.96(2)	2.11(3)	3.042(3)	163(5)

Symmetry transformations used to generate equivalent atoms:

#1 -x,-y+1,-z #2 x,-y+1,z-1/2 #3 -x,y,-z-1/2

#4 -x+1/2,-y+3/2,-z #5 -x+1/2,y+1/2,-z+1/2 #6 x,y-1,z

#7 x,-y+1,z+1/2

APPENDIX E

CRYSTAL STRUCTURE OF

1,2-BIS-(PHENYLPHOSPHINATO)ETHANE

Figure E.1. ORTEP representation of 1,2-bis(phenylphosphinato)ethane. Ellipsoids are drawn at 50% probability, and nonpolar hydrodgen atoms have been omitted for clarity.

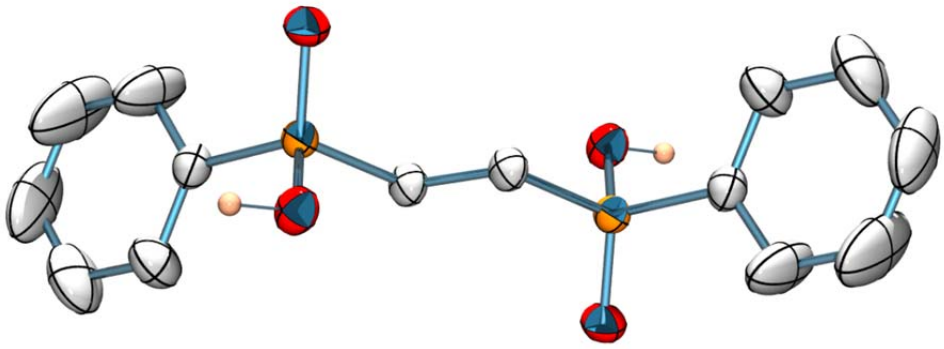

Figure E.2. Packing of 1,2-bis(phenylphosphinato)ethane, showing π-stacking and intramolecular hydrogen-bonding with waters of crystallization.

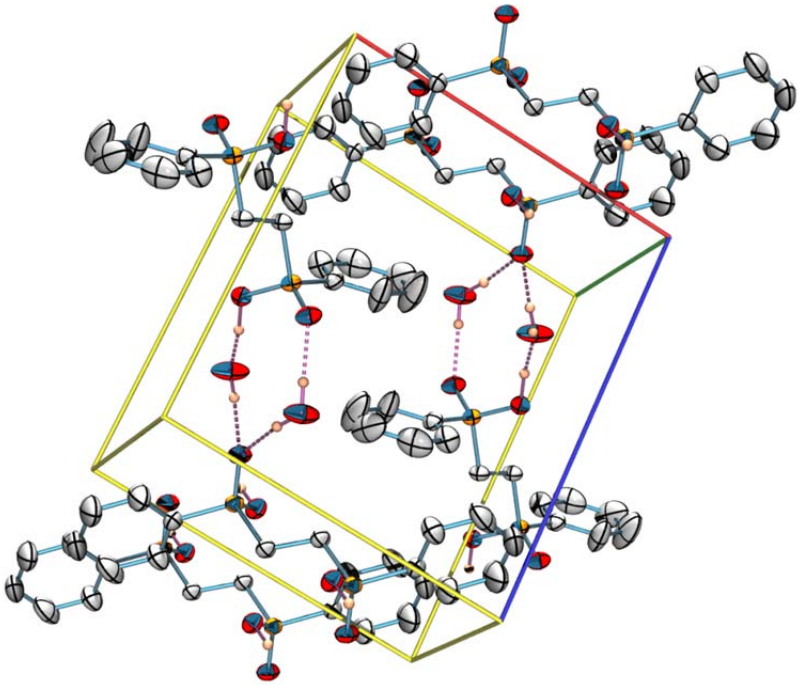

E.2. Crystallographic Data Tables

Table E.2.1. Crystal data and structure refinement for 1,2-bis(phenylphosphinato)-ethane.

Identification code	char11	
Empirical formula	C14 H20 O6 P2	
Formula weight	346.24	
Temperature	173(2) K	
Wavelength	0.71073 Å	
Crystal system	Monoclinic	
Space group	P2(1)/n	
Unit cell dimensions	a = 10.8280(16) Å	a= 90°.
	b = 6.2455(10) Å	b= 91.177(2)°.
	c = 12.861(2) Å	g = 90°.
Volume	869.5(2) $Å^3$	
Z	2	
Density (calculated)	1.322 Mg/m^3	
Absorption coefficient	0.273 mm^{-1}	
F(000)	364	
Crystal size	0.27 x 0.23 x 0.12 mm^3	
Theta range for data collection	2.43 to 27.00°.	
Index ranges	-13<=h<=13, -7<=k<=7, -16<=l<=16	
Reflections collected	9251	
Independent reflections	1888 [R(int) = 0.0213]	
Completeness to theta = 27.00°	100.0 %	
Absorption correction	Semi-empirical from equivalents	
Max. and min. transmission	0.9679 and 0.9298	
Refinement method	Full-matrix least-squares on F^2	
Data / restraints / parameters	1888 / 0 / 112	
Goodness-of-fit on F^2	1.093	
Final R indices [I>2sigma(I)]	R1 = 0.0390, wR2 = 0.1045	
R indices (all data)	R1 = 0.0431, wR2 = 0.1085	
Largest diff. peak and hole	0.409 and -0.385 e.$Å^{-3}$	

Table E.2.2. Atomic coordinates (x 10^4) and equivalent isotropic displacement parameters ($Å^2$x 10^3) for 1,2-bis(phenylphosphinato)ethane. U(eq) is defined as one third of the trace of the orthogonalized U^{ij} tensor.

	x	y	z	U(eq)
P(1)	8402(1)	1927(1)	5459(1)	28(1)
O(1)	7789(1)	487(2)	6217(1)	40(1)
O(2)	9208(1)	3728(2)	5950(1)	37(1)
C(1)	9482(2)	518(3)	4672(1)	32(1)
C(2)	7283(2)	3127(3)	4598(1)	36(1)
C(3)	6126(2)	2218(6)	4494(2)	83(1)
C(4)	5256(3)	3103(9)	3818(3)	122(2)
C(5)	5523(3)	4894(7)	3271(2)	95(1)
C(6)	6673(3)	5807(5)	3356(2)	76(1)
C(7)	7566(2)	4916(4)	4021(2)	53(1)
O(1S)	8284(2)	6587(3)	6995(1)	62(1)

Table E.2.3. Bond lengths [Å] and angles [°] for 1,2-bis(phenylphosphinato)ethane.

P(1)-O(1)	1.4928(13)
P(1)-O(2)	1.5500(13)
P(1)-C(2)	1.7883(18)
P(1)-C(1)	1.7927(16)
O(2)-H(1O)	1.06(3)
C(1)-C(1)#1	1.534(3)
C(1)-H(1B)	0.9900
C(1)-H(1C)	0.9900
C(2)-C(7)	1.380(3)
C(2)-C(3)	1.380(3)
C(3)-C(4)	1.383(4)
C(3)-H(3A)	0.9500
C(4)-C(5)	1.355(5)
C(4)-H(4A)	0.9500
C(5)-C(6)	1.373(5)
C(5)-H(5A)	0.9500
C(6)-C(7)	1.393(3)
C(6)-H(6A)	0.9500
C(7)-H(7A)	0.9500
O(1S)-H(1O)	1.40(3)
O(1S)-H(1S)	0.87(3)
O(1S)-H(2S)	0.91(4)
O(1)-P(1)-O(2)	115.11(8)
O(1)-P(1)-C(2)	110.63(8)
O(2)-P(1)-C(2)	108.45(8)
O(1)-P(1)-C(1)	112.15(8)
O(2)-P(1)-C(1)	102.64(8)
C(2)-P(1)-C(1)	107.32(8)
P(1)-O(2)-H(1O)	117.6(14)
C(1)#1-C(1)-P(1)	111.97(15)
C(1)#1-C(1)-H(1B)	109.2
P(1)-C(1)-H(1B)	109.2
C(1)#1-C(1)-H(1C)	109.2

P(1)-C(1)-H(1C)	109.2
H(1B)-C(1)-H(1C)	107.9
C(7)-C(2)-C(3)	119.5(2)
C(7)-C(2)-P(1)	121.16(15)
C(3)-C(2)-P(1)	119.37(18)
C(2)-C(3)-C(4)	120.1(3)
C(2)-C(3)-H(3A)	119.9
C(4)-C(3)-H(3A)	119.9
C(5)-C(4)-C(3)	120.4(3)
C(5)-C(4)-H(4A)	119.8
C(3)-C(4)-H(4A)	119.8
C(4)-C(5)-C(6)	120.3(2)
C(4)-C(5)-H(5A)	119.9
C(6)-C(5)-H(5A)	119.9
C(5)-C(6)-C(7)	120.0(3)
C(5)-C(6)-H(6A)	120.0
C(7)-C(6)-H(6A)	120.0
C(2)-C(7)-C(6)	119.7(2)
C(2)-C(7)-H(7A)	120.2
C(6)-C(7)-H(7A)	120.2
H(1O)-O(1S)-H(1S)	116(2)
H(1O)-O(1S)-H(2S)	122(2)
H(1S)-O(1S)-H(2S)	116(3)

Symmetry transformations used to generate equivalent atoms:

#1 -x+2,-y,-z+1

Table E.2.4. Anisotropic displacement parameters ($Å^2 x\ 10^3$)for 1,2-bis(phenyl-phosphinato)ethane. The anisotropic displacement factor exponent takes the form: $-2p^2[\ h^2 a^{*2} U^{11} + ... + 2\ h\ k\ a^*\ b^*\ U^{12}\ ]$.

	U^{11}	U^{22}	U^{33}	U^{23}	U^{13}	U^{12}
P(1)	30(1)	27(1)	28(1)	0(1)	5(1)	3(1)
O(1)	46(1)	34(1)	39(1)	6(1)	14(1)	3(1)
O(2)	35(1)	36(1)	40(1)	-8(1)	3(1)	0(1)
C(1)	35(1)	33(1)	28(1)	-2(1)	5(1)	6(1)
C(2)	31(1)	43(1)	34(1)	1(1)	2(1)	6(1)
C(3)	41(1)	131(3)	78(2)	43(2)	-13(1)	-22(2)
C(4)	41(1)	226(5)	97(2)	66(3)	-20(2)	-11(2)
C(5)	59(2)	166(4)	59(2)	28(2)	-8(1)	44(2)
C(6)	103(2)	72(2)	54(1)	20(1)	-8(1)	30(2)
C(7)	60(1)	46(1)	52(1)	10(1)	-8(1)	3(1)
O(1S)	105(2)	34(1)	50(1)	5(1)	38(1)	13(1)

Table E.2.5. Hydrogen coordinates (x 10^4) and isotropic displacement parameters (Å^{2}x 10^3) for 1,2-bis(phenylphosphinato)ethane.

	x	y	z	U(eq)
H(1B)	9039	-607	4270	38
H(1C)	9847	1527	4170	38
H(3A)	5926	983	4887	100
H(4A)	4467	2452	3737	146
H(5A)	4910	5519	2827	114
H(6A)	6861	7047	2961	91
H(7A)	8366	5537	4076	63
H(1O)	8750(20)	4910(40)	6401(19)	62(7)
H(1S)	7920(30)	6210(50)	7560(30)	86(10)
H(2S)	8010(30)	7830(60)	6700(30)	92(10)

Table E.2.6. Torsion angles [°] for 1,2-bis(phenylphosphinato)ethane.

O(1)-P(1)-C(1)-C(1)#1	-60.33(19)
O(2)-P(1)-C(1)-C(1)#1	63.78(18)
C(2)-P(1)-C(1)-C(1)#1	177.97(16)
O(1)-P(1)-C(2)-C(7)	162.61(16)
O(2)-P(1)-C(2)-C(7)	35.49(19)
C(1)-P(1)-C(2)-C(7)	-74.74(18)
O(1)-P(1)-C(2)-C(3)	-18.8(3)
O(2)-P(1)-C(2)-C(3)	-146.0(2)
C(1)-P(1)-C(2)-C(3)	103.8(2)
C(7)-C(2)-C(3)-C(4)	-0.3(5)
P(1)-C(2)-C(3)-C(4)	-178.9(3)
C(2)-C(3)-C(4)-C(5)	-1.5(6)
C(3)-C(4)-C(5)-C(6)	2.2(6)
C(4)-C(5)-C(6)-C(7)	-1.2(5)
C(3)-C(2)-C(7)-C(6)	1.3(4)
P(1)-C(2)-C(7)-C(6)	179.83(19)
C(5)-C(6)-C(7)-C(2)	-0.6(4)

Symmetry transformations used to generate equivalent atoms:
#1 -x+2,-y,-z+1

Table E.2.7. Hydrogen bonds for 1,2-bis(phenylphosphinato)ethane [Å and °].

D-H...A	d(D-H)	d(H...A)	d(D...A)	<(DHA)
O(2)-H(1O)...O(1S)	1.06(3)	1.40(3)	2.459(2)	173(2)
O(1S)-H(1S)...O(1)#2	0.87(3)	1.82(3)	2.687(2)	178(3)
O(1S)-H(2S)...O(1)#3	0.91(4)	1.78(4)	2.682(2)	167(3)

Symmetry transformations used to generate equivalent atoms:
#1 -x+2,-y,-z+1 #2 -x+3/2,y+1/2,-z+3/2 #3 x,y+1,z

REFERENCES CITED

Chapter I

(1) Spessard, G. O.; Miessler, G. L. *Organometallic Chemistry*; Prentice-Hall: Upper Saddle River N.J., 1997.

(2) Crabtree, R. H. *The Organometallic Chemistry of the Transition Metals*; 5th ed.; John Wiley and Sons, 2009.

(3) Fey, N.; Orpen, A. G.; Harvey, J. N. Building ligand knowledge bases for organometallic chemistry: Computational description of phosphorus(III)-donor ligands and the metal-phosphorus bond. *Coord. Chem. Rev.* **2009**, *253*, 704-722.

(4) van Leeuwen, P. W. *Homogeneous Catalysis: Understanding the Art*; Kluwer Academic Publishers: Dordrecht, 2004.

(5) Pignolet, L. *Homogeneous Catalysis with Metal Phosphine Complexes*; Modern Inorganic Chemistry; Plenum Press: New York, 1983.

(6) Tolman, W. *Activation of Small Molecules : Organometallic and Bioinorganic Perspectives*; Wiley-VCH: Weinheim, 2006.

(7) Cabbiness, D. K.; Margerum, D. W. Macrocyclic effect on the stability of copper(II) tetramine complexes. *J. Am. Chem. Soc.* **1969**, *91*, 6540-6541.

(8) Izatt, R. M.; Bradshaw, J. S.; Nielsen, S. A.; Lamb, J. D.; Christensen, J. J.; Sen, D. Thermodynamic and kinetic data for cation-macrocycle interaction. *Chem. Rev.* **1985**, *85*, 271-339.

(9) Izatt, R. M.; Pawlak, K.; Bradshaw, J. S.; Bruening, R. L. Thermodynamic and kinetic data for macrocycle interactions with cations and anions. *Chem. Rev.* **1991**, *91*, 1721-2085.

(10) Busch, D. H.; Farmery, K.; Goedken, V. L.; Katovic, V.; Melnyk, A. C.; Sperati, C. R.; Tokel, N. In *Bioinorganic Chemistry*; Advances in Chemistry; American Chemical Society, 1971; Vol. 100, pp. 44-78.

(11) Clay, R. M.; Corr, S.; Micheloni, M.; Paoletti, P. Non-cyclic reference ligands for tetraaza macrocycles. Synthesis and thermodynamic properties of a series of α,ω-di-N-methylated tetraaza ligands and their copper(II) complexes. *Inorg. Chem.* **1985**, *24*, 3330-3336.

(12) Frensdorff, H. K. Stability constants of cyclic polyether complexes with univalent cations. *J. Am. Chem. Soc.* **1971**, *93*, 600-606.

(13) Haymore, B. L.; Lamb, J. D.; Izatt, R. M.; Christensen, J. J. Thermodynamic origin of the macrocyclic effect in crown ether complexes of sodium(1+), potassium(1+), and barium(2+). *Inorg. Chem.* **1982**, *21*, 1598-1602.

(14) Sokol, L. S. W. L.; Ochrymowycz, L. A.; Rorabacher, D. B. Macrocyclic, ring size, and anion effects as manifested in the equilibrium constants and thermodynamic parameters of copper(II)-cyclic polythia ether complexes. *Inorg. Chem.* **1981**, *20*, 3189-3195.

(15) Desper, J. M.; Gellman, S. H.; Wolf, R. E.; Cooper, S. R. Enhanced nickel(II) chelation by gem-dimethyl-substituted macrocyclic tetrathioethers. *J. Am. Chem. Soc.* **1991**, *113*, 8663-8671.

(16) Toulhoat, C.; Vidal, M.; Vincens, M. Macrocyclic organophosphorus complexes of palladium(II), P-alkylated with saturated and unsaturated bridges. *Phosphorus, Sulfur Silicon Relat. Elem.* **1992**, *71*, 127-38.

(17) Lambert, B.; Desreux, J. F. Synthesis of macrocyclic polyphosphine oxides and phosphines by template cyclisation and demetallation. *Synthesis* **2000**, 1668-1670.

(18) Simulescu, V.; Ilia, G. Macrocycles and cavitands containing phosphorus. *J. Inclusion. Phenom. Macrocyclic Chem.* **2010**, *66*, 3-14.

(19) Caminade, A.; Majoral, J. P. Synthesis of phosphorus-containing macrocycles and cryptands. *Chem. Rev.* **1994**, *94*, 1183-1213.

(20) Markovskii, L. N.; Kal'chenko, V. I. Phosphorus-containing macroheterocyclic compounds. *Zh. Vses. Khim. O-va. im. D. I. Mendeleeva* **1985**, *30*, 528-35.

(21) Tsvetkov, E. N.; Bovin, A. N.; Syundyukova, V. K. The synthesis and complex forming capacity of phosphorus-containing macrocycles. *Russ. Chem. Rev.* **1988**, *57*, 776-800.

(22) Horner, L.; Kunz, H.; Walach, P. Organophosphorus compounds. 81. Synthesis of multimember oligophosphacycloalkanes. *Phosphorus* **1975**, *6*, 63-4.

(23) Horner, L.; Walach, P.; Kunz, H. Organophosphorus compounds, 87. Synthesis and reactions of cyclic phosphonium salts with 2 phosphorus atoms in 7,8,9,10 and 11 rings and 4 phosphorus atoms in 16,18 and 20 rings. *Phosphorus Sulfur Rel. Elem.* **1978**, *5*, 171-84.

(24) Kyba, E. P.; Hudson, C. W.; McPhaul, M. J.; John, A. M. Polyphosphino macrocyclic ligand systems. *J. Am. Chem. Soc.* **1977**, *99*, 8053-8054.

(25) Vögtle, F. A dlution principle apparatus. *Chem. Ind. (London)* **1972**, 346.

(26) Vögtle, F.; Wittig, G. A simple and inexpensive dilution apparatus. *J. Chem. Ed.* **1973**, *50*, 650.

(27) Davis, R. E.; Hudson, C. W.; Kyba, E. P. Properties and structure of a tetrakis(tert-phosphino) macrocycle. *J. Am. Chem. Soc.* **1978**, *100*, 3642-3643.

(28) Kyba, E. P.; John, A. M.; Brown, S. B.; Hudson, C. W.; McPhaul, M. J.; Harding, A.; Larsen, K.; Niedzwiecki, S.; Davis, R. E. Triligating 11-membered rings containing tert-phosphino sites. Synthesis and structure. *J. Am. Chem. Soc.* **1980**, *102*, 139-147.

(29) Kyba, E. P.; Davis, R. E.; Hudson, C. W.; John, A. M.; Brown, S. B.; McPhaul, M. J.; Liu, L.; Glover, A. C. Tetradentate 14-membered tert-phosphino-containing macrocycles. *J. Am. Chem. Soc.* **1981**, *103*, 3868-3875.

(30) Kyba, E. P.; Clubb, C. N.; Larson, S. B.; Schueler, V. J.; Davis, R. E. Synthesis of 14-membered phosphorus-sulfur P2S2 and P3S macrocycles which contain the 1-thio-2-(phenylphosphino)benzene moiety. Determination of stereochemistries of the free ligands and of a platinum(II) complex. *J. Am. Chem. Soc.* **1985**, *107*, 2141-2148.

(31) Kyba, E. P.; Davis, R. E.; Fox, M. A.; Clubb, C. N.; Liu, S. T.; Reitz, G. A.; Scheuler, V. J.; Kashyap, R. P. Phosphinomacrocycles. 16. Complexation of the nickel(II) triad with 14-membered macrocyclic P4-nSn (n = 2, 1, 0) ligands. Study of the effects on coordination of the relative configuration at the phosphines and the number and placement of thioether sites. *Inorg. Chem.* **1987**, *26*, 1647-1658.

(32) Kyba, E. P.; Liu, S. T. Phosphino macrocycles. 140. Synthesis of unusual phosphine ligands. Use of the 1-naphthylmethyl moiety as a P-H protecting group in the synthesis of a phosphino macrocycle that contains a secondary-phosphino ligating site. *Inorg. Chem.* **1985**, *24*, 1613-1616.

(33) Ciampolini, M.; Dapporto, P.; Nardi, N.; Zanobini, F. New phosphorus-containing macrocyclic sexidentate ligands: two isomers of 4,7,13,16-tetraphenyl-1,10-dioxa-4,7,13,16-tetraphosphacyclo-octadecane and crystal structures of their cobalt bis-(tetraphenylborate) complexes. *J. Chem. Soc., Chem. Commun.* **1980**, 177-178.

(34) Ciampolini, M.; Dapporto, P.; Dei, A.; Nardi, N.; Zanobini, F. Synthesis and characterization of the five diastereoisomers of the first crown ether type phosphorus-containing macrocycle: configurational and coordinative interdependence. *Inorg. Chem.* **1982**, *21*, 489-495.

(35) Ciampolini, M.; Dapporto, P.; Nardi, N.; Zanobini, F. Novel phosphorus-containing macrocyclic sexidentate ligands: Synthesis of (4R*, 7R*13S*, 16S*)-4,7,13,16-tetraphenyl-1,10-dithia-4,7,13,16-tetraphosphacyclo-octadecane and crystal structure of its nickel dibromide dihydrate complex. *Inorg. Chim. Acta* **1980**, *45*, L239-L240.

(36) Ciampolini, M.; Nardi, N.; Zanobini, F.; Cini, R.; Orioli, P. L. Sexidentate phosphorus-containing macrocyclic ligands. Synthesis of 1,10-dipropyl-4,7,13,16-tetraphenyl-1,10-diaza-4,7,13,16-tetraphospha-cyclooctadecane. *Inorg. Chim. Acta* **1983**, *76*, L17-L19.

(37) Laurent, B. A.; Grayson, S. M. Synthetic approaches for the preparation of cyclic polymers. *Chem. Soc. Rev.* **2009**, *38*, 2202-2213.

(38) Vincens, M.; Grimaldo-Moron, J. T.; Vidal, M. Synthesis of macrocyclic phosphine tetraoxides from the corresponding bisphosphonium bis oxides. *Tetrahedron* **1991**, *47*, 403.

(39) Venkataramu, S. D.; El-Deek, M.; Berlin, K. D. A novel carbon-phosphorus polycation heterocycle. *Tetrahedron Lett.* **1976**, *17*, 3365-3368.

(40) Vincens, M.; Grimaldo Moron, J. T.; Pasqualini, R.; Vidal, M. Synthese de nouveaux sels de tetraphosphonium macrocycliques. *Tetrahedron Lett.* **1987**, *28*, 1259-1262.

(41) Toulhoat, C.; Vincens, M.; Vidal, M. Polyoxydes de polyphopshines macrocycliques P-alkyles. *Bull. Soc. Chim. Fr.* **1993**, *130*, 647-654.

(42) Vincens, M.; Gong-Cheng, F.; Toulhoat, C.; Grimaldo-Moron, J. T.; Vidal, M. Synthese de nouveaux oxydes de tetraphosphines macrocycliques. *Tetrahedron Lett.* **1988**, *29*, 6247-6248.

(43) Li, G. Q.; Govind, R. Synthesis and characterization of a tetraphosphine macrocyclic ligand and its manganese(II) complexes. *Inorg. Chim. Acta* **1995**, *231*, 225-228.

(44) Toulhoat, C.; Vidal, M.; Vincens, M. Polyoxydes de polyphosphines bicycliques alkyles sur la phosphore. *Phosphorus, Sulfur Silicon Relat. Elem.* **1993**, *78*, 119.

(45) Baechler, R. D.; Mislow, K. Effect of structure on the rate of pyramidal inversion of acyclic phosphines. *J. Am. Chem. Soc.* **1970**, *92*, 3090-3093.

(46) Laporte, F.; Mercier, F.; Ricard, L.; Mathey, F. Tetraphosphorus macrocycles from phosphole tetramers. *J. Am. Chem. Soc.* **1994**, *116*, 3306-3311.

(47) Egan, W.; Tang, R.; Zon, G.; Mislow, K. Barriers to pyramidal inversion at phosphorus in phospholes, phosphindoles, and dibenzophospholes. *J. Am. Chem. Soc.* **1971**, *93*, 6205-6216.

(48) Avarvari, N.; Mézailles, N.; Ricard, L.; Floch, P. L.; Mathey, F. Silacalix-[n]-phosphaarenes: Macrocyclic ligands based on dicoordinate phosphorus centers. *Science* **1998**, *280*, 1587-1589.

(49) Avarvari, N.; Maigrot, N.; Ricard, L.; Mathey, F.; Le Floch, P. Synthesis and X-ray crystal structures of silacalix[n]phosphinines: the first sp^2-based phosphorus macrocycles. *Chem. Eur. J.* **1999**, *5*, 2109-2118.

(50) Mézailles, N.; Maigrot, N.; Hamon, S.; Ricard, L.; Mathey, F.; Le Floch Mixed phosphinine-ether macrocycles. *J. Org. Chem.* **2001**, *66*, 1054-1056.

(51) Morisaki, Y.; Ouchi, Y.; Fukui, T.; Naka, K.; Chujo, Y. Synthesis of oligomers including eight *P*-chiral centers and the construction of the 12-phosphacrown-4 skeleton. *Tetrahedron Lett.* **2005**, *46*, 7011-7014.

(52) Collman, J. P.; Schneider, P. W. Complexes of cobalt(III) and rhodium(III) with a cyclic tetradentate secondary amine. *Inorg. Chem.* **1966**, *5*, 1380-1384.

(53) Kalligeros, G. A.; Blinn, E. L. Strained five- and six-coordinated macrocyclic nickel(II) complexes. *Inorg. Chem.* **1972**, *11*, 1145-1148.

(54) Busch, D. H. Distinctive coordination chemistry and biological significance of complexes with macrocyclic ligands. *Acc. Chem. Res.* **1978**, *11*, 392-400.

(55) Rosen, W.; Busch, D. H. Octahedral nickel(II) complexes of some cyclic polyfunctional thioethers. *Inorg. Chem.* **1970**, *9*, 262-265.

(56) Lowry, D. J.; Helm, M. L. Synthesis of 1,4,7-Triphenyl-1,4,7-triphosphacyclononane: The first metal-free synthesis of a [9]-aneP3R3 ring. *Inorg. Chem.* **2010**, *49*, 4732-4734.

(57) Mason, L. J.; Moore, A. J.; Carr, A.; Helm, M. L. Lithium bis(2-phenylphosphidoethyl)phenyl-phosphine: A reactive phosphorus intermediate. *Heteroatom Chim.* **2007**, *18*, 675-678.

(58) Mizuta, T.; Onishi, M.; Miyoshi, K. Photolytic ring-opening polymerization of phosphorus-bridged [1]ferrocenophane coordinating to an organometallic fragment. *Organometallics* **2000**, *19*, 5005-5009.

(59) Mizuta, T.; Aotani, T.; Imamura, Y.; Kubo, K.; Miyoshi, K. Structure and properties of the macrocyclic tridentate ferrocenylphosphine ligand (-$PhPC_5H_4FeC_5H_4$-)$_3$. *Organometallics* **2008**, *27*, 2457-2463.

(60) Balueva, A. S.; Kuznetsov, R. M.; Litvinov, I. A.; Gubaidullin, A. T.; Nikonov, G. N. Cyclo-bis{1-[p-(p-phenylenomethyl)phenyl]-3,7-diphenyl-1,5,3,7-diazadiphosphacyclooctane} as the first representative of a new type of nitrogen-containing macroheterocyclic phosphines. *Mendeleev Commun.* **2000**, *10*, 120-121.

(61) Balueva, A. S.; Kuznetsov, R. M.; Ignat'eva, S. N.; Karasik, A. A.; Gubaidullin, A. T.; Litvinov, I. A.; Sinyashin, O. G.; Loennecke, P.; Hey-Hawkins, E. Self-assembly of novel macrocyclic aminomethylphosphines with hydrophobic intramolecular cavities. *Dalton Trans.* **2004**, 442-447.

(62) Naumov, R. N.; Karasik, A. A.; Kanunnikov, F. B.; Kozlov, A. V.; Latypov, S. K.; Domasevitch, K. V.; Hey-Hawkins, E.; Sinyashin, O. G. Synthesis of a chiral macrocyclic tetraphosphine - 1,9-di-R,R(and S,S)-alpha-methylbenzyl-3,7,11,15-tetramesityl-1,9-diaza-3,7,11,15-(RSSR)-tetraphosphacyclohexadecane. *Mendeleev Commun.* **2008**, *18*, 80-81.

(63) Naumov, R. N.; Karasik, A. A.; Sinyashin, O. G.; Loennecke, P.; Hey-Hawkins, E. Unexpected formation of a novel macrocyclic tetraphosphine: (RSSR)-1,9-dibenzyl-3,7,11,15-tetramesityl-1,9-diaza-3,7,11,15-tetraphosphacyclohexadecane. *Dalton Trans.* **2004**, 357-358.

(64) Naumov, R. N.; Karasik, A. A.; Kanunnikov, K. B.; Kozlov, A. V.; Latypov, S. K.; Domasevitch, K. V.; Hey-Hawkins, E.; Sinyashin, O. G. Synthesis of a chiral macrocyclic tetraphosphine -1,9-di-*R,R(*and *S,S*)-α-methylbenzyl-3,7,11,15-tetramesityl-1,9-diaza-3,7,11,15-(RSSR)-tetraphosphacyclohexadecane. *Mendeleev Commun.* **2008**, *18*, 80-81.

(65) Naumov, R. N.; Kozlov, A. V.; Kanunnikov, K. B.; Gomez-Ruiz, S.; Hey-Hawkins, E.; Latypov, S. K.; Karasik, A. A.; Sinyashin, O. G. The first example of stereoselective self-assembly of a cryptand containing four asymmetric intracyclic phosphane groups. *Tetrahedron Lett.* **2010**, *51*, 1034-1037.

(66) Naumov, R. N.; Karasik, A. A.; Kozlovi, A. V.; Latypov, S. K.; Krivolapov, D. B.; Dobrynin, A. B.; Litvinov, I. A.; Kataeva, O. N.; Sinyashin, O. G.; Loennecke, P.; Hey-Hawkins, E. Stereoselective synthesis and interconversions of 1,9-diaza-3,7,11,15-tetraphosphacyclohexadecanes. *Phosphorus, Sulfur Silicon Relat. Elem.* **2008**, *183*, 456-459.

(67) Karasik, A. A.; Naumov, R. N.; Spiridonova, Y. S.; Sinyashin, O. G.; Lönnecke, P.; Hey-Hawkins, E. Synthesis, molecular structure and coordination chemistry of the first 1-aza-3,7-diphosphacyclooctanes. *Z. Anorg. Allg. Chem.* **2007**, *633*, 205-210.

(68) Laughrey, Z. R.; Gibb, B. C. Macrocycle synthesis through templation. *Top. Curr. Chem.* **2005**, *249*, 67-125.

(69) Glueck, D. S. Metal-catalyzed nucleophilic carbon–heteroatom (C–X) bond formation: the role of M–X intermediates. *Dalton Trans.* **2008**, 5276.

(70) Diel, B. N.; Haltiwanger, R. C.; Norman, A. D. Metal-templated synthesis of a macrocyclic triphosphine-molybdenum complex, *fac*-$(CO)_3Mo(PHC_3H_6)_3$. *J. Am. Chem. Soc.* **1982**, *104*, 4700-4701.

(71) Diel, B. N.; Brandt, P. F.; Haltiwanger, R. C.; Hackney, M. L. J.; Norman, A. D. Metal-templated synthesis of macrocyclic (triphosphine)molybdenum complexes. *Inorg. Chem.* **1989**, *28*, 2811-2816.

(72) Coles, S. J.; Edwards, P. G.; Fleming, J. S.; Hursthouse, M. B. 1,5,9-Triphosphacyclododecane complexes of molybdenum and tungsten; crystal structure of tricarbonyl[1,5,9-tris(isopropyl)-1,5,9-triphosphacyclododecane]-molybdenum(0). *J. Chem. Soc., Dalton Trans.* **1995**, 1139.

(73) Edwards, P. G.; Fleming, J. S.; Liyanage, S. S.; Coles, S. J.; Hursthouse, M. B. Primary alkenyl phosphine complexes of chromium and molybdenum; synthesis and characterisation of tricarbonyl(1,5,9-triphosphacyclododecane)chromium(0). *J. Chem. Soc., Dalton Trans.* **1996**, 1801.

(74) Edwards, P. G.; Fleming, J. S.; Liyanage, S. S. Chromium and molybdenum complexes of tertiary alkyl and pendant donor triphosphamacrocycles. *J. Chem. Soc., Dalton Trans.* **1997**, 193-198.

(75) Jones, D. J.; Edwards, P. G.; Tooze, R. P.; Albers, T. The template synthesis of triaryl functionalised 1,5,9-triphosphacyclododecane on molybdenum using organocopper reagents. *J. Chem. Soc., Dalton Trans.* **1999**, 1045-1046.

(76) Edwards, P. G.; Newman, P. D.; Malik, K. M. A. Template synthesis of the first 1,4,7-triphosphacyclononane derivatives. *Angew. Chem., Int. Ed.* **2000**, *39*, 2922-2924.

(77) Edwards, P. G.; Haigh, R.; Li, D.; Newman, P. D. Template synthesis of 1,4,7-triphosphacyclononanes. *J. Am. Chem. Soc.* **2006**, *128*, 3818-3830.

(78) Edwards, P. G.; Whatton, M. L. Template synthesis of 9-membered triphospha-macrocycles with rigid o-phenylene backbone functions. *Dalton Trans.* **2006**, 442-450.

(79) Albers, T.; Edwards, P. G. Template synthesis of benzannulated triphosphacyclononanes-a new class of phosphacrowns via template assisted nucleophilic P-C bond formation. *Chem. Commun.* **2007**, 858-860.

(80) Price, A. J.; Edwards, P. G. A new template for the synthesis of triphosphorus macrocycles. *Chem. Commun.* **2000**, 899-900.

(81) Edwards, P. G.; Newman, P. D.; Hibbs, D. E. A new kinetic template synthesis of triphosphacyclodecanes. *Angewandte Chemie International Edition* **2000**, *39*, 2722-2724.

(82) Battle, A. R.; Edwards, P. G.; Haigh, R.; Hibbs, D. E.; Li, D.; Liddiard, S. M.; Newman, P. D. Synthesis and characterization of iron(II) complexes of 10- and 11-membered triphosphamacrocycles. *Organometallics* **2007**, *26*, 377-386.

(83) Bauer, E. B.; Ruwwe, J.; Hampel, F. A.; Szafert, S.; Gladysz, J. A.; Martín-Alvarez, J. M.; Peters, T. B.; Bohling, J. C.; Lis, T. Olefin metatheses in metal coordination spheres: novel trans-spanning bidentate and facially-spanning tridentate macrocyclic phosphine complexes. *Chem. Commun.* **2000**, 2261-2262.

(84) Driess, M.; Faulhaber, M.; Pritzkow, H. Multidentate, cyclic phosphorus ligands with a silicon-phosphorus backbone: Template synthesis of a 1,4,7-triphospha-2,3,5,6,8,9-hexasilacyclononane and a 1,3,5,7,9,11-hexaphospha-2,4,6,8,10,12-hexasilacyclododecane. *Angew. Chem. Int. Ed.* **1997**, *36*, 1892-1894.

(85) DelDonno, T. A.; Rosen, W. Studies of a fifteen-membered tetraphosphorus macrocyclic ligand. *Inorg. Chem.* **1978**, *17*, 3714-3716.

(86) DelDonno, T. A.; Rosen, W. Preparation of a tetraphosphine macrocyclic ligand. *J. Am. Chem. Soc.* **1977**, *99*, 8051-8052.

(87) Brauer, D. J.; Gol, F.; Hietkamp, S.; Peters, H.; Sommer, H.; Stelzer, O.; Sheldrick, W. S. Reaktionen koordinierter Liganden, XIV. Synthese eines vierzähnigen Phosphor-Makrocyclus im Palladium(II)-Templat. *Chem. Ber.* **1986**, *119*, 349-365.

(88) Mizuta, T.; Okano, A.; Sasaki, T.; Nakazawa, H.; Miyoshi, K. Palladium(II) and platinum(II) complexes of a tetraphosphamacrocycle. X-ray crystal structures of phosphorus analogs of a (tetramethylcyclam)metal complex. *Inorg. Chem.* **1997**, *36*, 200-203.

(89) Bartsch, R.; Hietkamp, S.; Morton, S.; Stelzer, O. Stereospecific synthesis of palladium(II) complexes of macrocyclic tetradentate phosphane ligands. *Angew. Chem. Int. Ed.* **1982**, *21*, 375-376.

(90) Bartsch, R.; Hietkamp, S.; Morton, S.; Peters, H.; Stelzer, O. Reactions of coordinated ligands. 12. Single-stage template syntheses of tetradentate macrocyclic phosphine complexes. *Inorg. Chem.* **1983**, *22*, 3624-3632.

(91) Bartsch, R.; Hietkamp, S.; Peters, H.; Stelzer, O. Reactions of coordinated ligands. 13. Template syntheses of 14- to 16-membered tetraphosphacycloalkanes using bis(tertiary phosphines) with protected carbonyl groups in the alkyl side chains. *Inorg. Chem.* **1984**, *23*, 3304-3309.

(92) Brauer, D. J.; Lebbe, T.; Stelzer, O. Template synthesis of macrocyclic multiphosphane ligands with functional groups. *Angew. Chem. Int. Ed.* **1988**, *27*, 438-439.

(93) Brauer, D. J.; Dörrenbach, F.; Lebbe, T.; Stelzer, O. Reaktionen koordinierter Liganden, XVIII. Templatsynthesen und Peripheriereaktionen makrocyclischer Multiphosphanliganden mit funktionellen Gruppen. *Chem. Ber.* **1992**, *125*, 1785-1794.

(94) Kang, Y. B.; Pabel, M.; Pathak, D. D.; Willis, A. C.; Wild, S. B. Copper(I)-facilitated methylation and cyclic alkylation of 1,2-phenylenebis(phosphine). *Main Group Chem.* **1995**, *1*, 89-98.

(95) Harnisch, J. A.; Angelici, R. J. Gold and platinum benzenehexathiolate complexes as large templates for the synthesis of 12-coordinate polyphosphine macrocycles. *Inorg. Chim. Acta* **2000**, *300-302*, 273-279.

(96) Baker, R. J.; Davies, P. C.; Edwards, P. G.; Farley, R. D.; Liyanage, S. S.; Murphy, D. M.; Yong, B. Early transition metal complexes of triphosphorus macrocycles. *Eur. J. Inorg. Chem.* **2002**, 1975-1984.

(97) Baker, R. J.; Edwards, P. G.; Gracia-Mora, J.; Ingold, F.; Abdul Malik, K. M. Manganese and rhenium triphosphorus macrocycle complexes and reactions with alkenes. *J. Chem. Soc., Dalton Trans.* **2002**, 3985-3992.

(98) Ciampolini, M.; Dapporto, P.; Nardki Nicoletta; Zanobini, F. Synthesis and characterization of some cobalt(II) and nickel(II) complexes of three diastereoisomers of the phosphorus-containing macrocycle 4,7,13,16-tetraphenyl-1,10-dioxa-4,7,13,16-tetraphosphacyclooctadecane. *Inorg. Chem.* **1983**, *22*, 13-17.

(99) Mercier, F.; Laporte, F.; Ricard, L.; Mathey, F.; Schröder, M.; Regitz, M. The use of a ten-membered tetraphosphole macrocycle to increase the lifetime of a palladium catalyst. *Angew. Chem. Int. Ed.* **1997**, *36*, 2364-2366.

(100) Le Floch, P.; Mathey, F. Transition metals in phosphinine chemistry. *Coord. Chem. Rev.* **1998**, *178-180*, 771-791.

(101) Mézailles, N.; Avarvari, N.; Maigrot, N.; Ricard, L.; Mathey, F.; Le Floch, P.; Cataldo, L.; Berclaz, T.; Geoffroy, M. Gold(I) and gold(0) complexes of phosphinine-based macrocycles. *Angew. Chem. Int. Ed.* **1999**, *38*, 3194-3197.

(102) Mingos, D. M. P. Theoretical and structural studies on organometallic cluster molecules. *Pure Appl. Chem.* **1980**, *52*, 705-712.

(103) Coles, S. J.; Edwards, P. G.; Fleming, J. S.; Hursthouse, M. B. Triphosphorus macrocycle complexes of divalent Group 6 transition metals; crystal structure of bromotricarbonyl-[1,5,9-tris(isopropyl)-1,5,9-triphosphacyclododecane]-molybdenum(II) tetraphenylborate. *J. Chem. Soc., Dalton Trans.* **1995**, 4091.

(104) Coles, S. J.; Edwards, P. G.; Fleming, J. S.; Hursthouse, M. B.; Liyanage, S. S. The liberation, characterisation and X-ray crystal structure of 1,5,9-triphospha-1,5,9-tris(2-propyl)cyclodecane. *Chem. Commun.* **1996**, 293.

(105) Edwards, P. G.; Fleming, J. S.; Liyanage, S. S. Stereoselective Synthesis of 1,5,9-Triphosphacyclododecane and tertiary derivatives. *Inorg. Chem.* **1996**, *35*, 4563-4568.

Chapter II

(1) *Annual Energy Review 2009*; U.S. Energy Information Administration: Washington, DC, 2010.

(2) Hugman, R. H.; Vidas, E. H.; Springer, P. S. *Chemical Composition of Discovered and Undiscovered Natural Gas in the U.S. Lower-48, Executive Summary*; Gas Research Institute: Chicago, IL, 1993.

(3) Tannehill, C. C.; Galvin, C. *Business Characteristics of the Natural Gas Conditioning Industry*; Gas Research Institute: Chicago, IL, 1993.

(4) Meyer, H. S. *GasTIPS*. 2000, p. 10.

(5) Kidnay, A. J.; Parrish, W. R. In *Fundamentals of Natural Gas Processing*; CRC Press, 2006; pp. 1-23.

(6) Kidnay, A. J.; Parrish, W. R. In *Fundamentals of Natural Gas Processing*; CRC Press, 2006; pp. 199-207.

(7) Lokhandwala, K. A.; Pinnau, I.; He, Z.; Amo, K. D.; DaCosta, A. R.; Wijmans, J. G.; Baker, R. W. Membrane separation of nitrogen from natural gas: A case study from membrane synthesis to commercial deployment. *J. Membr. Sci.* **2010**, *346*, 270-279.

(8) Lin, C. C. H.; Sawada, J. A.; Wu, L.; Haastrup, T.; Kuznicki, S. M. Anion-controlled pore size of titanium silicate molecular sieves. *J. Am. Chem. Soc.* **2009**, *131*, 609-614.

(9) Miller, W. K.; Gilbertson, J. D.; Leiva-Paredes, C.; Bernatis, P. R.; Weakley, T. J. R.; Lyon, D. K.; Tyler, D. R. Precursors to water-soluble dinitrogen carriers. Synthesis of water-soluble complexes of iron(II) containing water-soluble chelating phosphine ligands of the type 1,2-bis(bis(hydroxyalkyl)phosphino)ethane. *Inorg. Chem.* **2002**, *41*, 5453-5465.

(10) Gilbertson, J. D.; Szymczak, N. K.; Tyler, D. R. Reduction of N_2 to ammonia and hydrazine utilizing H_2 as the reductant. *J. Am. Chem. Soc.* **2005**, *127*, 10184-10185.

(11) Gilbertson, J. D.; Szymczak, N. K.; Crossland, J. L.; Miller, W. K.; Lyon, D. K.; Foxman, B. M.; Davis, J.; Tyler, D. R. Coordination chemistry of H_2 and N_2 in aqueous solution. Reactivity and mechanistic studies using trans-$Fe^{II}(P_2)_2X_2$-type complexes (P_2 = a chelating, water-solubilizing phosphine). *Inorg. Chem.* **2007**, *46*, 1205-1214.

(12) Caminade, A.; Majoral, J. P. Synthesis of phosphorus-containing macrocycles and cryptands. *Chem. Rev.* **1994**, *94*, 1183-1213.

(13) Mercier, F.; Laporte, F.; Ricard, L.; Mathey, F.; Schröder, M.; Regitz, M. The use of a ten-Membered tetraphosphole macrocycle to increase the lifetime of a palladium catalyst. *Angew. Chem. Int. Ed.* **1997**, *36*, 2364-2366.

(14) Däbritz, F.; Theumer, G.; Gruner, M.; Bauer, I. New conformational flexible phosphane and phosphane oxide macrobicycles. *Tetrahedron* **2009**, *65*, 2995-3002.

(15) Lowry, D. J.; Helm, M. L. Synthesis of 1,4,7-triphenyl-1,4,7-triphosphacyclononane: The first metal-free synthesis of a [9]-aneP_3R_3 ring. *Inorg. Chem.* **2010**, *49*, 4732-4734.

(16) Toulhoat, C.; Vidal, M.; Vincens, M. Polyoxydes de polyphosphines bicycliques alkyles sur la phosphore. *Phosphorus, Sulfur Silicon Relat. Elem.* **1993**, *78*, 119.

(17) Lambert, B.; Desreux, J. F. Synthesis of macrocyclic polyphosphine oxides and phosphines by template cyclisation and demetallation. *Synthesis* **2000**, 1668-1670.

(18) Cabbiness, D. K.; Margerum, D. W. Macrocyclic effect on the stability of copper(II) tetramine complexes. *J. Am. Chem. Soc.* **1969**, *91*, 6540-6541.

(19) Hinz, F. P.; Margerum, D. W. Effect of ligand solvation on the stability of metal complexes in solution. Explanation of the macrocyclic effect. *J. Am. Chem. Soc.* **1974**, *96*, 4993-4994.

(20) Busch, D. H.; Farmery, K.; Goedken, V. L.; Katovic, V.; Melnyk, A. C.; Sperati, C. R.; Tokel, N. In *Bioinorganic Chemistry*; Advances in Chemistry; American Chemical Society, 1971; Vol. 100, pp. 44-78.

(21) Izatt, R. M.; Bradshaw, J. S.; Nielsen, S. A.; Lamb, J. D.; Christensen, J. J.; Sen, D. Thermodynamic and kinetic data for cation-macrocycle interaction. *Chem. Rev.* **1985**, *85*, 271-339.

(22) DelDonno, T. A.; Rosen, W. Preparation of a tetraphosphine macrocyclic ligand. *J. Am. Chem. Soc.* **1977**, *99*, 8051-8052.

(23) Bartsch, R.; Hietkamp, S.; Morton, S.; Peters, H.; Stelzer, O. Reactions of coordinated ligands. 12. Single-stage template syntheses of tetradentate macrocyclic phosphine complexes. *Inorg. Chem.* **1983**, *22*, 3624-3632.

(24) Dogan, J.; Schulte, J. B.; Swiegers, G. F.; Wild, S. B. mechanism of phosphorus−carbon bond cleavage by lithium in tertiary phosphines. An optimized synthesis of 1,2-bis(phenylphosphino)ethane. *J. Org. Chem.* **2000**, *65*, 951-957.

(25) Bruker *SMART and SAINT*; Bruker AXS, Inc.: Madison, Wisconsin, USA, 2000.

(26) Sheldrick, G. M. *SADABS*; University of Göttingen: Germany, 1995.

(27) Sheldrick, G. M. A short history of SHELX. *Acta Crystallogr. A* **2008**, *64*, 112-122.

(28) Cecconi, F.; Di Vaira, M.; Midollini, S.; Orlandini, A.; Sacconi, L. Singlet ↔ quintet spin transitions of iron(II) complexes with a P_4Cl_2 donor set. X-ray structures of the compound $FeCl_2(Ph_2PCH{:}CHPPh_2)_2$ and of its acetone solvate at 130 and 295 K. *Inorg. Chem.* **1981**, *20*, 3423-3430.

(29) Chatt, J.; Hayter, R. G. 1079. Some hydrido-complexes of iron(II). *J. Chem. Soc.* **1961**, 5507.

(30) Girolami, G. S.; Wilkinson, G.; Galas, A. M. R.; Thornton-Pett, M.; Hursthouse, M. B. Synthesis and properties of the divalent 1,2-bis(dimethylphosphino)ethane (dmpe) complexes $MCl_2(dmpe)_2$ and $MMe_2(dmpe)_2$(M = Ti, V, Cr, Mn, or Fe). X-Ray crystal structures of $MCl_2(dmpe)_2$(M = Ti, V, or Cr), $MnBr_2(dmpe)_2$, $TiMe_{1.3}Cl_{0.7}(dmpe)_2$, and $CrMe_2(dmpe)_2$. *J. Chem. Soc., Dalton Trans.* **1985**, 1339.

(31) Mays, M. J.; Prater, B. E.; Wonchoba, E. R.; Parshall, G. W. trans - (Dinitrogen) bis [ethylenebis-(diethylphosphine)] hydridoiron(II) tetraphenylborate. *Inorg. Synth.* **1974**, *15*.

(32) Bellerby, J. M.; Mays, M. J.; Sears, P. L. Cationic low-spin bis[1,2-bis(dialkylphosphino)ethane]iron(II) complexes. *J. Chem. Soc., Dalton Trans.* **1976**, 1232.

(33) Baker, M. V.; Field, L. D.; Hambley, T. W. Diamagnetic ↔ paramagnetic equilibria in solutions of bis(dialkylphosphino)ethane complexes of iron. *Inorg. Chem.* **1988**, *27*, 2872-2876.

(34) Lewis, J.; Khan, M. S.; Kakkar, A. K.; Raithby, P. R.; Fuhrmann, K.; Friend, R. H. Synthesis and characterisation of a bulky chelating bis(phosphine) ligand, 1,2-bis(dinbutylphosphino)ethane (DBPE), and its iron metal coordinated complexes, $Fe(DBPE)_2Cl_2$ and $Fe(DBPE)_2$(---C[triple bond]C---$C_6H_5)_2$. *J. Organomet. Chem.* **1992**, *433*, 135-139.

(35) Antberg, M.; Dahlenburg, L. Oligophosphine ligands. XI. Hexacoordinate halogenoiron complexes $FeX_2[P(CH_2CH_2CH_2PMe_2)_3]$ (X = Cl, Br, I). *Inorg. Chim. Acta* **1985**, *104*, 51-54.

(36) Burrows, A. D.; Dodds, D.; Kirk, A. S.; Lowe, J. P.; Mahon, M. F.; Warren, J. E.; Whittlesey, M. K. Substitution and derivatization reactions of a water soluble iron(II) complex containing a self-assembled tetradentate phosphine ligand. *Dalton Trans.* **2007**, 570-580.

(37) Field, L. D.; Thomas, I. P.; Hambley, T. W.; Turner, P. Iron(II) complexes containing the 1,2-diphospholanoethane Ligand. *Inorg. Chem.* **1998**, *37*, 612-618.

(38) Woska, D.; Prock, A.; Giering, W. P. Determination of the stereoelectronic parameters of PF_3, PCl_3, PH_3, and $P(CH_2CH_2CN)_3$. The Quantitative Analysis of Ligand Effects (QALE). *Organometallics* **2000**, *19*, 4629-4638.

Chapter III

(1) Alder, R. W.; Bowman, P. S.; Steele, W. R. S.; Winterman, D. R. The remarkable basicity of 1,8-bis(dimethylamino)naphthalene. *Chem. Commun.* **1968**, 723-724.

(2) Kaljurand, I.; Kutt, A.; Soovali, L.; Rodima, T.; Maemets, V.; Leito, I.; Koppel, I. A. Extension of the self-consistent spectrophotometric basicity scale in acetonitrile to a full span of 28 pKa units: Unification of different basicity scales. *J. Org. Chem.* **2005**, *70*, 1019-1028.

(3) Terrier, F.; Halle, J. C.; Pouet, M. J.; Simonnin, M. P. The proton sponge as nucleophile. *J. Org. Chem.* **1986**, *51*, 409-411.

(4) Kurasov, L. A.; Pozharskii, A. F.; Kuz'menko, V. V.; Klyuev, N. A.; Chernyshev, A. I.; Goryaev, S. S.; Chikina, N. L. Peri-naphthylenediamines. VI. Nitration of 1,8-bis(dialkylamino)naphthalenes. *Zh. Org. Khim.* **1983**, *19*, 590-7.

(5) Ozeryanskii, V. A.; Pozharskii, A. F.; Fomchenkov, A. M. peri-Naphthylenediamines. 25. Evidence for the participation of a radical cation of 1,8-bis(dimethylamino)naphthalene ("proton sponge") in reactions with nitrating agents. The formation of 1,1'-binaphthyl "proton sponge" and the regioselective synthesis of 4-chloro-1,8-bis(dimethylamino)naphthalene. *Russ. Chem. Bull.* **1998**, *47*, 313-317.

(6) Vistorobskii, N. V.; Pozharskii, A. F. Peri-naphthylenediamines. X. Acylation of proton sponge. Approaches to phenalenones from it. *Zh. Org. Khim.* **1991**, *27*, 1543-52.

(7) Ryabtsova, O. V.; Pozharskii, A. F.; Ozeryanskii, V. A.; Vistorobskii, N. V. peri-Naphthylenediamines. 32. Reactions of 4,5-bis(dimethylamino)-1-naphthyllithium and 4,5-bis(dimethylamino)-1-naphthylmagnesium bromide with electrophilic agents. New representatives of double naphthalene “proton sponges” with the structures of 1,1"-binaphthyl ketone and 1,1"-binaphthylmethanol. *Russ. Chem. Bull.* **2001**, *50*, 854-859.

(8) Maresca, L.; Natile, G.; Fanizzi, F. P. On the carbon nucleophilicity of proton sponge. *J. Chem. Soc., Dalton Trans.* **1992**, 1867-8.

(9) Lee, Y.; Kitagawa, T.; Komatsu, K. Electron-Transfer-Induced Substitution of Alkylated C60 Chlorides with Proton Sponge. *J. Org. Chem.* **2004**, *69*, 263-269.

(10) Fenske, D.; Becher, H. J. 2,3-Bis(diphenylphosphino)maleic anhydride and diphenylphosphino derivatives of cyclobutenedione as ligands in metal carbonyls. *Chem. Ber.* **1974**, *107*, 117-22.

(11) Mao, F.; Tyler, D. R.; Keszler, D. Mechanism of the substitution reactions of the nineteen-electron cobalt carbonyl complex $Co(CO)_3L_2$[L_2 = 2,3-bis(diphenylphosphino)maleic anhydride]. *J. Am. Chem. Soc.* **1989**, *111*, 130-134.

(12) van Doorn, J.; A., J. H. G.; Meijboom, N. Formation and reactions of bis(phosphino)succinic anhydrides. *J. Chem. Soc., Perkin Trans. 2* **1990**, 479-85.

(13) Bruker *SMART and SAINT*; Bruker AXS, Inc.: Madison, Wisconsin, USA, 2000.

(14) Sheldrick, G. M. *SADABS*; University of Göttingen: Germany, 1995.

(15) Sheldrick, G. M. A short history of SHELX. *Acta Crystallogr. A* **2008**, *64*, 112-122.

(16) Pozharskii, A. F.; Ozeryanskii, V. A. In *The Chemistry of Anilines*; John Wiley & Sons Ltd., 2007; Vol. 2, pp. 931-1139.

(17) Einspahr, H.; Robert, J. B.; Marsh, R. E.; Roberts, J. D. Peri interactions: an X-ray crystallographic study of the structure of 1,8-bis(dimethylaminonaphthalene). *Acta Crystallogr. B* **1973**, *29*, 1611-1617.

(18) Korzhenevskaya, N. G.; Schroeder, G.; Brzezinski, B.; Rybachenko, V. I. Concept of superbasicity of 1,8-bis(dialkylamino)naphthalenes ("proton sponges"). *Russ. J. Org. Chem.* **2001**, *37*, 1603-1610.

(19) McKusick, B. C.; Heckert, R. E.; Cairns, T. L.; Coffman, D. D.; Mower, H. F. Cyanocarbon chemistry. VI.1 Tricyanovinylamines. *J. Am. Chem. Soc.* **1958**, *80*, 2806-2815.

(20) Martin, E. L.; Dickinson, C. L.; Roland, J. R. 4-(2-Cyano-3-maleimidyl)arylamines and Related Colored Compounds. *J. Org. Chem.* **1961**, *26*, 2032-2037.

(21) Martin, E. L. Substituted Maleic Anhydrides and the Corresponding Lactones of 3-Formylacrylic Acid. U.S. Patent 3,113,939. December 10, 1963.

(22) Kadlecek, D. E.; Hong, D.; Carroll, P. J.; Sneddon, L. G. Reactions of arachno-6,8-$C_2B_7H_{12}^-$ with electron deficient olefins: Syntheses of cyano-substituted carboranes. *Inorg. Chem.* **2004**, *43*, 1933-1942.

(23) Reichardt, C. Solvatochromic Dyes as solvent polarity indicators. *Chem. Rev.* **1994**, *94*, 2319-2358.

(24) Pozharskii, A. F.; Kuz'menko, V. V.; Aleksandrov, G. G.; Dmitrienko, D.V. Bis(dimethylamino)naphthalene. XIII. Solvatochromism and molecular structure of 1,8-bis(dimethylamino)-4-nitronaphthalene and its salt with chloric acid. *Russ. J. Org. Chem.* **1995**, *31*, 525.

(25) Mekh, M. A.; Pozharskii, A. F.; Ozeryanskii, V. A. Electrophilic substitution in 5,6-bis(diemthylamino)acenaphthylene as a route to push-pull proton sponges. *Polish J. Chem.* **2009**, *83*, 1609-1621.

(26) Abraham, M. H.; Grellier, P. L.; Prior, D. V.; Duce, P. P.; Morris, J. J.; Taylor, P. J. Hydrogen bonding. Part 7. A scale of solute hydrogen-bond acidity based on log K values for complexation in tetrachloromethane. *J. Chem. Soc., Perkin Trans. 2* **1989**, 699-711.

(27) Mulliken, R. S. Molecular compounds and their spectra. II. *J. Am. Chem. Soc.* **1952**, *74*, 811-824.

(28) Rosokha, S. V.; Kochi, J. K. The preorganization step in organic reaction mechanisms. Charge-transfer complexes as precursors to electrophilic aromatic substitutions. *J. Org. Chem.* **2002**, *67*, 1727-1737.

(29) Tomoi, M.; Suzuki, T.; Kakiuchi, H. Polymer-supported bases. 8. Synthesis and reactivity of polystyrene derivatives containing 1,8-bis(dimethylamino)naphthalene moieties. *Makromol. Chem. Rapid Commun.* **1987**, *8*, 291-6.

(30) Corma, A.; Iborra, S.; Rodríguez, I.; Sánchez, F. Immobilized proton sponge on inorganic carriers: The synergic effect of the support on catalytic activity. *J. Catal.* **2002**, *211*, 208-215.

(31) Macquarrie, D. J.; Hardy, J. J. E. Applications of functionalized chitosan in catalysis†. *Ind. Eng. Chem. Res.* **2005**, *44*, 8499-8520.

(32) Nishimura, S.; Kohgo, O.; Kurita, K.; Kuzuhara, H. Chemospecific manipulations of a rigid polysaccharide: syntheses of novel chitosan derivatives with excellent solubility in common organic solvents by regioselective chemical modifications. *Macromolecules* **1991**, *24*, 4745-4748.

Chapter IV

(1) Shaughnessy, K. H. Hydrophilic ligands and their application in aqueous-phase metal-catalyzed reactions. *Chem. Rev.* **2009**, *109*, 643-710.

(2) Cornlis, B.; Herrmann, W. A. *Aqueous-phase Organometallic Catalysis: Concepts and Applications*; 2nd ed.; Wiley-VCH, 2004.

(3) Zhang, D.; Wang, J.; Yue, Q. Synthesis, characterization and catalytic behaviors of water-soluble phosphine-sulfonato nickel methyl complexes bearing PEG-amine labile ligand. *J. Organomet. Chem.* **2010**, *695*, 903-908.

(4) Elie, B. T.; Levine, C.; Ubarretxena-Belandia, I.; Varela-Ramirez, A.; Aguilera, R. J.; Ovalle, R.; Contel, M. Water-soluble (phosphine)gold(I) complexes - applications as recyclable catalysts in a three-component coupling reaction and as antimicrobial and anticancer agents. *Eur. J. Inorg. Chem.* **2009**, 3421-3430.

(5) Kokkinos, N. C.; Lazaridou, A.; Nikolaou, N.; Papadogianakis, G.; Psaroudakis, N.; Chatzigakis, A. K.; Papadopoulos, C. E. Hydrogenation of a hydroformylated naphtha model (mixture of specific aldehydes) catalysed by Ru/TPPTS complex in aqueous media. *Appl. Catal., A* **2009**, *363*, 129-134.

(6) Mika, L. T.; Orha, L.; Farkas, N.; Horváth, I. T. Efficient synthesis of water-soluble alkyl-bis(m-sulfonated-phenyl)- and dialkyl-(m-sulfonated-phenyl)-phosphines and their evaluation in rhodium-catalyzed hydrogenation of maleic acid in water. *Organometallics* **2009**, *28*, 1593-1596.

(7) Maccaroni, E.; Dong, H.; Blacque, O.; Schmalle, H. W.; Frech, C. M.; Berke, H. Water soluble phosphine rhenium complexes. *J. Organomet. Chem.* **2010**, *695*, 487-494.

(8) Bechtold, E.; Reisz, J. A.; Klomsiri, C.; Tsang, A. W.; Wright, M. W.; Poole, L. B.; Furdui, C. M.; King, S. B. Water-soluble triarylphosphines as biomarkers for protein S-nitrosation. *ACS Chem. Biol.* **2010**, *5*, 405-414.

(9) Marzano, C.; Pellei, M.; Colavito, D.; Alidori, S.; Lobbia, G. G.; Gandin, V.; Tisato, F.; Santini, C. Synthesis, characterization, and in vitro antitumor properties of tris(hydroxymethyl)phosphine copper(I) complexes containing the new bis(1,2,4-triazol-1-yl)acetate ligand. *J. Med. Chem.* **2006**, *49*, 7317-7324.

(10) Ang, W. H.; Dyson, P. J. Classical and non-classical ruthenium-based anticancer drugs: towards targeted chemotherapy. *Eur. J. Inorg. Chem.* **2006**, *2006*, 4003-4018.

(11) Marzano, C.; Gandin, V.; Pellei, M.; Colavito, D.; Papini, G.; Lobbia, G. G.; Del Giudice, E.; Porchia, M.; Tisato, F.; Santini, C. In vitro antitumor activity of the water soluble copper(I) complexes bearing the tris(hydroxymethyl)phosphine ligand. *J. Med. Chem.* **2008**, *51*, 798-808.

(12) Porchia, M.; Benetollo, F.; Refosco, F.; Tisato, F.; Marzano, C.; Gandin, V. Synthesis and structural characterization of copper(I) complexes bearing N-methyl-1,3,5-triaza-7-phosphaadamantane (mPTA). *J. Inorg. Biochem.* **2009**, *103*, 1644-1651.

(13) Rimmer, R. D.; Richter, H.; Ford, P. C. A photochemical precursor for carbon monoxide release in aerated aqueous media. *Inorg. Chem.* **2010**, *49*, 1180-1185.

(14) Wang, K.; Hong, L.; Liu, Z. Exploring the water-soluble phosphine ligand as the environmentally friendly stabilizer for electroless nickel plating. *Ind. Eng. Chem. Res.* **2009**, *48*, 1727-1734.

(15) Hoffman, A. The action of hydrogen phosphide on formaldehyde. *J. Am. Chem. Soc.* **1921**, *43*, 1684-1688.

(16) Hoffman, A. The action of hydrogen phosphide on formaldehyde. III. *J. Am. Chem. Soc.* **1930**, *52*, 2995-2998.

(17) Petrov, K. A.; Parshina, V. A. Reactions of phosphines. III. Reactions of secondary phosphines with aldehydes and ketones. *Zh. Obshch. Khim.* **1961**, *31*, 3417-20.

(18) Hellmann; Bader, J.; Birkner, H.; Schumacher, O. Hydroxymethylphosphines, hydroxymethylphosphonium salts, and chloromethylphosphonium salts. *Justus Liebigs Ann. Chem.* **1962**, *659*, 49-63.

(19) Klötzer, D.; Mäding, P.; Münze, R. Preparation, complex formation, and characterization of 1,2-bis[bis(hydroxymethyl)phosphino]ethane. *Z. Chem.* **1984**, *24*, 224-225.

(20) Nieckarz, G. F.; Weakley, T. J. R.; Miller, W. K.; Miller, B. E.; Lyon, D. K.; Tyler, D. R. Generation of 19-electron adducts in aqueous solution using the water-soluble $(HOCH_2)_2PCH_2CH_2P(CH_2OH)_2$ ligand. *Inorg. Chem.* **1996**, *35*, 1721-1724.

(21) Reddy, V. S.; Katti, K. V.; Barnes, C. L. Hydroxymethyl bis(phosphines) and their palladium(II) and platinum(II) complexes formed via biphasic reactions. Crystal structure of $[Pd\{(HOH_2C)_2PC_6H_4P(CH_2OH)_2\}_2]Cl_2$. *J. Chem. Soc., Dalton Trans.* **1996**, 1301-1304.

(22) Daigle, D. J.; Reeves, W. A.; Donaldson, D. J. Reaction of THPOH [sodium hydroxide-neutralized tetrakis(hydroxymethyl)phosphonium chloride] with secondary amines. *Text. Res. J.* **1970**, *40*, 580-1.

(23) Märkl, G.; Jin, G. Y. Optically active N,N-bis(phosphinomethylene)amino acid esters and their molybdenum carbonyl complexes. *Tetrahedron Lett.* **1981**, *22*, 223-6.

(24) Daigle, D. J.; Frank, A. W. Chemistry of hydroxymethyl phosphorus compounds. Part IV. Ammonia, amines, and THPOH: a chemical approach to flame retardancy. *Text. Res. J.* **1982**, *52*, 751-5.

(25) Kellner, K.; Tzschach, A. Mannich reaction as a synthetic concept in phosphine chemistry. *Z. Chem.* **1984**, *24*, 365-75.

(26) Henderson, W.; Olsen, G. M.; Bonnington, L. S. Immobilised phosphines incorporating the chiral biopolymers chitosan and chitin. *J. Chem. Soc., Chem. Commun.* **1994**, 1863.

(27) Petach, H. H.; Henderson, W.; Olsen, G. M. $P(CH_2OH)_3$ - a new coupling reagent for the covalent immobilization of enzymes. *J. Chem. Soc., Chem. Commun.* **1994**, 2181-2.

(28) Durran, S. E.; Smith, M. B.; Slawin, A. M. Z.; Steed, J. W. The synthesis and co-ordination chemistry of new functionalised pyridylphosphines derived from Ph_2PCH_2OH. *J. Chem. Soc., Dalton Trans.* **2000**, 2771-2778.

(29) Smith, M. B.; Elsegood, M. R. Mannich-based condensation reactions as a practical route to new aminocarboxylic acid tertiary phosphines. *Tetrahedron Lett.* **2002**, *43*, 1299-1301.

(30) Zhang, Q.; Aucott, S.; Slawin, A.; Woollins, J. Synthesis and Coordination Chemistry of the New Unsymmetrical Ligand $Ph_2PCH_2NHC_6H_4PPh_2$. *Eur. J. Inorg. Chem.* **2002**, *2002*, 1635-1646.

(31) Durran, S. E.; Elsegood, M. R.; Hawkins, N.; Smith, M. B.; Talib, S. New functionalised ditertiary phosphines via phosphorus based Mannich condensation reactions. *Tetrahedron Lett.* **2003**, *44*, 5255-5257.

(32) Rakowski Dubois, M.; Dubois, D. L. Development of molecular electrocatalysts for CO_2 reduction and H_2 production/oxidation. *Acc. Chem. Res.* **2009**, *42*, 1974-1982.

(33) Curtis, C. J.; Miedaner, A.; Ciancanelli, R.; Ellis, W. W.; Noll, B. C.; Rakowski DuBois, M.; DuBois, D. L. $[Ni(Et_2PCH_2NMeCH_2PEt_2)_2]^{2+}$ as a functional model for hydrogenases. *Inorg. Chem.* **2003**, *42*, 216-227.

(34) Rakowski DuBois, M.; DuBois, D. L. The roles of the first and second coordination spheres in the design of molecular catalysts for H_2 production and oxidation. *Chem. Soc. Rev.* **2009**, *38*, 62.

(35) Yang, J. Y.; Bullock, R. M.; Shaw, W. J.; Twamley, B.; Fraze, K.; DuBois, M. R.; DuBois, D. L. Mechanistic insights into vatalytic H2 oxidation by Ni complexes containing a diphosphine ligand with a positioned amine base. *J. Am. Chem. Soc.* **2009**, *131*, 5935-5945.

(36) Pool, D. H.; DuBois, D. L. $[Ni(PPh_2NAr_2)_2(NCMe)][BF_4]_2$ as an electrocatalyst for H_2 production: PPh_2NAr_2 = 1,5-(di(4-(thiophene-3-yl)phenyl)-3,7-diphenyl-1,5-diaza-3,7-diphosphacyclooctane). *J. Organomet. Chem.* **2009**, *694*, 2858-2865.

(37) Yang, J. Y.; Bullock, R. M.; Dougherty, W. G.; Kassel, W. S.; Twamley, B.; DuBois, D. L.; Rakowski DuBois, M. Reduction of oxygen catalyzed by nickel diphosphine complexes with positioned pendant amines. *Dalton Trans.* **2010**, *39*, 3001.

(38) Wang, N.; Wang, M.; Zhang, T.; Li, P.; Liu, J.; Sun, L. A proton–hydride diiron complex with a base-containing diphosphine ligand relevant to the [FeFe]-hydrogenase active site. *Chem. Commun.* **2008**, 5800.

(39) Wang, N.; Wang, M.; Liu, J.; Jin, K.; Chen, L.; Sun, L. preparation, facile deprotonation, and rapid H/D exchange of the μ-hydride diiron model complexes of the [FeFe]-hydrogenase containing a pendant amine in a chelating diphosphine ligand. *Inorg. Chem.* **2009**, *48*, 11551-11558.

(40) Duan, L.; Wang, M.; Li, P.; Wang, N.; Wang, F.; Sun, L. Synthesis, protonation and electrochemical properties of trinuclear $NiFe_2$ complexes $Fe_2(CO)_6(\mu^3\text{-}S)_2[Ni(Ph_2PCH_2)_2NR]$ (R = n-Bu, Ph) with an internal pendant nitrogen base as a proton relay. *Inorg. Chim. Acta* **2009**, *362*, 372-376.

(41) Ezzaher, S.; Capon, J.; Gloaguen, F.; Pétillon, F. Y.; Schollhammer, P.; Talarmin, J.; Kervarec, N. Influence of a pendant amine in the second coordination sphere on proton transfer at a dissymmetrically disubstituted diiron system related to the [2Fe]H subsite of $[FeFe]H_2$ase. *Inorg. Chem.* **2009**, *48*, 2-4.

(42) Jeffery, J. C.; Odell, B.; Stevens, N.; Talbot, R. E. Self assembly of a novel water soluble iron(II) macrocyclic phosphine complex from tetrakis(hydroxymethyl)phosphonium sulfate and iron(II) ammonium sulfate: single crystal X-ray structure of the complex $[Fe(H_2O)_2\{RP(CH_2N(CH_2PR_2)CH_2)_2PR\}]SO_4\cdot 4H_2O$ (R = CH_2OH). *Chem. Commun.* **2000**, 101-102.

(43) Burrows, A. D.; Dodds, D.; Kirk, A. S.; Lowe, J. P.; Mahon, M. F.; Warren, J. E.; Whittlesey, M. K. Substitution and derivatization reactions of a water soluble iron(II) complex containing a self-assembled tetradentate phosphine ligand. *Dalton Trans.* **2007**, 570-580.

(44) Burrows, A. D.; Harrington, R. W.; Kirk, A. S.; Mahon, M. F.; Marken, F.; Warren, J. E.; Whittlesey, M. K. Synthesis, characterization, and electrochemistry of a series of iron(II) complexes containing self-assembled 1,5-diaza-3,7-diphosphabicyclo[3.3.1]nonane ligands. *Inorg. Chem.* **2009**, *48*, 9924-9935.

(45) Kühl, O.; Blaurock, S.; Sieler, J.; Hey-Hawkins, E. Metallatriphos complexes: synthesis and molecular structure of $[TpZr(OCH_2PPh_2)_3]$ (Tp=tris(pyrazolyl)hydroborate) and formation of the heterodinuclear complex $[TpZr(\mu\text{-}OCH_2PPh_2)_3Mo(CO)_3]$ with bridging phosphinoalkoxide ligands. *Polyhedron* **2001**, *20*, 2171-2177.

(46) He, Y.; Hinklin, R. J.; Chang, J.; Kiessling, L. L. Stereoselective *N*-glycosylation by Staudinger ligation. *Org. Lett.* **2004**, *6*, 4479-4482.

(47) Szymczak, N. K.; Braden, D. A.; Crossland, J. L.; Turov, Y.; Zakharov, L. N.; Tyler, D. R. Aqueous coordination chemistry of H_2: why is coordinated H_2 inert to substitution by water in trans-$Ru(P_2)_2(H_2)H^+$-type complexes (P_2 = a chelating phosphine)? *Inorg. Chem.* **2009**, *48*, 2976-2984.

(48) Bruker *SMART and SAINT*; Bruker AXS, Inc.: Madison, Wisconsin, USA, 2000.

(49) Sheldrick, G. M. *SADABS*; University of Göttingen: Germany, 1995.

(50) Sheldrick, G. M. A short history of SHELX. *Acta Crystallogr. A* **2008**, *64*, 112-122.

(51) Brunel, J. M.; Faure, B.; Maffei, M. Phosphine-boranes: synthesis, characterization and synthetic applications. *Coord. Chem. Rev.* **1998**, *178-180*, 665-698.

(52) Maier, L. Organic phosphorus compounds. XVIII. New method for the formation P-C-P bonds (preparation of di-, tri- and tetratertiary phosphines). *Helv. Chim. Acta* **1965**, *48*, 1034-9.

(53) Maier, L. Organic phosphorus compounds. XXII. Preparation and properties of diprimary α,ω-diphosphinoalkanes. *Helv. Chim. Acta* **1966**, *49*, 842-51.

(54) Gilbertson, J. D.; Szymczak, N. K.; Tyler, D. R. H_2 activation in aqueous solution: Formation of *trans*-$[Fe(DMeOPrPE)_2H(H_2)]^+$ via the heterolysis of H_2 in water. *Inorg. Chem.* **2004**, *43*, 3341-3343.

(55) Pensee, A. A. L.; Bickley, J.; Higgins, S. J. Homoleptic iron(II)-diphosphine and -diarsine complexes: syntheses, characterization and redox properties. *J. Chem. Soc., Dalton Trans.* **2002**, 3241-3244.

(56) Gilbertson, J. D.; Szymczak, N. K.; Crossland, J. L.; Miller, W. K.; Lyon, D. K.; Foxman, B. M.; Davis, J.; Tyler, D. R. Coordination chemistry of H_2 and N_2 in aqueous solution. Reactivity and mechanistic studies using trans-$Fe^{II}(P_2)_2X_2$-type complexes (P_2 = a chelating, water-solubilizing phosphine). *Inorg. Chem.* **2007**, *46*, 1205-1214.

(57) Tramontini, M. *Mannich Bases: Chemistry and Uses*; CRC Press: Boca Raton, 1994.

(58) Kellner, K.; Seidel, B.; Tzschach, A. Organoarsen-verbindungen : XXXIII. Synthese und reaktionsverhalten der [alpha]-aminomethylphosphine und -arsine. *J. Organomet. Chem.* **1978**, *149*, 167-176.

(59) Imamoto, T.; Kusumoto, T.; Suzuki, N.; Sato, K. Phosphine oxides and lithium aluminum hydride-sodium borohydride-cerium(III) chloride: synthesis and reactions of phosphine-boranes. *J. Am. Chem. Soc.* **1985**, *107*, 5301-5303.

(60) Redmore, D. Chemistry of phosphorous acid: new routes to phosphonic acids and phosphate esters. *J. Org. Chem.* **1978**, *43*, 992-996.

(61) Bates, J. I.; Gates, D. P. Diphosphiranium (P2C) or diphosphetanium (P2C2) cyclic cations: Different fates for the electrophile-initiated cyclodimerization of a phosphaalkene. *J. Am. Chem. Soc.* **2006**, *128*, 15998-15999.

(62) van der Knap, T.; Bickelhaupt, F. A nucleophilic reaction of a phosphaalkene: the methylation of mesityldiphenylmethylenephosphine. *Tetrahedron Lett.* **1982**, *23*, 2037-2040.

(63) Igau, A.; Baceiredo, A.; Gruetzmacher, H.; Pritzkow, H.; Bertrand, G. Synthesis, reactivity, and crystal structure of the first methylenephosphonium ion: a severely twisted valence isoelectronic olefin. *J. Am. Chem. Soc.* **1989**, *111*, 6853-6854.

Chapter V

(1) Glueck, D. S. Metal-catalyzed nucleophilic carbon–heteroatom (C–X) bond formation: the role of M–X intermediates. *Dalton Trans.* **2008**, 5276.

(2) Kang, Y. B.; Pabel, M.; Pathak, D. D.; Willis, A. C.; Wild, S. B. Copper(I)-facilitated methylation and cyclic alkylation of 1,2-phenylenebis(phosphine). *Main Group Chem.* **1995**, *1*, 89-98.

(3) Lambert, B.; Desreux, J. F. Synthesis of macrocyclic polyphosphine oxides and phosphines by template cyclisation and demetallation. *Synthesis* **2000**, 1668-1670.

(4) Dogan, J.; Schulte, J. B.; Swiegers, G. F.; Wild, S. B. mechanism of phosphorus−carbon bond cleavage by lithium in tertiary phosphines. An optimized synthesis of 1,2-bis(phenylphosphino)ethane. *J. Org. Chem.* **2000**, *65*, 951-957.

(5) Bruker *SMART and SAINT*; Bruker AXS, Inc.: Madison, Wisconsin, USA, 2000.

(6) Sheldrick, G. M. *SADABS*; University of Göttingen: Germany, 1995.

(7) Sheldrick, G. M. A short history of SHELX. *Acta Crystallogr. A* **2008**, *64*, 112-122.

(8) Mohr, B.; Brooks, E. E.; Rath, N.; Deutsch, E. X-ray structural and NMR characterization of the copper(I) dimer $[Cu(dmpe)_2]_2(BF_4)_2$, where dmpe is 1,2-bis(dimethylphosphino)ethane. *Inorg. Chem.* **1991**, *30*, 4541-4545.

(9) Saito, K.; Saijo, S.; Kotera, K.; Date, T. Asymmetric hydrogenation catalyzed by rhodium complex with a new chiral bisphosphine derived from L-threonine. *Chem. Pharm. Bull.* **1985**, *33*, 1342-1350.

(10) Lewis, J. S.; Heath, S. L.; Powell, A. K.; Zweit, J.; Blower, P. J. Diphosphine bifunctional chelators for low-valent metal ions. Crystal structures of the copper(I) complexes $[CuClL^1_2]$ and $[CuL^1_2][PF_6]$ [L^1 = 2,3-bis(diphenylphosphino)maleic anhydride]. *J. Chem. Soc., Dalton Trans.* **1997**, 855-862.

(11) Blue, E. D.; Davis, A.; Conner, D.; Gunnoe, T. B.; Boyle, P. D.; White, P. S. Synthesis, solid-state crystal structure, and reactivity of a monomeric copper(I) anilido complex. *J. Am. Chem. Soc.* **2003**, *125*, 9435-9441.

(12) Townsend, J. M.; Blount, J. F.; Sun, R. C.; Zawoiski, S.; Valentine, D. Novel copper complexes of chiral diphosphines: preparation, structure, and use to form rhodium complex catalysts for chiral hydrogenations. *J. Org. Chem.* **1980**, *45*, 2995-2999.

(13) di Nicola, C.; Effendy; Fazaroh, F.; Pettinari, C.; Skelton, B. W.; Somers, N.; White, A. H. Structural characterization of 1:1 adducts of silver(I) (pseudo-) halides (AgX, X = NCO, Cl, Br, I) with $Ph_2E(CH_2)EPh_2$ (E = P, As) ('dp(p/a)m') and 4:3 adducts of copper(I) halide (CuX, X = Cl, Br, I), containing trinuclear cations, of the form $[X_2Ag_3(dppm)_3]X$ and $[X_2Cu_3(dppm)_3](CuX_2)$ and the novel neutral $[(OCN)_3Ag_3(dpam)_3]$. *Inorg. Chim. Acta* **2005**, *358*, 720-734.

(14) Mao, Z.; Chao, H.; Hui, Z.; Che, C.; Fu, W.; Cheung, K.; Zhu, N. 3[(d_{x2-y2}, d_{xy})(p_z)] Excited states of binuclear copper(I) phosphine complexes: Effect of copper–ligand and copper–copper interactions on excited state properties and photocatalytic reductions of the 4,4′-dimethyl-2,2′-bipyridinium ion in alcohols. *Chem. Eur. J.* **2003**, *9*, 2885-2894.

(15) Darensbourg, D. J.; Chao, C. S.; Reibenspies, J. H.; Bischoff, C. J. Crystal structure and reactivity of bis[bis(1,2-dimethylphosphino)ethane]copper(2+) bis(tetracarbonylcobalt)curprate(2-): staggered and eclipsed conformations of $[(CO)_4CoCuCo(CO)_4]^-$ anions. *Inorg. Chem.* **1990**, *29*, 2153-2157.

(16) Nadasdi, T. T.; Stephan, D. W. Heterobimetallic derivatives of cyclopentadienyltitanium bis(dithiolate) anions: $[CpTi(S(CH_2)_nS)_2M]_x$ and $CpTi(S(CH_2)_nS)_2ML$ (M = Cu, Rh; n = 2, 3). *Inorg. Chem.* **1994**, *33*, 1532-1538.

(17) Marstokk, K.; Moellendal, H. Structural and conformational properties of 1,2-diphosphinoethane as studied by microwave spectroscopy and ab initio calculations. *Acta Chem. Scand.* **1996**, *50*, 875-884.

(18) Berners-Price, S. J.; Johnson, R. K.; Mirabelli, C. K.; Faucette, L. F.; McCabe, F. L.; Sadler, P. J. Copper(I) complexes with bidentate tertiary phosphine ligands: solution chemistry and antitumor activity. *Inorg. Chem.* **1987**, *26*, 3383-3387.

(19) Berners-Price, S. J.; Sadler, P. J. Phosphines and metal phosphine complexes: Relationship of chemistry to anticancer and other biological activity. *Struct Bonding* **1988**, *70*, 27-102.

(20) Lewis, J. S.; Zweit, J.; Blower, P. J. Effect of ligand and solvent on chloride ion coordination in anti-tumour copper(I) diphosphine complexes: Synthesis of $[Cu(dppe)_2]Cl$ and analogous complexes (dppe = 1,2-bis(diphenylphosphino)ethane). *Polyhedron* **1998**, *17*, 513-517.

(21) Marzano, C.; Gandin, V.; Pellei, M.; Colavito, D.; Papini, G.; Lobbia, G. G.; Del Giudice, E.; Porchia, M.; Tisato, F.; Santini, C. In vitro antitumor activity of the water soluble copper(I) complexes bearing the tris(hydroxymethyl)phosphine ligand. *J. Med. Chem.* **2008**, *51*, 798-808.

(22) Marzano, C.; Pellei, M.; Colavito, D.; Alidori, S.; Lobbia, G. G.; Gandin, V.; Tisato, F.; Santini, C. Synthesis, characterization, and in vitro antitumor properties of tris(hydroxymethyl)phosphine copper(I) complexes containing the new bis(1,2,4-triazol-1-yl)acetate ligand. *J. Med. Chem.* **2006**, *49*, 7317-7324.

(23) Alidori, S.; Gioia Lobbia, G.; Papini, G.; Pellei, M.; Porchia, M.; Refosco, F.; Tisato, F.; Lewis, J. S.; Santini, C. Synthesis, in vitro and in vivo characterization of 64Cu(I) complexes derived from hydrophilic tris(hydroxymethyl)phosphane and 1,3,5-triaza-7-phosphaadamantane ligands. *J Biol Inorg Chem* **2007**, *13*, 307-315.

(24) Lewis, J. S.; Zweit, J.; Dearling, J. L. J.; Rooney, B. C.; Blower, P. J. Copper(I) bis(diphosphine) complexes as a basis for radiopharmaceuticals for positron emission tomography and targeted radiotherapy. *Chem. Commun.* **1996**, 1093-1094.

(25) Cho, C.; Phuong Thuy Pham, T.; Jeon, Y.; Yun, Y. Influence of anions on the toxic effects of ionic liquids to a phytoplankton Selenastrum capricornutum. *Green Chem.* **2008**, *10*, 67.